The impact of ageing, gamma(γ)-irradiation, and varying concentrations of phosphate on the stability and solubility of biogenic iron oxides (BIOS) in the presence of *Shewanella putrefaciens* CN32

Tarek Najem

Thesis submitted to the Faculty of Graduate and Postdoctoral Studies, in partial fulfillment of the requirements for the M. Sc. Degree in Earth Sciences, Specialization in Chemical and Environmental Toxicology

Ottawa-Carleton Geoscience Centre
and
University of Ottawa
Ottawa, Canada

Abstract

The redox cycling of iron is intimately linked to the cycling of C, S, N, P as well as the speciation, mobility, and bioavailability of various toxic contaminants in soils and sediments. Within these environments, the cycling of iron is catalytically driven by iron-oxidizing (FeOB) and iron reducing bacteria (FeRB) which mediate the formation, transformation, and dissolution of various iron-bearing minerals. Under oxic conditions, FeOB promote the formation of iron oxides on or in close proximity of their cell walls and extracellular polymeric substances, and such composite, termed biogenic iron oxides (BIOS), offers highly reactive heterogenous sites that efficiently immobilize trace metals and contaminants alike. However, under reducing conditions, FeRB mediate the reductive dissolution of BIOS and in turn lead to the remobilization of associated contaminants. Conversely, contaminants may become immobilized by secondary iron minerals that form from the metabolic activity of FeRB. Therefore, determining the factors that influence the reactivity of BIOS, as well as the formation of secondary iron minerals is of critical importance to develop a better understanding of the geochemical cycling of iron and in turn the transport of contaminants in the environment. This thesis investigated (1) the impact of simulated diagenesis (ageing for ~5 years at 4ºC) on the mineral stability and reactivity of BIOS towards reduction by *Shewanella putrefaciens* CN32, (2) the effects of phosphate at an environmentally relevant (10µM) and excess (3.9mM) concentration on the rates and extent of microbial reduction of synthetic 2-line ferrihydrite and BIOS, as well as the formation of secondary iron minerals, and (3) the impact of sterilization by γ-irradiation on the mineral stability and reactivity of BIOS. It was found that simulated diagenesis did not affect the mineralogical composition of BIOS but significantly lowered the reactivity of BIOS towards microbial reduction. The concentration of phosphate was found to have contrasting effects on the rates of reduction of ferrihydrite and BIOS,

but in general, excess concentration of phosphate enhanced the extent of Fe(III) reduction. The formation of a specific secondary iron mineral was also found to depend on the concentration of phosphate, as well as, in the case for BIOS, the presence of intermixed cell derived organic matter. γ-irradiation did not alter the mineralogy and reactivity of BIOS towards microbial reduction, and it was concluded to be a suitable technique to sterilize BIOS.

Résumé

Le cycle redox du fer est intimement lié aux cycles du C, S, N et P, ainsi qu'à la spéciation, la mobilité et la biodisponibilité de divers contaminants toxiques dans les sols et les sédiments. Dans ces environnements, le cycle du fer est contrôlé en partie par des bactéries oxydantes (FeOB) et réductrices (FeRB) du fer, lesquelles peuvent influencer la formation, la transformation et la dissolution de divers minéraux riches en fer. Sous des conditions oxiques, les FeOB permettent la formation d'oxydes de fer près de leur membrane cellulaire et sur leurs substances exopolymériques, ce qui crée un mélange souvent appelé oxydes de fer biogéniques (BIOS) lesquels sont très efficaces pour immobiliser les contaminants solubles. Sous des conditions réductrices, les FeRB peuvent cependant faciliter la dissolution réductive du BIOS et ainsi remettre en solution tous les contaminants sorbés. Ces mêmes contaminants peuvent toutefois être immobilisés de nouveau par des minéraux secondaires formés lors de la réduction des oxydes de fer biogéniques. Il demeure donc important d'étudier la réactivité du BIOS ainsi que la formation de minéraux secondaires afin de mieux comprendre le cycle du fer et des contaminants. La présente thèse s'est donc intéressée à 1) l'effet de la diagenèse (sur une période de 5 ans à 4ºC) sur la stabilité et la réactivité de BIOS lors de leur réduction en présence de *Shewanella putrefaciens* CN32, 2) l'effet de faibles (10µM) et de grandes (3.9mM) concentrations de phosphate sur la réduction microbienne de la ferrihydrite à 2 lignes et du BIOS, ainsi que l'effet sur la minéralogie des minéraux secondaires et 3) l'impact de la stérilisation par radiation gamma sur la stabilité et la réactivité des BIOS. Les résultats démontrent que la diagenèse n'affecte pas la composition minéralogique du BIOS mais diminue de façon significative leur réactivité lors de leur réduction microbienne. La concentration de phosphate a eu des effets différents sur les taux de réduction de la ferrihydrite et du BIOS; les concentrations élevées ont augmenté le taux de réduction. Les

résultats indiquent aussi que la formation de minéraux secondaires lors de la réduction est contrôlée par la concentration de phosphate ainsi que part la présence de matière organique dans le cas du BIOS. Finalement, la stérilisation gamma n'altère pas la minéralogie et la réactivité du BIOS lors de la réduction. Cette technique de stérilisation est donc appropriée.

Acknowledgments

I would like to express my deepest gratitude to my supervisor Dr. Danielle Fortin for, teaching, mentoring, directing, and encouraging me, and her scientific support during this research. Her patience and positive attitude made my experience a remarkable one, I feel privileged to have known and allowed to work with Dr. Fortin. A special thank you to Dr. Sean Langley, Dr. Erika Revesz, and Bob Chlebek for always taking the time to answer all of my questions, the completion of this thesis would not have been possible without their support and expertise.

My sincerest thanks to: Brandon Khan, Maeve Moriarty, Maria Stefanescu, Liz Ashby, Justin Whitaker, Sarina Cotroneo, and Ed Bryson, for their support, friendship, and making the experience of graduate studies a special one. I'm indebted to my friends Dr. Nimal de Silva and Maeve Moriarty, for sharing their expertise with me throughout my studies, the plethora of knowledge they provided me with regards to analytical techniques and analytical instruments is immeasurable, I feel privileged to have been allowed to get to know and learn from them.

During the course of M. Sc. I had the opportunity to work with and to know many technicians, and graduate and undergraduate students, i.e. Tara Kell, Ping Zhang, Smita Mohanty, Sarah Agosta, Emily Meyers, Fiona D'Arcy, Ashley Chen, and Stéphane Aubin, I thank them all for their support and friendship, I learned a lot and shared a great time.

Finally, I dedicate this work to the special people in my life, my parents, girlfriend, brother, sister and her husband. Thank you for your unconditional support and love.

Table of Contents

List of Tables

List of Figures

Preface

This thesis is organized as manuscripts for publication. As such, the chapters may contain some repetition of Chapter 1 of this thesis. The entire thesis was written by the candidate and all the results presented in this thesis are based on measurements performed by the candidate. The experiments include: synthesis of synthetic 2-line ferrihydrite, and all of the microbial reduction experiments carried out with aged BIOS, non- and γ-irradiated BIOS, and synthetic 2-line ferrihydrite. Collection and preparation of BIOS samples from Chalk River were performed by Dr. Sean Langley and Dr. Danielle Fortin. Collection and preparation of BIOS samples from Calumet Mine were performed by the candidate, Sarina Cotroneo, and Dr. Danielle Fortin. SEM imaging was performed by Dr. Erika Revesz at the University of Ottawa. Bulk XRD analyses were carried out by the candidate with supervision and training provided by Dr. Tara Kell at the University of Ottawa. ICP analyses were performed by Dr. Nimal de Silva at the University of Ottawa. Maeve Moriarty carried out the PHREEQ-C modeling and provided assistance with ICP analyses, LOI, and bulk XRD. Finally, all the calculations and statistical analyses were performed by the candidate.

Chapter 1: General Introduction

1. Biogenic Iron Oxides

1.1. Occurrence and formation

Biogenic iron oxides (BIOS) are defined as a composite mixture of fine grained iron oxides (collectively referring to Fe(III)-oxyhydroxides, Fe(III)-hydroxides, and Fe(III)-oxides) and cell derived organic matter, which form from the metabolic activity of a diverse range of species of Fe(II)-oxidizing bacteria (FeOB) that inhabit a broad range of environments, including: pH-neutral and acidic, oxic, oxic-anoxic, anoxic, and hydrothermal settings (Ferris et al., 1999; Ferris et al., 2000; Fortin and Langley, 2005; Kappler and Straub, 2005; Melton et al., 2014). Although the chemical oxidation of dissolved Fe(II) by molecular O_2 is very rapid at circumneutral pH and O_2 saturated conditions (half-life of ~5 minutes) (Stumm and Morgan, 2012), microaerophilic FeOB, such as *Gallionella* spp. and *Leptothrix* spp., are capable of competing with O_2 for Fe(II) by occupying limited oxic-anoxic zones that are characterized by elevated concentrations of Fe(II) and low pO_2 (Fortin and Langley, 2005; Hedrich et al., 2011). These conditions occur in a broad range of environments, including: hydrothermal sea vents (Kennedy et al., 2003; Langley et al., 2009a; Toner et al., 2009; Toner et al., 2012), soils (Cismasu et al., 2016), wetland plant rhizospheres (Emerson et al., 1999), lake sediments (Fortin et al., 1993), mining impacted environments (Banfield et al., 2000; Chan et al., 2004; Fabisch et al., 2016), and ferriferous groundwater discharge zones (James and Ferris, 2004; Blöthe and Roden, 2009; Gault et al., 2011). Within these environments, the formation of BIOS stems from the direct and indirect role of bacteria (Fortin and Langley, 2005). Directly, FeOB derive energy from the oxidation of Fe(II) to Fe(III) and promote the precipitation of iron oxides on or in close proximity of their cell surfaces or extracellular polymeric substances (EPS), such as twisted stalks and sheaths generated by the

FeOB *Gallionella ferruginea* and *Leptothrix ochracea*, respectively (Chan et al., 2004; Fortin and Langley, 2005; Kappler and Straub, 2005; Chan et al., 2009; Chan et al., 2011). Indirectly, due to the presence of negatively charged functional groups (e.g. carboxyl, phosphoryl, and hydroxyl groups) on cell surfaces, bacteria, including non-Fe metabolizing bacteria, and extracellular surfaces act as passive heterogeneous templates for the sorption, nucleation, and precipitation of iron oxides that formed chemically in solution (Konhauser, 1997; Warren and Ferris, 1998; Châtellier et al., 2001; Châtellier et al., 2004; Fortin and Langley, 2005; Rancourt et al., 2005).

FeOB face the challenge of the precipitation of poorly soluble iron mineral crusts onto the surfaces of metabolizing cells that could potentially impair cellular function by limiting the diffusion of nutrients into and waste away from the metabolizing cell, eventually leading to death (Kappler and Newman, 2004; Chan et al., 2011; Saini and Chan, 2013; Posth et al., 2014). FeOB, however, have developed a number of strategies to deal with such dilemma, and as will be discussed later, species specific strategies have important consequences on the long-term stability and therefore the reactivity of the mineral fraction. In the case for the microaerophilic FeOB, *Gallionella ferruginea* and *Leptothrix ochracea*, it was recently proposed that these bacteria produce EPS (twisted stalks or sheaths) in order to direct the precipitation of iron oxides away from the metabolizing cells (Chan et al., 2011). Another potential advantage of such strategy is the enhancement of metabolic energy generation promoted by the formation of a proton gradient formed from reactions involving Fe(II) (e.g. proton generation from the autocatalytic oxidation of Fe(II)) (Chan et al., 2004). Recent work has also shown that marine and freshwater stalk-forming microaerophilic FeOB, *Mariprofundus ferrooxydans* PV-1 and *Gallionellales* strain R-1, respectively, maintain a hydrophilic and low, near-neutral cell surface charge thereby preventing the attraction of the positively charged iron oxides to the metabolizing cell surfaces (Saini and

Chan, 2013). Thus, these FeOB have developed a well-coordinated strategy to prevent the encrustation of metabolizing cells by iron oxide deposits (Saini and Chan, 2013). Another possible advantage of the production of Fe-encrusted EPS is the binding of toxic heavy metals (e.g. Cu, Ni, Zn) lowering their free concentration in solution to less toxic levels for the bacteria as was recently observed for pure-cultures of the anoxygenic photoautotrophic FeOB *Rhodobacter ferrooxidans* strain SW2 (Hao et al., 2016). Metabolically driven modification of the microenvironment adjacent to the metabolizing cell was proposed to be a another strategy utilized by some anoxygenic photoautotrophic and nitrate-reducing FeOB (Kappler and Newman, 2004; Schädler et al., 2009; Posth et al., 2014), in which case acidification of the local environment around the cell enhances the solubility of iron oxides thereby preventing their precipitation on the metabolizing cells, consequently iron oxides are loosely associated with the cell surfaces (Kappler and Newman, 2004; Schädler et al., 2009). For example, using a pH-sensitive fluorescent dye combined with fluorescence microscopy, Hegler et al. (2010) showed that the pH adjacent to the photoautotrophic FeOB *Thiodictyon* sp. strain F4 was ~6.0 which was lower than the pH of the bulk medium (pH of 6.6). Recent work suggested that the formation of loosely associated biogenic Fe(III) minerals with the cells of the anoxygenic photoautotrophic FeOB *Rhodobacter ferrooxidans* strain SW2 and *Rhodopseudomonas palustris* could act as a protective barrier against UV-irradiation, findings which have important implications for ancient oceans and banded iron formation (Gauger et al., 2015). Another strategy proposed to avoid cell encrustation includes the production of organic ligands (e.g. citrate) to solubilize and complex Fe(III) (Schädler et al., 2009; Toner et al., 2009). However, it is important to note that FeOB may utilize a combination of the aforementioned strategies to avoid cell encrustation (Schädler et al., 2009).

1.2. Mineralogy and environmental significance

The most common iron oxide that precipitates in close association of the cells and/or their EPS within BIOS formed from the activity of microaerophilic FeOB is a short-ranged ordered phase that resembles the poorly crystalline mineral 2-line ferrihydrite, but also minor amounts of the crystalline iron oxides lepidocrocite, goethite, akaganeite, or hematite, comprising the remainder (Chan et al., 2004; Hallberg and Ferris, 2004; Fortin and Langley, 2005; Chan et al., 2009; Chan et al., 2011; Gault et al., 2011). 2-line ferrihydrite is common in soils, sediments, and aqueous environments, and it is an environmentally important iron oxide as it is considered to be the most efficient adsorbent of nutrients (e.g., PO_4^{-3}), trace metals (e.g., Cu, Co, Zn, etc.), and organic and inorganic contaminants (e.g., As), as a result of its high surface area compared to other iron phases (Table 1) (Tessier et al., 1996; Cornell and Schwertmann, 2003; Baken et al., 2015).

Table 1-1: Surface area of different iron oxides. Values obtained from Cornell and Schwertmann (2003).

Mineral	**Surface Area (m^2 g^{-1})**
2-line Ferrihydrite ($Fe(OH)_3$)	100-700
Lepidocrocite (γ-FeOOH)	15-260
Goethite (α-FeOOH)	8-200
Maghemite (γ-Fe_2O_3)	8-130
Hematite (α-Fe_2O_3)	4-100
Magnetite (Fe_3O_4)	2-27

The incorporation of cells and/or their EPS within BIOS, however, modifies the properties of the mineral fraction, thus BIOS exhibit distinct properties from their synthetic mineral counterparts. BIOS possess lower crystallinity and smaller particle size (Châtellier et al., 2001; Châtellier et al., 2004; Rancourt et al., 2005), different morphologies (Posth et al., 2014), lower surface area, and an overall negative surface charge compared to synthetic iron oxides which are positively charged under pH-neutral conditions (Kleinert et al., 2011). Consequently, BIOS exhibit

different sorptive capacity and properties towards metal(loid)s, and, as will be discussed later, susceptibility towards microbial Fe(III) reduction. Previous studies have demonstrated the capability of BIOS to immobilize a significant amount of metal(loid)s under laboratory and natural settings, which has been attributed to the presence of the organic fraction that provides additional binding sites. Therefore, the effectiveness of BIOS at immobilizing metal(loid)s increases with decreasing iron content, hence an increase in the relative proportion of organic matter (Ferris et al., 1999; Ferris et al., 2000). Hao et al. (2016) assessed the sorption and partitioning of heavy metals (Au, Cd, Cr, CrO_4^{-2}, Cu, Hg, Ni, Pd, tributyltin, and Zn) to bacteria-EPS-iron oxide aggregates formed by a pure culture of the photoautotrophic FeOB *Rhodobacter ferrooxidans* strain SW2. These authors found that the heavy metals were preferentially bound by microbial cells and their EPS, and that Fe(III) and Fe(II) competed for the same sites, particularly on EPS. Eickhoff et al. (2014), however, found that synthetic 2-line ferrihydrite adsorbed a higher amount of Ni^{2+} when compared to that of biogenic 2-line ferrihydrite produced by a pure culture of the freshwater and marine photoautotrophic FeOB *Rhodobacter ferrooxidans* SW2 and *Rhodovulum iodosum*, respectively, which was attributed to the competition between Ni^{2+} and cell derived organic matter for sorption sites on the biogenic 2-line ferrihydrite. In contrast, Langley et al. (2009b) showed that BIOS dominated by *Leptothrix*-like sheath structures were more efficient at binding Sr^{2+} (S_{max} of 3.41µmol/g) than synthetic 2-line ferrihydrite (S_{max} of 1µmol/g). Martinez et al. (2003) suggested that BIOS formed from the activity of microaerophilic FeOB provide heterogeneous reactive sites whereby some heavy metals preferentially bind to the mineral fraction while others preferentially bind to the organic fraction. BIOS dominated by *Gallionella*-like stalks that formed within mine water (pH 6.0) contaminated with heavy metals were found to efficiently scavenge heavy metals, Cu, in particular, was found to preferentially bind to the iron oxide fraction

(Fabisch et al., 2016). Similarly, BIOS formed from the activity of microaerophilic FeOB within a mining impacted environment (pH 7.1) were found to efficiently scavenge arsenic from solution (As:Fe ~0.40 mol/mol) (Keim, 2011). Hohmann et al. (2011) investigated the effectiveness of BIOS formed by a pure strain of the nitrate-reducing FeOB *Acidovorax* sp. strain BoFeN1 to immobilize arsenic by adding variable concentrations (50, 200, or 500µM) of As(V) to a growth medium to which an active population of Fe(II) respiring bacteria were added. These authors found that BIOS immobilized a significant proportion of As(V) via coprecipitation, but As(V) had a significant effect on the mineralogy of BIOS, in which case at low concentrations of As(V) goethite was the dominant mineral that formed and with increasing As(V) concentrations the proportion of 2-line ferrihydrite was found to progressively increase at the expense of goethite (up to ~30%). Collectively, these studies show that BIOS could potentially provide a natural and an efficient attenuating mechanism for different contaminants in various environments, particularly within environments impacted by mining activity. Consequently, however, the mobility and fate of associated contaminants are dependent on the redox state of iron.

1.3. Mineral stability under oxic conditions

According to the Ostwald step rule, or the rule of stages, 2-line ferrihydrite, which is the least stable and most soluble iron phase, is expected to be the first iron phase to precipitate following the oxidation of Fe(II) and the hydrolysis of Fe(III), because the nucleation of ferrihydrite nanoparticles is kinetically favored (Stumm and Morgan, 2012). Once formed, 2-line ferrihydrite eventually transforms into thermodynamically stable iron oxide phases such as goethite and/or hematite, which are the most stable end members under oxic conditions (Cornell and Schwertmann, 2003), the kinetics of which strongly depend on the prevailing geochemical conditions (e.g. pH and temperature) (Cornell and Schwertmann, 2003). For example, at ambient

temperature (25°C) it took ~4 years for 2-line ferrihydrite to fully transform (~95%) into crystalline phases at neutral pH conditions, whereas it took only a few hours for full transformation to occur at alkaline pH conditions (pH 12) (Cornell and Schwertmann, 2003; Schwertmann et al., 2004). Transformation may proceed via two competing pathways, including: (1) dissolution of precursor ferrihydrite nanoparticles and the subsequent precipitation of goethite (dissolution-reprecipitation), or (2) dehydration-aggregation and internal rearrangement of ferrihydrite nanoparticles to form hematite (solid-state transformation) (Cornell and Schwertmann, 2003). Which pathway predominates, mainly depends on the prevailing geochemical conditions (e.g. temperature, pH, ionic strength, etc.) (Cornell and Schwertmann, 2003). For example, at pH neutral conditions hematite formation from precursor 2-line ferrihydrite predominates over a wide temperature range (4 - 90ºC), pH-conditions in which the solubility of 2-line ferrihydrite is at a minimum (Cornell and Schwertmann, 2003). The transformation of a highly reactive mineral to crystalline phases has important ecological and environmental implications, as the varying properties of the iron phases influence their biogeochemical reactivity and in turn affect the mobility and fate of nutrients and contaminants that are associated with the iron phase. For example, as shown in Table 1 the transformation of 2-line ferrihydrite into goethite or hematite reduces the surface area and thus the available binding sites to uptake contaminants, in which case such transformation may lead to the desorption and remobilization of adsorbed contaminants (Ford et al., 1997; Cornell and Schwertmann, 2003; Vu and Moreau, 2015). In contrast, such transformation may lead to the structural incorporation of adsorbed contaminants into crystalline phases leading to stronger contaminant-iron oxide association, which is particularly desirable because crystalline iron oxides are recalcitrant to microbial Fe(III) reduction (Roden and Zachara, 1996; Hansel et al., 2003; Nielsen et al., 2014; Das et al., 2015).

Naturally occurring iron oxides rarely occur as pure phases, instead they are often closely associated with impurities such as Al, Si, P, As, and organic matter (e.g. humic acids and cell derived organic matter) (Fortin et al., 1993; Tessier et al., 1996; Cornell and Schwertmann, 2003). With the exception of Mn(II) and Fe(II), impurities adsorbed and/or incorporated by ferrihydrite often result in a concentration dependent effect on the kinetics and extent of transformation, and in turn modify the identity/proportion of the mineral products that form (Cornell, 1988; Ford et al., 1997; Cornell and Schwertmann, 2003). Impurities may also completely inhibit transformation, presumably by either blocking dissolution sites on ferrihydrite and the nucleation of crystalline phases in solution, or linking ferrihydrite nanoparticles into an immobile network thereby preventing their aggregation (Cornell and Schwertmann, 2003). For example, increasing the concentration of silicate (Si/Fe mol ratio 0.001-0.1) was found to progressively inhibit the transformation of 2-line ferrihydrite into goethite at 70°C and alkaline conditions (pH 11), and where transformation occurred, silicate was found to promote the formation of hematite (Cornell et al., 1987). Similarly, the degree of transformation of 2-line ferrihydrite coprecipitated with increasing concentrations of phosphate (P/Fe mol ratio 0-0.03) progressively diminished, and where transformation occurred, phosphate was found to promote the formation of hematite over goethite (Galvez et al., 1999). Schwertmann et al. (2000) conducted long term experiments where 2-line ferrihydrite was aged for 16 years at ambient temperature (25°C) and pH-neutral conditions in the presence of different clay minerals. The clay minerals allophane and soil smectite were found to retard the rate and extent of transformation of ferrihydrite, in which case only ~50% or 80% of ferrihydrite was transformed in the presence of either allophane or soil smectite, respectively, which was attributed to the adsorption of Al and Si released from the clay minerals to the surface of ferrihydrite.

Organic matter or organic acids can also stabilize 2-line ferrihydrite preventing its transformation to goethite or hematite (Cornell and Schwertmann, 2003). For example, naturally occurring 2-line ferrihydrite containing organic matter (carbon content of 10.23%) was boiled in an alkaline solution, conditions which strongly favor the formation of goethite (Schwertmann, 1966). However, the mineralogy of natural ferrihydrite remained the same whereas synthetic ferrihydrite fully transformed into goethite (Schwertmann, 1966). Kennedy et al. (2004) coprecipitated 2-line ferrihydrite in the presence of variable amounts of non Fe-metabolizing bacteria, *Bacillus subtilis*, and subjected the synthetic bacteria-ferrihydrite composites to aqueous heating at 80°C for 2 days. These authors found that hematite formation was progressively inhibited with increasing cell content, and concluded that inhibition occurs when 50% of the total Fe was present as 2-line ferrihydrite and the remainder is bound/complexed as ferric iron. Within the same study, Kennedy et al. (2004) subjected marine BIOS formed from the activity of microaerophilic FeOB to similar conditions and found that BIOS resisted transformation into hematite. These authors attributed the inhibition of transformation to the binding of 2-line ferrihydrite particles to microbial functional groups, which constrained particle aggregation required for hematite formation. In contrast to BIOS formed from the activity of microaerophilic FeOB, biogenic 2-line ferrihydrite precipitated by the anoxygenic photoautotroph *R. ferrooxidans* strain SW2 transformed into lepidocrocite and goethite after ageing for ~1 month (Kappler and Newman, 2004). Such transformation was attributed to the acidification of the cell local environment which could have induced transformation via acid-catalyzed dissolution (Kappler and Newman, 2004; Hegler et al., 2010). Most of the studies conducted so far to determine the mineral stability and reactivity of BIOS formed from the activity of microaerophilic FeOB have been carried out within short-time scales, therefore the long term mineral stability of BIOS is unknown.

For example, Chan et al. (2009) showed that mineral transformation into akaganeite can in fact occur in the immediate vicinity of microbial exudates in naturally occurring BIOS formed the activity of microaerophilic FeOB. Chan et al. (2009) further suggested that such transformation may not occur during short-time scales (in the order of weeks). Rather, transformation may occur during longer time scales (in the order of months). These findings highlight the need for a broader investigation of the long term mineral stability of BIOS formed from the activity of microaerophilic FeOB under controlled settings, and given the context above, such knowledge would be useful to predict the reactivity of BIOS and in turn the possible impact on contaminant mobility in the environment.

2. Dissimilatory Iron Reducing Bacteria

One of the factors that govern the impact of iron oxides on the mobility and bioavailability of associated contaminants is the exposure of iron oxides to anaerobic conditions, which favor the reductive dissolution of iron oxides that can be mediated by dissimilatory iron reducing bacteria (DIRB) or hydrogen sulfide (HS^-). Under pH-neutral and non-sulfidogenic conditions, the reductive dissolution of iron oxides is principally mediated by DIRB, such as *Geobacter* spp. and *Shewanella* spp., which couple the oxidation of organic matter or H_2 to the reduction of Fe(III) generating Fe(II), and energy required for growth and function (Lovley et al., 2004). The ability of DIRB to reduce iron oxides is dependent on the physicochemical properties of the mineral, including: surface area, aggregation state, crystallinity, morphology, and solubility of the iron phase (Roden and Zachara, 1996; Bonneville et al., 2004; Bonneville et al., 2009; Cutting et al., 2009). Typically, the rate and extent of microbial Fe(III) reduction increases with increasing surface area (Table 1), therefore 2-line ferrihydrite is considered to be the most bioavailable Fe(III)-phase whereas crystalline iron oxides, such as hematite, goethite, and magnetite, are

generally recalcitrant to microbial Fe(III) reduction (Roden and Zachara, 1996). Under pH-neutral conditions, however, DIRB face the challenge of utilizing the poorly soluble iron oxides as terminal electron acceptors, because iron oxides cannot pass the cell membrane (Lovley et al., 2004). Consequently, DIRB have developed a number of strategies to transfer electrons to iron oxides, including: (1) electron transfer via direct contact between bacteria and the mineral surface mediated by outer membrane-bound proteins (c-type cytochromes) or conductive pili-like appendages called "nanowires" (Lovley et al., 2004; Gorby et al., 2006), (2) electron transfer by endogenous compounds generated by *Shewanella* spp. such as flavins that chelate Fe(III) and function as electron shuttles (Marsili et al., 2008; Von Canstein et al., 2008), and (3) electron transfer by exogenous redox-active compounds such as quinones and dissolved or solid-phase humic substances that also function as electron shuttles (Lovley et al., 2004; Roden et al., 2010). Through these processes, DIRB mediate a number of reactions that have important consequences on the environment, in particular the reductive dissolution of iron oxides may lead to the remobilization of adsorbed contaminants, which could have detrimental impacts on human health as prominently discussed for arsenic (Cummings et al., 1999; Islam et al., 2004; Tufano et al., 2008; Borch et al., 2009; Masue-Slowey et al., 2011; Muehe et al., 2013a).

The generation of Fe(II) from microbial activity, however, can lead to the formation of secondary iron minerals that differ in redox reactivity and sorption capacity. For example, the mixed valent Fe(II)/Fe(III) iron oxides, magnetite and green-rust are common end products formed from the microbial reduction of 2-line ferrihydrite or lepidocrocite (Fredrickson et al., 1998; Ona-Nguema et al., 2002; Glasauer et al., 2003; O'Loughlin, 2008; O'Loughlin et al., 2010). Their formation stems from the instability of 2-line ferrihydrite and lepidocrocite in the presence of Fe(II), in which case Fe(II) generated by DIRB adsorbs onto the surface of the 2-line ferrihydrite

or lepidocrocite transferring an electron to the oxide thereby catalyzing their transformation into magnetite or green rust (Cornell and Schwertmann, 2003; Hansel et al., 2003; Hansel et al., 2005). Proposed mechanisms of transformation include reductive dissolution-reprecipitation mechanism or solid-state transformation mechanism (Hansel et al., 2003; Hansel et al., 2005). It is noteworthy to mention that the catalytic action of Fe(II) is significant, in which case full transformation of 2-line ferrihydrite into crystalline phases can be achieved within days in the presence of Fe(II) under anoxic conditions as opposed to years (~4) in the absence of Fe(II) at 25ºC and oxic pH-neutral conditions (Hansel et al., 2003; Schwertmann et al., 2004; Hansel et al., 2005). Goethite and lepidocrocite have also been reported to form from the microbial reduction of 2-line ferrihydrite, in which case Fe(II) mediates transformation via reductive dissolution-reprecipitation mechanism (Zachara et al., 2002; Hansel et al., 2003). Alternatively, depending on the geochemical conditions, discrete Fe(II)-bearing secondary iron minerals such as vivianite ($Fe_3(PO_4)_2 \cdot 8H_2O$) or siderite ($FeCO_3$) may form from the reduction of iron oxides (Fredrickson et al., 1998; Zachara et al., 1998; Zachara et al., 2002). The formation of secondary iron minerals have important consequences on subsurface environments, in particular goethite, magnetite, and green rust, as they are capable of transforming and/or sequestering the released contaminants adsorption and/or structural incorporation as was previously illustrated by a number of laboratory-based studies for Zn, Ni, Sr, Cd, and As (Cooper et al., 2000; Parmar et al., 2000; Parmar, 2001; Roden et al., 2002; Tufano et al., 2008; Borch et al., 2009; Muehe et al., 2013a; Muehe et al., 2013b; Muehe et al., 2013c). Therefore, given the ecological importance of DIRB, an extensive amount of research has been conducted to determine the factors that influence the rate and extent of Fe(III) reduction, as well as the secondary iron minerals that form.

Research to date indicates that in addition to the physicochemical properties of the Fe(III)-phase, concentration of DIRB (Roden and Zachara, 1996; Zegeye et al., 2007; O'Loughlin et al., 2010), geochemical conditions (e.g. pH, bicarbonate as buffer, etc.) (Fredrickson et al., 1998; Zachara et al., 2002), presence of oxyanions (e.g. PO_4^{-3}, MoO_4^{-2}, etc.) (Fredrickson et al., 1998; O'Loughlin et al., 2010), presence of electron shuttles (Fredrickson et al., 1998), presence and nature of dissolved organic carbon (O'Loughlin, 2008), and orientation of the incubation vessel (Dippon et al., 2015), affect the rate and extent of microbial Fe(III) reduction thereby influencing the flux of Fe(II), and in turn dictating the identity and properties of the mineral products (Hansel et al., 2003; Hansel et al., 2005). Thus, the formation of a specific mineral phase does not depend on the strain of DIRB but rather on the concentration and flux of Fe(II), presence of phosphate, and the prevailing geochemical conditions. For example, in the absence of phosphate, Hansel et al. (2005) showed that 2-line ferrihydrite transforms into lepidocrocite and goethite at low Fe(II) loading (<1.0 mM Fe(II)/g 2-line ferrihydrite) whereas magnetite, lepidocrocite, and goethite are the dominant products at high Fe(II) loadings (>1.0 mM Fe(II)/g 2-line ferrihydrite), the proportion of which depended on anions present in solution including Cl^-, SO_4^{-2}, and HCO_3^-.

2.1. Effects of phosphate on microbial Fe(III) reduction

The effects of the concentration of phosphate on the rate and extent of microbial Fe(III) reduction have been extensively studied, primarily as a result of its strong and common association with iron oxides in the environment, but as a limiting nutrient it is also of environmental concern where excessive fertilization of agricultural land occurs (Baken et al., 2015). Fredrickson et al. (1998) compared the rate and extent of reduction of 2-line ferrihydrite in the presence (~3.9mM) and absence of phosphate, and found that phosphate, in the presence of electron shuttles, enhanced the rate and extent of Fe(III) reduction, and promoted the formation of vivianite and green rust at

the expense of magnetite. In contrast, Borch et al. (2007) found that increasing the amount of pre-adsorbed phosphate to the surface of 2-line ferrihydrite significantly lowered the extent of Fe(III) reduction, and promoted the formation of magnetite and green-rust at the expense of goethite, while preserving a significant proportion of 2-line ferrihydrite. Amstaetter et al. (2012) reported that the addition of 0.8mM phosphate lowered the rate but not the extent of reduction of ferrrihydrite, while goethite and magnetite formed in the absence of phosphate, magnetite formed in phosphate treated experiments. In contrast, O'Loughlin et al. (2010) found that the addition of phosphate at a concentration of 0.5mM lowered the rate but enhanced the extent of lepidocrocite reduction and promoted the formation of green rust, whereas magnetite was the sole end product formed in the absence of phosphate. Kukkadapu et al. (2004) found that phosphate at a concentration of 20mM enhanced the rate and extent of reduction of synthetic Si-substituted 2-line ferrihydrite, and promoted the formation of vivianite at the expense of green rust and magnetite. Therefore, the addition of phosphate may promote microbial Fe(III) reduction by functioning as a nutrient thereby stimulating the growth and activity of DIRB (Fredrickson et al., 1998), or inhibit microbial Fe(III) reduction by blocking available sites on the mineral surface (Borch et al., 2007; O'Loughlin et al., 2010; Amstaetter et al., 2012). Nonetheless, the addition of phosphate affects the identity and proportion of secondary iron minerals. However, while these studies and several others revealed the intricate biomineralization pathways of iron oxides with varying concentrations of phosphate, these studies utilized pure synthetic iron oxides as terminal electron acceptors, which are not truly analogous to naturally occurring iron oxides, where such minerals are associated with organic and inorganic impurities.

2.2. Effects of impurities on microbial Fe(III) reduction

Impurities associated with iron oxides modify their physicochemical properties including crystallinity, morphology, aggregation state, surface area, and solubility, thereby influencing the rate and extent of microbial Fe(III) reduction and in turn dictating the identity/proportion of secondary iron minerals that form (Fredrickson et al., 2001; Cornell and Schwertmann, 2003; Jones et al., 2009; Ekstrom et al., 2010; Cismasu et al., 2011; Hansel et al., 2011; Masue-Slowey et al., 2011; Piepenbrock et al., 2011; Amstaetter et al., 2012; Henneberry et al., 2012; O'Loughlin et al., 2013; Shimizu et al., 2013). Ekstrom et al. (2010) showed that the rates and extent of Fe(III) reduction of Al-substituted 2-line ferrihydrite by DIRB decreased with increasing Al-content (0-13 mol% (Al/Al+Fe)). Hansel et al. (2011) later revealed that secondary mineralization of Al-substituted 2-line ferrihydrite by means of Fe(II)-induced reduction was progressively diminished with increasing Al-content (0-24 mol% (Al/Al+Fe)). Diminished reduction and mineralization was attributed to the decrease in solubility of Al-bearing ferrihydrite (Ekstrom et al., 2010; Hansel et al., 2011). The adsorption or incorporation of organic matter (purified standard humic substances or naturally occurring organic matter) by ferrihydrite significantly affect the rate and extent of microbial Fe(III) reduction and Fe(II)-mediated mineralization (Jones et al., 2009; Pédrot et al., 2011; Piepenbrock et al., 2011; Amstaetter et al., 2012; Henneberry et al., 2012; Shimizu et al., 2013; Chen et al., 2015). Pédrot et al. (2011) found that iron oxides coprecipitated with standard humic substances were reduced ~8x faster than pure lepidocrocite by *Shewanella putrefaciens* CIP 80.40 T. Shimizu et al. (2013) investigated the effects of varying concentrations of standard humic acid coprecipitated with 2-line ferrihydrite (C/Fe 0-4.8) on Fe(III) reduction by *Shewanella putrefaciens* CN32. Humic acids at low C/Fe ratios (C/Fe $\leq$ 1.8) were found to decrease reduction, whereas higher C/Fe ratios (C/Fe $\geq$ 1.8) were reported to enhance reduction. The varying

concentration of humic acids also influenced the proportion of the secondary iron minerals that formed, in which case the proportion of green-rust increased at the expense of magnetite and goethite with increasing C/Fe ratios. In contrast to Shimizu et al. (2013), Eusterhues et al. (2014) found that increasing the concentration of naturally occurring organic matter coprecipitated with 2-line ferrihydrite (C/Fe 0-2.83) decreased reduction by *Geobacter bremensis* and inhibited the formation of goethite. The discrepancy between the studies could be attributed to the different strain of DIRB utilized and to the different properties of organic matter used in each study. Langley et al. (2009c) investigated the reactivity of BIOS formed from the activity of microaerophilic FeOB in the presence of *Shewanella putrefaciens* CN32 and found that BIOS were reduced at a much higher rate than a synthetic analogue, 2-line ferrihydrite. The enhanced reduction was attributed to the presence of cell derived organic matter which stimulated reduction by providing additional nutrient sources for DIRB, acting as electron shuttles, or complexing released Fe(II) thereby preventing it from blocking reactive sites on the mineral fraction (Langley et al., 2009c). This suggests that any contaminants associated with BIOS could be easily remobilized into the environment as demonstrated by Langley et al. (2009d). However, while these studies assessed the reactivity of BIOS and the fate of metal contaminants associated with BIOS under reducing conditions, these studies were conducted under conditions that poorly represent the environment, i.e., high concentration of phosphate (3.9mM), conditions which likely enhance the metabolic activity of DIRB and favor the formation of vivianite (Langley et al., 2009a; Langley et al., 2009c; Langley et al., 2009d). Thus, the influence of varying concentration of phosphate on the rate and extent of reduction of BIOS, as well as the identity and properties of the mineral products that form has not been investigated. Such knowledge would be useful to predict the reactivity of BIOS and the identity of the biominerlization products that form under environmentally relevant

conditions, and in turn the possible impact on contaminant mobility in the environment. Given the context above, however, it is expected that the intermixed organic fraction to influence the identity, proportion, and properties of the mineral products that form during the reduction of BIOS, particularly in the absence or presence of low amount of phosphate.

3. Gamma (γ)-irradiation

Studies conducted to date to determine the reactivity of BIOS, in particular BIOS that formed from the activity of microaerophilic FeOB, have been carried out utilizing naturally occurring BIOS, necessitating the need to sterilize the samples in order to prevent reactions mediated by the native microbial communities during storage and experimental duration (Langley et al., 2009a; Langley et al., 2009c; Langley et al., 2009d). These studies utilized gamma(γ)-irradiation as a sterilization technique at doses ranging from 14 to 48 kGy (Langley et al., 2009a; Langley et al., 2009c; Langley et al., 2009d). Sterilization by γ-irradiation proceeds either directly or indirectly. Directly, the ionizing energy causes direct damage to cell DNA. Indirectly, sterilization proceeds by reactive radical species that form from the radiolysis of cellular H_2O (e.g. $^{\bullet}OH$, $^{\bullet}e_{aq}^-$, $^{\bullet}H$, H_2O_2, $^{\bullet}O_2^-$), which may react with proteins, nucleic acids, and lipids causing cleavage of carbon-carbon bonds leading to the depolymerization of complex organic matter ultimately leading to cell death (McNamara et al., 2003; Yakabuskie et al., 2011; Brown et al., 2015). Ideally, sterilization should eliminate all viable microbes while causing no significant changes in the physicochemical properties of the sample (McNamara et al., 2003). The efficiency of γ-irradiation as a sterilization and minimally invasive technique has been compared with a number of other sterilization techniques such as autoclaving, and the application of poisons and fumigants (e.g. sodium azide, chloroform, mercuric chloride) (McNamara et al., 2003). While some studies identify γ-irradiation as an effective and minimally invasive technique, others suggest otherwise

indicating that irradiation driven alteration of the physicochemical properties of soils/sediments may be related to the properties, mineralogy and organic matter content of the soil/sediment (McNamara et al., 2003; Schaller et al., 2011). One of the most common change observed for soils/sediments following γ-irradiation is the increase in dissolved organic carbon, likely originating from radiation induced depolymerization of complex organic matter (including microorganisms) within the sample (Salonius et al., 1967; Tuominen et al., 1994; McNamara et al., 2003; Bank et al., 2008; Berns et al., 2008; Schaller et al., 2011; Brown et al., 2015). In contrast, the effects of γ-irradiation on the physical properties of soils/sediments are variable. Wolf et al. (1989) γ-sterilized a number of different soils (dosage of 50-60 kGy) and observed no significant changes in their surface area. Similarly, Herbert et al. (2005) found no significant changes in the mineralogy and surface area of mine tailings following irradiation to a final dose of 10 or 25kGy. In contrast, Lotrario et al. (1995) observed a 16% decline in soil surface area following γ-irradiation (10 kGy). More recently, Schaller et al. (2011) found that γ-irradiation (4x 15kGy) of sediments with high organic carbon content (9.5%) led to a significantly higher remobilization of arsenic and uranium into solution when compared to non-sterilized sediments. Bank et al. (2008) found that γ-irradiated sediments (final dose of 20kGy) adsorbed a significantly higher amount of U(VI) than non-sterilized sediments which was attributed to irradiation induced alteration of the cation exchange capacity of the sediment and the partial reduction of goethite to Fe(II). Berns et al. (2008) found that γ-irradiation (36 kGy) altered the aggregation state of soil and in turn increased the surface area. In contrast, the exposure of various clay minerals to a high dosage of γ-irradiation (1.1 MGy) slightly altered the surface area of select minerals, whereas in other minerals (e.g. smectite) irradiation induced reduction of Fe(III) to Fe(II) leading to an overall decline in cation exchange capacity (Plötze et al., 2003). On the other hand, the exposure of

synthetic 2-line ferrihydrite and hematite to a similar dose (1 MGy) was found to alter their crystalline structure, and enhance their bioavailability to microbial Fe(III) reduction by *Shewanella oneidensis* MR-1 in the presence of an electron shuttle (Brown et al., 2014). Even at lower doses (0.6 and 38.6 kGy), however, γ-irradiation may have enhanced the bioavailability of Fe(III) in sediments to microbial reduction by *Geobacter sulfurreducens* (Brown et al., 2015). Thus, radiation driven alteration of the physicochemical properties and oxidation state of iron may lead to an over-or under-estimation of their reactivity and may in turn influence the secondary iron products that form during microbial Fe(III) reduction. The effects of γ-irradiation on the physicochemical properties and reactivity of BIOS have not been investigated. If γ-irradiation does indeed alter the reactivity of BIOS, rates of reduction of γ-irradiated BIOS from past studies may not reflect the true reactivity of BIOS. Therefore, research into the effects of γ-irradiation on BIOS is required.

4. Objectives and Hypotheses

The objectives of this thesis are:

1. To investigate the effects of long term ageing on the mineralogical composition and reactivity of sterile BIOS formed from the activity of microaerophilic FeOB that have been preserved at 4°C for several years (~5) in order to simulate early diagenesis. The reactivity of aged BIOS was assessed in the presence of a model DIRB, *Shewanella putrefaciens* CN32. In order to determine any changes in the mineralogical composition, as well as the susceptibility of aged BIOS towards microbial reduction, the results were compared with previously published data which correspond to "fresh" BIOS (Langley et al., 2009a; Gault et al., 2011). Based on the study of Kennedy et al. (2004), it is hypothesized that the mineralogy of the aged BIOS will be the same as the fresh BIOS. It is also expected the rates of reduction, and thus the reactivity, of aged BIOS will be very similar to those measured for fresh BIOS since the mineralogy is not expected to change.
2. To investigate the effects of phosphate at high (3.9 mM) and environmentally relevant (10 μM) concentrations on the rate and extent of reduction of BIOS formed from the activity of microaerophilic FeOB and synthetic 2-line ferrihydrite, in the presence of *Shewanella putrefaciens* CN32. To determine the effects of varying concentrations of phosphate on the secondary iron minerals that form. It is hypothesized that the concentration of phosphate will have a significant effect on the rate and extent of reduction of BIOS and 2-line ferrihydrite. It is expected that the concentration of phosphate and the presence of cell derived organic matter to influence the identity of the secondary iron minerals that form.
3. To investigate the impact of γ-irradiation on the susceptibility of BIOS formed from the activity of microaerophilic FeOB to microbial reduction. Based on the current literature, it

is hypothesized that γ-irradiation will enhance the susceptibility of BIOS towards microbial reduction.

References

Amstaetter, K., Borch, T., Kappler, A., 2012. Influence of humic acid imposed changes of ferrihydrite aggregation on microbial Fe(III) reduction. Geochim. Cosmochim. Acta, 85, 326-341.

Baken, S., Verbeeck, M., Verheyen, D., Diels, J., Smolders, E., 2015. Phosphorus losses from agricultural land to natural waters are reduced by immobilization in iron-rich sediments of drainage ditches. Water research, 71, 160-170.

Banfield, J.F., Welch, S.A., Zhang, H., Ebert, T.T., Penn, R.L., 2000. Aggregation-Based Crystal Growth and Microstructure Development in Natural Iron Oxyhydroxide Biomineralization Products. Science, 289, 751-754.

Bank, T.L., Kukkadapu, R.K., Madden, A.S., Ginder-Vogel, M., Baldwin, M., Jardine, P., 2008. Effects of gamma-sterilization on the physico-chemical properties of natural sediments. Chem. Geol., 251, 1-7.

Berns, A., Philipp, H., Narres, H.D., Burauel, P., Vereecken, H., Tappe, W., 2008. Effect of gamma-sterilization and autoclaving on soil organic matter structure as studied by solid state NMR, UV and fluorescence spectroscopy. European Journal of Soil Science, 59, 540-550.

Blöthe, M., Roden, E.E., 2009. Microbial Iron Redox Cycling in a Circumneutral-pH Groundwater Seep. Appl. Environ. Microbiol., 75, 468-473.

Bonneville, S., Behrends, T., Van Cappellen, P., 2009. Solubility and dissimilatory reduction kinetics of iron(III) oxyhydroxides: A linear free energy relationship. Geochim. Cosmochim. Acta, 73, 5273-5282.

Bonneville, S., Van Cappellen, P., Behrends, T., 2004. Microbial reduction of iron(III) oxyhydroxides: effects of mineral solubility and availability. Chem. Geol., 212, 255-268.

Borch, T., Kretzschmar, R., Kappler, A., Cappellen, P.V., Ginder-Vogel, M., Voegelin, A., Campbell, K., 2009. Biogeochemical Redox Processes and their Impact on Contaminant Dynamics. Environ. Sci. Technol., 44, 15-23.

Borch, T., Masue, Y., Kukkadapu, R.K., Fendorf, S., 2007. Phosphate imposed limitations on biological reduction and alteration of ferrihydrite. Environ. Sci. Technol., 41, 166-172.

Brown, A.R., Boothman, C., Pimblott, S.M., Lloyd, J.R., 2015. The impact of gamma radiation on sediment microbial processes. Appl. Environ. Microbiol., 81, 4014-4025.

Brown, A.R., Wincott, P.L., LaVerne, J.A., Small, J.S., Vaughan, D.J., Pimblott, S.M., Lloyd, J.R., 2014. The impact of γ radiation on the bioavailability of Fe (III) minerals for microbial respiration. Environ. Sci. Technol., 48, 10672-10680.

Chan, C.S., De Stasio, G., Welch, S.A., Girasole, M., Frazer, B.H., Nesterova, M.V., Fakra, S., Banfield, J.F., 2004. Microbial polysaccharides template assembly of nanocrystal fibers. Science, 303, 1656-8.

Chan, C.S., Fakra, S.C., Edwards, D.C., Emerson, D., Banfield, J.F., 2009. Iron oxyhydroxide mineralization on microbial extracellular polysaccharides. Geochim. Cosmochim. Acta, 73, 3807-3818.

Chan, C.S., Fakra, S.C., Emerson, D., Fleming, E.J., Edwards, K.J., 2011. Lithotrophic iron-oxidizing bacteria produce organic stalks to control mineral growth: implications for biosignature formation. ISME J, 5, 717-27.

Châtellier, X., Fortin, D., West, M.M., Leppard, G.G., Ferris, F.G., 2001. Effect of the presence of microbial surfaces during the synthesis of Fe oxides by oxidation of ferrous ions. European Journal of Mineralogy, 13, 705-714.

Châtellier, X., West, M.M., Rose, J., Fortin, D., Leppard, G.G., Ferris, F.G., 2004. Characterization of Iron-Oxides Formed by Oxidation of Ferrous Ions in the Presence of Various Microbial Species and Inorganic Ligands. Geomicrobiology Journal, 21, 99-112.

Chen, C., Kukkadapu, R., Sparks, D.L., 2015. Influence of coprecipitated organic matter on fe2+(aq)-catalyzed transformation of ferrihydrite: Implications for carbon dynamics. Environ. Sci. Technol., 49, 10927-10936.

Cismasu, A.C., Michel, F.M., Tcaciuc, A.P., Tyliszczak, T., Brown, J.G.E., 2011. Composition and structural aspects of naturally occurring ferrihydrite. Comptes Rendus Geoscience, 343, 210-218.

Cismasu, A.C., Williams, K.H., Nico, P.S., 2016. Iron and Carbon Dynamics during Aging and Reductive Transformation of Biogenic Ferrihydrite. Environ. Sci. Technol., 50, 25-35.

Cooper, D.C., Picardal, F., Rivera, J., Talbot, C., 2000. Zinc Immobilization and Magnetite Formation via Ferric Oxide Reduction by Shewanella putrefaciens 200. Environ. Sci. Technol., 34, 100-106.

Cornell, R., 1988. The influence of some divalent cations on the transformation of ferrihydrite to more crystalline products. Clay Minerals, 23, 329-332.

Cornell, R., Giovanoli, R., Schindler, P., 1987. Effect of silicate species on the transformation of ferrihydrite into goethite and hematite in alkaline media. Clays and Clay Minerals, 35, 21-28.

Cornell, R.M., Schwertmann, U., 2003. The iron oxides: structure, properties, reactions, occurrences and uses. John Wiley & Sons.

Cummings, D.E., Caccavo, F., Fendorf, S., Rosenzweig, R.F., 1999. Arsenic mobilization by the dissimilatory Fe (III)-reducing bacterium Shewanella alga BrY. Environ. Sci. Technol., 33, 723-729.

Cutting, R.S., Coker, V.S., Fellowes, J.W., Lloyd, J.R., Vaughan, D.J., 2009. Mineralogical and morphological constraints on the reduction of Fe(III) minerals by Geobacter sulfurreducens. Geochim. Cosmochim. Acta, 73, 4004-4022.

Das, S., Essilfie-Dughan, J., Hendry, M.J., 2015. Fate of adsorbed arsenate during phase transformation of ferrihydrite in the presence of gypsum and alkaline conditions. Chem. Geol., 411, 69-80.

Dippon, U., Schmidt, C., Behrens, S., Kappler, A., 2015. Secondary Mineral Formation During Ferrihydrite Reduction by Shewanella oneidensis MR-1 Depends on Incubation Vessel Orientation and Resulting Gradients of Cells, Fe2+ and Fe Minerals. Geomicrobiology Journal, 32, 878-889.

Eickhoff, M., Obst, M., Schröder, C., Hitchcock, A.P., Tyliszczak, T., Martinez, R.E., Robbins, L.J., Konhauser, K.O., Kappler, A., 2014. Nickel partitioning in biogenic and abiogenic ferrihydrite: The influence of silica and implications for ancient environments. Geochim. Cosmochim. Acta, 140, 65-79.

Ekstrom, E.B., Learman, D.R., Madden, A.S., Hansel, C.M., 2010. Contrasting effects of Al substitution on microbial reduction of Fe(III) (hydr)oxides. Geochim. Cosmochim. Acta, 74, 7086-7099.

Emerson, D., Weiss, J.V., Megonigal, J.P., 1999. Iron-Oxidizing Bacteria Are Associated with Ferric Hydroxide Precipitates (Fe-Plaque) on the Roots of Wetland Plants. Appl. Environ. Microbiol., 65, 2758-2761.

Eusterhues, K., Hädrich, A., Neidhardt, J., Küsel, K., Keller, T., Jandt, K., Totsche, K., 2014. Reduction of ferrihydrite with adsorbed and coprecipitated organic matter: microbial reduction by Geobacter bremensis vs. abiotic reduction by Na-dithionite. Biogeosciences, 11, 4953-4966.

Fabisch, M., Freyer, G., Johnson, C., Büchel, G., Akob, D., Neu, T., Küsel, K., 2016. Dominance of 'Gallionella capsiferriformans' and heavy metal association with Gallionella-like stalks in metal-rich pH 6 mine water discharge. Geobiology, 14, 68-90.

Ferris, F., Konhauser, K., Lyven, B., Pedersen, K., 1999. Accumulation of metals by bacteriogenic iron oxides in a subterranean environment. Geomicrobiology Journal, 16, 181-192.

Ferris, F.G., Hallberg, R., Lyven, B., Pedersen, K., 2000. Retention of strontium, cesium, lead and uranium by microbial iron oxides from a subterranean environment. Applied Geochemistry, 15, 1035-1042.

Ford, R.G., Bertsch, P.M., Farley, K.J., 1997. Changes in Transition and Heavy Metal Partitioning during Hydrous Iron Oxide Aging. Environ. Sci. Technol., 31, 2028-2033.

Fortin, D., Langley, S., 2005. Formation and occurrence of biogenic iron-rich minerals. Earth-Science Reviews, 72, 1-19.

Fortin, D., Leppard, G.G., Tessier, A., 1993. Characteristics of lacustrine diagenetic iron oxyhydroxides. Geochim. Cosmochim. Acta, 57, 4391-4404.

Fredrickson, J.K., Zachara, J.M., Kennedy, D.W., Dong, H., Onstott, T.C., Hinman, N.W., Li, S.-m., 1998. Biogenic iron mineralization accompanying the dissimilatory reduction of hydrous ferric oxide by a groundwater bacterium. Geochim. Cosmochim. Acta, 62, 3239-3257.

Fredrickson, J.K., Zachara, J.M., Kukkadapu, R.K., Gorby, Y.A., Smith, S.C., Brown, C.F., 2001. Biotransformation of Ni-substituted hydrous ferric oxide by an Fe(III)-reducing bacterium. Environ. Sci. Technol., 35, 703-712.

Galvez, N., Barron, V., Torrent, J., 1999. Effect of phosphate on the crystallization of hematite, goethite, and lepidocrocite from ferrihydrite. Clays and Clay Minerals, 47, 304-311.

Gauger, T., Konhauser, K., Kappler, A., 2015. Protection of phototrophic iron (II)-oxidizing bacteria from UV irradiation by biogenic iron (III) minerals: Implications for early Archean banded iron formation. Geology, 43, 1067-1070.

Gault, A.G., Ibrahim, A., Langley, S., Renaud, R., Takahashi, Y., Boothman, C., Lloyd, J.R., Clark, I.D., Ferris, F.G., Fortin, D., 2011. Microbial and geochemical features suggest iron redox cycling within bacteriogenic iron oxide-rich sediments. Chem. Geol., 281, 41-51.

Glasauer, S., Weidler, P.G., Langley, S., Beveridge, T.J., 2003. Controls on Fe reduction and mineral formation by a subsurface bacterium. Geochim. Cosmochim. Acta, 67, 1277-1288.

Gorby, Y.A., Yanina, S., McLean, J.S., Rosso, K.M., Moyles, D., Dohnalkova, A., Beveridge, T.J., Chang, I.S., Kim, B.H., Kim, K.S., 2006. Electrically conductive microbial nanowires produced by Shewanella oneidensis strain MR-1 and other microorganisms. Proceedings of the National Academy of Sciences, 103, 11358-11363.

Hallberg, R., Ferris, F.G., 2004. Biomineralization by Gallionella. Geomicrobiology Journal, 21, 325-330.

Hansel, C.M., Benner, S.G., Fendorf, S., 2005. Competing Fe(II)-Induced Mineralization Pathways of Ferrihydrite. Environ. Sci. Technol., 39, 7147-7153.

Hansel, C.M., Benner, S.G., Neiss, J., Dohnalkova, A., Kukkadapu, R.K., Fendorf, S., 2003. Secondary mineralization pathways induced by dissimilatory iron reduction of ferrihydrite under advective flow. Geochim. Cosmochim. Acta, 67, 2977-2992.

Hansel, C.M., Learman, D.R., Lentini, C.J., Ekstrom, E.B., 2011. Effect of adsorbed and substituted Al on Fe(II)-induced mineralization pathways of ferrihydrite. Geochim. Cosmochim. Acta, 75, 4653-4666.

Hao, L., Guo, Y., Byrne, J.M., Zeitvogel, F., Schmid, G., Ingino, P., Li, J., Neu, T.R., Swanner, E.D., Kappler, A., 2016. Binding of heavy metal ions in aggregates of microbial cells, EPS and biogenic iron minerals measured in-situ using metal-and glycoconjugates-specific fluorophores. Geochim. Cosmochim. Acta, 180, 66-96.

Hedrich, S., Schlomann, M., Johnson, D.B., 2011. The iron-oxidizing proteobacteria. Microbiology, 157, 1551-64.

Hegler, F., Schmidt, C., Schwarz, H., Kappler, A., 2010. Does a low-pH microenvironment around phototrophic FeII-oxidizing bacteria prevent cell encrustation by FeIII minerals? FEMS Microbiol. Ecol., 74, 592-600.

Henneberry, Y.K., Kraus, T.E.C., Nico, P.S., Horwath, W.R., 2012. Structural stability of coprecipitated natural organic matter and ferric iron under reducing conditions. Organic Geochemistry, 48, 81-89.

Herbert, R.B., Malmström, M., Ebenå, G., Salmon, U., Ferrow, E., Fuchs, M., 2005. Quantification of abiotic reaction rates in mine tailings: Evaluation of treatment methods for eliminating iron-and sulfur-oxidizing bacteria. Environ. Sci. Technol., 39, 770-777.

Hohmann, C., Morin, G., Ona-Nguema, G., Guigner, J.-M., Brown, G.E., Kappler, A., 2011. Molecular-level modes of As binding to Fe (III)(oxyhydr) oxides precipitated by the anaerobic nitrate-reducing Fe (II)-oxidizing Acidovorax sp. strain BoFeN1. Geochim. Cosmochim. Acta, 75, 4699-4712.

Islam, F.S., Gault, A.G., Boothman, C., Polya, D.A., Charnock, J.M., Chatterjee, D., Lloyd, J.R., 2004. Role of metal-reducing bacteria in arsenic release from Bengal delta sediments. Nature, 430, 68-71.

James, R.E., Ferris, F.G., 2004. Evidence for microbial-mediated iron oxidation at a neutrophilic groundwater spring. Chem. Geol., 212, 301-311.

Jones, A.M., Collins, R.N., Rose, J., Waite, T.D., 2009. The effect of silica and natural organic matter on the Fe(II)-catalysed transformation and reactivity of Fe(III) minerals. Geochim. Cosmochim. Acta, 73, 4409-4422.

Kappler, A., Newman, D.K., 2004. Formation of Fe(III)-minerals by Fe(II)-oxidizing photoautotrophic bacteria 1. Geochim. Cosmochim. Acta, 68, 1217-1226.

Kappler, A., Straub, K.L., 2005. Geomicrobiological Cycling of Iron. Reviews in Mineralogy and Geochemistry, 59, 85-108.

Keim, C.N., 2011. Arsenic in biogenic iron minerals from a contaminated environment. Geomicrobiology Journal, 28, 242-251.

Kennedy, C., Martinez, R., Scott, S.D., Ferris, F., 2003. Surface chemistry and reactivity of bacteriogenic iron oxides from Axial Volcano, Juan de Fuca Ridge, north-east Pacific Ocean. Geobiology, 1, 59-69.

Kennedy, C.B., Scott, S.D., Ferris, F.G., 2004. Hydrothermal phase stabilization of 2-line ferrihydrite by bacteria. Chem. Geol., 212, 269-277.

Kleinert, S., Muehe, E.M., Posth, N.R., Dippon, U., Daus, B., Kappler, A., 2011. Biogenic Fe (III) minerals lower the efficiency of iron-mineral-based commercial filter systems for arsenic removal. Environ. Sci. Technol., 45, 7533-7541.

Konhauser, K.O., 1997. Microbial iron biomineralisation in nature. FEMS Microbiol. Rev., 20, 315-326.

Kukkadapu, R.K., Zachara, J.M., Fredrickson, J.K., Kennedy, D.W., 2004. Biotransformation of two-line silica-ferrihydrite by a dissimilatory fe (iii)-reducing bacterium: Formation of carbonate green rust in the presence of phosphate. Geochim. Cosmochim. Acta, 68, 2799-2814.

Langley, S., Igric, P., Takahashi, Y., Sakai, Y., Fortin, D., Hannington, M.D., Schwarz-Schampera, U., 2009a. Preliminary characterization and biological reduction of putative biogenic iron oxides (BIOS) from the Tonga-Kermadec Arc, southwest Pacific Ocean. Geobiology, 7, 35-49.

Langley, S., Gault, A.G., Ibrahim, A., Takahashi, Y., Renaud, R., Fortin, D., Clark, I.D., Ferris, F.G., 2009b. Sorption of Strontium onto Bacteriogenic Iron Oxides. Environ. Sci. Technol., 43, 1008-1014.

Langley, S., Gault, A., Ibrahim, A., Renaud, R., Fortin, D., Clark, I.D., Ferris, F.G., 2009c. A Comparison of the Rates of Fe(III) Reduction in Synthetic and Bacteriogenic Iron Oxides by Shewanella putrefaciens CN32. Geomicrobiology Journal, 26, 57-70.

Langley, S., Gault, A.G., Ibrahim, A., Takahashi, Y., Renaud, R., Fortin, D., Clark, I.D., Ferris, F.G., 2009d. Strontium desorption from bacteriogenic iron oxides (BIOS) subjected to microbial Fe(III) reduction. Chem. Geol., 262, 217-228.

Lotrario, J., Stuart, B., Lam, T., Arands, R., O'Connor, O., Kosson, D., 1995. Effects of sterilization methods on the physical characteristics of soil: implications for sorption isotherm analyses. Bull. Environ. Contam. Toxicol., 54, 668-675.

Lovley, D.R., Holmes, D.E., Nevin, K.P., 2004. Dissimilatory Fe(III) and Mn(IV) Reduction, Adv. Microb. Physiol. Academic Press, pp. 219-286.

Marsili, E., Baron, D.B., Shikhare, I.D., Coursolle, D., Gralnick, J.A., Bond, D.R., 2008. Shewanella secretes flavins that mediate extracellular electron transfer. Proceedings of the National Academy of Sciences, 105, 3968-3973.

Martinez, R.E., Smith, D.S., Pedersen, K., Ferris, F.G., 2003. Surface chemical heterogeneity of bacteriogenic iron oxides from a subterranean environment. Environ. Sci. Technol., 37, 5671-7.

Masue-Slowey, Y., Loeppert, R.H., Fendorf, S., 2011. Alteration of ferrihydrite reductive dissolution and transformation by adsorbed As and structural Al: Implications for As retention. Geochim. Cosmochim. Acta, 75, 870-886.

McNamara, N.P., Black, H.I.J., Beresford, N.A., Parekh, N.R., 2003. Effects of acute gamma irradiation on chemical, physical and biological properties of soils. Applied Soil Ecology, 24, 117-132.

Melton, E.D., Swanner, E.D., Behrens, S., Schmidt, C., Kappler, A., 2014. The interplay of microbially mediated and abiotic reactions in the biogeochemical Fe cycle. Nat Rev Micro, 12, 797-808.

Muehe, E.M., Scheer, L., Daus, B., Kappler, A., 2013a. Fate of Arsenic during Microbial Reduction of Biogenic versus Abiogenic As–Fe(III)–Mineral Coprecipitates. Environ. Sci. Technol., 47, 8297-8307.

Muehe, E.M., Adaktylou, I.J., Obst, M., Zeitvogel, F., Behrens, S., Planer-Friedrich, B., Kraemer, U., Kappler, A., 2013b. Organic carbon and reducing conditions lead to cadmium immobilization by secondary Fe mineral formation in a pH-neutral soil. Environ. Sci. Technol., 47, 13430-13439.

Muehe, E.M., Obst, M., Hitchcock, A., Tyliszczak, T., Behrens, S., Schröder, C., Byrne, J.M., Michel, F.M., Krämer, U., Kappler, A., 2013c. Fate of Cd during microbial Fe (III) mineral reduction by a novel and Cd-tolerant Geobacter species. Environ. Sci. Technol., 47, 14099-14109.

Nielsen, S.S., Kjeldsen, P., Hansen, H.C.B., Jakobsen, R., 2014. Transformation of natural ferrihydrite aged in situ in As, Cr and Cu contaminated soil studied by reduction kinetics. Applied Geochemistry, 51, 293-302.

O'Loughlin, E.J., 2008. Effects of electron transfer mediators on the bioreduction of lepidocrocite (γ-FeOOH) by Shewanella putrefaciens CN32. Environ. Sci. Technol., 42, 6876-6882.

O'Loughlin, E.J., Gorski, C.A., Scherer, M.M., Boyanov, M.I., Kemner, K.M., 2010. Effects of Oxyanions, Natural Organic Matter, and Microbial Cell Numbers on the Bioreduction of Lepidocrocite (γ-FeOOH) and the Formation of Secondary Mineralization Products. Environ. Sci. Technol., 44, 4570-4576.

O'Loughlin, E.J., Boyanov, M.I., Flynn, T.M., Gorski, C.A., Hofmann, S.M., McCormick, M.L., Scherer, M.M., Kemner, K.M., 2013. Effects of bound phosphate on the bioreduction of lepidocrocite (γ-feooh) and maghemite (γ-Fe_2O_3) and formation of secondary minerals. Environ. Sci. Technol., 47, 9157-9166.

Ona-Nguema, G., Abdelmoula, M., Jorand, F., Benali, O., Gehin, A., Block, J.-C., Génin, J.-M.R., 2002. Iron (II, III) hydroxycarbonate green rust formation and stabilization from lepidocrocite bioreduction. Environ. Sci. Technol., 36, 16-20.

Parmar, N., Warren, L.A., Roden, E.E., Ferris, F.G., 2000. Solid phase capture of strontium by the iron reducing bacteria Shewanella alga strain BrY. Chem. Geol., 169, 281-288.

Parmar, Y.G., TJ Beveridge, FG Ferris, N, 2001. Formation of green rust and immobilization of nickel in response to microbial reduction of hydrous ferric oxide. Geomicrobiology Journal, 18, 375-385.

Pédrot, M., Le Boudec, A., Davranche, M., Dia, A., Henin, O., 2011. How does organic matter constrain the nature, size and availability of Fe nanoparticles for biological reduction? J. Colloid Interface Sci., 359, 75-85.

Piepenbrock, A., Dippon, U., Porsch, K., Appel, E., Kappler, A., 2011. Dependence of microbial magnetite formation on humic substance and ferrihydrite concentrations. Geochim. Cosmochim. Acta, 75, 6844-6858.

Plötze, M., Kahr, G., Stengele, R.H., 2003. Alteration of clay minerals—gamma-irradiation effects on physicochemical properties. Applied Clay Science, 23, 195-202.

Posth, N.R., Canfield, D.E., Kappler, A., 2014. Biogenic Fe(III) minerals: From formation to diagenesis and preservation in the rock record. Earth-Science Reviews, 135, 103-121.

Rancourt, D.G., Thibault, P.-J., Mavrocordatos, D., Lamarche, G., 2005. Hydrous ferric oxide precipitation in the presence of nonmetabolizing bacteria: Constraints on the mechanism of a biotic effect. Geochim. Cosmochim. Acta, 69, 553-577.

Roden, E.E., Kappler, A., Bauer, I., Jiang, J., Paul, A., Stoesser, R., Konishi, H., Xu, H., 2010. Extracellular electron transfer through microbial reduction of solid-phase humic substances. Nature geoscience, 3, 417-421.

Roden, E.E., Leonardo, M.R., Ferris, F.G., 2002. Immobilization of strontium during iron biomineralization coupled to dissimilatory hydrous ferric oxide reduction. Geochim. Cosmochim. Acta, 66, 2823-2839.

Roden, E.E., Zachara, J.M., 1996. Microbial Reduction of Crystalline Iron(III) Oxides: Influence of Oxide Surface Area and Potential for Cell Growth. Environ. Sci. Technol., 30, 1618-1628.

Saini, G., Chan, C., 2013. Near-neutral surface charge and hydrophilicity prevent mineral encrustation of Fe-oxidizing micro-organisms. Geobiology, 11, 191-200.

Salonius, P.O., Robinson, J.B., Chase, F.E., 1967. A comparison of autoclaved and gamma-irradiated soils as media for microbial colonization experiments. Plant and Soil, 27, 239-248.

Schädler, S., Burkhardt, C., Hegler, F., Straub, K., Miot, J., Benzerara, K., Kappler, A., 2009. Formation of cell-iron-mineral aggregates by phototrophic and nitrate-reducing anaerobic Fe (II)-oxidizing bacteria. Geomicrobiology Journal, 26, 93-103.

Schaller, J., Weiske, A., Dudel, E.G., 2011. Effects of gamma-sterilization on DOC, uranium and arsenic remobilization from organic and microbial rich stream sediments. Sci. Total Environ., 409, 3211-3214.

Schwertmann, U., 1966. Inhibitory Effect of Soil Organic Matter on the Crystallization of Amorphous Ferric Hydroxide. Nature, 212, 645-646.

Schwertmann, U., Friedl, J., Stanjek, H., Schulze, D., 2000. The effect of clay minerals on the formation of goethite and hematite from ferrihydrite after 16 years' ageing at 25 C and pH 4–7. Clay Minerals, 35, 613-623.

Schwertmann, U., Stanjek, H., Becher, H.-H., 2004. Long-term in vitro transformation of 2-line ferrihydrite to goethite/hematite at 4, 10, 15 and 25 C. Clay Minerals, 39, 433-438.

Shimizu, M., Zhou, J., Schröder, C., Obst, M., Kappler, A., Borch, T., 2013. Dissimilatory Reduction and Transformation of Ferrihydrite-Humic Acid Coprecipitates. Environ. Sci. Technol., 47, 13375-13384.

Stumm, W., Morgan, J.J., 2012. Aquatic chemistry: chemical equilibria and rates in natural waters, 126. John Wiley & Sons.

Tessier, A., Fortin, D., Belzile, N., DeVitre, R.R., Leppard, G.G., 1996. Metal sorption to diagenetic iron and manganese oxyhydroxides and associated organic matter: Narrowing the gap between field and laboratory measurements. Geochim. Cosmochim. Acta, 60, 387-404.

Toner, B.M., Berquó, T.S., Michel, F.M., Sorensen, J.V., Templeton, A.S., Edwards, K.J., 2012. Mineralogy of iron microbial mats from Loihi Seamount. Frontiers in Microbiology, 3.

Toner, B.M., Santelli, C.M., Marcus, M.A., Wirth, R., Chan, C.S., McCollom, T., Bach, W., Edwards, K.J., 2009. Biogenic iron oxyhydroxide formation at mid-ocean ridge hydrothermal vents: Juan de Fuca Ridge. Geochim. Cosmochim. Acta, 73, 388-403.

Tufano, K.J., Reyes, C., Saltikov, C.W., Fendorf, S., 2008. Reductive processes controlling arsenic retention: revealing the relative importance of iron and arsenic reduction. Environ. Sci. Technol., 42, 8283-8289.

Tuominen, L., Kairesalo, T., Hartikainen, H., 1994. Comparison of methods for inhibiting microbial activity in sediment. Appl. Environ. Microbiol., 60, 3454-3457.

Von Canstein, H., Ogawa, J., Shimizu, S., Lloyd, J.R., 2008. Secretion of flavins by Shewanella species and their role in extracellular electron transfer. Appl. Environ. Microbiol., 74, 615-623.

Vu, H.P., Moreau, J.W., 2015. Thiocyanate adsorption on ferrihydrite and its fate during ferrihydrite transformation to hematite and goethite. Chemosphere, 119, 987-993.
Warren, L.A., Ferris, F.G., 1998. Continuum between sorption and precipitation of Fe (III) on microbial surfaces. Environ. Sci. Technol., 32, 2331-2337.
Wolf, D., Dao, T., Scott, H., Lavy, T., 1989. Influence of sterilization methods on selected soil microbiological, physical, and chemical properties. J. Environ. Qual., 18, 39-44.
Yakabuskie, P., Joseph, J., Keech, P., Botton, G., Guzonas, D., Wren, J., 2011. Iron oxyhydroxide colloid formation by gamma-radiolysis. Phys. Chem. Chem. Phys., 13, 7198-7206.
Zachara, J.M., Fredrickson, J.K., Li, S.-M., Kennedy, D.W., Smith, S.C., Gassman, P.L., 1998. Microbial reduction of crystalline Fe3+ oxides in single phase suspensions and subsurface materials. American Mineralogist, 83, 1426-1443.
Zachara, J.M., Kukkadapu, R.K., Fredrickson, J.K., Gorby, Y.A., Smith, S.C., 2002. Biomineralization of poorly crystalline Fe (III) oxides by dissimilatory metal reducing bacteria (DMRB). Geomicrobiology Journal, 19, 179-207.
Zegeye, A., Ruby, C., Jorand, F., 2007. Kinetic and thermodynamic analysis during dissimilatory γ-FeOOH reduction: formation of green rust 1 and magnetite. Geomicrobiology Journal, 24, 51-64.

Chapter 2: A comparison of Fe(III) reduction rates between fresh and aged biogenic iron oxides (BIOS) by *Shewanella putrefaciens* CN32

Tarek Najem[a], Sean Langley[b], Danielle Fortin[a*]

[a] Department of Earth and Environmental Sciences, University of Ottawa, 25 Templeton St., Ottawa, Ontario, Canada K1N 6N5
[b] Natural Resources Canada, Canmet MINING, 555 Booth Street, Ottawa, Ontario, Canada, K1A 0G1

[*] Corresponding author: dfortin@uottawa.ca

Manuscript published in *Chemical Geology*[1]

[1]Najem, T., Langley, S., Fortin, D., 2016. A comparison of Fe(III) reduction rates between fresh and aged biogenic iron oxides (BIOS) by *Shewanella putrefaciens* CN32. Chem. Geol., 439, 1-12.

Abstract

This study compared the chemical and physical properties of freshwater biogenic iron oxides (BIOS) aged at 4°C for ~5 years in the dark to simulate early diagenesis to previously published findings from fresh samples. In addition, the reactivity of aged BIOS in the presence of a well-characterized iron reducing bacterium, *Shewanella putrefaciens* CN32, was investigated. The composition and proportion of the iron minerals were examined using XRD, Fe k-edge EXAFS, and chemical extractions, and results were similar in both fresh and aged BIOS. Aged BIOS were dominated by 2-line ferrihydrite indicating that the intermixed microbial cells and their exudates inhibited the transformation of 2-line ferrihydrite into crystalline phases. However, despite the similarity of mineralogy between aged and fresh BIOS, the rates of microbial iron reduction in aged BIOS were found to be significantly lower than that of their fresh counterparts. Further characterization of aged BIOS by TEM revealed unique morphologies which were not previously observed in fresh BIOS. TEM also showed thickly coated microbial exudates and presumably those formed as a result of continued accretion or aggregation of iron oxide nanoparticles. Aggregation of the iron oxide particles and subsequent decrease in solubility are likely responsible for the low rates of microbial iron reduction in aged BIOS. Phase stability and aggregation in BIOS have important implications for the long-term reactivity of BIOS and the preservation of organic matter in the environment.

Keywords: BIOS, Ferrihydrite, Ageing, Aggregation, Iron reduction, *Shewanella putrefaciens*

1. Introduction

Iron oxides (collectively referring to iron oxyhydroxides, iron hydroxides, and iron oxides) are ubiquitous in a diverse range of surface and subsurface environments, and they occur as a spectrum of phases, ranging from well-defined crystalline mineral phases, such as goethite (α-FeOOH) and lepidocrocite (γ-FeOOH), to poorly-ordered mineral phases, such as 2-line ferrihydrite (approx. $Fe(OH)_3$) (Cornell and Schwertmann, 2003). Iron oxides are well recognized for their ability to exert a major control on the mobility and fate of nutrients and (in)organic contaminants in the environment. In particular, ferrihydrite is considered to be one of the most effective sorbent of contaminants, primarily as a result of its high surface area and reactivity (Tessier et al., 1996; Roden and Zachara, 1996; Cornell and Schwertmann, 2003). Ferrihydrite is often one of the first solid phases that precipitate following the hydrolysis of Fe(III), formed from the abiotic and/or biotic oxidation of Fe(II), however it is thermodynamically unstable with respect to crystalline iron oxides (Cornell and Schwertmann, 2003). With time and depending on the prevalent conditions (e.g. pH, temperature) ferrihydrite transforms into goethite and/or hematite which are the most stable end members in the environment (Cornell and Schwertmann, 2003). Such transformation has important ecological and environmental implications, as the varying properties of the iron phases influence their biogeochemical reactivity and in turn the mobility and fate of nutrients and contaminants that are associated with the iron phase. For example, recrystallization of ferrihydrite may result in less reactive site density with consequent release of contaminants (Ford et al., 1997; Cornell and Schwertmann, 2003; Vu and Moreau, 2015), but also the possible structural incorporation of associated contaminants into crystalline phases leading to stronger contaminant-iron oxide association (Ford et al., 1997; Cornell and Schwertmann, 2003; Nielsen et al., 2014). Furthermore, in anoxic environments iron oxides serve as terminal electron

acceptors for iron-reducing bacteria (FeRB), with ferrihydrite being the most bioavailable iron phase (Roden and Zachara, 1996; Urrutia et al., 1998; Roden et al., 2000; Hansel et al., 2003; Hansel et al., 2004; Hansel et al., 2005). FeRB solubilize iron oxides into Fe(II) and, as a consequence, contaminants associated with ferrihydrite are readily released back into the environment. In contrast, crystalline iron oxides are more recalcitrant to microbial reduction (Roden and Zachara, 1996; Urrutia et al., 1998; Roden et al., 2000; Hansel et al., 2003; Hansel et al., 2004; Hansel et al., 2005).

In the environment, iron oxides rarely exist as pure phases. Instead, they frequently contain impurities such as Al and Si, and they are often intimately associated with organic matter, in particular intact and/or partially degraded microbial cells and extracellular exudates (Fortin et al., 1993; Cornell and Schwertmann, 2003; Chan et al., 2004; Chan et al., 2009). Such intimate association occurs as a consequence of the active (i.e. metabolic) and passive (i.e. chemical) role of bacteria in the oxidation of Fe(II), which leads to the precipitation of iron oxides directly on or in close proximity to microbial cells and their extracellular exudates (Konhauser, 1997; Chan et al., 2004; Fortin and Langley, 2005; Kappler and Straub, 2005; Chan et al., 2009; Chan et al., 2011; Melton et al., 2014; Posth et al., 2014). The most common iron oxide that forms in association with microbial surfaces is a short-range ordered phase that resembles 2-line-ferrihydrite, along with minor amounts of crystalline phases such as akaganeite, lepidocrocite, goethite, or hematite comprising the remainder (Hallberg and Ferris, 2004; Chan et al., 2004; Fortin and Langley, 2005; Chan et al., 2009; Gault et al., 2011; Chan et al., 2011). These so-called biogenic iron oxides (BIOS) are found in a broad range of environments, including hydrothermal sea vents (Kennedy et al., 2003; Toner et al., 2009; Langley et al., 2009a; Toner et al., 2012), wetland plant rhizospheres (Emerson et al., 1999), lake sediments (Fortin et al., 1993), anoxic

sediments and aquifers (Fortin and Langley, 2005), mining impacted environments (Banfield et al., 2000; Chan et al., 2004), and groundwater discharge zones (James and Ferris, 2004; Blöthe and Roden, 2009; Gault et al., 2011), and they exhibit distinct properties compared to their synthetic counterparts. BIOS exhibit smaller particle size and lower crystallinity (Châtellier et al., 2001; Châtellier et al., 2004; Rancourt et al., 2005), and a slightly higher redox potential suggesting that BIOS are more reducible by FeRB than their synthetic counterparts (Langley et al., 2009a; Langley et al., 2009b; Langley et al., 2009c; Piepenbrock et al., 2014). BIOS also contain an organic component which offers additional heterogeneous and highly reactive sites that can immobilize a significant amount of contaminants (Ferris et al., 1999; Ferris et al., 2000; Martinez et al., 2003; Langley et al., 2009d; Moon and Peacock, 2013).

The incorporation of microbial cells and/or their exudates influences the kinetics and pathways of transformation and crystal growth of BIOS. For example, Kennedy et al. (2004) subjected synthetic 2-line ferrihydrite and marine BIOS to aqueous heating at 80°C for 2 days, and found that synthetic 2-line ferrihydrite transformed into hematite, whereas BIOS did not transform into crystalline phases. In agreement with several studies (Banfield et al., 2000; Kennedy et al., 2003; Toner et al., 2009; Toner et al., 2012; Vollrath et al., 2013), Kennedy et al. (2004) concluded that the organic fraction associated with BIOS plays a role in inhibiting transformation. However, Chan et al. (2009) showed that mineral transformation into akaganeite can occur in the immediate vicinity of microbial exudates in naturally occurring BIOS. Chan et al. (2009) further suggested that such transformation may not occur during short-time scales (in the order of weeks). Rather, transformation may occur during longer time scales (in the order of months). These findings highlight the need for a broader investigation of the long term mineral stability of BIOS, and given

the context above, such knowledge would be useful to predict the reactivity of BIOS and in turn the possible impact on contaminant mobility in the environment.

The present study investigates the mineralogical composition of sterile BIOS samples that have been preserved at 4°C for several years (~5) in order to simulate early diagenesis. They are referred to as "aged" BIOS throughout the paper. In addition, the present study investigates the reactivity of aged BIOS in the presence of a model FeRB, *Shewanella putrefaciens* CN32 (*S. putrefaciens* CN32). In order to determine any changes in the mineralogical composition, as well as the susceptibility of aged BIOS towards microbial reduction, the results presented herein are compared with previously published data which correspond to "fresh" BIOS (Langley et al., 2009b; Gault et al., 2011).

2. Material and methods

2.1. BIOS collection

BIOS samples were collected during the spring of 2007 from a circumneutral-pH wetland located on the property of the Canadian Nuclear Laboratories (CNL) in Chalk River, Ontario, Canada (see Figure S1 for a map of the site and sampling locations). A detailed description of the site along with the geochemical parameters of the surface waters, sampling methods, and processing can be found in Langley et al. (2009b), Gault et al. (2011), and Gault et al. (2012) (see Table S1 for selected physicochemical parameters of groundwater-derived surface waters measured for sample sites with BIOS deposition). For the present study, the BIOS samples originated from 2 sites situated along an anoxic and Fe(II)-rich groundwater discharge zone and were abbreviated CR-01 and CR-02. CR-01 corresponds to a site that was situated within 1m of the groundwater discharge point, whereas CR-02 corresponds to a site that was approximately 10m downstream from CR-01. The reactivity of fresh BIOS towards the microbial reduction by *S.*

putrefaciens CN32 was previously investigated by Langley et al. (2009b). For their reduction experiments, the fresh BIOS originated from the same site but a different location adjacent to CR-02, which was abbreviated as CR-03 (Figure S1). Given that mineralogy of the BIOS collected from the different locations was dominated by 2-line ferrihydrite (see Figure S2), it is very likely that the reactivity of BIOS among the different locations was similar.

2.2. BIOS sterilization and simulated diagenesis

In order to avoid microbial transformation of BIOS during storage and processing, BIOS were previously sterilized after their collection by gamma (γ-) irradiation to a final dose of 14 kGray (Langley et al., 2009b). Previous studies indicate that a dose of 14 kGray is sufficient to sterilize the samples without inducing unwanted mineralogical alteration in BIOS (McNamara et al., 2003; Langley et al., 2009b). Subsequently, the sterile wet samples were aged in the dark at 4°C for several years (~5) in order to simulate diagenesis.

2.3. Mineralogy and surface area of aged BIOS

The bulk mineralogy of aged BIOS was determined by X-ray diffraction (XRD). Prior to analysis, samples were dried in a Coy Labs anaerobic chamber with an atmosphere of 95:5 N_2:H_2, and then ground into a fine powder using a mortar and pestle. XRD analysis was performed using a Philips PW1830 X-ray diffractometer, operating at 45 kV and 40 mA using Cu-Kα radiation. Diffraction data were collected over the 10–70° 2Θ range using a step size of 0.02°. Further quantification of iron-bearing minerals in aged BIOS was performed by extended x-ray absorption fine structure (EXAFS) as previously described by Gault et al. (2011).

BET N_2 surface area measurements on duplicate samples prepared in the same manner as XRD and EXAFS were carried out using a Micromeritics 3Flex Surface Characterization

Analyzer. Samples were degassed under N_2 flow at a temperature of 50°C for 24 hours before N_2 adsorption measurements.

2.4. Chemical quantification of iron-bearing mineral fractions in aged BIOS

To quantify the amorphous and crystalline iron fractions in aged BIOS, non-sequential chemical extraction was performed in triplicates following the methods of Kostka and Luther (1994). Briefly, a known amount of wet sample was accurately weighed into 20mL scintillation vials followed by the immediate addition of a specific chemical extractant, including: HCl (0.5M – duration of 1 hour), ascorbate (pH 8.0 – duration of 24 hours), oxalate (pH 3.0 – performed in the dark for 48 hours), and dithionite (pH 4.8 – duration of 4 hours). The amount of iron extracted with HCl is operationally defined to represent the amorphous iron fraction as well as adsorbed Fe(II) and any Fe(II) associated with acid volatile sulfides (AVS) and silicates, in particular chlorite (Kostka and Luther, 1994). The amount of iron extracted with ascorbate is considered to represent the amorphous iron fraction only. The amount of iron extracted with oxalate is similar to that of HCl, however oxalate may overestimate the amorphous iron fraction and underestimate the crystalline iron fraction (Kostka and Luther, 1994). Finally, dithionite extracts all reactive iron fractions including those extracted by HCl as well as crystalline iron fractions (Kostka and Luther, 1994). Subsequent to each extraction, the concentration of iron was determined spectrophotometrically using the ferrozine assay (Stookey, 1970; Kostka and Luther, 1994). The pseudo-total iron content of the BIOS samples was determined by suspending 0.1g of wet sample into 6mL ultrapure (18 MΩ•cm) water (UPW), and fully digested by the addition of 4mL of 30% H_2O_2 and 2mL trace metal grade HNO_3 followed by heating at 70°C overnight (Langley et al., 2009b). Subsequently, the digested samples were filtered (0.2 µm) and diluted into 1% trace metal grade HNO_3 (1:10) and analyzed by inductively coupled plasma — optical emission spectroscopy

using a Varian Vista-PRO CCD Simultaneous ICP-OES, operating under standard conditions. The water content of BIOS was determined by placing wet sample into pre-weighed 20mL glass scintillation vials and drying to a constant weight at 70°C to express the amount of iron per gram/milligram dry weight of sample.

2.5. Chemical composition of BIOS

To determine the chemical composition of BIOS, a known amount of dry crushed sample was suspended in an ammonium oxalate/oxalic acid solution (pH 3.0) and agitated for 2 hours in the dark (Loeppert and Inskeep, 1996; Cismasu et al., 2011). Subsequently, the digests were filtered (0.2µm) and analyzed with ICP-OES for the elements Fe, Al, Si, and P. As previously described, this extraction procedure supposedly provides the chemical composition of the amorphous iron fraction with little effect on detrital crystalline aquifer material such as quartz and some clay minerals (Loeppert and Inskeep, 1996; Cismasu et al., 2011). Other elements such as Cd, Co, Cr, Cu, Ni and Zn were not analyzed due to their low concentration (Langley et al., 2009d). To determine the organic matter content of BIOS, weight loss on ignition (LOI) was carried out in duplicate by heating a known amount of oven-dried (100ºC) crushed sample in a muffle furnace at 365°C for 24 hours.

2.6. Reduction experiments

In order to compare the reactivity of aged BIOS to that of fresh BIOS, aged BIOS were subjected to anaerobic conditions in the presence of *S. putrefaciens* CN32. The reduction experiments were conducted in microcosms comprised of 1L acid-washed Kimax bottles with 700mL of sterile chemically defined medium (CDM) (pH ~7.00) with the following composition: 20mM sodium lactate as the electron donor, 3.9mM sodium phosphate, 4mM 1,4-

piperazinediethanesulfonic acid (PIPES) buffer, trace element salts, and 4mM total Fe in the form of aged BIOS as determined by ICP-OES (Section 2.4) (Glasauer et al., 2003; Langley et al., 2009b). Cell cultures of *S. putrefaciens* CN32 were prepared according to the methodology of Langley et al. (2009b). Subsequently, the microcosms were inoculated with the prepared cells to yield an initial cell number of ~10^7 CFU/mL. All reduction experiments were conducted in triplicate, from three separate preparations of growth medium, cells, and iron oxides, and cell-free controls were included. The microcosms to which cells were added are referred to as "biotic" microcosms, whereas controls are referred to as "abiotic" microcosms.

Sampling of each system was performed immediately following the addition of the cells (time 0), at 3 hours, 6 hours, and 24 hours post-inoculation, followed by once daily for a total of 5 days. At each time point, sub-sample suspensions from the microcosms were analyzed for Eh, pH, cell viability of *S. putrefaciens* CN32, total and soluble Fe(II), total Fe and P, and total soluble Fe and P as previously described (Langley et al., 2009b). Eh and pH were monitored utilizing standard laboratory meters and probes, whereas cell viability was monitored by colony counts on trypticase soy agar (TSA) plates (Glasauer et al., 2003; Langley et al., 2009b). Total Fe(II) was determined by immediately dispensing 0.5mL of the suspension into 4.5mL of 0.5M trace metal grade HCl for 24 hours at ambient temperature, after which the concentration of Fe(II) was determined spectrophotometrically using the ferrozine assay (Stookey, 1970). For the determination of total Fe and P, 6mL of the suspension was digested by addition of 4 mL of 30% H_2O_2 and 2 mL of concentrated trace metal grade HNO_3 at 70°C for 24 hours and analyzed by ICP-OES. Soluble Fe(II) was determined by filtering the suspension (0.2 μm) and transferring 0.5mL of the filtrate into 4.5mL HCl, followed by analysis with ferrozine, as described for total Fe(II). Total soluble

Fe and P were determined by digesting 6mL of the filtered suspension followed by analysis as described for total Fe and P.

Post-reduction mineral precipitates that formed during microbial reduction were analyzed by XRD as described in Section 2.3. Prior to analysis, post-reduction minerals were harvested by centrifugation (4200 rpm), washed multiple times with anoxic UPW, and dried under anaerobic conditions.

2.7. Electron microscopy

Transmission electron microscopy (TEM) observation of aged BIOS was performed at the University of Guelph (Ontario, Canada) using a Philips CM 10 microscope operating at 80 kV. The microscope is coupled to a Soft-imaging Systems (SiS) Morada CCD camera, controlled by a SiSiTEM software, and an EDAX Sapphire X-ray detector. The samples were embedded in resin and thin sectioned according to the protocol of Langley and Beveridge (1999). Aged BIOS samples were also observed by scanning electron microscopy (SEM) with a JEOL JSM-6610LV microscope operating at 20 kV at the University of Ottawa (Ontario, Canada). Prior to observation, samples for SEM analysis were prepared by placing a thin layer of dry samples on a carbon tape attached to a sample holder.

3. Results

3.1. Mineralogy and surface area of BIOS

XRD patterns obtained from aged BIOS are presented and compared to those of fresh BIOS in Figure 1. Generally, the diffraction patterns of aged BIOS were similar to those of fresh BIOS. The patterns contained two broad reflections centered at d-spacings of ~2.5 and 1.5 Å, which are characteristic of the poorly ordered iron oxide mineral, 2-line ferrihydrite (Cornell and

Schwertmann, 2003). Additional peaks could be discerned, which belong to the crystalline iron oxides, goethite and lepidocrocite. Other sharp peaks correspond to silicate minerals including quartz, feldspar, and mica, which comprise the bulk of the aquifer material (Langley et al., 2009b; Gault et al., 2011).

Similar to XRD, Fe K-edge EXAFS spectra obtained from aged BIOS were similar to those of fresh BIOS (Figure 2). Linear combination fitting of model iron oxy(hydr)oxide mineral Fe K-edge EXAFS spectra to aged BIOS from sites CR-01 and CR-02 indicated that 2-line ferrihydrite comprised the bulk of the iron-bearing minerals (71 and 76%), while the inclusion of lepidocrocite (17%) and goethite (12 and 6%) improved the fit (Figure 2; Table 1). A comparison of the proportions of iron-bearing minerals between fresh and aged BIOS reveals no major differences in the mineralogy and the observed variability is well within the reported detection limit and fitting errors of ~5% of total Fe (Table 1) (Gault et al. 2011).

BET analysis determined a surface area of 80±9 and 150±30 m^2/g for aged BIOS from sites CR-01 and CR-02, respectively.

3.2. Chemical quantification of iron-bearing fractions in aged BIOS

The amount of iron extracted from aged BIOS by different chemical treatments is presented in Table 2. In both samples, no significant difference was observed between the amount of iron extracted by HCl and ascorbate (determined by t-test, $p>0.05$). Therefore, both HCl and ascorbate extractions are estimators of the amorphous iron fraction in aged BIOS. In contrast, in both samples, the amount of iron extracted by oxalate was significantly higher than the amount extracted by either HCl or ascorbate ($p<0.05$). The amount of iron extracted from both samples by dithionite was found to agree with the amount determined by ICP-OES (data not shown); therefore, dithionite is an estimator of the total iron pool. In both samples, the amount of iron extracted by

dithionite was significantly higher than the amount of iron extracted by HCl and ascorbate ($p<0.05$). In contrast, no significant difference was observed between dithionite and oxalate extractable iron from aged BIOS from site CR-01 ($p>0.05$), however the amount of iron extracted by dithionite is significantly higher than the amount of iron extracted by oxalate from aged BIOS from site CR-02 ($p<0.05$). This is in agreement with Kostka and Luther (1994) who found that oxalate overestimates the amorphous iron fraction and underestimates the crystalline iron fraction, presumably due to the presence of Fe(II) which catalyzes the dissolution of crystalline iron oxides. Oxalate extractable Fe(II) was found to be 3±0.6 and 2±0.1 mg/gdwt for aged BIOS from sites CR-01 and CR-02, respectively. The slightly higher concentration of Fe(II) in aged BIOS from site CR-01 would likely further catalyze the dissolution of the crystalline iron fractions in the presence of oxalate, thus explaining the similarity to the amount of iron extracted by dithionite. This would also apply to aged BIOS from site CR-02, but due to the lower concentration of Fe(II) it is likely that a lower amount of the crystalline iron fraction was dissolved in the presence of oxalate explaining the overestimation of the amorphous iron fraction and the underestimation of the crystalline fraction.

Previous studies found that ascorbate quantitatively and selectively dissolves the amorphous iron fraction thus ascorbate was used to represent such fraction in this paper (Kostka and Luther, 1994; Hyacinthe et al., 2006; Raiswell et al., 2010). The proportion of the amorphous iron fraction in aged BIOS from sites CR-01 and CR-02 was determined to be 66±5 and 70±4%, respectively (Table 2). In agreement with previous studies (Kostka and Luther, 1994; Hyacinthe et al., 2006; Raiswell et al., 2010), the amorphous iron mineral fraction determined by ascrobate was found to be within the range of the proportion of 2-line ferrihydrite determined by Fe K-edge EXAFS (Tables 1 and 2). By using the total and amorphous iron fractions determined by dithionite

and ascorbate, respectively, it is possible to calculate the proportion of the crystalline iron fraction, which was determined to be 30±6 and 28±4% for aged BIOS from sites CR-01 and CR-02, respectively (Table 2). Within error, the crystalline fraction determined by extractions corresponds to the sum of the proportions of lepidocrocite and goethite determined by Fe K-edge EXAFS (Tables 1 and 2).

3.3. Chemical composition of aged BIOS

The chemical composition of the amorphous iron fraction of aged BIOS is given in Table 3. Analysis by ICP-OES revealed Fe concentrations ranging from 20 to 30%, with Al:Fe mol ratios ranging from 0.01 to 0.02, Si:Fe mol ratios ranging from 0.06 to 0.08, and P:Fe mol ratios ranging from 0.003 to 0.004. An organic matter content of 21 and 28% was detected by LOI in BIOS from sites CR-01 and CR-02, respectively (Table 3).

The amount of iron extracted with oxalate was found to agree with the amount of iron extracted with ascorbate, suggesting that oxalate selectively dissolved the amorphous iron fraction (data not shown). The difference between the amount of iron determined by oxalate in this case and the amount discussed in the previous section (3.2) could be attributed to a number of factors. Following the methods of Loeppert and Inskeep (1996), the extractions were carried out using dry samples prior to a 2 hour extraction period. It is possible that drying the samples in open air oxidized Fe(II) thereby preventing the catalyzed dissolution of the crystalline iron fractions as was previously found. In contrast, in the methods of Kostka and Luther (1994), the oxalate extractions were performed by using wet samples for a duration of 48 hours. It is also possible that the duration of extraction time could have played a role. Nonetheless, the concentration of the selected elements presented in Table 3 can be confidently said to represent those that are associated with the amorphous fraction.

3.4. Electron microscopy

SEM and TEM micrographs of aged BIOS from sites CR-01 and CR-02 showed the abundance of typical structures associated with neutrophilic iron oxidizing bacteria, including sheaths reminiscent of *Leptothrix ochracea*, as was previously observed with fresh BIOS (Figure 3a and b) (Langley et al., 2009b; Gault et al., 2011). TEM thin sections of fresh and aged BIOS showed that the cell structures were coated with an electron dense precipitate (Figure 4). However, in some instances, we observed a difference in the thickness of the electron dense precipitate when comparing fresh and aged BIOS. In fresh BIOS, the thickness of the precipitate was 100-200 nm thick (Langley et al., 2009b), in contrast the precipitate associated with aged BIOS was observed to be occasionally thicker with an approximate thickness of 300 nm (Figure 4b compared to Figure 4a). In some instances, sheath structures belonging to aged BIOS appeared to be coated by coarse minerals (Figure 4c). Energy dispersive X-ray spectroscopy (EDS) analysis of the precipitate associated with the cell structures generated spectra with strong signals corresponding to Fe and O, and weaker signals belonging to Al, Si and other trace elements, as was previously observed (data not shown) (Langley et al., 2009b).

TEM thin sections of aged BIOS further revealed unique morphological features which were not previously observed in fresh BIOS. We observed linear structures which appear to have formed within sheaths. These structures appeared parallel to the orientation of the sheaths (Figure 4d and e). Needle or lath-like structures morphologically similar to those of lepidocrocite were occasionally observed surrounding sheath structures (Figure 4f) (Fortin et al., 1993). The lepidocrocite-like crystals were variable in length and width, typically ranging between 100-1000nm in length and averaging ~30nm in width. In most cases, the lepidocrocite-like crystals appeared to be randomly oriented, but in one case some crystals appeared to be oriented in a

specific direction, forming parallel lineations (Figure 4f). No obvious differences in morphology were noted between aged BIOS from sites CR-01 and CR-02 as the morphologies described above were observed in both samples suggesting that the observed mineral development or "growth" occurred as a consequence of ageing.

3.5. Reduction of aged BIOS

3.5.1. Abiotic microcosms

Throughout the experiment, no significant changes in the different parameters measured and no microbial growth was observed in all the abiotic microcosms (data not shown). The only change observed was the gradual decline of Eh. Within the first 24 hours following the storage of the microcosms in the anaerobic chamber, Eh declined by an average of 40mV (corrected to the standard hydrogen electrode; SHE) and continued to gradually decline throughout the remainder of the experiment (Figure S3a and b). Such decline represents the equilibration of the microcosms with the anaerobic atmosphere (Langley et al., 2009b).

3.5.2. Biotic microcosms

Similar trends were observed in the different parameters measured from all biotic microcosms. Within the first 24 hours, Eh dropped dramatically by an average of 270mV in all biotic microcosms. However, Eh continued to decline until day 2 at which point the levels reached a steady state for the remaining duration of the experiment (Figure S3a and b). In all the biotic microcosms cell counts increased from an average of 6.6×10^7 CFU/mL to an average maximum of 1.8×10^8 CFU/mL after 24 hours of incubation which gradually declined throughout the experiment and reached an average of 8.8×10^7 CFU/mL at the end of the experiment (Figure S3c

and d). pH increased from ~7.00 to an average maximum of 7.14 and continued to fluctuate throughout the experiment (Figure S3e and f).

The change of total Fe(II) relative to total Fe, as well as the change of soluble P relative to total P throughout the reduction period for both fresh and aged BIOS are presented in Figure 5 (data for total Fe(II), soluble Fe(II), and total Fe are provided in Figure S4). The initial concentration of total Fe(II) was low for aged BIOS at an average of 2% of the total Fe. In contrast, initial concentration of total Fe(II) was ~25% of the total Fe for fresh BIOS (Figure 5). This suggests that Fe(II) was chemically oxidized during storage, probably by molecular O_2 or via autocatalysis. During the reduction of aged BIOS, an initial lag in the production of Fe(II) was noted until 6 hours at which point it rapidly increased to ~26% of the total Fe by day 1 (Figure 5). Total Fe(II) continued to increase reaching ~44% and ~40% of the total Fe for aged BIOS from sites CR-01 and CR-02, respectively, by day 2. However, the production of Fe(II) continued to increase slowly and reached a steady state for the remaining duration of the experiment (Figure 5). In contrast, previous work showed that during the reduction of fresh BIOS, total Fe(II) reached ~70% of the total Fe at day 1 and increased to ~90% of the total Fe at day 2 (Figure 5) (Langley et al., 2009b). The maximum percentages of reduced Fe measured for the aged BIOS from sites CR-01 and CR-02 were 60±9and 50±10%, respectively (Table 4). In contrast, previous work showed that the maximum percentage of reduced Fe for fresh BIOS was 98±3% (Table 4) (Langley et al., 2009b). No significant difference was observed in the maximum amount of reduced Fe between aged BIOS from sites CR-01 and CR-02 ($p>0.05$), however a significant difference was observed when compared to fresh BIOS ($p<0.05$) (Table 4).

The initial concentration of soluble P in aged BIOS systems was 100% of total P which gradually declined throughout the reduction period, reaching an average of ~47% of total P at the

termination of the experiment (Figure 5). The gradual decline of soluble P was also observed during the reduction of fresh BIOS, in which case soluble P decreased from an initial concentration of 67% to 40% of the total P at day 5 and continued to decline to ~31% of the total P at day 7 (Figure 5) (Langley et al., 2009b).

3.5.3. Rates of reduction

Maximum rates of microbial reduction of the aged BIOS were calculated by linear regression of selected time points that correspond to the period of maximum total Fe(II) accumulation (Langley et al., 2009b). A summary of the regression data is presented in Table 4, which shows a significant difference between the reduction rates of aged BIOS and fresh BIOS ($p<0.05$). The reduction rates of aged BIOS from sites CR-01 and CR-02 were determined to be 0.23 ± 0.03 day^{-1} and 0.21 ± 0.03 day^{-1}, respectively, whereas the reduction rate of fresh BIOS was 0.47 ± 0.02 day^{-1} (Table 4) (Langley et al., 2009b). No significant difference was observed between the reduction rates of aged BIOS from sites CR-01 and CR-02 ($p>0.05$), however both were significantly lower than that of fresh BIOS ($p<0.05$).

3.5.4. Post-reduction minerals

XRD analysis of the post-reduction mineral precipitates that formed during Fe reduction indicate that vivianite ($Fe_3(PO_4)_2 \cdot 8H_2O$) formed in all biotic microcosms (Figure S5). The formation of vivianite as a secondary mineral was previously observed and was expected given the high concentrations of phosphate (3.9mM) in the medium (Glasauer et al., 2003; Langley et al., 2009b). In contrast, no changes in mineralogy of the abiotic microcosms were observed (data not shown).

4. Discussion

4.1. Mineralogy

The transformation of ferrihydrite into crystalline phases proceeds by the dissolution of precursor ferrihydrite nanoparticles followed by the precipitation of the crystalline phase in the bulk solution (dissolution-reprecipitation), or through dehydration-aggregation and internal re-arrangement of ferrihydrite nanoparticles (solid-state transformation) (Cornell and Schwertmann, 2003). Phase transformation is accompanied by crystal growth which proceeds by two mechanisms: coarsening and aggregation (Penn, 2004; Burleson and Penn, 2006; Cölfen and Antonietti, 2008a; Cölfen and Antonietti, 2008b; De Yoreo et al., 2015). Coarsening, also referred to as Ostwald ripening, involves the growth of larger crystals at the expense of the dissolving smaller crystals by diffusion of molecular-scale species to the surface of existing nuclei, whereas aggregation involves particle-mediated crystal growth, namely oriented aggregation (Banfield et al., 2000; Penn, 2004; Burleson and Penn, 2006; Cölfen and Antonietti, 2008a; Cölfen and Antonietti, 2008b; De Yoreo et al., 2015). Oriented aggregation proceeds by the self-assembly and orientation of primary crystallites, through Brownian motion and rotation, to achieve structural compatibility and the formation of new secondary crystals (Banfield et al., 2000; Penn, 2004; Burleson and Penn, 2006; Cölfen and Antonietti, 2008a; Cölfen and Antonietti, 2008b; Yuwono et al., 2010; De Yoreo et al., 2015). Crystal growth is achieved by desorption of water and/or adsorbed molecules at the interfaces of aggregated primary crystallites to form iron-oxygen bonds (Banfield et al., 2000; Penn, 2004; Burleson and Penn, 2006; Cölfen and Antonietti, 2008a; Cölfen and Antonietti, 2008b; Yuwono et al., 2010; De Yoreo et al., 2015). The pathway and kinetics of transformation and crystal growth are primarily controlled by pH and temperature of the system (Cornell and Schwertmann, 2003; Penn, 2004; Burleson and Penn, 2006). For example, goethite

formation from precursor ferrihydrite is favored at pH 4 and 12 with crystal growth being dominated by coarsening at low pH, and a combination of aggregation and coarsening at higher pH (Cornell and Schwertmann, 2003; Burleson and Penn, 2006). Impurities (e.g., Al, Si, and P) present in solution and/or adsorbed/incorporated by the iron oxide influence the rate of transformation and the secondary mineral products that form, and in some cases completely inhibit the transformation of ferrihydrite (Cornell and Schwertmann, 2003). It has been previously noted by several studies that microbial cells and/or their exudates inhibit the transformation of ferrihydrite into crystalline phases (Banfield et al., 2000; Kennedy et al., 2004; Toner et al., 2009; Toner et al., 2012; Vollrath et al., 2013). Our XRD and EXAFS results are in agreement with this notion, which show that 2-line ferrihydrite remains as the dominant mineral in our samples, even after ~5 years of ageing. In contrast, synthetic 2-line ferrihydrite aged for the same period of time and under similar conditions employed in this study, partially transformed (~40%) into a mixture of goethite and hematite (Schwertmann et al., 2004). In synthetic 2-line ferrihydrite-bacteria coprecipitates, Kennedy et al. (2004) attributed the inhibition of transformation to the binding of ferrihydrite particles to microbial functional groups, which constrained particle rotation and oriented aggregation required for crystal growth. In our samples, the abundance of mineralized sheaths, as evidenced by SEM/TEM micrographs (Figures 3 and 4), suggests that most of the iron oxides are bound by microbial exudates. Sheaths are acidic polysaccharides with carboxyl functional groups that spatially correlate with the distribution of iron oxides (Chan et al., 2009). Therefore, binding of ferrihydrite nanoparticles to carboxyl functional groups would likely inhibit transformation in a similar manner proposed by Kennedy et al. (2004) and others (Banfield et al., 2000; Toner et al., 2009; Toner et al., 2012; Vollrath et al., 2013).

Further examination of the mineralogy of aged BIOS by XRD and Fe K-edge EXAFS revealed the presence of the crystalline iron oxide phases; lepidocrocite and goethite, as was previously observed with fresh BIOS (Gault et al., 2011). The relatively broad XRD peaks corresponding to lepidocrocite and goethite in aged and fresh BIOS suggests that these minerals exist as nanoparticulate phases, in accordance with TEM images (Figures 1 and 4f). The similarity of peak intensity and broadening of such phases between aged and fresh BIOS further indicate that crystal growth at the expense of 2-line ferrihydrite was inhibited (Figure 1). This is further supported by Fe K-edge EXAFS, which shows a similarity of the proportion of the iron minerals analyzed between aged and fresh BIOS (Table 1). These observations are in agreement with previous studies. For instance, in a laboratory based study, Vollrath et al. (2013) found that the biotic oxidation of Fe(II) by *Leptothrix cholodnii* Appels led to the formation and stabilization of nanoparticulate lepidocrocite crystals, whereas in the absence of bacteria the initially formed lepidocrocite crystals progressively grew at the expense of 2-line ferrihydrite and/or from available Fe(II) in solution. Vollrath et al. (2013) attributed the inhibition of crystal growth to the presence of microbial cells and their exudates. In contrast, Kappler and Newman (2004) found that biogenic 2-line ferrihydrite precipitated by the anoxygenic photoautotroph *Rhodobacter ferrooxidans* strain SW2 transformed into lepidocrocite and goethite after ageing for ~1 month. Such transformation was attributed to the presence of small amounts of Fe(II) in solution or potentially produced by the microbial reduction of Fe(III), which stimulated the dissolution of 2-line ferrihydrite and the precipitation of crystalline phases (Kappler and Newman, 2004). Another possibility is that the acidification of the cell local environment could have induced transformation via acid-catalyzed dissolution (Kappler and Newman, 2004; Hegler et al., 2010). Such a strategy is used to escape mineral cell encrustation and entombment, and leads to the diffusion of Fe(III) and precipitation

of iron oxides away from the cell suggesting that ferrihydrite particles are not specifically bound by microbial surfaces (Kappler and Newman, 2004; Hegler et al., 2010). In contrast, microaerophilic iron oxidizing bacteria such as *Leptothrix* spp. and *Gallionella* spp. produce extracellular polymeric substances such as sheaths and twisted stalks, respectively, to specifically bind Fe(III) away from the metabolizing cells (Figures 3 and 4) (Chan et al., 2004; Chan et al., 2009; Chan et al., 2011; Saini and Chan, 2013). Such binding strategy would likely lead to a higher amount of ferrihydrite particles closely associated with microbial surfaces as opposed to *Rhodobacter ferrooxidans* SW2 or synthetic ferrihydrite-bacteria coprecipitates (as mentioned above). This suggests that microbial exudates are likely to stabilize ferrihydrite particles not only against oriented aggregation as previously described, but also against dissolution and coarsening.

In addition to biotic factors stabilizing BIOS against transformation, inorganic impurities (e.g. Al, Si, and P) may also play a role. Al, Si (as silicate), and P (as phosphate) are well known for their ability to retard or inhibit the transformation of ferrihydrite presumably by blocking dissolution sites on ferrihydrite and the nucleation of crystalline phases in solution (Cornell et al., 1987; Galvez et al., 1999; Schwertmann et al., 2000a; Schwertmann et al., 2000b; Cornell and Schwertmann, 2003; Jones et al., 2009; Hansel et al., 2011). For example, Schwertmann et al. (2000a) showed that the transformation of 2-line ferrihydrite into goethite/hematite aged for ~20 years at 25°C, progressively diminished as coprecipitated Al content increased (0-1 mol/mol Al/(Al+Fe)). Likewise, the degree of transformation of 2-line ferrihydrite coprecipitated with phosphate progressively diminished as the concentration of phosphate increased (P/Fe mol ratio 0-0.03) (Galvez et al., 1999). Recently, Toner et al. (2012) found that marine iron microbial mats comprised of low-ordered ferrihydrite coated with amorphous silica resisted transformation after ageing for 0.5-1 year at 4°C as well as during a hydrothermal treatment at 400°C. Toner et al.

(2012) attributed the inhibition of transformation primarily due to the high concentrations of Si (Si:Fe mol ratio of 0.1-0.3) and, possibly, P (P:Fe mol ratio of 0.03-0.17). Similarly, Kennedy et al. (2004) attributed the inhibition of hydrothermal transformation of marine iron microbial mats in part due to the presence of microbial cells and their exudates, as previously discussed, but also due to inorganic impurities, particularly Si which was found in concentrations ranging from 18 to 26% by weight. In comparison with previous studies, the concentrations of Si and P associated with ferrihydrite in our samples were much lower (Table 3). Although, appreciable amounts of Si were found in our samples ranging from 0.06 to 0.08 mol/mol Si:Fe, suggesting that Si could potentially contribute to the stability of ferrihydrite. In contrast, given their low concentrations, Al and P are not expected to significantly contribute to stabilizing ferrihydrite (Galvez et al., 1999; Schwertmann et al., 2000a; Cornell and Schwertmann, 2003). It is important to note that the concentration of Al and Si given in Table 3 may not represent the species that are in direct association with ferrihydrite (i.e. adsorbed or structurally incorporated) (Cismasu et al., 2011). It is possible that individual nm Al- and Si-containing phases could potentially exist as surface precipitates (Cismasu et al., 2011). These fractions may be extractable with ammonium oxalate/oxalic acid leading to an overestimation of Al and Si fractions that are adsorbed and/or structurally incorporated by ferrihydrite (Cismasu et al., 2011). Therefore, given the high organic matter content in our samples (21-28 wt%), we attribute the stability of BIOS from sites CR-01 and CR-02 primarily to the presence of bacteria and their exudates.

4.2 Electron microscopy

TEM thin sections of aged BIOS revealed morphologically distinct features when compared to those of fresh BIOS suggesting that some mineralogical development or "growth" had occurred as a consequence of ageing (Figure 4). Most notably, the structures we observed

appeared to be thickly coated by an aggregated electron-dense mineral phase that did not appear to exhibit well-defined crystallographic features. Based on past and present data, it is likely that the electron-dense precipitate is primarily composed of 2-line ferrihydrite (Langley et al., 2009b). Although, goethite could potentially occur in these precipitates as was previously inferred from ESEM X-ray spot analysis of crystallites that formed on stalks produced by *Gallionella* spp. in freshwater BIOS (Hallberg and Ferris, 2004). Using this approach, Hallberg and Ferris (2004) showed that precipitation of iron on stalks proceeds by a multistep process, whereby crystalline iron oxide, presumably hematite, initially forms inside the fibers of the young stalk. Subsequently, as the stalk ages, the initially formed iron precipitates act as a template for the inorganic precipitation and accretion of iron oxides thereby forming a mixture of ferrihydrite and goethite on the surface of the stalk fibers (Hallberg and Ferris, 2004). Inorganic precipitation of iron oxides proceeds by the chemical oxidation of Fe(II) by stalk-bound iron oxides (autocatalysis) (Hallberg and Ferris, 2004; Vollrath et al., 2013). Inorganic precipitation of iron oxides on microbial surfaces is also likely to proceed by the oxidation of Fe(II) by molecular oxygen leading to the formation of ferrihydrite or goethite nanoparticles in solution that later passively adsorb to reactive surfaces (Warren and Ferris, 1998; Langley et al., 2009b). Similarly, it is possible that in our samples that microbial sheaths act as "nuclei" for continued adsorption/accretion or aggregation of ferrihydrite nanoparticles that initially formed away from the microbial structures thereby forming the "thick" electron-dense precipitate (Figure 4b). In freshwater BIOS, Chan et al. (2009) observed a range of iron mineralization where some remnant microbial structures appeared to be less mineralized while others appeared to be more thickly coated. Chan et al. (2009) also observed structures that were thickly coated by coarse crystalline minerals, as observed in the present study (Figure 4c). In agreement with our observations, the "gradient" of iron mineralization observed by Chan et al.

(2009) was speculated to occur as a consequence of ageing, possibly through the aforementioned processes.

Further examination of TEM thin sections of aged BIOS revealed striations in the mineral phase which were oriented parallel to the longitudinal axis of the sheaths (Figure 4d and e). These structures could potentially harbor crystalline iron oxides which may have formed through recrystallization and oriented aggregation (Section 4.1). This notion is supported by several lines of evidence. For instance, Chan et al. (2004) found that microbial filaments collected from biofilms contained elongated oriented akaganeite pseudo-single crystals, and attributed the formation of akaganeite to ageing, presumably by the recrystallization of an "amorphous" iron oxide and oriented aggregation within the filaments. Akaganeite, or possibly goethite, was also found to form within *Gallionella*-like stalks collected from another freshwater iron microbial mat (Chan et al., 2009). Chan et al. (2009) also observed intact and broken *Leptothrix* spp. sheaths with structures similar to those observed in the present study, which were found to become more pronounced in older broken sheaths (Figure 4d and e). Although such structures were not examined by high resolution TEM, Chan et al. (2009) speculated that they may contain crystalline iron oxides. Chan et al. (2009) further speculated that mineral transformation within close vicinity of microbial surfaces is likely to occur during long timescales (in the order of months). Our observations are in agreement with previous studies, suggesting that mineral transformation in BIOS may occur within close vicinity of microbial surfaces as a consequence of long term ageing, possibly by oriented aggregation.

It is important to keep in mind that in thin-sections if the section plane does not happen to pass through any unique features or crystalline minerals, they will be eliminated from subsequent analysis (Langley et al., 2009b). For example, we observed lepidocrocite-like crystals surrounding

sheath structures (Figure 4f). Some crystals appeared to be randomly oriented while others appeared to be oriented or radiating outward from the sheath. While recrystallization and oriented aggregation could have occurred within sheaths as a consequence of ageing, whether or not the lepidocrocite-like crystals aggregated in an oriented fashion due to ageing is difficult to determine. This is because lepidocrocite-like crystals were not previously observed in fresh BIOS, probably due to their low abundance (Table 1), thus making a direct comparison difficult (Langley et al., 2009b; Langley et al., 2009d). In fact, during a short-term study (in the order of days), Chan et al. (2011) observed lepidocrocite crystals "radiating" from stalks produced by a pure culture of *Mariprofundus ferrooxydans*. Therefore, it is possible that the observed oriented or "radiating" lepidocrocite crystals were previously present in fresh BIOS (Figure 4f). The same argument could be used against the features that were previously discussed (Figure 4b-e). However, due to their abundance in both aged samples (CR-01 and CR-02), and the fact that we have not previously observed them over many years of studying fresh BIOS from the same site, we favor the explanation that their formation is due primarily to ageing (Figure 4b-e).

4.3. Anaerobic reduction of aged BIOS

A comparison of the rates of iron reduction between fresh and aged BIOS revealed unexpected results. We found that the rates and extent of iron reduction of aged BIOS from sites CR-01 and CR-02 were significantly lower than that of fresh BIOS collected from site CR-03 (Figure 5, Table 4). There are several factors that influence the rate and extent of iron reduction by FeRB. These factors include: cell concentration (O'Loughlin et al., 2010), surface area (Roden and Zachara, 1996), particle aggregation (Roden and Zachara, 1996; Roden, 2003; Cutting et al., 2009), crystallinity and morphology (Cutting et al., 2009), solubility (Bonneville et al., 2004; Bonneville et al., 2009), Fe(II) concentration (Roden and Zachara, 1996; Urrutia et al., 1998;

Fredrickson et al., 1998), and the presence of organic ligands (Urrutia et al., 1999). In the present study, the measured changes in viable cell numbers along with Eh and pH throughout the course of the experiment were comparable to those measured previously (Figure S3) (Langley et al., 2009b). This suggests that other factors related to the physical state of aged BIOS are responsible for the lower reduction rates and extent, rather than the health or number of viable cells.

Surface area is often used as a quantitative indicator of the reactive site density available for microbial iron reduction (Roden and Zachara, 1996; Roden, 2003). Accordingly, surface area could be used as a predictor of the potential iron reduction rate whereby an increase in mineral surface area tends to promote the microbial iron reduction and vice versa (Roden and Zachara, 1996; Roden, 2003). BET analysis determined a surface area of 80±9 and 150±30 m^2/g for aged BIOS from sites CR-01 and CR-02, respectively, while the surface area of fresh BIOS was previously determined to be ~90m^2/g (Kennedy et al., 2011). In contrast to BIOS, the surface area of synthetic ferrihydrite varies between 200-700 m^2/g (Cornell and Schwertmann, 2003). The lower surface area determined for BIOS could be attributed to the low N_2-surface area of microbial exudates, and occlusion of interparticle pores of ferrihydrite by microbial cells and/or exudates (Mikutta et al., 2008). Nevertheless, the surface area measurements of aged BIOS were found to be in the range of those of fresh BIOS. As a result, one might expect microbial iron reduction of aged BIOS to proceed at the same rate as fresh BIOS, although this was clearly not the case (Figure 5, Table 4). It is important to note that the surface area determined for multiple samples was found to be highly inconsistent, likely due to the variable distribution of microbial cells and exudates in the subsamples analyzed. This suggests that surface area may not be a reliable indicator of mineral bioavailability, especially in BIOS. Such notion is supported by our results and several other studies. For example, given that the surface area of aged BIOS from site CR-01 is ~2× lower than

that of aged BIOS from site CR-02, it would be expected that aged BIOS from site CR-01 would be less reducible, however comparable reduction rates were observed for the two sites (Table 4). Similarly, Langley et al. (2009a) found that the rates and extent of microbial iron reduction of marine BIOS collected from different sites were not significantly different than each other, despite a substantial difference in the surface area between the two sites. Likewise, Ekstrom et al. (2010) found that while the surface area of aluminous ferrihydrites did not significantly change as Al content increased (0-13% mol/mol Al/(Al+Fe)), the microbial reduction rate and extent of reduction by *S. putrefaciens* CN32 progressively diminished as Al content increased. Recent studies further indicate that particle aggregation (Cutting et al., 2009), crystallinity and morphology (Cutting et al., 2009), and solubility (Bonneville et al., 2004; Bonneville et al., 2009), as opposed to surface area, are the main factors that control the rates and extent of microbial iron reduction. It is possible that these factors are the controlling variables here.

Indeed, it appears that particle aggregation and possible development in crystallinity within sheath structures are responsible for the lower rates and extent of microbial iron reduction in aged BIOS (Figure 5, Table 4), and such notion is supported by our TEM micrographs of aged BIOS (Figure 4b-e). Particle aggregation would likely lead to a loss of available surface area, and inhibit the relatively large FeRB from entering interior aggregate pore spaces/interfaces leading to low iron reduction rates (Roden and Zachara, 1996; Roden, 2003). Such changes may not be reflected in BET surface area analysis (Roden and Zachara, 1996). The influence of particle aggregation on the reactivity of synthetic ferrihydrite towards microbial and chemical iron reduction was previously investigated. Aggregation of 2-line ferrihydrite particles due to dehydration was found to substantially reduce the rate of microbial iron reduction, which was found to be even lower than that of crystalline goethite, despite possessing a higher surface area than goethite (Roden and

Zachara, 1996). Similarly, ageing of 2-line ferrihydrite in suspension led to the formation of networked-aggregates, which substantially reduced the rate of chemical dissolution by ascorbate (Raiswell et al., 2010). This suggests that particle aggregation is also likely to lower mineral solubility which also influences the rates of microbial iron reduction. Taken together, it is very likely that ageing led to particle aggregation and subsequent reduction in mineral solubility, consequently leading to the lower rates of iron reduction determined in this study (Table 4).

The maximum amount of iron reduced in aged BIOS from sites CR-01 and CR-02 was determined to be 62±9 and 50±10%, respectively. This amount appears to be in the range of the ascorbate iron extractable fraction (Table 2), suggesting that 2-line ferrihydrite was selectively and almost completely reduced by *S. putrefaciens* CN32 while leaving the crystalline iron oxides, lepidocrocite and goethite, intact. This is in agreement with Hyacinthe et al. (2006), who showed that the maximum amount of iron extracted by ascorbate linearly correlates with the maximum concentration of Fe(III) reduced by *S. putrefaciens* 200R. This could also provide an explanation for the observed apparent cessation of Fe(II) production, given that goethite is recalcitrant towards microbial reduction (Roden and Zachara, 1996; Roden et al., 2000; Glasauer et al., 2003; Hansel et al., 2003; Hansel et al., 2004; Hansel et al., 2005). In contrast, lepidocrocite could be reduced by *S. putrefaciens* CN32 but this is likely to occur at a lower rate than 2-line ferrihydrite and within a longer time span than 5 days (Figure 5), which is due to the lower surface area of lepidocrocite (Roden and Zachara, 1996; Roden, 2003; Cornell and Schwertmann, 2003). Alternatively, as reduction proceeds the formed biogenic Fe(II) could saturate the mineral surface thereby blocking the remaining iron fractions to microbial attachment and subsequent reduction (Roden and Zachara, 1996; Urrutia et al., 1998; Fredrickson et al., 1998). With continued Fe(II) production, the solution becomes saturated with respect to vivianite due to the high concentration of phosphate

(3.9mM) in solution, leading to the precipitation of vivianite and the decline in soluble phosphorus (Figure 5). XRD analysis of the post-reduction mineral precipitates identified vivianite as the dominant mineral; however, we could not identify any peaks corresponding to lepidocrocite or goethite, probably due to their low abundance and the attenuation of their peaks by vivianite (Figure S5).

In contrast to our results, fresh BIOS from site CR-03 were fully reduced (Table 4). XRD analysis of the fresh BIOS from site CR-03 showed that the mineralogy was dominated by 2-line ferrihydrite (Figure S2, Langley et al., 2009b). Further characterization of the fresh BIOS from site CR-03 by Fe K-edge EXAFS and selected area electron diffraction failed to reveal any crystalline phases (Langley et al., 2009b). However, given the heterogeneity of the samples, it's possible that crystalline phases may occur within isolated regions and the failure to detect any crystalline phases could be attributed to the analytical constraints of the techniques (Langley et al., 2009b). Nonetheless, it's clear that, on a bulk scale, fresh BIOS from site CR-03 were dominated by 2-line ferrihydrite and it's likely that the proportion of 2-line ferrihydrite in such samples was higher than those collected from CR-01 and CR-02. This could explain the higher amount of iron reduced in fresh BIOS, however as previously discussed, as reduction proceeds biogenic Fe(II) would thermodynamically constrain further reduction, and yet fresh BIOS were fully reduced. Langley et al. (2009b) attributed the enhanced microbial iron reduction rate and extent of fresh BIOS to the presence of organic matter (microbial cells and exudates). Organic matter would complex the formed biogenic Fe(II) making Fe(III) reduction thermodynamically more favorable by preventing Fe(II) from saturating mineral surfaces (Urrutia et al., 1999; Langley et al., 2009b; Muehe et al., 2013). Furthermore, organic matter could be potentially used as additional nutrients or electron donors for microbial iron reduction, and as electron shuttles (Langley et al., 2009b).

Shewanella strains are also capable of producing flavin compounds capable of electron shuttling and Fe(III) complexation (Marsili et al., 2008). Electron shuttles would preclude the requirement for *S. putrefaciens* CN32 to be in direct contact of the mineral surface and allow FeRB to better access complex interstices of the solid (Fredrickson et al., 1998; Zachara et al., 1998). Taken together, these processes were previously shown to enhance the rate and extent of microbial reduction of both poorly ordered and crystalline iron oxides (Fredrickson et al., 1998; Zachara et al., 1998; Urrutia et al., 1999; Cutting et al., 2009; Muehe et al., 2013), providing an explanation for the full reduction of fresh BIOS observed by Langley et al. (2009b).

In our samples, it is possible that the aforementioned processes enhanced the reduction of the aggregated 2-line ferrihydrite particles. Electron shuttles, whether produced or provided by the organic matter, would allow FeRB to access interior aggregate pore spaces and interfaces leading to the full reduction of 2-line ferrihydrite. However, the question arises as to why, in aged BIOS, the crystalline fractions were not reduced despite the "enhancement" provided by organic matter as well as the capability of FeRB to produce flavin compounds. At this time, we can only speculate that ageing possibly influenced the properties of the crystalline iron oxide fractions. However, it is important to note that the reduction experiments were conducted over a short duration of time (Figure 5). Therefore, it is very likely that full reduction of the crystalline phases in aged BIOS may occur over a longer time span.

5. Conclusions

Ageing of freshwater BIOS at 4°C for ~5 years was found to have a profound impact on their reactivity with respect to microbial iron reduction. Ageing, on the other hand, did not influence the composition and proportion of iron-bearing minerals within aged BIOS when compared to fresh BIOS as determined by XRD, EXAFS, and chemical extractions. 2-line

ferrihydrite remained as the dominant Fe-bearing mineral in aged BIOS, likely due to the stabilization of the ferrihydrite nanoparticles by microbial cells and exudates against transformation. The rates of reduction of aged BIOS from sites CR-01 and CR-02 were found to be significantly lower than that of fresh BIOS from site CR-03, despite the similarity of the mineralogy between the sites. TEM observations suggest that aggregation and possible development in crystallinity within sheath structures are likely responsible for the low rates of microbial iron reduction in aged BIOS. 2-line ferrihydrite in aged BIOS was, however, fully reduced indicating that it remains bioavailable. The impact of ageing on the long-term reactivity of BIOS has important consequences on the dynamics of iron and carbon cycling in the environment. The lower reactivity of BIOS as a consequence of ageing suggests that aggregated 2-line ferrihydrite nanoparticles are likely to protect the organic matter from degradation, which leads to the preservation of organic matter in the environment for extended periods of time. In turn, organic matter plays an important role in stabilizing the bioavailable 2-line ferrihydrite against further transformation. Our results show that the effects of ageing on the reactivity of BIOS are likely to occur during long time scales under conditions that are relevant to early diagenesis. This also suggests that the reactivity of BIOS in natural environments may not be easy to predict, and therefore the effects of ageing on the reactivity of BIOS have to be considered within the framework of iron biogeochemistry.

Acknowledgements

The present research was entirely funded by a NSERC Discovery grant to D. Fortin. The authors are very thankful to E. Revesz and D. Moyles for performing the electron microscopy, N. De Silva for running the ICP analyses and A. Gault for doing the Fe-EXAFS interpretation. We

also wish to thank the personnel of the Canadian Nuclear Laboratories (CNL) for giving us access to their site in Chalk River, ON, Canada.

References

Banfield, J.F., Welch, S.A., Zhang, H., Ebert, T.T., Penn, R.L., 2000. Aggregation-based crystal growth and microstructure development in natural iron oxyhydroxide biomineralization products. Science, 289, 751-754.

Blöthe, M., Roden, E.E., 2009. Microbial iron redox cycling in a circumneutral-ph groundwater seep. Appl. Environ. Microbiol., 75, 468-473.

Bonneville, S., Van Cappellen, P., Behrends, T., 2004. Microbial reduction of iron (III) oxyhydroxides: Effects of mineral solubility and availability. Chem. Geol., 212, 255-268.

Bonneville, S., Behrends, T., Van Cappellen, P., 2009. Solubility and dissimilatory reduction kinetics of iron (III) oxyhydroxides: A linear free energy relationship. Geochim. Cosmochim. Acta, 73, 5273-5282.

Burleson, D.J., Penn, R.L., 2006. Two-step growth of goethite from ferrihydrite. Langmuir, 22, 402-409.

Chan, C.S., De Stasio, G., Welch, S.A., Girasole, M., Frazer, B.H., Nesterova, M.V., Fakra, S., Banfield, J.F., 2004. Microbial polysaccharides template assembly of nanocrystal fibers. Science, 303, 1656-8.

Chan, C.S., Fakra, S.C., Edwards, D.C., Emerson, D., Banfield, J.F., 2009. Iron oxyhydroxide mineralization on microbial extracellular polysaccharides. Geochim. Cosmochim. Acta, 73, 3807-3818.

Chan, C.S., Fakra, S.C., Emerson, D., Fleming, E.J., Edwards, K.J., 2011. Lithotrophic iron-oxidizing bacteria produce organic stalks to control mineral growth: Implications for biosignature formation. ISME J, 5, 717-27.

Châtellier, X., Fortin, D., West, M.M., Leppard, G.G., Ferris, F.G., 2001. Effect of the presence of microbial surfaces during the synthesis of fe oxides by oxidation of ferrous ions. Eur. J. Mineral., 13, 705-714.

Châtellier, X., West, M.M., Rose, J., Fortin, D., Leppard, G.G., Ferris, F.G., 2004. Characterization of iron-oxides formed by oxidation of ferrous ions in the presence of various microbial species and inorganic ligands. Geomicrobiol. J., 21, 99-112.

Cismasu, A.C., Michel, F.M., Tcaciuc, A.P., Tyliszczak, T., Brown, J.G.E., 2011. Composition and structural aspects of naturally occurring ferrihydrite. CR Geosci., 343, 210-218.

Cölfen, H., Antonietti, M., 2008a. Nonclassical crystallization, in: Cölfen, H., Antonietti, M. (Eds.), Mesocrystals and nonclassical crystallization. John Wiley & Sons, Ltd., New York, pp. 73-101.

Cölfen, H., Antonietti, M., 2008b. Self-assembly and self-organization, in: Cölfen, H., Antonietti, M. (Eds.), Mesocrystals and nonclassical crystallization. John Wiley & Sons, Ltd., New York, pp. 103-106.

Cornell, R., Giovanoli, R., Schindler, P., 1987. Effect of silicate species on the transformation of ferrihydrite into goethite and hematite in alkaline media. Clays Clay Miner., 35, 21-28.

Cornell, R.M., Schwertmann, U., 2003. The Iron Oxides: Structure, Properties, Reactions, Occurrences and Uses, second ed. John Wiley & Sons, Ltd., New York.

Cutting, R.S., Coker, V.S., Fellowes, J.W., Lloyd, J.R., Vaughan, D.J., 2009. Mineralogical and morphological constraints on the reduction of Fe (III) minerals by *Geobacter sulfurreducens*. Geochim. Cosmochim. Acta, 73, 4004-4022.

De Yoreo, J.J., Gilbert, P.U.P.A., Sommerdijk, N.A.J.M., Penn, R.L., Whitelam, S., Joester, D., Zhang, H., Rimer, J.D., Navrotsky, A., Banfield, J.F., Wallace, A.F., Michel, F.M.,

Meldrum, F.C., Cölfen, H., Dove, P.M., 2015. Crystallization by particle attachment in synthetic, biogenic, and geologic environments. Science, 349.
Ekstrom, E.B., Learman, D.R., Madden, A.S., Hansel, C.M., 2010. Contrasting effects of Al substitution on microbial reduction of Fe (III) (hydr)oxides. Geochim. Cosmochim. Acta, 74, 7086-7099.
Emerson, D., Weiss, J.V., Megonigal, J.P., 1999. Iron-oxidizing bacteria are associated with ferric hydroxide precipitates (Fe-plaque) on the roots of wetland plants. Appl. Environ. Microbiol., 65, 2758-2761.
Ferris, F., Konhauser, K., Lyven, B., Pedersen, K., 1999. Accumulation of metals by bacteriogenic iron oxides in a subterranean environment. Geomicrobiol. J., 16, 181-192.
Ferris, F.G., Hallberg, R., Lyven, B., Pedersen, K., 2000. Retention of strontium, cesium, lead and uranium by microbial iron oxides from a subterranean environment. Appl. Geochem., 15, 1035-1042.
Ford, R.G., Bertsch, P.M., Farley, K.J., 1997. Changes in transition and heavy metal partitioning during hydrous iron oxide aging. Environ. Sci. Technol., 31, 2028-2033.
Fortin, D., Leppard, G.G., Tessier, A., 1993. Characteristics of lacustrine diagenetic iron oxyhydroxides. Geochim. Cosmochim. Acta, 57, 4391-4404.
Fortin, D., Langley, S., 2005. Formation and occurrence of biogenic iron-rich minerals. Earth-Sci. Rev., 72, 1-19.
Fredrickson, J.K., Zachara, J.M., Kennedy, D.W., Dong, H., Onstott, T.C., Hinman, N.W., Li, S.-m., 1998. Biogenic iron mineralization accompanying the dissimilatory reduction of hydrous ferric oxide by a groundwater bacterium. Geochim. Cosmochim. Acta, 62, 3239-3257.
Galvez, N., Barron, V., Torrent, J., 1999. Effect of phosphate on the crystallization of hematite, goethite, and lepidocrocite from ferrihydrite. Clays Clay Miner., 47, 304-311.
Gault, A.G., Ibrahim, A., Langley, S., Renaud, R., Takahashi, Y., Boothman, C., Lloyd, J.R., Clark, I.D., Ferris, F.G., Fortin, D., 2011. Microbial and geochemical features suggest iron redox cycling within bacteriogenic iron oxide-rich sediments. Chem. Geol., 281, 41-51.
Gault, A.G., Langley, S., Ibrahim, A., Renaud, R., Takahashi, Y., Boothman, C., Lloyd, J.R., Clark, I.D., Ferris, F.G., Fortin, D., 2012. Seasonal changes in mineralogy, geochemistry and microbial community of bacteriogenic iron oxides (BIOS) deposited in a circumneutral wetland. Geomicrobiol. J., 29, 161-172.
Glasauer, S., Weidler, P.G., Langley, S., Beveridge, T.J., 2003. Controls on Fe reduction and mineral formation by a subsurface bacterium. Geochim. Cosmochim. Acta, 67, 1277-1288.
Hallberg, R., Ferris, F.G., 2004. Biomineralization by gallionella. Geomicrobiol. J., 21, 325-330.
Hansel, C.M., Benner, S.G., Neiss, J., Dohnalkova, A., Kukkadapu, R.K., Fendorf, S., 2003. Secondary mineralization pathways induced by dissimilatory iron reduction of ferrihydrite under advective flow. Geochim. Cosmochim. Acta, 67, 2977-2992.
Hansel, C.M., Benner, S.G., Nico, P., Fendorf, S., 2004. Structural constraints of ferric (hydr)oxides on dissimilatory iron reduction and the fate of Fe(II). Geochim. Cosmochim. Acta, 68, 3217-3229.
Hansel, C.M., Benner, S.G., Fendorf, S., 2005. Competing Fe(II)-induced mineralization pathways of ferrihydrite. Environ. Sci. Technol., 39, 7147-7153.
Hansel, C.M., Learman, D.R., Lentini, C.J., Ekstrom, E.B., 2011. Effect of adsorbed and substituted al on Fe(II)-induced mineralization pathways of ferrihydrite. Geochim. Cosmochim. Acta, 75, 4653-4666.

Hegler, F., Schmidt, C., Schwarz, H., Kappler, A., 2010. Does a low-ph microenvironment around phototrophic Fe(II)-oxidizing bacteria prevent cell encrustation by Fe(III) minerals? FEMS Microbiol. Ecol., 74, 592-600.

Hyacinthe, C., Bonneville, S., Van Cappellen, P., 2006. Reactive iron(III) in sediments: Chemical versus microbial extractions. Geochim. Cosmochim. Acta, 70, 4166-4180.

James, R.E., Ferris, F.G., 2004. Evidence for microbial-mediated iron oxidation at a neutrophilic groundwater spring. Chem. Geol., 212, 301-311.

Jones, A.M., Collins, R.N., Rose, J., Waite, T.D., 2009. The effect of silica and natural organic matter on the Fe(II)-catalysed transformation and reactivity of Fe(III) minerals. Geochim. Cosmochim. Acta, 73, 4409-4422.

Kappler, A., Newman, D.K., 2004. Formation of Fe(III)-minerals by Fe(II)-oxidizing photoautotrophic bacteria 1. Geochim. Cosmochim. Acta, 68, 1217-1226.

Kappler, A., Straub, K.L., 2005. Geomicrobiological cycling of iron. Reviews in Mineralogy and Geochemistry, 59, 85-108.

Kennedy, C., Martinez, R., Scott, S.D., Ferris, F., 2003. Surface chemistry and reactivity of bacteriogenic iron oxides from axial volcano, juan de fuca ridge, north-east pacific ocean. Geobiology, 1, 59-69.

Kennedy, C.B., Scott, S.D., Ferris, F.G., 2004. Hydrothermal phase stabilization of 2-line ferrihydrite by bacteria. Chem. Geol., 212, 269-277.

Kennedy, C.B., Gault, A.G., Fortin, D., Clark, I.D., Ferris, F.G., 2011. Retention of iodide by bacteriogenic iron oxides. Geomicrobiol. J., 28, 387-395.

Konhauser, K.O., 1997. Microbial iron biomineralisation in nature. FEMS Microbiol. Rev., 20, 315-326.

Kostka, J.E., Luther, G.W., 1994. Partitioning and speciation of solid phase iron in saltmarsh sediments. Geochim. Cosmochim. Acta, 58, 1701-1710.

Langley, S., Beveridge, T.J., 1999. Effect of o-side-chain-lipopolysaccharide chemistry on metal binding. Appl. Environ. Microbiol., 65, 489-498.

Langley, S., Igric, P., Takahashi, Y., Sakai, Y., Fortin, D., Hannington, M.D., Schwarz-Schampera, U., 2009a. Preliminary characterization and biological reduction of putative biogenic iron oxides (BIOS) from the tonga-kermadec arc, southwest pacific ocean. Geobiology, 7, 35-49.

Langley, S., Gault, A., Ibrahim, A., Renaud, R., Fortin, D., Clark, I.D., Ferris, F.G., 2009b. A comparison of the rates of Fe(III) reduction in synthetic and bacteriogenic iron oxides by shewanella putrefaciens cn32. Geomicrobiol. J., 26, 57-70.

Langley, S., Gault, A.G., Ibrahim, A., Takahashi, Y., Renaud, R., Fortin, D., Clark, I.D., Ferris, F.G., 2009c. Strontium desorption from bacteriogenic iron oxides (BIOS) subjected to microbial Fe(III) reduction. Chem. Geol., 262, 217-228.

Langley, S., Gault, A.G., Ibrahim, A., Takahashi, Y., Renaud, R., Fortin, D., Clark, I.D., Ferris, F.G., 2009d. Sorption of strontium onto bacteriogenic iron oxides. Environ. Sci. Technol., 43, 1008-1014.

Loeppert, R.H., Inskeep, W.P., 1996. Iron, in: Sparks, D.L., Page, A.L., Helmke, P.A., Loeppert, R.H. (Eds.), Methods of soil analysis part 3—chemical methods. Sssa book series. Soil Science Society of America, American Society of Agronomy, Madison, WI., pp. 639-664.

Marsili, E., Baron, D.B., Shikhare, I.D., Coursolle, D., Gralnick, J.A., Bond, D.R., 2008. Shewanella secretes flavins that mediate extracellular electron transfer. PNAS, 105, 3968-3973.

Martinez, R.E., Smith, D.S., Pedersen, K., Ferris, F.G., 2003. Surface chemical heterogeneity of bacteriogenic iron oxides from a subterranean environment. Environ. Sci. Technol., 37, 5671-7.

McNamara, N.P., Black, H.I.J., Beresford, N.A., Parekh, N.R., 2003. Effects of acute gamma irradiation on chemical, physical and biological properties of soils. Appl. Soil Ecol., 24, 117-132.

Melton, E.D., Swanner, E.D., Behrens, S., Schmidt, C., Kappler, A., 2014. The interplay of microbially mediated and abiotic reactions in the biogeochemical fe cycle. Nat Rev Micro, 12, 797-808.

Mikutta, C., Mikutta, R., Bonneville, S., Wagner, F., Voegelin, A., Christl, I., Kretzschmar, R., 2008. Synthetic coprecipitates of exopolysaccharides and ferrihydrite. Part I: Characterization. Geochim. Cosmochim. Acta, 72, 1111-1127.

Moon, E.M., Peacock, C.L., 2013. Modelling Cu(II) adsorption to ferrihydrite and ferrihydrite–bacteria composites: Deviation from additive adsorption in the composite sorption system. Geochim. Cosmochim. Acta, 104, 148-164.

Muehe, E.M., Scheer, L., Daus, B., Kappler, A., 2013. Fate of arsenic during microbial reduction of biogenic versus abiogenic As–Fe(III)–mineral coprecipitates. Environ. Sci. Technol., 47, 8297-8307.

Nielsen, S.S., Kjeldsen, P., Hansen, H.C.B., Jakobsen, R., 2014. Transformation of natural ferrihydrite aged in situ in As, Cr and Cu contaminated soil studied by reduction kinetics. Appl. Geochem., 51, 293-302.

O'Loughlin, E.J., Gorski, C.A., Scherer, M.M., Boyanov, M.I., Kemner, K.M., 2010. Effects of oxyanions, natural organic matter, and microbial cell numbers on the bioreduction of lepidocrocite (γ-FeOOh) and the formation of secondary mineralization products. Environ. Sci. Technol., 44, 4570-4576.

Penn, R.L., 2004. Kinetics of oriented aggregation. J. Phys. Chem. B., 108, 12707-12712.

Piepenbrock, A., Schröder, C., Kappler, A., 2014. Electron transfer from humic substances to biogenic and abiogenic Fe(III) oxyhydroxide minerals. Environ. Sci. Technol., 48, 1656-1664.

Posth, N.R., Canfield, D.E., Kappler, A., 2014. Biogenic Fe(III) minerals: From formation to diagenesis and preservation in the rock record. Earth. Sci. Rev., 135, 103-121.

Raiswell, R., Vu, H.P., Brinza, L., Benning, L.G., 2010. The determination of labile Fe in ferrihydrite by ascorbic acid extraction: Methodology, dissolution kinetics and loss of solubility with age and de-watering. Chem. Geol., 278, 70-79.

Rancourt, D.G., Thibault, P.-J., Mavrocordatos, D., Lamarche, G., 2005. Hydrous ferric oxide precipitation in the presence of nonmetabolizing bacteria: Constraints on the mechanism of a biotic effect. Geochim. Cosmochim. Acta, 69, 553-577.

Roden, E.E., Zachara, J.M., 1996. Microbial reduction of crystalline iron(III) oxides: Influence of oxide surface area and potential for cell growth. Environ. Sci. Technol., 30, 1618-1628.

Roden, E.E., Urrutia, M.M., Mann, C.J., 2000. Microbial reductive dissolution of crystalline Fe(III) oxide in continuous-flow column reactors. Appl. Environ. Microbiol., 66, 1062-1065.

Roden, E.E., 2003. Fe(III) oxide reactivity toward biological versus chemical reduction. Environ. Sci. Technol., 37, 1319-1324.

Saini, G., Chan, C., 2013. Near-neutral surface charge and hydrophilicity prevent mineral encrustation of fe-oxidizing micro-organisms. Geobiology, 11, 191-200.

Schwertmann, U., Friedl, J., Stanjek, H., Schulze, D.G., 2000a. The effect of al on Fe oxides. Xix. Formation of Al-substituted hematite from ferrihydrite at 25 c and ph 4 to 7. Clays Clay Miner., 48, 159-172.

Schwertmann, U., Friedl, J., Stanjek, H., Schulze, D., 2000b. The effect of clay minerals on the formation of goethite and hematite from ferrihydrite after 16 years' ageing at 25ºC and pH 4–7. Clay Minerals, 35, 613-623.

Schwertmann, U., Stanjek, H., Becher, H.-H., 2004. Long-term in vitro transformation of 2-line ferrihydrite to goethite/hematite at 4, 10, 15 and 25ºC. Clay Minerals, 39, 433-438.

Stookey, L.L., 1970. Ferrozine---a new spectrophotometric reagent for iron. Anal. Chem., 42, 779-781.

Tessier, A., Fortin, D., Belzile, N., DeVitre, R.R., Leppard, G.G., 1996. Metal sorption to diagenetic iron and manganese oxyhydroxides and associated organic matter: Narrowing the gap between field and laboratory measurements. Geochim. Cosmochim. Acta, 60, 387-404.

Toner, B.M., Santelli, C.M., Marcus, M.A., Wirth, R., Chan, C.S., McCollom, T., Bach, W., Edwards, K.J., 2009. Biogenic iron oxyhydroxide formation at mid-ocean ridge hydrothermal vents: Juan de fuca ridge. Geochim. Cosmochim. Acta, 73, 388-403.

Toner, B.M., Berquó, T.S., Michel, F.M., Sorensen, J.V., Templeton, A.S., Edwards, K.J., 2012. Mineralogy of iron microbial mats from loihi seamount. Front. Microbiol., 3.

Urrutia, M.M., Roden, E.E., Fredrickson, J.K., Zachara, J.M., 1998. Microbial and surface chemistry controls on reduction of synthetic Fe(III) oxide minerals by the dissimilatory iron-reducing bacterium shewanella alga. Geomicrobiol. J., 15, 269-291.

Urrutia, M.M., Roden, E.E., Zachara, J.M., 1999. Influence of aqueous and solid-phase Fe(II) complexants on microbial reduction of crystalline iron(iii) oxides. Environ. Sci. Technol., 33, 4022-4028.

Vollrath, S., Behrends, T., Koch, C.B., Cappellen, P.V., 2013. Effects of temperature on rates and mineral products of microbial Fe(II) oxidation by leptothrix cholodnii at microaerobic conditions. Geochim. Cosmochim. Acta, 108, 107-124.

Vu, H.P., Moreau, J.W., 2015. Thiocyanate adsorption on ferrihydrite and its fate during ferrihydrite transformation to hematite and goethite. Chemosphere, 119, 987-993.

Warren, L.A., Ferris, F.G., 1998. Continuum between sorption and precipitation of Fe (III) on microbial surfaces. Environ. Sci. Technol., 32, 2331-2337.

Yuwono, V.M., Burrows, N.D., Soltis, J.A., Penn, R.L., 2010. Oriented aggregation: Formation and transformation of mesocrystal intermediates revealed. J. Am. Chem. Soc., 132, 2163-2165.

Zachara, J.M., Fredrickson, J.K., Li, S.-M., Kennedy, D.W., Smith, S.C., Gassman, P.L., 1998. Microbial reduction of crystalline Fe3+ oxides in single phase suspensions and subsurface materials. Am. Mineral., 83, 1426-1443.

Tables

Table 2-1: Proportions of iron-bearing phases in fresh and aged BIOS from sites CR-01 and CR-02 determined by best fits of iron K-edge EXAFS spectra.

Table 2-2: Non-sequential chemical extractions of the solid iron phase of aged BIOS from sites CR-01 and CR-02. Also shown are the bioavailable and crystalline iron fractions determined by the ascorbate extraction. Data represent means (± one standard deviation) of 3 replicates for each chemical treatment.

Table 2-3: Chemical composition of aged BIOS from sites CR-01 and CR-02 determined by ammonium oxalate/oxalic acid extraction. Solid phase Fe and loss on ignition (LOI) are expressed in wt%, whereas Al:Fe, Si:Fe, and P:Fe are expressed as mole ratios. Data represent means (± one standard deviation) of 3 replicates for element determination and 2 replicates for LOI.

Table 2-4: Maximum percentage of total Fe reduced, linear reduction rates and correlation coefficients for the linear reduction rates for fresh BIOS from site CR-03 and aged BIOS from sites CR-01 and CR-02. Data represent means (± one standard deviation) of 3 replicate experiments for each BIOS sample collected.

Table 2-1: Proportions of iron-bearing phases in fresh and aged BIOS from sites CR-01 and CR-02 determined by best fits of iron K-edge EXAFS spectra.

	Proportion of Iron-bearing Mineral (%)		
Sample	2-Line ferrihydrite	Lepidocrocite	Goethite
CR-01 Fresh[a]	70	22	8
CR-02 Fresh[a]	61	27	12
CR-01 Aged	71	17	12
CR-02 Aged	76	17	6

[a]Source: Gault et al. (2011).

Table 2-2: Non-sequential chemical extractions of the solid iron phase of aged BIOS from sites CR-01 and CR-02. Also shown are the bioavailable and crystalline iron fractions determined by the ascorbate extraction. Data represent means (± one standard deviation) of 3 replicates for each chemical treatment.

	Solid Phase Iron (mg/gdwt)				Fraction (%)	
Sample	HCl (H)	Ascorbate (A)	Oxalate (O)	Dithionite (D)	Amorphous[a]	Crystalline[b]
CR-01 Aged	190±6	180±10	260±9	270±10	66±5	30±6
CR-02 Aged	320±5	340±15	410±10	470±10	70±4	28±4

[a]Amorphous fraction calculated from: $\left(\frac{A}{D}\right)\times 100$

[b]Crystalline fraction calculated from: $\left(\frac{D-A}{D}\right)\times 100$

Table 2-3: Chemical composition of aged BIOS from sites CR-01 and CR-02 determined by ammonium oxalate/oxalic acid extraction. Solid phase Fe and loss on ignition (LOI) are expressed in wt%, whereas Al:Fe, Si:Fe, and P:Fe are expressed as mole ratios. Data represent means (± one standard deviation) of 3 replicates for element determination and 2 replicates for LOI.

Element	CR-01	CR-02
Fe	20±1	30±2
Al:Fe	0.02±0.001	0.01±0.001
Si:Fe	0.06±0.003	0.08±0.004
P:Fe	0.004±0.001	0.003±0.001
LOI	21±2	28±3

The limits of detection for the elements analyzed (ppm): Fe 0.004, Al 0.001, P 0.009, Si 0.005.

Table 2-4: Maximum percentage of total Fe reduced, linear reduction rates and correlation coefficients for the linear reduction rates for fresh BIOS from site CR-03 and aged BIOS from sites CR-01 and CR-02. Data represent means (± one standard deviation) of 3 replicate experiments for each BIOS sample collected.

Sample	Maximum Fe reduced (%)	Reduction Rate (day^{-1})	R^2
CR-03 Fresh[a]	98±3	0.47±0.02	0.942
CR-01 Aged	60±9	0.23±0.03	0.975
CR-02 Aged	50±10	0.21±0.03	0.960

[a]Source: Langley et al. (2009b).

Figures

Figure 2-1: X-ray diffraction patterns of fresh and aged BIOS from sites CR-01 and CR-02 compared to standard reference lines for 2-line ferrihydrite, lepidocrocite and goethite. The mineralogy of aged BIOS is similar to that of fresh BIOS. The sharp peaks correspond to silicate weathering minerals whereas the broad reflections centered around 1.5 and 2.5Å correspond to 2-line ferrihydrite (F). Other broad peaks correspond to nanoparticulate lepidocrocite (L) and goethite (G). All patterns have been vertically separated on an arbitrary y-axis, for clarity.

Figure 2-2: Normalized iron K-edge EXAFS spectra for aged and fresh BIOS from sites CR-01 and CR-02, and standard minerals. The data for BIOS are displayed as solid black lines while the best fits from linear combinations of standards (listed in Table 1) are represented as dotted red lines. Data for fresh BIOS were obtained from Gault et al. (2011).

Figure 2-3: (A) SEM image of aged BIOS showing the abundance of sheath like structures (arrows) reminiscent of the iron oxidizing bacteria *Leptothrix* spp., scale bar = 2μm. (B) TEM image of aged BIOS in thin section, arrows point to *Leptothrix*-like sheaths in cross-section and longitudinal section, scale bar = 250nm.

Figure 2-4: TEM images of mineralized sheath structures from fresh BIOS (A) and aged BIOS (B-F) in thin section. (C) Arrow points to coarse and possibly crystalline minerals surrounding a sheath structure. (D) and (E) Arrows point to lineations parallel to the orientation of the sheath. (F) Needle or lath-like crystals reminiscent of those belonging to lepidocrocite crystals surrounding a sheath structure, arrows point to oriented lepidocrocite-like crystals which seem to form parallel lineations. All scale bars = 250nm.

Figure 2-5: Changes in total Fe(II)/total Fe (●) and soluble P/total P (○) during the reduction of fresh BIOS from site CR-03 and aged BIOS from sites CR-01 and CR-02 by *S. putrefaciens* CN32. Data markers represent means and standard deviations of 3 replicate experiments. Solid lines represent 3-parameter sigmoid lines of best fit to the data. Correlation coefficients (R^2) of the fitted lines are 0.984 (fresh BIOS from site CR-03), 0.967 (aged BIOS from site CR-01), and 0.967 (aged BIOS from site CR-02). For fresh BIOS, data corresponding to total Fe(II) and P were obtained from Langley et al. (2009b).

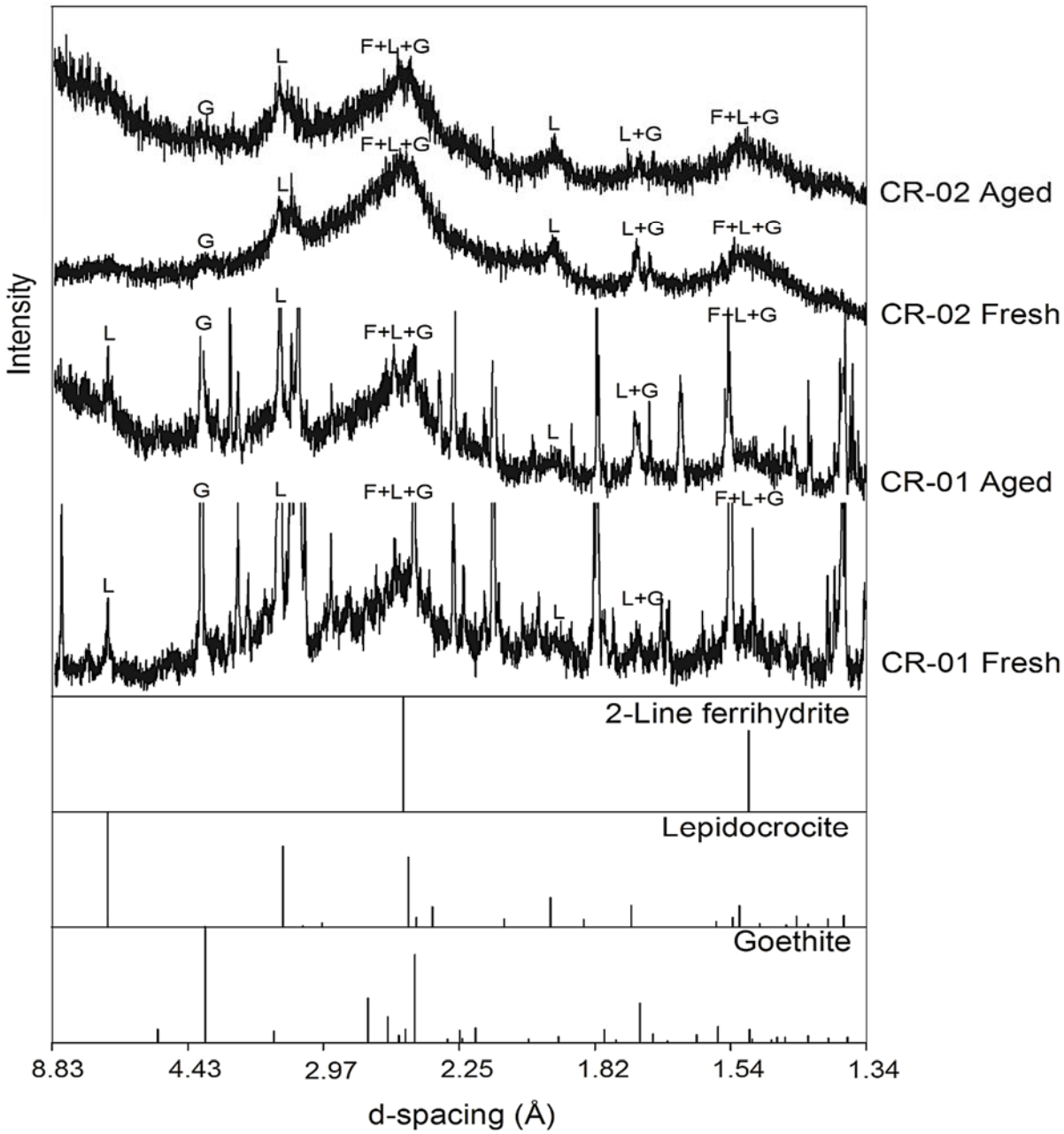

Figure 2-1: X-ray diffraction patterns of fresh and aged BIOS from sites CR-01 and CR-02 compared to standard reference lines for 2-line ferrihydrite, lepidocrocite and goethite. The mineralogy of aged BIOS is similar to that of fresh BIOS. The sharp peaks correspond to silicate weathering minerals whereas the broad reflections centered around 1.5 and 2.5Å correspond to 2-line ferrihydrite (F). Other broad peaks correspond to nanoparticulate lepidocrocite (L) and goethite (G). All patterns have been vertically separated on an arbitrary y-axis, for clarity.

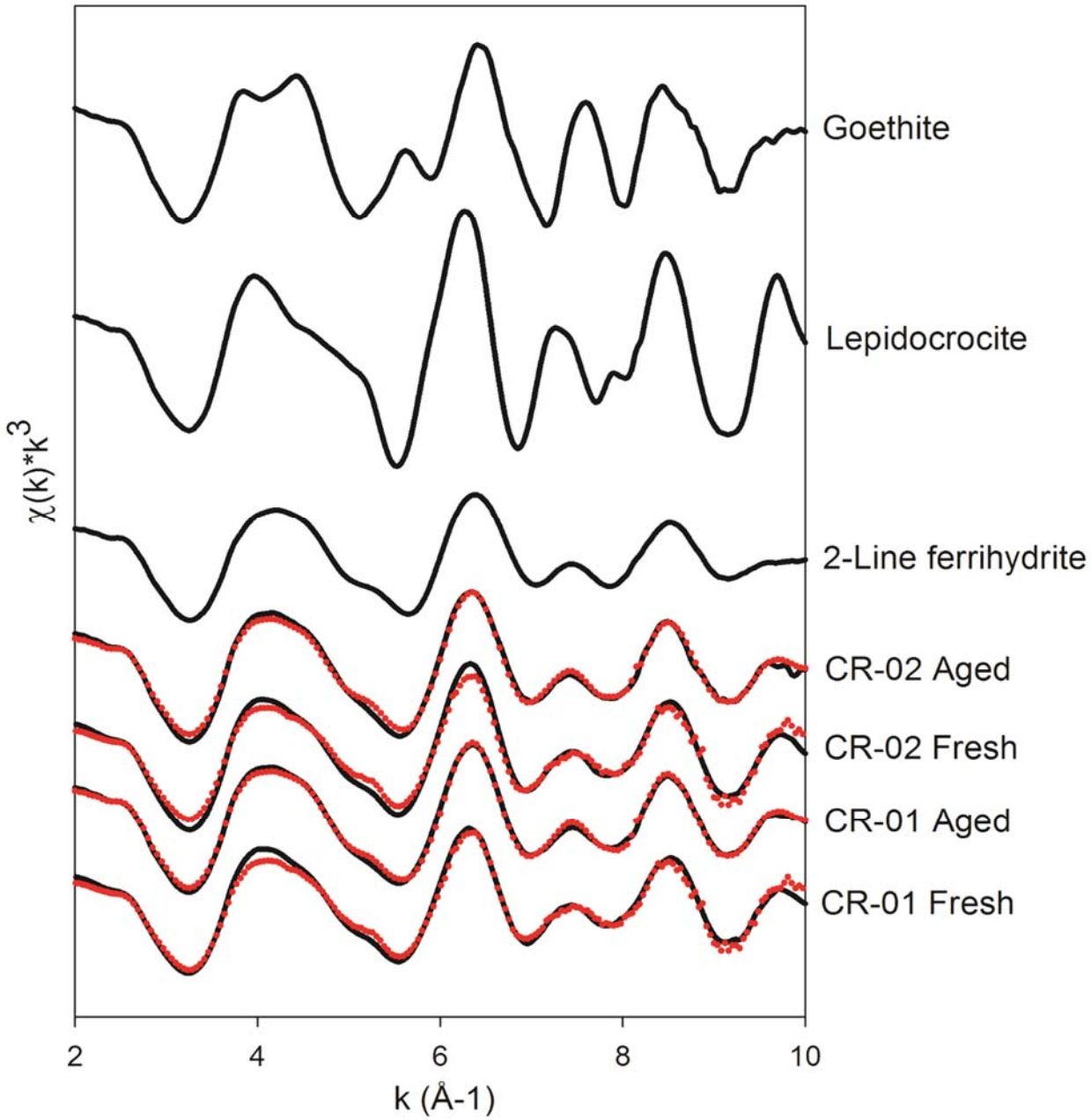

Figure 2-2: Normalized iron K-edge EXAFS spectra for aged and fresh BIOS from sites CR-01 and CR-02, and standard minerals. The data for BIOS are displayed as solid black lines while the best fits from linear combinations of standards (listed in Table 1) are represented as dotted red lines. Data for fresh BIOS were obtained from Gault et al. (2011).

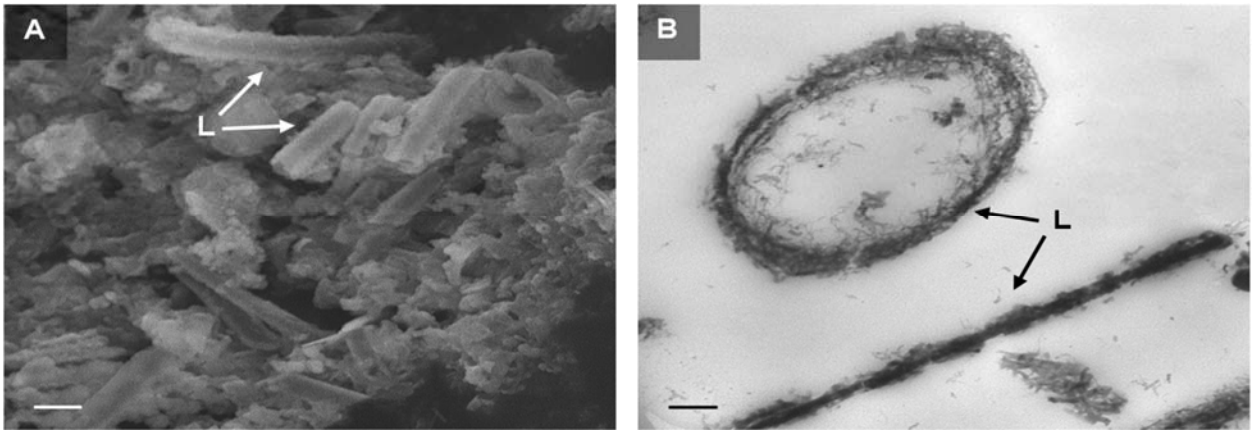

Figure 2-3: (A) SEM image of aged BIOS showing the abundance of sheath like structures (arrows) reminiscent of the iron oxidizing bacteria *Leptothrix* spp., scale bar = 2μm. (B) TEM image of aged BIOS in thin section, arrows point to *Leptothrix*-like sheaths in cross-section and longitudinal section, scale bar = 250nm.

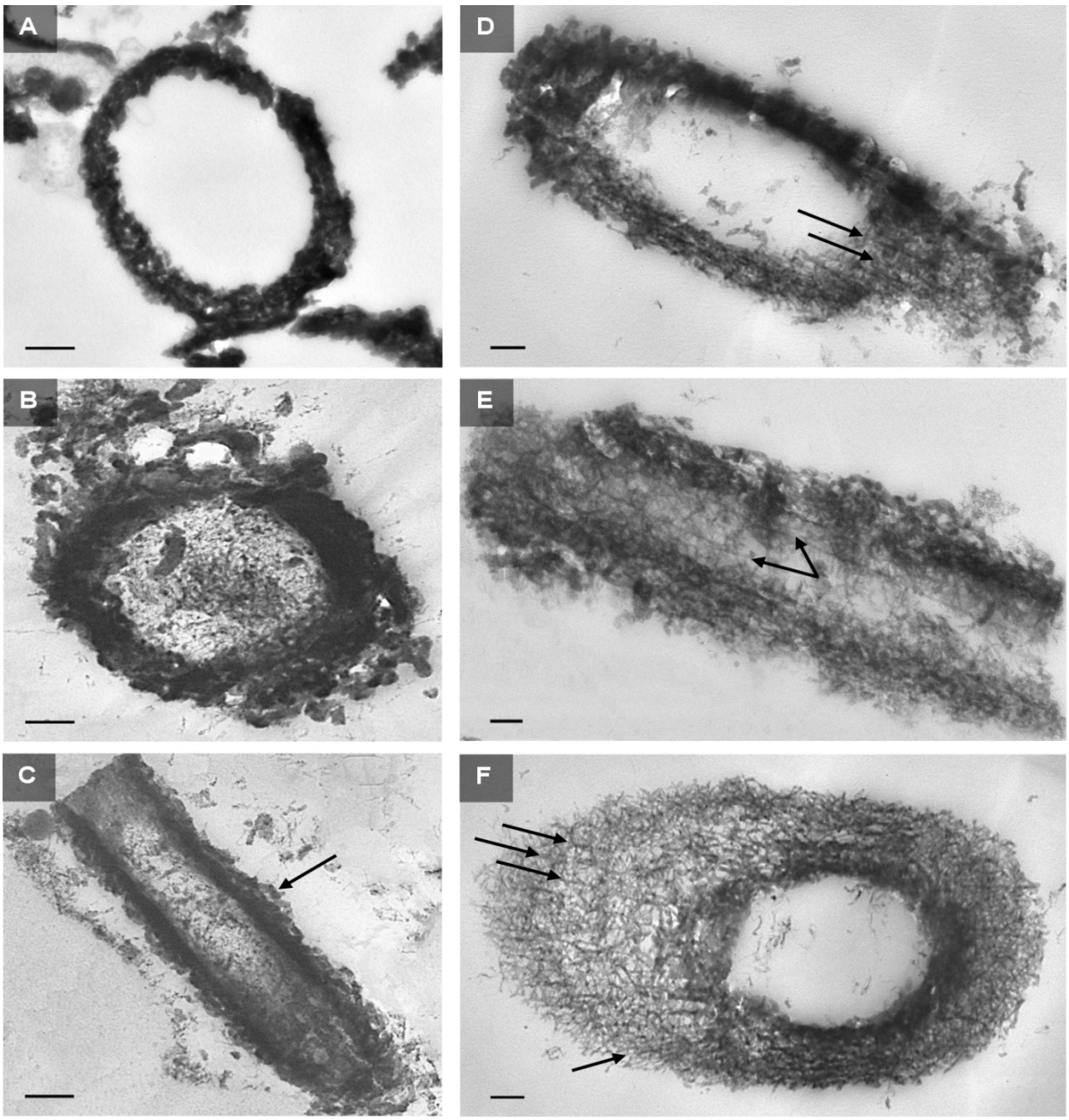

Figure 2-4: TEM images of mineralized sheath structures from fresh BIOS (A) and aged BIOS (B-F) in thin section. (C) Arrow points to coarse and possibly crystalline minerals surrounding a sheath structure. (D) and (E) Arrows point to lineations parallel to the orientation of the sheath. (F) Needle or lath-like crystals reminiscent of those belonging to lepidocrocite crystals surrounding a sheath structure, arrows point to oriented lepidocrocite-like crystals which seem to form parallel lineations. All scale bars = 250nm.

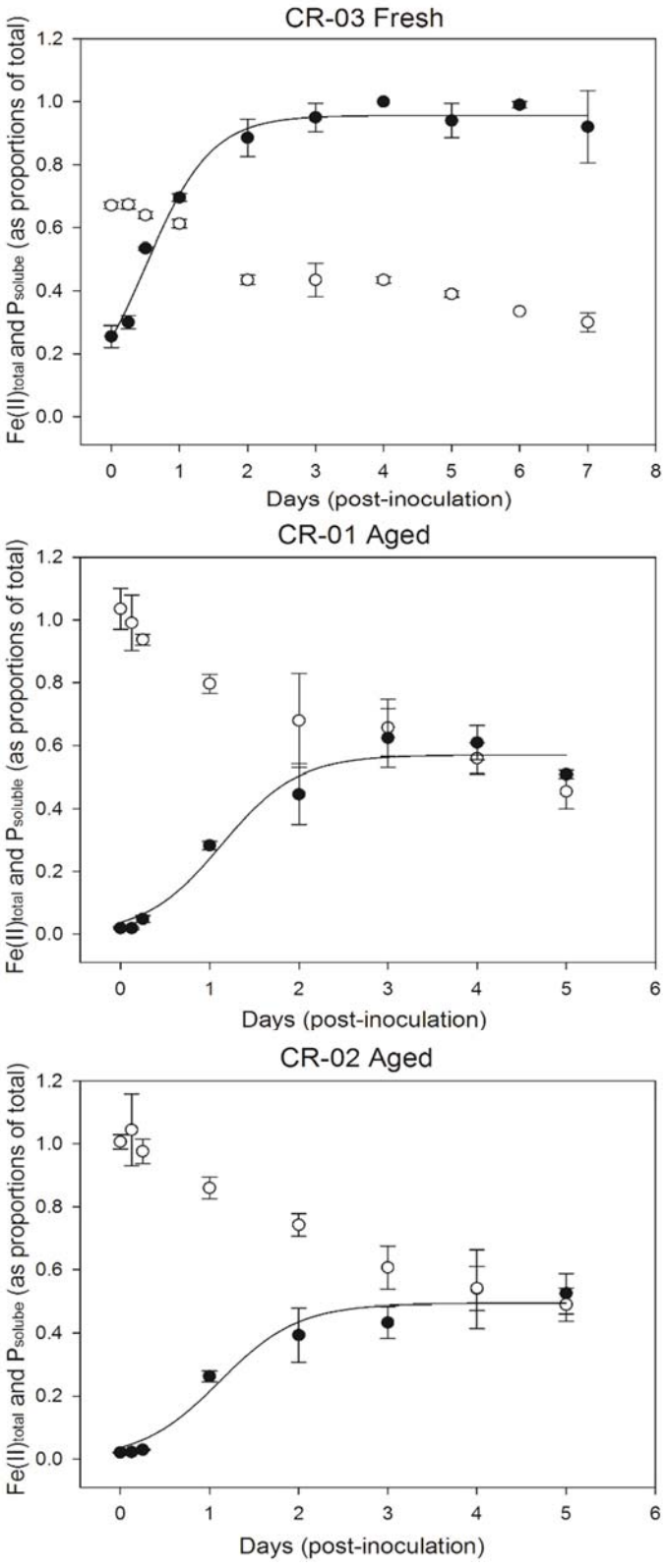

Figure 2-5: Changes in total Fe(II)/total Fe (●) and soluble P/total P (○) during the reduction of fresh BIOS from site CR-03 and aged BIOS from sites CR-01 and CR-02 by *S. putrefaciens* CN32. Data markers represent means and standard deviations of 3 replicate experiments. Solid lines represent 3-parameter sigmoid lines of best fit to the data. Correlation coefficients (R^2) of the fitted lines are 0.984 (fresh BIOS from site CR-03), 0.967 (aged BIOS from site CR-01), and 0.967 (aged BIOS from site CR-02). For fresh BIOS, data corresponding to total Fe(II) and P were obtained from Langley et al. (2009b).

Supplementary material

A comparison of Fe(III) reduction rates between fresh and aged biogenic iron oxides (BIOS) by *Shewanella putrefaciens* CN32

Tarek Najem[a], Sean Langley[b], Danielle Fortin[a*]

[a] Department of Earth and Environmental Sciences, University of Ottawa, 25 Templeton St., Ottawa, Ontario, Canada K1N 6N5
[b] Natural Resources Canada, Canmet MINING, 555 Booth Street, Ottawa, Ontario, Canada, K1A 0G1

[*] Corresponding author: dfortin@uottawa.ca

Table S1: Phyiscochemical parameters of groundwater-derived surface waters measured at Chalk River sites CR-01 and CR-02 during the spring of 2007. Data obtained from Gault et al. (2012).

Site	pH	Eh (mV)	Temp (ºC)	Dissolved O_2 (µM)	Fe (µM)	Fe(II) (µM) [a]	Si (µM)
CR-01	6.02	+247	8.0	155	77.7	85.1	178
CR-02	6.14	+248	8.4	342	30.7	35.8	196

[a] Dissolved Fe(II) exceeded total dissolved Fe by 10-17%.

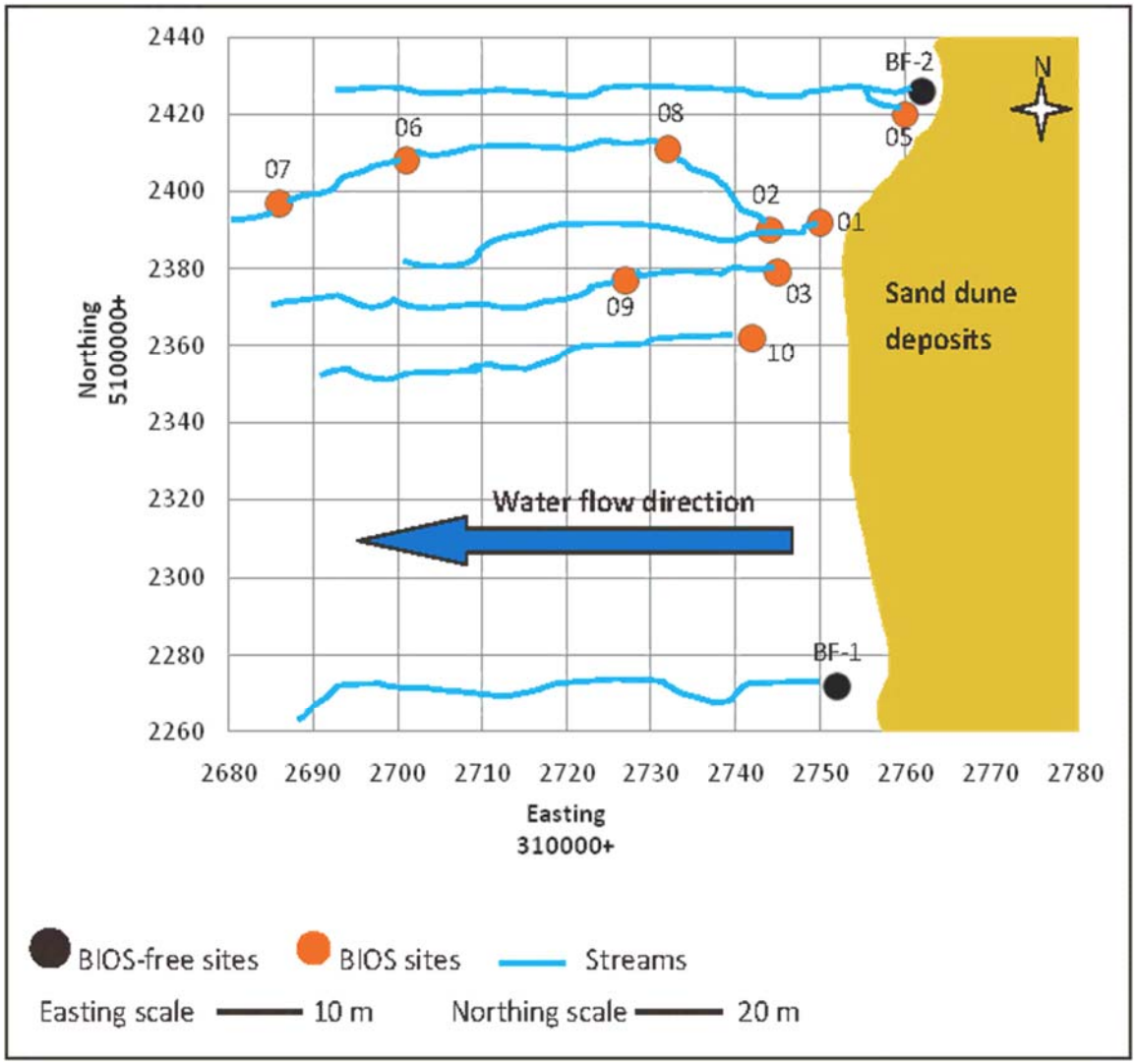

Figure S1: Map of the circumneutral-pH wetland located on the property of the Canadian Nuclear Laboratories (CNL) in Chalk River, Ontario, Canada representing the sites (marked circles) from which BIOS were collected. Sampling points were mapped with UTM coordinates. Data obtained from Ibrahim and Fortin (2010).

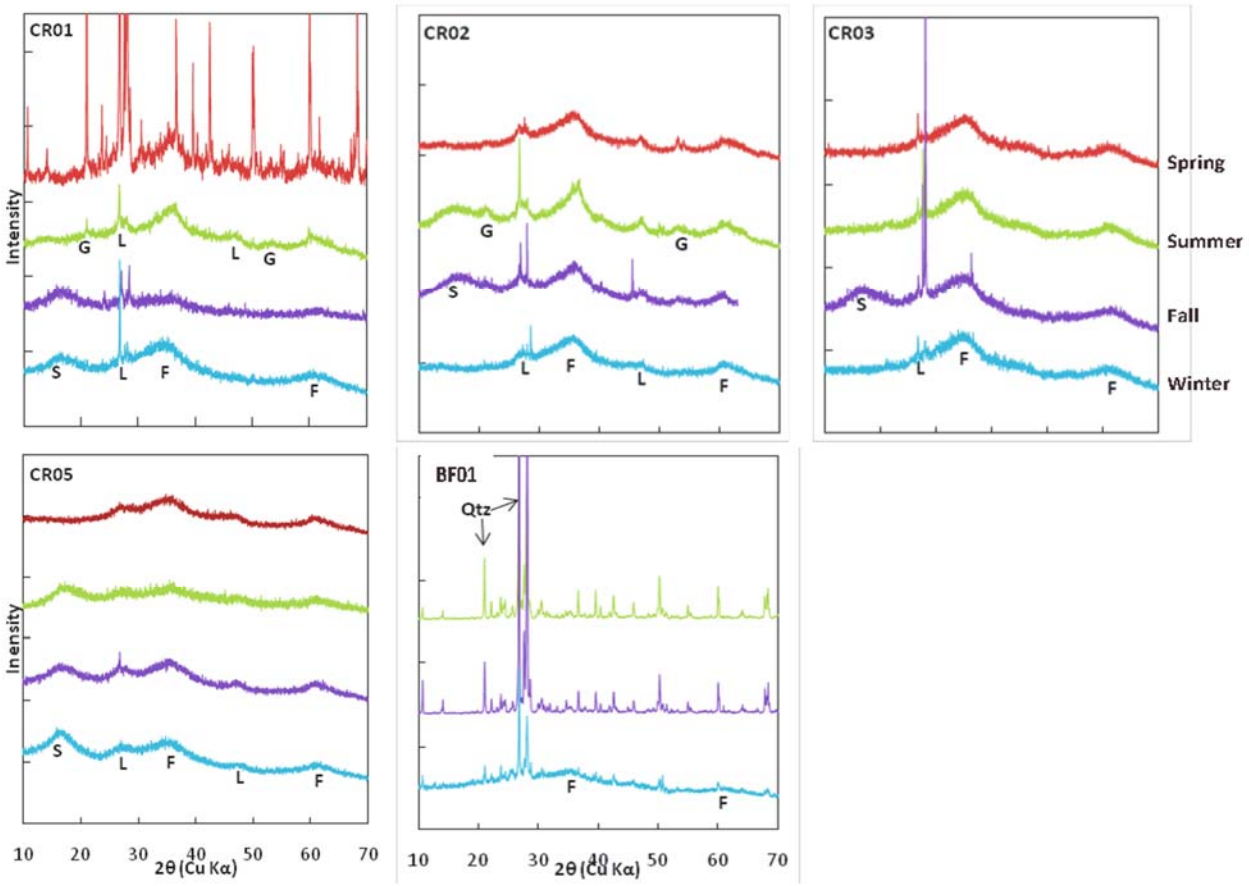

Figure S2: Seasonal x-ray diffraction patterns of BIOS collected from the different sites spaced throughout the circumneutral-pH wetland. The BIOS collected from the different locations are dominated by 2-line ferrihydrite (F) with minor amounts of lepidocrocite (L) and goethite (G). S corresponds to the sample holder. Sharper peaks correspond to silicate weathering minerals. Data obtained from Ibrahim and Fortin (2010).

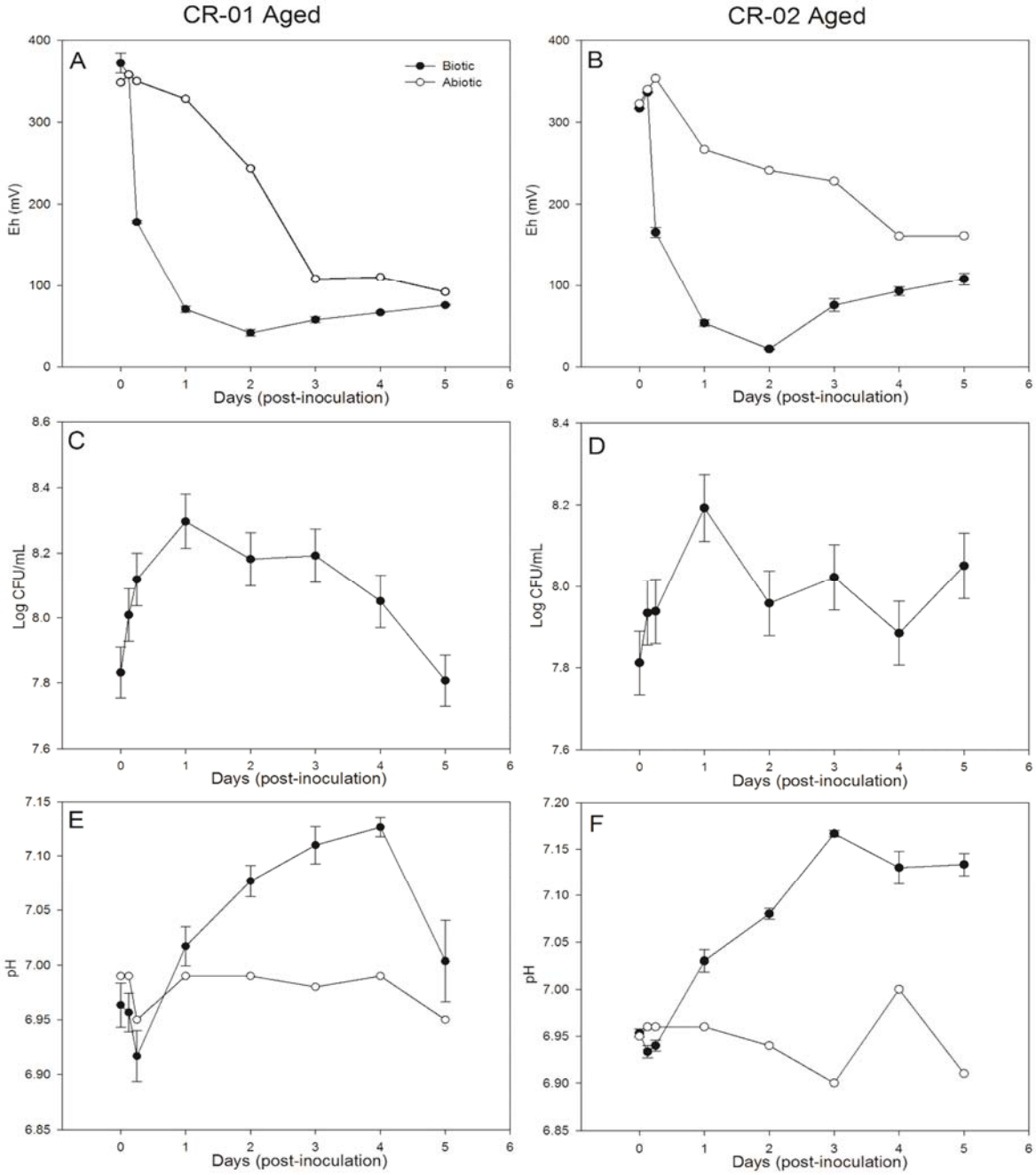

Figure S3: Changes in redox potential (Eh, mV), cell concentration of *Shewanella putrefaciens* CN32 (CFU/mL), and pH during the reduction of aged BIOS from sites CR-01 (A, C, and E) and CR-02 (B, D, and F). Biotic (●) refers to microcosms inoculated with iron-reducing bacteria whereas abiotic (○) refers to microcosms without bacteria. No growth of bacteria in abiotic microcosms was observed. Data markers corresponding to biotic microcosms represent means and standard deviations of 3 replicate experiments.

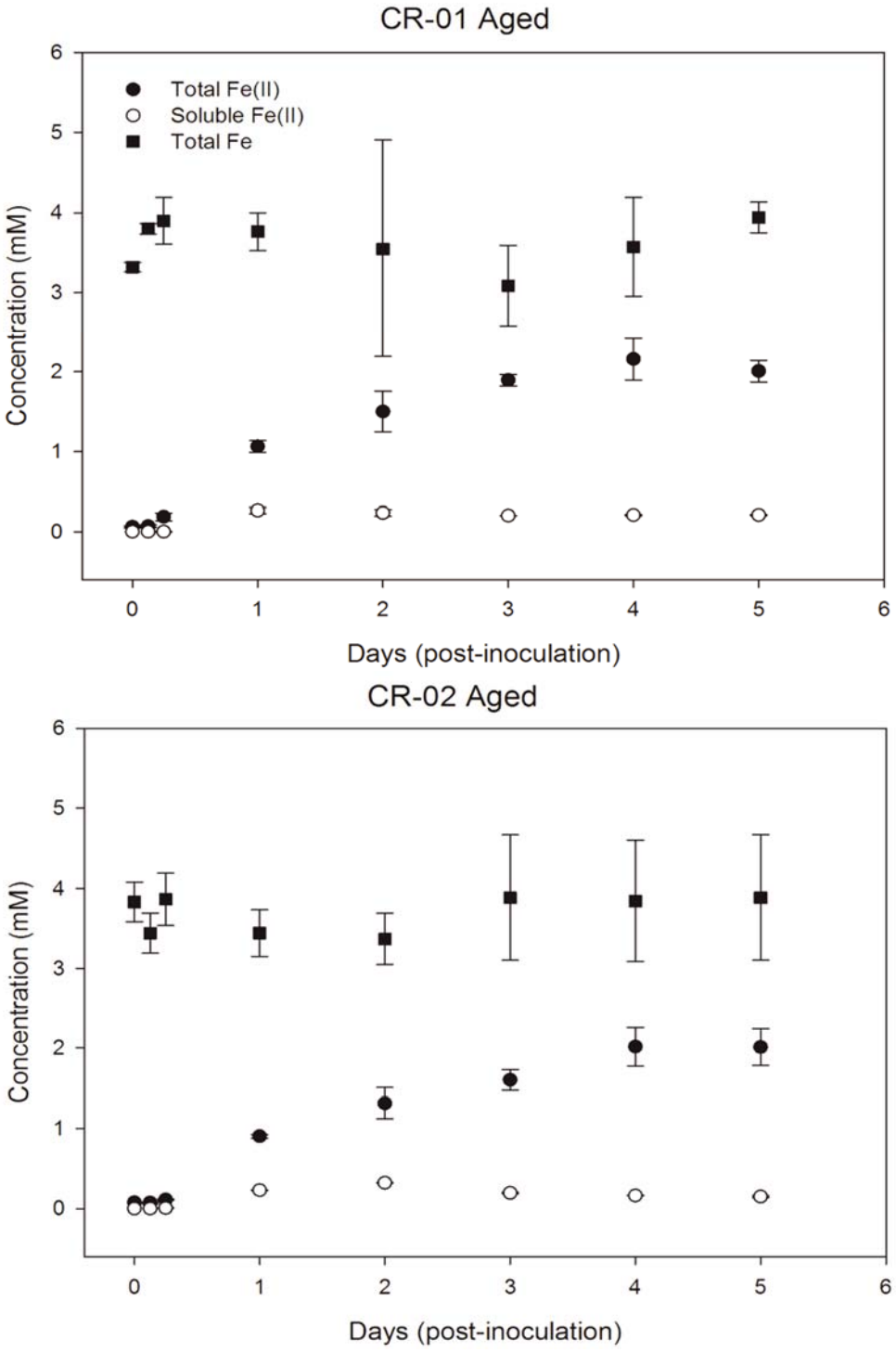

Figure S4: Changes in total Fe(II) and soluble Fe(II) during the microbial reduction of aged BIOS collected from sites CR-01 and CR-02 by the iron reducing bacteria *Shewanella putrefaciens* CN32. Also shown total Fe.

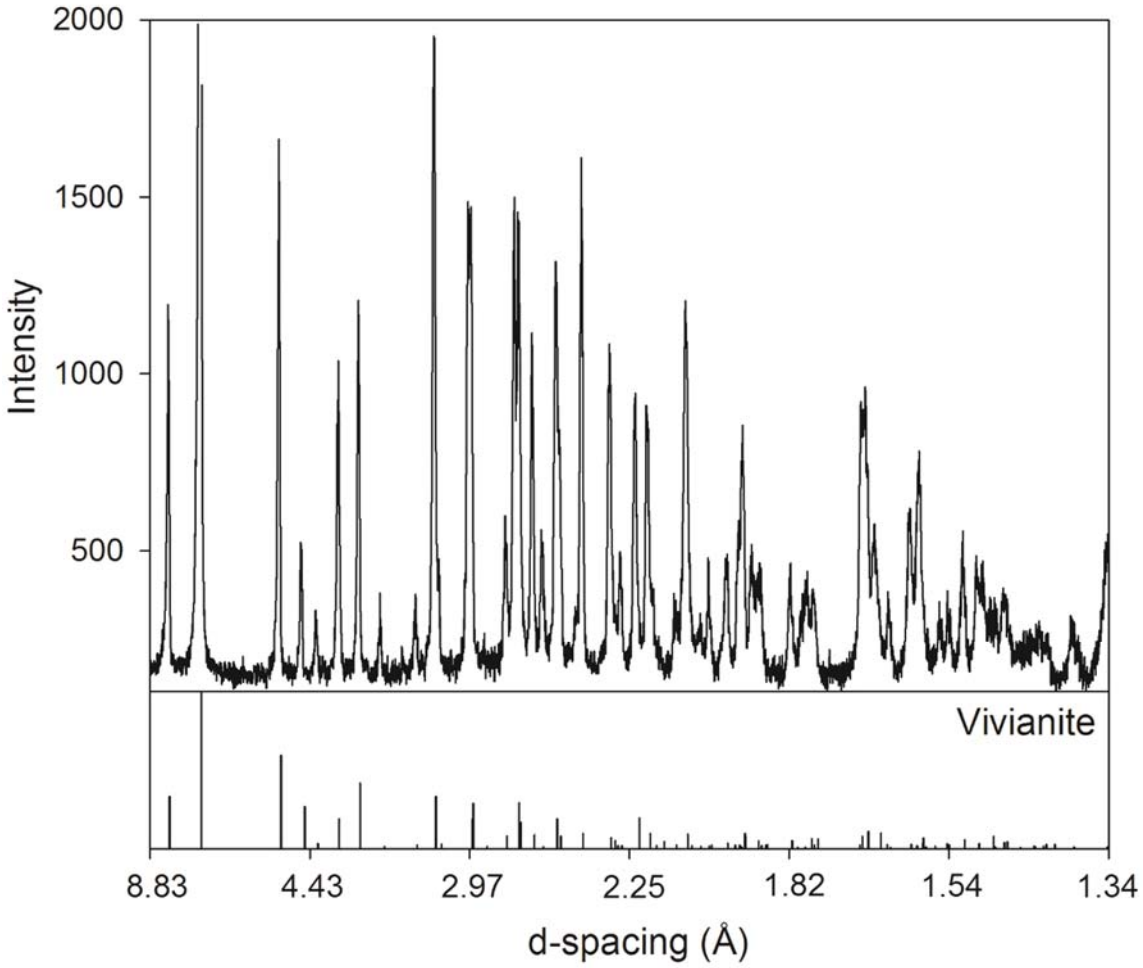

Figure S5: X-ray diffraction pattern of post-reduction iron mineral precipitates remaining after the reduction of aged BIOS, which indicates the formation of the crystalline Fe(II) mineral vivianite ($Fe_3(PO_4)_2 \cdot 8H_2O$).

References

Gault, A.G., Langley, S., Ibrahim, A., Renaud, R., Takahashi, Y., Boothman, C., Lloyd, J.R. Clark, I.D., Ferris, F.G., Fortin, D., 2012. Seasonal changes in mineralogy, geochemistry and microbial community of bacteriogenic iron oxides (bios) deposited in a circumneutral wetland. Geomicrobiology Journal, 29, 161-172.

Ibrahim, A. and Fortin, D., 2010. Biogeochemical mapping of bacteriogenic iron oxides in a freshwater wetland at Chalk River, Ontario, Canada. Master's thesis, University of Ottawa, pp 70.

Chapter 3: Effects of γ-irradiation and varying concentrations of phosphate and molybdate on the stability and reactivity of biogenic iron oxides (BIOS) in the presence of *Shewanella putrefaciens* CN32

Tarek Najem[a], Maeve Moriarty[a], Danielle Fortin[a]

[a] Department of Earth and Environmental Sciences, University of Ottawa, 25 Templeton St., Ottawa, Ontario, Canada K1N 6N5

To be submitted to a journal (*Chemical Geology*)

Abstract

This study investigated the effects of phosphate at environmentally relevant (10μM) and excess (3.9mM) concentration, and varying concentrations of molybdate (0, 0.14, or 0.28mM) on the rate and extent of Fe(III) reduction of synthetic 2-line ferrihydrite and biogenic iron oxides (BIOS) that have been frozen for ~2 years at -15ºC in the presence of a well characterized dissimilatory iron reducing bacteria, *Shewanella putrefaciens* CN32. This study also investigated the impact of sterilization by γ-irradiation at a dose of 14kGy on the susceptibility of frozen BIOS towards microbial reduction. The concentration of phosphate had contrasting effects on the rates of Fe(III) reduction, but, overall, excess concentration enhanced the extent of Fe(III) reduction. Likewise, molybdate had contrasting effects on the rates and extent of Fe(III) reduction, the effects of which depended on the concentration of phosphate and, in the case of BIOS, the presence of intermixed cell derived organic matter. It was also found that the concentration of phosphate and molybdate, and in the case of BIOS, the intermixed cell derived organic matter, influenced the formation of a specific secondary iron mineral phase. The effects of phosphate and intermixed cell derived organic on the rates and extent of BIOS reduction, as well as the formation of secondary iron minerals have important implications on the mobility and fate of contaminants in the environment. Sterilization by γ-irradiation eliminated all culturable native bacteria and had no significant impact on the mineralogy of BIOS, as well as the susceptibility of BIOS towards microbial reduction. Freezing of BIOS was found to promote the aggregation of iron oxide nanoparticles which reduced the susceptibility of BIOS towards microbial reduction. The effects of freezing on the reactivity of BIOS, which is a natural phenomenon in the environment, have to be considered within the framework of iron biogeochemistry.

1. Introduction

Fe(III) oxides, Fe(III) hydroxides, and Fe(III) oxyhydroxides (henceforth referred to as iron oxides) such as hematite (Fe_2O_3), ferrihydrite (approx. $Fe(OH)_3$), and goethite (α-FeOOH), are key mineral assemblages in soils, sediments, and aqueous environments. Due to their abundance in the environment and high surface reactivity, iron oxides are well known for their ability to control the mobility and bioavailability of various (in)organic contaminants, nutrients, and trace metals primarily through sorption reactions (Tessier et al., 1996; Cornell and Schwertmann, 2003; Baken et al., 2015). In addition to regulating the geochemistry of various environments, iron oxides serve as terminal electron acceptors for dissimilatory iron reducing bacteria (DIRB) with ferrihydrite being the principal form of Fe(III) utilized by DIRB, primarily as a result of its high reactivity and surface area in comparison to other Fe(III) phases (Roden and Zachara, 1996; Lovley et al., 2004; Hansel et al., 2004; Bonneville et al., 2004; Bonneville et al., 2009). Under anaerobic conditions, DIRB couple the oxidation of organic matter to the reductive dissolution of iron oxides generating energy for growth and function, and Fe(II) (Lovley et al., 2004). Through this process, DIRB mediate a number of reactions that have important consequences on subsurface environments. For example, DIRB are capable of coupling the oxidation of aromatic hydrocarbons to the reduction of Fe(III) playing a role in the bioremediation of contaminated environments (Lovley et al., 2004), whereas the reduction of iron oxides may lead to the re-mobilization of adsorbed toxic contaminants, which can have detrimental impacts as prominently discussed for As (Cummings et al., 1999; Islam et al., 2004; Tufano et al., 2008; Borch et al., 2009; Masue-Slowey et al., 2011; Muehe et al., 2013a). Adding to the complexity of these systems, is the tendency of "biogenic" Fe(II) to interact with the surface of Fe(III) minerals enhancing the reductive capacity of Fe(II) towards redox sensitive (in)organic contaminants

influencing their mobility and toxicity (Buerge and Hug, 1999; McCormick et al., 2002; Lee and Batchelor, 2002; Borch et al., 2009), but also mediating the dynamic recrystallization of thermodynamically stable and crystalline iron oxide phases (e.g. goethite and hematite) leading to the release or structural incorporation of metal contaminants (Cooper et al., 2000; Cooper et al., 2005; Frierdich and Catalano, 2012a; Frierdich and Catalano, 2012b; Boland et al., 2014). In contrast, the interaction of biogenic Fe(II) with the poorly crystalline and thermodynamically unstable iron oxide, ferrihydrite, catalyzes its transformation into secondary iron minerals such as lepidocrocite, goethite, magnetite, and green rust (Fredrickson et al., 1998; Cornell and Schwertmann, 2003; Hansel et al., 2003a; Hansel et al., 2004; Hansel et al., 2005; Hansel et al., 2011). Depending on the conditions, however, Fe(II) may also precipitate as discrete Fe(II)-bearing secondary iron minerals such as siderite, or vivianite (Fredrickson et al., 1998; Zachara et al., 1998; Zachara et al., 2002). The formation of secondary iron minerals have important consequences on subsurface environments, in particular goethite, magnetite, and green rust, as they are capable of transforming and/or sequestering the released contaminants (ex. Sr, Zn, Ni, Cd, and As) (Cooper et al., 2000; Parmar et al., 2000; Parmar, 2001; Roden et al., 2002; Kocar et al., 2006; Tufano et al., 2008; Borch et al., 2009; Muehe et al., 2013c; Muehe et al., 2013a; Muehe et al., 2013b), and their potential to influence the biogeochemical cycling of organic carbon (Tang et al., 2016). In addition, although the transformation of ferrihydrite into the crystalline phases goethite or magnetite, which possess lower surface area may result in less reactive site density available to bind contaminants, the incorporation of contaminants into the structure of these phases during transformation may be particularly desirable because they are recalcitrant to microbial Fe(III) reduction (Roden and Zachara, 1996; Fredrickson et al., 1998; Hansel et al., 2003a; Hansel et al., 2004). Therefore, given the ecological and environmental importance of microbial Fe(III)

reduction, an extensive amount of research has been conducted to determine the factors that influence the rate and extent of reduction of iron oxides, as well as the secondary iron mineral products that form.

The effects of phosphate in particular have been extensively studied, primarily as a result of its strong and common association with iron oxides in the environment, but as a nutrient it is also of environmental concern where excessive fertilization of agricultural land occurs (Baken et al., 2015). The addition of phosphate may promote microbial Fe(III) reduction by functioning as a nutrient thereby stimulating the growth and activity of DIRB (Fredrickson et al., 1998; Glasauer et al., 2003; Kukkadapu et al., 2004), or inhibit microbial Fe(III) reduction by blocking available sites on the mineral surface (Borch et al., 2007; O'Loughlin et al., 2010; Amstaetter et al., 2012). Nonetheless, the addition of phosphate affects the identity and proportion of secondary iron minerals. For example, Fredrickson et al. (1998) compared the rate and extent of reduction of 2-line ferrihydrite in the presence (~3.9mM) and absence of phosphate, and found that phosphate, in the presence of electron shuttles, enhanced the rate and extent of Fe(III) reduction, and promoted the formation of vivianite and green rust at the expense of magnetite. In contrast, Borch et al. (2007) found that increasing the amount of pre-adsorbed phosphate to the surface of 2-line ferrihydrite significantly lowered the extent of Fe(III) reduction, and promoted the formation of magnetite and green-rust at the expense of goethite, while preserving a significant proportion of 2-line ferrihydrite. While these studies and several others revealed the intricate biomineralization pathways of iron oxides with varying concentrations of phosphate, these studies utilized pure synthetic iron oxides as terminal electron acceptors.

Within natural environments iron oxides rarely exist as pure phases, instead they are often closely associated with impurities (e.g. Al, Si) and organic matter, in particular intact and/or

partially degraded microbial cells and extracellular polymeric substances (Fortin et al., 1993; Cornell and Schwertmann, 2003; Chan et al., 2004; Chan et al., 2009). Such mixture of minerals and cell derived organic matter, termed biogenic iron oxides (BIOS), forms as a consequence of metabolic and chemical oxidation of Fe(II) to Fe(III) and the subsequent precipitation of iron oxides on or in close proximity of cell derived organic matter (Chan et al., 2004; Fortin and Langley, 2005; Ferris, 2005; Chan et al., 2009; Chan et al., 2011; Melton et al., 2014). The most common iron oxide phase that precipitates is 2-line ferrihydrite, but also minor amounts of lepidocrocite and/or goethite comprising the remainder (<30% of total Fe) (Chan et al., 2011; Gault et al., 2011). BIOS form in a broad range of environments, e.g. ferriferous groundwater discharge zones (James and Ferris, 2004; Gault et al., 2011), and they possess properties distinct from their synthetic mineral counterparts. BIOS possess lower crystallinity and smaller particle size (Châtellier et al., 2001; Châtellier et al., 2004), different morphologies (Posth et al., 2014), and an overall negative surface charge compared to synthetic iron oxides which are positively charged under pH-neutral conditions (Kleinert et al., 2011). Consequently, BIOS exhibit different sorptive capacity and properties towards metal(loid)s, and susceptibility towards microbial Fe(III) reduction. Recent studies have shown that BIOS are capable of immobilizing a significant amount of metal(loid)s under laboratory and natural conditions (Ferris et al., 1999; Ferris et al., 2000; Langley et al., 2009a; Fabisch et al., 2016; Hao et al., 2016), but they are particularly more susceptible to microbial Fe(III) reduction than a mineralogically similar synthetic iron oxide (Langley et al., 2009b; Langley et al., 2009c), which has been attributed to, in part, the presence of cell derived organic matter. This suggests that any contaminants associated with BIOS could be easily remobilized into the environment as demonstrated by Langley et al. (2009c). However, while these studies assessed the reactivity of BIOS and the fate of metal contaminants associated

with BIOS under reducing conditions, these studies were conducted under conditions that poorly represent the environment, i.e., high concentration of phosphate (3.9mM), conditions which likely enhance the metabolic activity of DIRB and favor the formation of vivianite (Langley et al., 2009b; Langley et al., 2009c; Langley et al., 2009d). Thus, the influence of varying concentration of phosphate on the rate and extent of reduction of BIOS, as well as the identity and properties of the mineral products that form has not been investigated. In addition to influencing the properties and enhancing the reduction of BIOS, cell derived organic matter was previously shown to stabilize BIOS against phase transformation under various conditions (Banfield et al., 2000; Kennedy et al., 2004; Najem et al., 2016). Therefore, it is expected that the intermixed organic fraction to influence the formation of secondary iron minerals.

Studies conducted to date to determine the reactivity of BIOS have been carried out utilizing naturally occurring BIOS, necessitating the need to sterilize the samples in order to prevent reactions mediated by the native microbial communities during storage and experimental duration (Langley et al., 2009b; Langley et al., 2009c; Langley et al., 2009d). These studies utilized gamma(γ)-irradiation as a sterilization technique at doses ranging from 14 to 48kGy (Langley et al., 2009b; Langley et al., 2009c; Langley et al., 2009d). Although the effects of γ-irradiation on the physicochemical properties of soils and sediments have been extensively studied (McNamara et al., 2003), the reported effects are somewhat conflicting. While some studies identify γ-sterilization as an effective and minimally invasive technique, others suggest otherwise indicating that irradiation driven alteration of the physicochemical properties of soils/sediments may be related to the properties, mineralogy and organic matter content of the soil/sediment (McNamara et al., 2003; Schaller et al., 2011). Reported irradiation induced changes at doses ranging from 10-60kGy include: the radiolytic degradation of complex organic matter leading to the increase in

dissolved organic matter and nutrients (Salonius et al., 1967; Tuominen et al., 1994; Bank et al., 2008; Berns et al., 2008; Schaller et al., 2011; Brown et al., 2015), decrease or increase in surface area (Lotrario et al., 1995; Berns et al., 2008), decrease in aggregation state of soils (Berns et al., 2008), reduction of lattice Fe(III) in clays and goethite (Plötze et al., 2003; Bank et al., 2008), and modification of cation exchange capacity leading to enhanced desorption or adsorption of contaminants (Plötze et al., 2003; Bank et al., 2008; Schaller et al., 2011; Borisover et al., 2016). At similar doses, however, others found no significant changes in surface area or bulk mineralogy (Wolf et al., 1989; Herbert et al., 2005; Langley et al., 2009b). Recently, the exposure of synthetic 2-line ferrihydrite and hematite to a high dosage of γ-irradiation (1 MGy) was found to alter their crystalline structure, and enhance their bioavailability to microbial Fe(III) reduction in the presence of an electron shuttle (Brown et al., 2014). Even at lower doses (0.6 and 38.6 kGy), however, γ-irradiation may have enhanced the bioavailability of Fe(III) to microbial reduction in sediments (Brown et al., 2015). Thus, radiation driven alteration of the physicochemical properties and oxidation state of iron may lead to an over-or under-estimation of their reactivity and may in turn influence the secondary iron products that form during microbial Fe(III) reduction. The effects of γ-irradiation on the physicochemical properties and reactivity of BIOS have not been investigated. If γ-irradiation does indeed alter the reactivity of BIOS, rates of reduction of γ-irradiated BIOS from past studies may not reflect the true reactivity of BIOS. Therefore, research into the effects of γ-irradiation on BIOS is required.

In the present study, we investigate the effects of phosphate at high (3.9mM) and environmentally relevant (10μM, Praharaj and Fortin, 2008) concentrations on the rate and extent of reduction of BIOS in the presence of a model DIRB, *Shewanella putrefaciens* CN32, and characterize the secondary iron minerals that form. We also assess the impact of γ-irradiation on

the reactivity of BIOS towards microbial Fe(III) reduction. Such knowledge would be useful to predict the reactivity of BIOS and the identity of the secondary iron minerals that form under environmentally relevant conditions, and in turn the possible impact on contaminant mobility in the environment.

2. Material and methods

2.1. Site description, sample collection and preparation

BIOS samples were collected from the grounds of the New Calumet Mine located on the Grand Calumet Island, Quebec, Canada. Throughout the 26 years of operation (1944-1970), ~3.8 million tonnes of massive sulfide ore deposits consisting of sphalerite, galena, and pyrrhotite were extracted, and a total of ~2.5 million tonnes of mine tailings were deposited on site and distributed between three piles (MacLatchy, 2013). The three piles were previously given the names: the Gobi Desert, Mount Sinai, and the Beaver Dam (MacLatchy, 2013). Visual observations of the mine tailings suggest that they are rich in iron oxides indicating that significant oxidation in the upper layers had occurred. The tailings are, however, slightly alkaline (pH 7-8.5), which is due to the presence of carbonate-rich minerals in the host bedrock (Moorhouse, 1941; Praharaj and Fortin, 2008). Extensive BIOS deposits form where anoxic, pH-neutral, and Fe(II)-rich groundwater is discharged along the base of the Beaver Dam tailings. The BIOS form at shallow depths (~5cm) near the groundwater discharge point and at greater depths (~0.5m) further downstream. BIOS were collected from four sites spaced throughout the BIOS impacted wetland. The first site, abbreviated as CA-04, was situated within 2-3m of the groundwater discharge point at the base of the tailings, whereas sites CA-03, CA-02, and CA-01 were situated approximately 4-5, 15, and 35m downstream from CA-04, respectively. A detailed description of the sampling sites along with the physicochemical parameters of the surface waters, sampling methods, and processing can be

found in Cotroneo and Fortin (2013) (see Table S1 for selected physicochemical parameters of groundwater-derived surface waters measured for sample sites with BIOS deposition). For the present study, the BIOS samples were collected during the spring of 2013 from sites CA-04 and CA-03 and stored in the dark at -15ºC for ~2 years in order to avoid the microbial transformation of BIOS during storage. BIOS were stored at -15ºC because we previously found that the long-term storage of non-sterile BIOS at 4ºC led to the change of the colour of BIOS from orange-brown to black, suggesting the formation of iron sulfide species as a consequence of the activity of sulfate reducing bacteria (SRB) (Praharaj and Fortin, 2008). Frozen subsamples were later sterilized by γ-irradiation at a dose rate of 0.8-1.0 kGy/hour (final dose of 14kGy) and stored in the dark at -15ºC until use (Langley et al., 2009b). Sterility was tested by aseptically inoculating γ-irradiated samples into sterile tryptic soy broth (TSB). Following 3 days of incubation, the TSB-sample mix was plated onto tryptic soy agar (TSA) plates and checked daily for 4 days. Growth was never observed in any of these tests, suggesting that γ-irradiation was effective in eliminating or rendering inactive a substantial proportion of culturable native bacteria.

Hydrous ferric oxide (HFO) was synthesized by the rapid addition of sterile 1M NaOH to sterile 2M $FeCl_3 \cdot 6H_2O$ followed by repeated washing with autoclaved ultrapure (18 MΩ·cm) water (UPW) (Glasauer et al., 2003; Langley et al., 2009b). The final gel-suspension was adjusted to pH 7.00 and stored in the dark at 4ºC. To prevent the aggregation or potential transformation of HFO (Cornell and Schwertmann, 2003; Raiswell et al., 2010), long term storage was avoided. Therefore, HFO was prepared 1 week prior to use in experiments.

2.2. Bulk mineralogy

The bulk mineralogy of BIOS and HFO was determined by X-ray diffraction (XRD). Prior to analysis, subsamples were dried in a fume-hood and thoroughly crushed with a mortar and

pestle. XRD analysis was performed using a Rigaku Ultima IV diffractometer, with a Cu-Kα X-ray source, operating at 45 kV and 40 mA. Continuous scans were run from10–80° 2Θ using a step size of 0.02° at a rate of 0.6°/minute.

2.3. Non-sequential chemical extractions

Chemical quantification of the Fe-bearing mineral fractions in BIOS was carried out by following the methods of Kostka and Luther (1994). The chemical extraction scheme involves the addition of a specific chemical extractant to a known amount of wet sample. The chemical extractants include: HCl (0.5M – duration of 1 hour), ascorbate (pH 8.0 – duration of 24 hours), oxalate (pH 3.0 – performed in the dark for 48 hours), and dithionite (pH 4.8 – duration of 4 hours). Each chemical extracts a specific Fe-bearing fraction, such that the amount of Fe extracted with HCl is operationally defined to represent the amorphous Fe fraction as well as adsorbed Fe(II) and any Fe(II) associated with acid volatile sulfides (AVS), and silicates, in particular chlorite (Kostka and Luther, 1994). Whereas, the amount of Fe extracted with ascorbate is considered to represent the amorphous Fe fraction only (Kostka and Luther, 1994; Hyacinthe et al., 2006; Raiswell et al., 2010). The amount of Fe extracted with oxalate is similar to that of HCl, however oxalate may overestimate the amorphous Fe fraction and underestimate the crystalline Fe fraction (Kostka and Luther, 1994). Finally, dithionite extracts all reactive Fe fractions including those extracted by HCl as well as crystalline Fe fractions (Kostka and Luther, 1994). Subsequent to each extraction, the concentration of Fe was determined spectrophotometrically using the ferrozine assay (Stookey, 1970; Kostka and Luther, 1994; Viollier et al., 2000). The water content of BIOS was determined by placing wet sample into pre-weighed 20mL glass scintillation vials and drying to a constant weight at 70°C to express the amount of Fe per gram/milligram dry weight of sample.

2.4. Inductively coupled plasma—optical emission spectrometry

The chemical composition of BIOS and HFO was determined by suspending a known amount of wet sample into 6mL UPW, and fully digested by the addition of 4mL 30% H_2O_2 and 2mL trace metal grade HNO_3 followed by heating at 70°C for 24 hours (Langley et al., 2009b). Subsequently, the digests were filtered (0.2 μm) and diluted into 1% trace metal grade HNO_3 (1:10) and analyzed with inductively coupled plasma — optical emission spectroscopy using a Varian Vista-PRO CCD Simultaneous ICP-OES, operating under standard conditions.

2.5. Organic matter content of BIOS

To determine the organic matter content of BIOS, weight loss on ignition (LOI) was carried out in duplicate by heating a known amount of oven-dried sample in a muffle furnace at 375°C for 24 hours.

2.6. Microbial medium and preparation of cultures

Fe(III) reduction batch experiments were conducted in "microcosms" comprised of 1L acid-washed Kimax bottles with 700mL of sterile chemically defined medium (CDM) (pH ~7.00) with the following composition: 20mM sodium lactate as the electron donor, 4mM 1,4-piperazinediethanesulfonic acid (PIPES) buffer, and trace mineral salts (2.20mM NH_4Cl, 1.20mM KCl, 0.61mM $CaCl_2$, 0.07mM nitrilotriacetic acid, 0.11mM $MgSO_4 \cdot 7H_2O$, 0.15mM NaCl, 27μM $MnSO_4 \cdot H_2O$, 8.6μM $ZnCl_2$, 3.2μM $FeSO_4 \cdot 7H_2O$, 6.1μM $CaCl_2 \cdot 2H_2O$, 3.8μM $CoCl_2 \cdot 6H_2O$, 0.93μM $Na_2MoO_4 \cdot 2H_2O$, 0.68μM $Na_2WO_4 \cdot 2H_2O$, 0.91μM $NiCl_2 \cdot 6H_2O$, 0.36μM $CuSO_4 \cdot 5H_2O$, 0.19μM $AlK(SO_4)_2 \cdot 12H_2O$, 1.5μM H_3BO_3) (Zachara et al., 1998; Glasauer et al., 2003; Langley et al., 2009b). In order to determine the effects of the concentration of phosphate on the rates of microbial Fe(III) reduction and the secondary Fe minerals that form, the reduction experiments

were conducted with 10μM or 3.9mM of phosphate ($NaH_2PO_4 \bullet H_2O$). The CDM was amended with 4mM total Fe in the form of either γ-irradiated BIOS, non-irradiated BIOS, or HFO (Langley et al., 2009b). One day prior to amending CDM with BIOS and the start of reduction experiments, frozen BIOS were allowed to thaw at room temperature, weighed into sterile falcon centrifuge tubes, and stored in the dark at 4ºC.

In order to compare the microbial reduction rates of γ-irradiated BIOS and non-irradiated BIOS, sodium molybdate ($Na_2MoO_4 \bullet 2H_2O$) was added as a specific inhibitor of SRB to CDM amended with non-irradiated BIOS. Previous studies suggested that the appropriate concentration of molybdate to inhibit SRB should be equimolar to that of ambient sulfate (Oremland and Capone, 1988; Avramescu et al., 2011). The concentration of sulfate in CDM was determined to be ~0.14mM, thus molybdate was added from a sterile 0.2M stock solution (pH ~7.00) to a final concentration of ~0.14mM (1:1 molybdate:sulfate). However, it is important to note that sulfate in the groundwater-derived surface waters reached concentrations greater than 8mM at sites CA-04 and CA-03 (Table S1). This suggests that the addition of wet BIOS to CDM could potentially serve as additional sources of sulfate. Therefore, in order to account for such contribution, additional experiments were conducted where molybdate was added to a final concentration of 0.28mM (2:1 molybdate:sulfate). Previous studies have, however, shown that the addition of molybdate to a final concentration of ~0.5mM led to reduced rates of microbial Fe(III) reduction of lepidocrocite (O'Loughlin et al., 2010). Therefore, in order to determine the combined influence of phosphate (10μM or 3.9mM) and molybdate (1:1 or 2:1 molybdate:sulfate) on the rates of microbial Fe(III) reduction and the secondary Fe minerals that form, Fe(III) reduction batch experiments were conducted with HFO as the sole electron acceptor. The experimental set-up and a summary of the treatments used in this study are summarized in Table 1.

Microbial Fe(III) reduction experiments were conducted with a well characterized, facultative, dissimilarity Fe(III)-reducing bacterium, *Shewanella putrefaciens* strain CN32 (*S. putrefaciens* CN32). *S. putrefaciens* CN32 was routinely cultured aerobically on TSA plates at room temperature (~22°C). Microbial cells were prepared according to the protocols of Glasauer et al. (2003) and Langley et al. (2009b). Briefly, cells were prepared by inoculating 50mL of TSB with a colony of *S. putrefaciens* CN32 aseptically transferred from TSA plates, and kept on a rotary shaker at 125 rpm for 24 hours at 22°C. Subsequently, 0.5mL of the culture was transferred into 50mL of 50:50 CDM:TSB mixtures containing various combinations of phosphate (390μM or 3.9mM) and molybdate (1:1 or 2:1 molybdate:sulfate). After 24 hours, the sub-culturing procedure was repeated with 95:5, 99:1 (CDM:TSB) solutions and finally 100% CDM with various combinations of phosphate and molybdate to acclimate the bacteria to depleted nutrients and microcosm conditions (Glasauer et al., 2003; Langley et al., 2009b). The choice of using 390μM of phosphate rather than 10μM for microbial growth was employed in order to have sufficient amounts of bacteria at the end of the growth/acclimation process. Following the acclimation period, the bacteria were harvested by centrifugation at 2500 rpm and re-suspended into 2 mL of 100% sterile CDM. Additionally, for bacteria acclimatized with 390μM of phosphate, the bacteria were washed once with sterile CDM in order to avoid the possible carryover of phosphate into the microcosms with low phosphate (10μM). Subsequently, the BioRad Protein Assay II dye reagent was used to standardize the concentrated cell suspension in order for the microcosms to contain a cell density of ~10^7 CFU/mL (Glasauer et al., 2003; Langley et al., 2009b). The experiments were conducted in triplicate (non-irradiated BIOS and HFO) and duplicate (γ-irradiated BIOS), and controls to which no bacteria were added were included. Prior to inoculation with *S. putrefaciens* CN32, the microcosms were wrapped in aluminum foil in order to avoid potential photochemical

reactions. Subsequently, the microcosms were moved into a Coy Labs anaerobic chamber with an atmosphere of 95:5 N_2:H_2 and inoculated with *S. putrefaciens* CN32. Throughout the paper, we refer to the microcosms to which cells were added as "biotic" microcosms, whereas controls to which no bacteria were added are referred to as "control" microcosms.

2.7. Sampling and analyses

Sampling of each system was performed immediately following the addition of the cells (time 0) and then periodically at selected time points. Sampling was carried out by vigorously shaking the microcosm bottles to suspend the iron oxides into solution. Subsequently 20mL of the suspension was immediately poured into a sterile 20mL scintillation vial. All sub-samples were then taken from this aliquot, in order to minimize the potential contamination of the microcosms (Langley et al., 2009b). At each time point, the sub-sample suspensions were analyzed for redox potential (Eh), pH, cell viability of *S. putrefaciens* CN32, total and dissolved Fe(II), and total Fe. Additionally, for batch experiments conducted with BIOS as the sole electron acceptors, dissolved sulfide was measured. Eh and pH were monitored utilizing standard laboratory meters and probes, whereas cell viability was determined by colony counts on TSA plates (Glasauer et al., 2003; Langley et al., 2009b). Dissolved Fe(II) was determined by filtering (0.22 μm) 10mL of the suspension into an acid-washed 20mL scintillation vial, 0.5mL of the filtrate was immediately dispensed into 4.5mL of 0.5M trace metal grade HCl and allowed to react for 24 hours in the anaerobic chamber. In order to determine the concentration of dissolved sulfide, sub-samples of the filtrate were fixed with Cline reagents in amber vials and allowed to react for 20 minutes in the dark, subsequently the concentration was determined spectrophotometrically at an absorbance of 670nm (Cline, 1969). Fe(II) associated with the solid phase (total Fe(II)) was determined by dispensing 0.5mL of the unfiltered iron oxide suspension into 4.5mL of 0.5M HCl and allowed to

react for 24 hours in the anaerobic chamber. The concentrations of dissolved Fe(II) and total Fe(II) were determined spectrophotometrically using the ferrozine assay (Stookey, 1970; Viollier et al., 2000). The concentration of total Fe(II) was also determined spectrophotometrically using 1,10-phenanthroline, because, in some instances, we found that ferrozine gave unstable readings when determining the concentration of Fe(II), specifically Fe(II) associated with BIOS suspensions (see Figure S1 for stability tests). The efficiency of extracting the solid suspension in 0.5M HCl for 24 hours to completely recover Fe(II) associated with the secondary iron minerals, in particular magnetite, was confirmed in this study and previous studies (Fredrickson et al., 1998; Glasauer et al., 2003). In agreement with Glasauer et al. (2003), we found that extracting the solid suspension in 3M or 6M HCl for 24 hours gave identical results to a 24-hour extraction in 0.5M HCl (see Table S2).

To determine total Fe, 6mL of the iron oxide suspension was digested with the addition of 4 mL 30% H_2O_2 and 2 mL of concentrated trace metal grade HNO_3 at 70°C for 24 hours. Once cooled, 100µL of the digest was mixed with 900µL of reducing agent for 30 minutes (0.28M hydroxylamine hydrochloride in 0.05M N-(2-hydroxyethyl)piperazine-N'-(2-ethanesulfonic acid) (HEPES) buffer). Subsequently, the concentration of Fe(II) was determined using the ferrozine assay as previously described. In order to confirm the concentrations of P and Mo, as well as to determine the fate of P and Mo throughout the reduction period, 6mL of the filtered suspensions from all control microcosms and 1 biotic microcosm from each experiment at the beginning and end of the experimental period were digested in H_2O_2/HNO_3 as previously described. Subsequently 1mL of the H_2O_2/HNO_3 digests were diluted into 10mL UPW and analyzed with ICP-OES.

Post-reduction secondary mineral precipitates that formed during microbial Fe(III) reduction were analyzed by XRD as described in Section 2.2, using an air sensitive sample holder

in order to prevent oxidation of potential Fe(II)-bearing minerals. Prior to analysis, post-reduction minerals were harvested by centrifugation (2500 rpm), washed multiple times with anoxic UPW, and dried under anaerobic conditions.

2.8. Electron microscopy

BIOS samples and post-reduction mineral precipitates were observed by scanning electron microscopy (SEM) with a JEOL JSM-6610LV microscope operating at 20 kV at the University of Ottawa (Ontario, Canada). Prior to observation, samples for SEM analysis were prepared by placing a thin layer of dry samples on a carbon tape attached to a sample holder.

3. Results

3.1. Mineralogy

X-ray diffraction patterns of HFO, and BIOS collected from sites CA-04 and CA-03 are shown in Figure 1. Generally, the diffraction patterns contained two broad reflections centered at ~2.5 and 1.5 Å, which are characteristic of the poorly ordered iron oxide mineral, 2-line ferrihydrite (Cornell and Schwertmann, 2003). In addition, BIOS collected from site CA-04 contained another mineral phase with a sharp peak centered at d-spacing of ~2.5 Å which corresponded to magnetite. The presence of magnetite was also confirmed by holding a magnet next to the samples. No magnetite was detected by XRD or the magnet test in the BIOS samples collected from site CA-03. BIOS collected from site CA-03, however, contained another mineral phase with broad sharp peaks centered at d-spacings of ~5.0, 4.2, 3.4, 2.7, 2.6, 2.4, 2.3, 2.2, 1.7, and 1.6Å, which was identified as goethite. Other sharp peaks likely correspond to calcite and silicate minerals such as quartz, which comprise the bulk of the host bedrock material (Moorhouse, 1941). Figure 1 also shows a comparison of the mineralogy between “fresh” BIOS, which

correspond to samples that were analyzed soon after collection, and those that have been frozen for ~2 years. Generally, the diffraction patterns of frozen BIOS were similar to those of fresh BIOS indicating that storage and ageing did not adversely affect the mineralogy of the samples. No major differences were observed between the diffraction patterns of γ-irradiated and non-irradiated samples (data not shown), indicating that, under the conditions of this study, γ-irradiation did not significantly alter the mineralogy of the samples (Langley et al., 2009b).

3.2. Chemical extractions and chemical composition

Table 2 shows the amount of Fe obtained from BIOS collected from sites CA-04 and CA-03 using different chemical extractants. In both samples, no significant difference was found between the amount of Fe extracted by HCl and ascorbate (determined by t-test, $p>0.05$), suggesting that other sources such as AVS and silicates do not significantly contribute to the Fe pool. This is further supported by the low amount of Fe(II) extracted by 0.5M HCl, which was found to be 25.7±2.9 or 31.5±3.2 mg/gdwt for BIOS samples collected from sites CA-04 or CA-03, respectively. Therefore, HCl and ascorbate extractions are estimators of the amorphous Fe fraction. The amount of Fe extracted from both samples by dithionite was found to agree with the amount extracted by HNO_3/H_2O_2 and determined by ICP-OES (Table S3); therefore, dithionite is an estimator of the total Fe pool. In both samples, the amount of Fe extracted by dithionite or oxalate was found to be significantly higher than the amount of Fe extracted by HCl and ascorbate ($p<0.05$). For BIOS samples from site CA-04, the amount of Fe extracted with oxalate was found to be significantly higher than the amount of Fe extracted with dithionite ($p<0.05$). In contrast, for BIOS samples collected from site CA-03, no significant difference was found between the amount of Fe extracted with oxalate and dithionite ($p>0.05$). This is in agreement with Kostka and Luther (1994) who found that oxalate overestimates the amorphous iron fraction and underestimates the

crystalline iron fraction, presumably due to the presence of Fe(II) which catalyzes the dissolution of crystalline iron oxides. Oxalate extractable Fe(II) was found to be 9.6±0.7 and 7.0±4.2mg/gdwt for BIOS samples collected from sites CA-04 and CA-03, respectively. Therefore, the presence of oxalate extractable Fe(II) would likely further catalyze the dissolution of any crystalline iron fractions in the samples, thereby explaining the similarity to the amount of Fe extracted by dithionite. The higher amount of Fe extracted with oxalate compared to that which was extracted by dithionite for BIOS samples collected from site CA-04 could be potentially attributed to the heterogeneity of the sample (Table 2).

Table 2 further shows the proportions of the amorphous Fe fraction and the crystalline Fe fraction in BIOS samples collected from sites CA-04 and CA-03. Although the amount of Fe determined by 0.5M HCl and ascorbate was found to be similar between each treatment for both sites, ascorbate was selected to represent the amorphous Fe fraction. This is based on previous studies which indicate that ascorbate selectively extracts the amorphous Fe fraction (Kostka and Luther, 1994; Hyacinthe et al., 2006; Raiswell et al., 2010). Therefore, the proportion of the amorphous Fe fraction in BIOS from sites CA-04 and CA-03 was determined to be 88.2±3.4 and 74.1±3.8%, respectively (Table 2). By using the total and amorphous Fe fractions determined by dithionite and ascorbate, respectively, it is possible to calculate the proportion of the crystalline Fe fraction, which was determined to be 11.8±3.6 and 25.9±4.8% for BIOS collected from sites CA-04 and CA-03, respectively (Table 2).

The chemical composition of BIOS collected from sites CA-04 and CA-03, as well as HFO are given in Table 3. For BIOS, analysis by ICP-OES revealed Fe concentrations ranging from 22 to 40wt%, with Zn concentration of ~0.20wt% in both samples, and Pb concentrations ranging from 0.01 to 0.08wt%, whereas the concentrations of P and Mo were found to be below the

detection limit of the instrument (Table 3). An organic matter content of 10.3% was detected by LOI for BIOS collected from site CA-04, which was found to increase further downstream to 15.1% for BIOS collected from site CA-03 (Table 3). For HFO, the Fe concentration was determined to be ~47wt%, and the Zn concentration was determined to be 0.004wt%, whereas the concentrations of P, Pb and Mo were below the detection limit of the instrument (Table 3).

3.3. Electron microscopy of BIOS

SEM micrographs of BIOS from sites CA-04 and CA-03 revealed the abundance of typical structures associated with neutrophilic FeOB, including sheaths and twisted stalks reminiscent of *Leptothrix* spp. and *Gallionella* spp., respectively, as was previously observed with fresh BIOS (Figure 2a and b) (Cotroneo and Fortin, 2013). The structures appeared intact, suggesting that freezing did not significantly influence the integrity of the samples. Energy dispersive X-ray spectroscopy (EDS) analysis of the precipitate associated with the cell structures generated spectra with strong signals corresponding to Fe and O, and weaker signals belonging to Al, Si and Ca, likely originating from silicate minerals and calcium carbonate, which comprise the bulk of the bedrock material (data not shown) (Moorhouse, 1941).

3.4. Microbial reduction of HFO and BIOS

3.4.1. HFO

Changes in the redox potential (Eh), pH, and CFU during the microbial reduction of HFO conducted with 3.9mM or 10μM of phosphate in the absence or presence of molybdate:sulfate concentration of 1:1 or 2:1 are shown in Figures S2-S4. In general, as Fe(III) reduction commenced, Eh significantly declined across all biotic microcosms reaching a minimum value of ~ -300mV or ~-200mV (corrected to the standard hydrogen electrode; SHE) within microcosms

containing 3.9mM or 10µM of phosphate, respectively. It was also noted that reducing conditions were established at a faster rate within microcosms containing 3.9mM of phosphate when compared to those containing 10µM of phosphate (Figures S2 and S3). Throughout the experimental duration, pH gradually increased across all biotic microcosms reaching maximum values of 7.14-7.30 or 7.30-7.45 within microcosms to which 3.9mM or 10µM of phosphate was added, respectively (Figures S2 and S3). Initial cell counts across all biotic microcosms were in the order of 7.1×10^7 - 8.6×10^7 CFU/mL (Figure S4). Plate counts indicated that the cells remained viable, and, interestingly, even within biotic microcosms containing 10µM of phosphate the cell counts remained in order of 10^7 CFU/mL throughout the duration of the experiment (Figure S4b). Cell counts, however, eventually declined across all biotic microcosms reaching 2.6×10^7, 6.4×10^7, or 6.7×10^7 CFU/mL at day 14 within biotic microcosms containing 3.9mM phosphate and molybdate:sulfate concentrations of 0:1, 1:1, or 2:1, respectively (Figure S4a). Similarly, cell counts declined to reach 2.5×10^7, 9.8×10^6, or 8.2×10^6 CFU/mL at termination of the experiment within biotic microcosms containing molybdate:sulfate concentrations of 0:1, 1:1, or 2:1, respectively, and 10µM of phosphate (Figure S4b). In contrast to the biotic microcosms, no significant changes in pH were observed and no viable microbial cells were detected across all control microcosms (Figure S2 and S3). The only change observed within the control microcosms was the gradual decline in Eh, which could be attributed to the equilibration of the microcosms with the anaerobic atmosphere (Langley et al., 2009b) (Figure S2 and S3). Although the addition of molybdate (molybdate:sulfate concentrations of 1:1 or 2:1) did not appear to significantly impact the changes of Eh, pH, and CFU throughout the duration of the experiment (Figures S2-S4), one notable change was observed during the initial stages of the experiment. In which case, upon the addition of molybdate (1:1 or 2:1 molybdate:sulfate) to microcosms containing HFO and

10μM of phosphate, pH slightly increased to ~7.1 from an initial value of 7.05, such change, however, was not observed for microcosms containing 3.9mM of phosphate likely due to the additional buffering capacity of phosphate.

Changes in the proportions of total Fe(II) and dissolved Fe(II) relative to total Fe during the reduction of HFO are shown in Figure 3. Within the biotic microcosms, Fe(III) reduction commenced after an initial lag period, in which case significant increases in the proportion of total Fe(II) were not observed until day 2 or day 3 for experiments conducted with 3.9mM or 10μM of phosphate, respectively (Figure 3). As reduction commenced, the proportion of total Fe(II) gradually increased throughout the duration of the experiment reaching a maximum of 75-80% or 40-50%within 14 days of inoculation within biotic microcosms containing 3.9mM or 10μM of phosphate, respectively (Figure 3, Table 4). As reduction proceeded within the biotic microcosms containing 3.9mM phosphate, the proportion of dissolved Fe(II) reached an average maximum of ~6% at day 4 which declined to ~3% and remained at that level for the remaining duration of the experiment, suggesting that most of the Fe(II) was associated with the solid phase (Figure 3). In contrast, the proportion of dissolved Fe(II) in the biotic microcosms containing 10μM of phosphate reached a maximum of 26-30% of total Fe (Figure 3). Across all biotic microcosms containing 10μM of phosphate, the concentration of dissolved Fe(II) accounted for ~60% of the total Fe(II) production, suggesting that most of the Fe(II) released from the microbial Fe(III) reduction remained in solution. In contrast to the biotic microcosms, no significant changes in total Fe(II) were noted throughout the duration of the experiment and only negligible amounts of dissolved Fe(II) were present in the control microcosms (Figure 3).

The initial concentration of dissolved phosphate within microcosms containing 3.9mM of phosphate was found to be ~3.1mM in the control and selected biotic microcosms, which declined

and reached ~2.6mM in the control microcosms at the termination of the experiment (Table S4). In contrast, the concentration of dissolved phosphate declined to lower values reaching ~1.47, 1.57, or 1.61mM in selected biotic microcosms with molybdate:sulfate concentrations of 0:1, 1:1, or 2:1, respectively (Table S4). Initial molybdate concentrations were found to be ~0.14mM or 0.30mM in the control and selected biotic microcosms with molybdate:sulfate concentration of 1:1, or 2:1, respectively. The concentration of molybdate slightly declined within the control microcosms with molybdate:sulfate concentration of 2:1 reaching ~0.28mM at termination of the experiment, whereas the concentration of molybdate in the control microcosm with a molybdate:sulfate concentration of 1:1 remained unchanged (Table S4). Similarly, the concentration of molybdate slightly declined reaching ~0.13 or 0.26mM within the selected biotic microcosms containing molybdate:sulfate concentration of 1:1 or 2:1, respectively, at termination of the experiment (Table S4).

In contrast to the microcosms containing 3.9mM of phosphate, the initial concentrations of dissolved molybdate within microcosms containing 10μMof phosphate were found to be 50-60% of the total molybdate, indicating that molybdate was quickly scavenged from solution (Table S4). The concentration of molybdate continued to decline and reached ~0.05 or 0.14mM in the control microcosms with molybdate:sulfate concentrations of 1:1 or 2:1, respectively, at termination of the experiment (Table S4). The concentration of molybdate, however, declined to lower values reaching ~0.02 or 0.06mM within selected biotic microcosms with molybdate:sulfate concentrations of 1:1 or 2:1, respectively, at termination of the experiment (Table S4). The concentration of phosphate within batch experiments conducted with 10μM of phosphate was found to be below the detection limit of the instrument, confirming the low amount of phosphate

added. Also, in the microcosms to which no molybdate was added, the molybdenum concentration was found to be below the detection limit of the instrument.

3.4.2. BIOS

3.4.2.1 Non-irradiated BIOS

Changes in Eh, pH, and CFU within batch experiments conducted with various combinations of phosphate (3.9mM or 10µM) and molybdate (molybdate:sulfate concentration of 1:1 or 2:1) with non-irradiated BIOS from sites CA-04 or CA-03 as the sole electron acceptor are shown in Figures S5-S9. Similar trends in the changes of Eh were observed across all biotic microcosms suggesting that, as opposed to HFO and regardless of the phosphate concentration, reducing conditions were established at an equal rate and extent (Figures S5-S9). Eh values across all biotic microcosms reached a minimum value of ~ -200mV, which continued to fluctuate throughout the duration of the experiment (Figures S5-S8). In contrast to the biotic microcosms, one notable difference was observed between control microcosms containing 3.9mM or 10µM of phosphate, in which case reducing conditions were established at a faster rate in control microcosms with 3.9mM of phosphate as opposed to those containing 10µM of phosphate (Figures S5-S8). In all biotic microcosms, as microbial Fe(III) reduction commenced, pH increased to a maximum of 7.4-7.5 and continued to fluctuate throughout the duration of the experiment (Figures S5-S8). Similar trends were observed in the changes of pH across all control microcosms (Figures S5-S8), with the exception of the control microcosm containing BIOS from site CA-04, 3.9mM of phosphate, and molybdate:sulfate concentration of 1:1, in which case a decline in pH to 6.33 was observed at termination of the experiment (Figure S5). It is important to note that in contrast to batch experiments conducted with HFO and 10µM of phosphate, no changes in pH were observed following the addition of molybdate to the microcosms containing 10µM of phosphate. Initial cell

counts were in the order of 6.0 x 10^7 - 6.8 x 10^7 CFU/mL across all biotic microcosms (Figure S9). In contrast to batch experiments conducted with HFO and 3.9mM of phosphate, cell counts increased to 1.2 x 10^8 – 1.9 x 10^8 CFU/mL within biotic microcosms containing 3.9mM of phosphate within 2 days of inoculation and remained at those levels for 4-10 days, after which cell counts gradually declined to 3.0x 10^7 - 5x 10^7 CFU/mL at termination of the experiment (Figure S9). In contrast to batch experiments conducted with HFO, cell counts exhibited an overall decline throughout the duration of the experiment reaching 4.0 x 10^6 - 1.0x 10^7 CFU/mL at termination of the experiment (Figure S9). No viable cells belonging to *S. putrefaciens* CN32 were detected in the control microcosms; however, we observed the growth of undefined bacteria which likely originated from the native microbial population within the samples. As previously observed with batch experiments conducted with HFO, the addition of molybdate (molybdate:sulfate concentration of 1:1 or 2:1) did not appear to influence the changes of Eh, pH, and CFU throughout the duration of the experiment (Figures S5-S9).

Despite the addition of molybdate, sulfide production was detected in all microcosms, with the exception of control microcosms containing 10µM of phosphate (Figures S10 and S11). Regardless of the concentration of molybdate, the production of sulfide was found to commence earlier in biotic microcosms containing 3.9mM of phosphate when compared to microcosms containing 10µM of phosphate (Figures S10 and S11). Sulfide was detected at day 6 with initial concentrations ranging from 0.10 to 0.34µM and continued to increase for the remaining duration of the experiment to reach maximum concentrations of 7.28 – 9.27µM in the biotic microcosms with 3.9mM of phosphate (Figures S10 and S11).Some notable differences were observed in biotic microcosms containing10µM of phosphate, in which case sulfide was detected 12-14 days post-inoculation within batch experiments conducted with BIOS from site CA-04, whereas in batch

experiments conducted with BIOS from site CA-03, sulfide was detected 16 days post-inoculation (Figures S10 and S11). In all biotic microcosms containing 10μM of phosphate, sulfide concentrations reached maximum values of 1.0-3.77μMat termination of the experiment (Figures S10 and S11). Sulfide in control microcosms with 3.9mM of phosphate was detected at day 8, however the concentration of sulfide remained low throughout the duration of the experiment within the range of 0.30 – 2.0μM, and reached maximum concentrations of 3.0 – 6.5μM at termination of the experiment (Figures S10 and S11). One notable exception was the control microcosm containing 3.9mM of phosphate and molybdate:sulfate concentration of 1:1 conducted with BIOS from site CA-04, in which case sulfide concentration reached a maximum of ~8.5μM at day 12 and declined to ~4.00μM at termination of the experiment (Figures S10). It is important to note that the concentration of sulfide was found to be highly variable across all biotic microcosms reflecting the heterogeneous abundance of the native SRB within the samples (Figures S10 and S11).

Changes in the proportions of total Fe(II) and dissolved Fe(II) relative to total Fe during the reduction of non-irradiated BIOS are shown in Figures 4 and 5. As previously mentioned, in some instances we noted that ferrozine gave unstable readings when determining the concentration of total Fe(II), and for that reason we used 1,10-phenanthroline as a "check." In general, we found that a reaction time of 10 minutes with ferrozine was sufficient to give identical readings to those determined by 1,10-phenanthroline (see Figures S12 and S13 for a comparison between the two methods). Overall, the reduction of non-irradiated BIOS showed the same general pattern as HFO, with some notable differences. Regardless of the phosphate concentration, the initial lag period between culture inoculation and the onset of iron reduction was either abbreviated or absent (Figures 4 and 5 compared to Figure 3). Within the biotic batch experiments conducted with BIOS

from site CA-04 with 3.9mM of phosphate and molybdate:sulfate concentrations of 1:1 or 2:1, the proportion of total Fe(II) gradually increased from an initial value of ~5% and reached ~60% at day 8 or 9, at which point the proportion of total Fe(II) appeared to have reached a plateau (Figure 4). However, the plateau period lasted for 4-6 days at which point the proportion of total Fe(II) continued to increase and reached maximum values of ~90 or 85% at termination of the experiment in biotic microcosms with molybdate:sulfate concentrations of 1:1 or 2:1, respectively (Figure 4 and Table 4). The reduction of BIOS from site CA-03 with 3.9mM of phosphate showed the same general pattern for the reduction BIOS from site CA-04, with some notable differences (Figures 4 and 5). During the reduction of BIOS from site CA-03, the proportion of total Fe(II) increased from an initial value of ~5% to reach ~50% at day 6 for biotic microcosms with molybdate:sulfate concentration of 1:1 and ~30% at day 4 for biotic microcosms with molybdate:sulfate concentration of 2:1, at which point the proportion of total Fe(II) appeared to have reached a plateau (Figure 5). The plateau period lasted for ~8 days after which the proportion of total Fe(II) continued to increase and reached a maximum value of ~90% at termination of the experiment (Figure 5 and Table 4). As reduction commenced across all biotic microcosms with 3.9mM of phosphate, the proportion of dissolved Fe(II) increased from an initial value of 0% to a maximum value of ~10% at day 4 which then declined to ~5% at day 6 and remained at that level for the remaining duration of the experiment (Figures 4 and 5).

Similar trends were observed in the changes of the proportion of total Fe(II) during the microbial reduction of BIOS from sites CA-04 or CA-03 conducted with 10μM of phosphate and molybdate:sulfate concentrations of 1:1 or 2:1 (Figures 4 and 5). For biotic batch experiments conducted with BIOS from site CA-04, the proportion of total Fe(II) gradually increased from an initial value of ~5% and reached ~60% at day 9, at which point the proportion of total Fe(II)

reached a plateau (Figure 4). However, the proportion of total Fe(II) continued to slowly increase and reached a maximum value of ~73% at termination of the experiment in biotic microcosms with molybdate:sulfate concentrations of 1:1 or 2:1 (Figure 4 and Table 4). Similarly, the proportion of total Fe(II) in biotic batch experiments conducted with BIOS from site CA-03 gradually increased from an initial value of ~5% to ~50% at day 10, which continued to slowly increase to reach maximum values of ~65or 70% at termination of the experiment in biotic microcosms with molybdate:sulfate concentrations of 1:1 or 2:1, respectively (Figure 5 and Table 4). Within all biotic microcosms with 10μM of phosphate, dissolved Fe(II) increased as total Fe(II) increased and accounted for ~80% of the total Fe(II) production, suggesting that most of the Fe(II) released from the microbial Fe(III) reduction remained in solution (Figures 4 and 5). The higher amount of dissolved Fe(II) in batch experiments conducted with non-irradiated BIOS and 10μM of phosphate than those conducted with HFO further indicates that a lower amount of Fe(II) was associated with the solid phase.

Fe(III) reduction was found to occur within all control microcosms, which commenced after 8-12 days of incubation (Figures 4 and 5). In general, it appears that Fe(III) reduction commenced sooner within microcosms containing 3.9mM of phosphate when compared to those containing 10μM of phosphate (Figures 4 and 5). Interestingly, once Fe(III) reduction proceeded within the control microcosms containing 3.9mM of phosphate, it occurred rapidly such that the proportion of total Fe(II) increases to maximum values of 70-80% within 2-3 days (Figures 4 and 5, Table S5). One notable exception was the control microcosm with 3.9mM of phosphate and molybdate:sulfate concentration of 1:1 conducted with BIOS from site CA-04, in which case total Fe(II) slowly increased to a maximum value of ~50% (Figure 4, Table S5). As observed with biotic microcosms containing 3.9mM of phosphate, the proportion of dissolved Fe(II) remained low

throughout the incubation period reaching maximum values of 6-9% (Figures 4 and 5). In contrast to control microcosms with 3.9mM of phosphate, the proportion of total Fe(II) within control microcosms with containing 10μM of phosphate was found to increase at a slower rate (Figures 4 and 5). In all the control microcosms with 10μM of phosphate, the proportion of total Fe(II) reached maximum values of 30-45% at termination of the experiment with dissolved Fe(II) accounting for 60-75% of the total Fe(II) (Figures 4 and 5, Table S5).

Initial concentrations of dissolved phosphate within all control and selected biotic microcosms containing 3.9mM of phosphate were within the range of 3.1-3.8mM (Table S4). The concentration of phosphate declined to ~1.2mM at the termination of the experiment across all microcosms, with the exception of the control microcosm containing 3.9mM of phosphate and molybdate:sulfate concentration of 1:1 conducted with BIOS from site CA-04, in which case the concentration of phosphate declined to ~2mM at termination of the experiment (Table S4). In all control and selected biotic microcosms containing 10μM of phosphate, the concentration of dissolved phosphate was found to be below the detection limit of the instrument. Initial molybdate concentrations were within the range of 0.12-0.14mM or 0.25-0.30mM in all control and selected biotic microcosms with molybdate:sulfate concentration of 1:1, or 2:1, respectively, with high and low concentration of phosphate (Table S4).This suggests that, in contrast to batch experiments conducted with HFO and 10μM of phosphate, molybdate was not as quickly scavenged from solution. As observed with batch experiments conducted with HFO and 3.9mM of phosphate, the concentration of molybdate slightly declined at termination of the experiment within microcosms containing 3.9mM of phosphate (Table S4). In contrast, the concentration of molybdate declined to lower values reaching 0.08-0.09mM or 0.14-0.20mM at termination of the experiment in microcosms with molybdate:sulfate concentration of 1:1 or 2:1, respectively, and 10μM of

phosphate (Table S4). However, in comparison to batch experiments conducted with HFO and 10μM of phosphate, it appears that most of the molybdate remained in solution (Table S4).

3.4.2.2 γ-irradiated BIOS

Similar trends were observed in the changes of Eh, pH, and CFU during the reduction of γ-irradiated BIOS when compared to those observed during the reduction of non-irradiated BIOS (Figures S14-S16). One exception was that Eh reached a minimum value of ~ -135mV during the reduction of γ-irradiated BIOS from sites CA-04 or CA-03 within batch experiments conducted with 10μM of phosphate (Figures S14 and S15). In contrast to the biotic microcosms, no significant changes in the different parameters measured were observed in the control microcosms, other than the gradual decline of Eh (Figure S14 and S15). We also did not observe any growth of viable bacteria within the control microcosms including those belonging to *S. putrefaciens* CN32, suggesting that γ-irradiation was effective in eliminating or rendering inactive a substantial proportion of culturable native bacteria. However, despite the apparent effectiveness of γ-irradiation in sterilizing the samples, minor sulfide production was detected in the biotic microcosms containing 3.9mM of phosphate (Figure S17). As previously observed with non-irradiated BIOS, sulfide was detected at day 6 with initial concentrations ranging from 0.06 to 0.12μM (Figure S16). However, in comparison to experiments conducted with non-irradiated BIOS and 3.9mM of phosphate, the concentration of sulfide remained low throughout the duration of the experiment reaching maximum values of 0.15-0.3μM (Figure S17). In contrast, no sulfide production was detected in the control microcosms or biotic microcosms containing 10μM of phosphate.

Changes in the proportion of total and dissolved Fe(II) during the microbial reduction of γ-irradiated BIOS are shown in Figures 4 and 5. Fe(III) reduction of γ-irradiated BIOS from sites

CA-04 or CA-03 followed the same general pattern observed with non-irradiated BIOS in the presence of 3.9mM of phosphate (Figures 4 and 5).The maximum amounts of Fe(III) reduced for γ-irradiated BIOS from sites CA-04 or CA-03 reached ~70% or 65%, respectively, in the presence of 3.9mM of phosphate, whereas the maximum amounts of Fe(III) reduced in the presence of 10μM of phosphate for γ-irradiated BIOS from sites CA-04 or CA-03 reached ~40% or 30%, respectively (Figures 4 and 5, Table 4). The proportion of dissolved Fe(II) during the reduction of γ-irradiated BIOS from sites CA-04 or CA-03 in the presence of 10μM of phosphate reached ~60% of total Fe(II) as opposed to ~80% of total Fe(II) determined during the reduction of non-irradiated BIOS (Figures 4 and 5). In contrast to the biotic microcosms, no significant changes in total Fe(II) were noted throughout the duration of the experiment and only negligible amounts of dissolved Fe(II) were present in the control microcosms (Figures 4 and 5).

Initial concentrations of dissolved phosphate within control and selected biotic microcosms with 3.9mM of phosphate were within the range of 3.81-3.86mM (Table S4). Within the biotic microcosms, the concentration of phosphate declined to 1.64-1.88mM at termination of the experiment (Table S4). In contrast, phosphate slightly declined within control microcosms reaching 3.22mM at termination of the experiment (Table S4). Across all microcosms containing 3.9mM of phosphate, the molybdate concentration was determined to be below the detection limit of the instrument.

3.5. Statistical analyses: rate and extent of Fe(III) reduction

The rates of reduction of HFO, non- and γ-irradiated BIOS by *S. putrefaciens* CN32 were calculated by linear regression of selected time points that correspond to the period of maximum accumulation of total Fe(II) relative to total Fe. A summary of the regression data is presented in Table 4. In the case for non-irradiated BIOS, the rates of Fe(III) reduction in the presence of *S.*

putrefaciens CN32 were calculated during the early stages of the experiment prior to the detection of sulfide in order to avoid the possible overestimation of Fe(III) reduction due to the production of sulfide. The rates of reduction within the control microcosms conducted with non-irradiated BIOS were calculated using a similar approach, a summary of the regression data is given in Table S5. It is important to note that the rates of Fe(III) reduction within control microcosms conducted with non-irradiated BIOS and 3.9mM of phosphate were calculated during the later stages of the experiment, therefore Fe(III) reduction was likely induced by both the activity of native bacteria and sulfide (Figures 4 and 5, S10 and S11). In order to determine the effects of the concentration of molybdate and/or phosphate on the rates and extent of Fe(III) reduction across all treatments in the presence of *S. putrefaciens* CN32, two factor ANOVA and in some cases, single factor ANOVA analyses were conducted. A detailed and thorough analysis of the statistics is given in the Appendix (see Tables S6-S35), here we present the general significant trends determined from the data.

The rates of HFO reduction by *S. putrefaciens* CN32 within experiments conducted with 3.9mM of phosphate and molybdate:sulfate concentrations of 0:1, 1:1, or 2:1 were determined to be, respectively, 0.065±0.011, 0.080±0.010, or 0.087±0.016 day^{-1}(Table 4). Interestingly, the rates of reduction of HFO by *S. putrefaciens* CN32 in the presence of 10μM of phosphate and molybdate:sulfate concentrations of 0:1, 1:1, or 2:1 approached those determined in the presence of 3.9mM of phosphate, in which case the rates were determined to be 0.054±0.004, 0.073±0.005, or 0.086±0.005 day^{-1}, respectively (Table 4). In general, the concentration of molybdate did not significantly influence the rate or extent of reduction of HFO in the presence of 3.9mM of phosphate ($p>0.05$, Table 4). In contrast, the concentration of molybdate significantly enhanced the rate and extent of reduction of HFO in the presence of 10μM of phosphate ($p<0.05$, Table 4).

Overall, the concentration of phosphate did not significantly influence the rate of reduction ($p>0.05$, Table 4), but did influence the extent of reduction of HFO, in which case a significantly higher amount of Fe(III) was reduced in the presence of 3.9mM of phosphate when compared to those determined in the presence of 10μM of phosphate ($p<0.05$, Table 4).

The rates of reduction of non-irradiated BIOS from site CA-04 by *S. putrefaciens* CN32 within batch experiments conducted with molybdate:sulfate concentrations of 1:1 or 2:1 were determined to be, in the presence of 3.9mM of phosphate, 0.066±0.004 or 0.066±0.012 day^{-1}, respectively, whereas in the presence of 10μM of phosphate, the rates were determined to be 0.066±0.006 or 0.067±0.006 day^{-1}, respectively (Table 4). The rates of reduction of non-irradiated BIOS from site CA-03 by *S. putrefaciens* CN32 within batch experiments conducted with molybdate:sulfate concentrations of 1:1 or 2:1 approached those determined for non-irradiated BIOS from site CA-04 in the presence of 3.9mM of phosphate, which were determined to be 0.070±0.005 or 0.061±0.010 day^{-1}, respectively (Table 4). In contrast, the rates of reduction of non-irradiated BIOS from site CA-03 by *S. putrefaciens* CN32 within batch experiments conducted with 10μM of phosphate and molybdate:sulfate concentrations of 1:1 or 2:1 were much lower, in which case the rates were determined to be 0.047±0.005 or 0.046±0.006 day^{-1}, respectively (Table 4). Overall, in contrast to experiments conducted with HFO and regardless of the concentration of phosphate, the concentration of molybdate did not significantly affect the rate or extent of reduction of non-irradiated BIOS (although there are some exceptions, see Appendix) ($p>0.05$, Table 4). In contrast, the concentration of phosphate influenced the extent of reduction of non-irradiated BIOS from both sites, in which case a significantly higher amount of Fe(III) was reduced in the presence of 3.9mM phosphate when compared to those determined in the presence of 10μM of phosphate ($p<0.05$, Table 4). The concentration of phosphate did not significantly

influence the rate of reduction of non-irradiated BIOS from site CA-04 ($p>0.05$, Table 4), but did significantly influence the rate of reduction of non-irradiated BIOS from site CA-03, in which case the rates were significantly higher in the presence of 3.9mM of phosphate when compared to those determined in the presence of 10μM of phosphate ($p<0.05$, Table 4). In general, it appears that the rate and extent of reduction for non-irradiated BIOS from sites CA-04 and CA-03 did not significantly vary in the presence of 3.9mM of phosphate and at corresponding molybdate concentrations (although there are some exceptions, see Appendix) ($p>0.05$, Table 4). In contrast, non-irradiated BIOS from site CA-04 were reduced at a significantly faster rate than non-irradiated BIOS from site CA-03 in the presence of 10μM of phosphate ($p<0.05$, Table 4). In general, it appears that the extent of reduction of non-irradiated BIOS from sites CA-04 and CA-03 in the presence of 10μM of phosphate was, more-or-less, equal (see Appendix for pairwise comparisons) (Table 4).

The rates of reduction of γ-irradiated BIOS from sites CA-04 or CA-03 by *S. putrefaciens* CN32 in the presence of 3.9mM of phosphate approached those determined for non-irradiated BIOS, in which case the rates were determined to be 0.068±0.006 or 0.061±0.015 day^{-1}, respectively (Table 4). In contrast, in the presence of 10μM of phosphate, the rates of reduction of γ-irradiated BIOS from sites CA-04 or CA-03 by *S. putrefaciens* CN32 were slow, in which the case the rates were determined to be 0.035±0.005 or 0.028±0.001 day^{-1}, respectively (Table 4). The concentration of phosphate had a significant effect on the rate and extent of reduction of γ-irradiated BIOS, in which case BIOS were reduced faster and to a higher extent in the presence of 3.9mM of phosphate when compared to those determined in the presence of 10μM of phosphate ($p<0.05$, Table 4). At corresponding phosphate concentration, no significant difference was found between the rates of reduction between the two sites indicating that BIOS from both sites were

equal in reactivity ($p>0.05$, Table 4). In contrast, it appears that a significantly higher amount of Fe(III) was reduced for γ-irradiated BIOS from CA-04 when compared to that of γ-irradiated BIOS from site CA-03 at corresponding phosphate concentrations ($p<0.05$, Table 4).

Across the entire dataset for experiments conducted with 3.9mM of phosphate, the rates of reduction did not significantly vary suggesting that the rates of reduction for γ-irradiated BIOS were not significantly different than those determined for non-irradiated BIOS and in turn, the rates of reduction of non- and γ-irradiated BIOS did not significantly differ from the rates of reduction for HFO at corresponding molybdate concentrations (see Appendix for pairwise comparisons) ($p>0.05$, Table 4). In contrast, for experiments conducted with 10μM of phosphate, regardless of the molybdate concentration the rates of reduction of non-irradiated BIOS were significantly higher than those determined for γ-irradiated BIOS ($p<0.05$, Table 4). For experiments conducted with 10μM of phosphate, the rate of reduction of HFO was found to be significantly higher than that of γ-irradiated BIOS (in the absence of molybdate) ($p<0.05$, Table 4), at corresponding molybdate concentrations the rates of reduction of HFO were also significantly higher than those determined for non-irradiated from site CA-03 ($p<0.05$, Table 4). In contrast, under the same conditions, no significant difference was observed between the rates of reduction of HFO and non-irradiated BIOS from site CA-04 in the presence of molybdate:sulfate concentration of 1:1 ($p>0.05$, Table S31). However, the rate of reduction of HFO was significantly higher than that of non-irradiated BIOS from site CA-04 determined in the presence of molybdate:sulfate concentration of 2:1 and 10μM of phosphate ($p<0.05$, Table S31). In general, non-irradiated BIOS were reduced to a significantly higher extent than γ-irradiated BIOS at corresponding phosphate concentrations ($p<0.05$, Table 4). Although it may appear that non-irradiated BIOS were reduced to a higher extent than HFO in the presence of 3.9mM of

phosphate (Table 4), it is important to note that experiments conducted with HFO and molybdate were terminated after 14 days in comparison to experiments conducted with non-irradiated BIOS which were terminated after 17-19 days (Figures 3-5). Therefore, it is possible for HFO reduction to continue as observed with experiments conducted with HFO but without molybdate which reached ~90% (Table 4 and Figure 3). Nonetheless, statistical analysis revealed that a significantly higher amount of Fe(III) was reduced for non-irradiated BIOS than HFO in the presence of either 1:1 or 2:1 molybdate:sulfate concentration ($p<0.05$, Table 4). For experiments conducted with 3.9mM of phosphate, HFO in the absence of molybdate was reduced to a significantly higher extent than γ-irradiated BIOS (within 18 days of reduction) ($p<0.05$, Table 4). At corresponding molybdate:sulfate concentrations, a significantly higher amount of Fe(III) was reduced for non-irradiated BIOS when compared to HFO in the presence of 10μM of phosphate ($p<0.05$, Table 4). Under similar conditions, however, no significant difference was found between the maximum amount of Fe(III) reduced for HFO (in the absence of molybdate) and γ-irradiated BIOS from site CA-04 ($p>0.05$, Table 4), but a significantly higher amount of HFO was reduced when compared to that of γ-irradiated BIOS from site CA-03 ($p<0.05$, Table 4).

Interestingly, the rate and extent of reduction of non-irradiated BIOS from sites CA-04 or CA-03 by the native bacteria (control microcosms), although highly variable, were lower than or approached those determined in the presence of *S. putrefaciens* CN32 (Tables 4 and S5). In general, the concentrations of molybdate and phosphate did not significantly influence the rate of reduction by the native bacteria (two factor ANOVA without replication, $p>0.05$, Table S5), and it seems that a higher amount of Fe(III) was reduced in the presence of 3.9mM of phosphate when compared to those determined in the presence of 10μM of phosphate by the native bacteria (Table S5), but two-way ANOVA without replicates revealed that the extent of reduction did not

significantly vary as a function of the concentration of phosphate or molybdate ($p>0.05$, Table S5). A comparison in the rate and extent of reduction between the two sites at corresponding phosphate and molybdate concentrations, reveals no significant difference indicating that BIOS from both sites were reduced at an equal rate and to the same degree (two-way ANOVA without replication $p>0.05$, Table S5). At corresponding molybdate concentrations and in the presence of 3.9mM of phosphate, the rates of reduction of non-irradiated BIOS by the native bacteria were not significantly different than those determined in the presence of *S. putrefaciens* CN32 (determined by t-test $p>0.05$, Tables 4 and S5). Under the same conditions, the rates of reduction of non-irradiated BIOS by the native bacteria did not significantly differ than those determined for HFO (at corresponding molybdate concentrations) and γ-irradiated BIOS (determined by t-test $p>0.05$, Tables 4 and S5). One exception was that the rate of reduction of HFO by *S. putrefaciens* CN32 was significantly higher than the rate of reduction of non-irradiated BIOS from site CA-04 by the native bacteria in the presence of molybdate:sulfate concentration of 1:1 and 3.9mM of phosphate (determined by t-test $p<0.05$, Tables 4 and S5). In contrast to experiments conducted with 3.9mM of phosphate, the rates of reduction determined for non-irradiated BIOS in the presence of *S. putrefaciens* CN32 were significantly higher than the rates of reduction by the native bacteria at corresponding molybdate concentrations and in the presence of 10μM of phosphate (determined by t-test $p<0.05$, Tables 4 and S5). One exception was that the rate of reduction of non-irradiated BIOS from site CA-03 by *S. putrefaciens* CN32 and the native bacteria in the presence of molybdate:sulfate concentrations of 1:1 and 10μM of phosphate did not significantly differ (determined by t-test $p>0.05$, Tables 4 and S5). Interestingly, regardless of the molybdate concentration and in the presence of 10μM of phosphate, the rates of reduction of non-irradiated BIOS by the native bacteria were not significantly different than those determined for γ-irradiated

BIOS (determined by t-test $p>0.05$, Tables 4 and S5). In contrast, under the same conditions, the rates of reduction of HFO by *S. putrefaciens* CN32 were significantly higher than the rates of reduction of non-irradiated BIOS by the native bacteria (determined by t-test $p<0.05$, Tables 4 and S5). Interestingly, the maximum amounts of Fe(III) reduced by the native bacteria approached those determined in the presence of *S. putrefaciens* CN32 within experiments conducted with 3.9mM of phosphate (Tables 4 and S5).

3.6. Post-reduction secondary minerals

Solid phase transformation products of HFO and BIOS, where Fe(III) reduction had occurred, were different in appearance from the starting material. Their appearance also varied with the concentration of phosphate, in which case a light-green or dark-brown precipitate formed within microcosms containing 3.9mM or 10µM of phosphate, respectively. Where sulfide production had occurred, a black precipitate was found to form which was more obvious within microcosms containing 10µM of phosphate. In some instances, we also observed a colour change of the media from light-yellow/green to red within microcosms containing molybdate, 3.9mM of phosphate, and where sulfide production had occurred. In order to identify the mineral products, the residual minerals were analyzed with XRD and SEM. Regardless of the molybdate concentration, vivianite ($Fe_3(PO_4)_2 \cdot 8H_2O$) was the dominant product in all experiments conducted with 3.9mM of phosphate, it was clearly identified by XRD (Figures 7, S18 and S19), and its distinctive pinacoidal and bladed morphology (Figure 10A-C). The vivianite crystallites varied in size ranging from 5-40µm, and were often intergrown and aggregated (Figure 10B and C). Consistent with vivianite, energy dispersive X-ray spectroscopy (EDS) analysis of the precipitates generated spectra with strong signals corresponding to Fe, P, and O (Figure S22A and B). EDS analysis of the post-reduction precipitates that formed within biotic microcosms containing

molybdate and 3.9mM of phosphate conducted with non-irradiated BIOS also generated minor peaks corresponding to S, Mo, Na, and Ca (Figure S22A and B). Peaks which belong to Mo, however, were not observed in EDS spectra for vivianite precipitates that formed from the microbial reduction of HFO in the presence of molybdate (data not shown).

A greater diversity of minerals was observed for experiments conducted with 10μM of phosphate. XRD analysis of the residual mineral products that formed from the microbial reduction of HFO in the presence of 10μM of phosphate showed that goethite formed across all treatments (Figure 7). XRD analysis of such precipitates revealed another phase, which was identified as magnetite (Figure 7). The formation of magnetite, however, was found to be dependent on the concentration of molybdate, in which case as the concentration of molybdate increased the peaks for magnetite were found to diminish (Figure 7). Magnetite and goethite were also identified within the post-reduction residual products originating from the biotic microcosms conducted with BIOS from site CA-04 in the presence of 10μM of phosphate with and without the addition of molybdate (Figure 8). However, the dependency of magnetite formation on the molybdate concentration was not as obvious for these samples as those that formed from the reduction of HFO (Figures 7 and 8). Goethite was found to be the dominant residual mineral across all experiments conducted with BIOS from site CA-03 in the presence of 10μM of phosphate (Figure 9). No obvious differences were observed between the treatments for experiments conducted with BIOS, indicating that molybdate did not have a significant effect on the formation of minerals (Figures 8 and 9). SEM micrographs of the post-reduction residual products that formed in the presence of 10μM of phosphate showed the formation of aggregates (Figure 10D-F), but where it had formed, the individual crystallites of magnetite were not resolvable by SEM (Figure 10D and F). EDS analysis of these precipitates generated spectra with strong peaks corresponding to Fe, and minor peaks

corresponding to Mo (Figure S22 C-E). EDS analysis of the post-reduction residual products originating from biotic microcosms conducted with BIOS also generated minor peaks corresponding to P, Na, Ca, K, Si, and Al, but no sulfide was detected (Figure S22C and D). No vivianite was detected by either XRD or SEM within the post-reduction residual products originating from biotic microcosms conducted with 10μM of phosphate.

A similar suit of minerals was observed within the post-reduction residual products originating from the microcosms conducted with non-irradiated BIOS without the addition of *S. putrefaciens* CN32 (Figures S18-S21). It is important to note that, where sulfide production had occurred, sulfide containing minerals such as mackinawite or pyrrhotite were not detected by XRD across all treatments conducted with BIOS.

4. Discussion

4.1. Mineralogy of BIOS

XRD analysis of BIOS from sites CA-04 and CA-03 revealed that the precipitates were comprised of the poorly ordered iron oxide 2-line ferrihydrite, and the crystalline iron oxides magnetite or goethite (Figure 1). Quantification of the Fe-bearing mineral fractions within the BIOS samples by chemical extractions further showed that ferrihydrite made up the bulk of the samples (74-88%), with magnetite or goethite comprising a smaller proportion (12-26%, Table 2). The formation of a specific biogenic mineral phase depends on the prevailing geochemical conditions (e.g. pH, temperature), the rate of Fe(II) oxidation, and the presence of coprecipitating foreign species which may alter the identity and crystallinity of a mineral (Cornell and Schwertmann, 2003; Vollrath et al., 2013; Posth et al., 2014). The rapid oxidation of Fe(II) by coupled biotic and abiotic reactions with subsequent hydrolysis of iron within iron microbial mats often lead to the formation of 2-line ferrihydrite (Cornell and Schwertmann, 2003). Where

determined, the mineralogy of naturally occurring BIOS has often been reported to be dominated by a poorly ordered iron-bearing phase that resembles 2-line ferrihydrite as observed in this study (Figure 1) (Banfield et al., 2000; Chan et al., 2004; Chan et al., 2009; Toner et al., 2009; Langley et al., 2009b; Chan et al., 2011; Gault et al., 2011; Toner et al., 2012). The presence of crystalline iron oxides within naturally occurring BIOS has also been previously reported by a number of studies (Banfield et al., 2000; Chan et al., 2004; Hallberg and Ferris, 2004; Chan et al., 2009; Gault et al., 2011). For example, by means of ESEM X-ray spot analysis of iron oxides that formed within and outside of stalks produced by freshwater *Gallionella* spp., Hallberg and Ferris (2004) found that a crystalline iron-bearing phase with iron and oxygen atomic ratios similar to that of hematite first forms within the stalks. Subsequently, the initial precipitate acts as a template for continued precipitation and accretion of iron oxides whereby goethite and ferrihydrite form on the surface of stalks, thus, according to the model of Hallberg and Ferris (2004), precipitation occurs as a multistep process. In another study, Vollrath et al. (2013) found that lepidocrocite and ferrihydrite formed from the biotic oxidation of Fe(II) by a pure culture of FeOB, *Leptothrix cholodnii* Appels. A comparison between lepidocrocite formed in the presence and absence of bacteria revealed that biogenic lepidocrocite formed as nanoparticulates whereas abiogenic lepidocrocite formed as larger crystallites (Vollrath et al., 2013). Crystalline iron oxides found in close association of FeOB are often reported to occur as nanoparticulate phases, indicating that cell derived organic matter influence the size and characteristics of associated iron oxides (Gault et al., 2011; Vollrath et al., 2013). Such notion is supported by laboratory-based studies which showed that the oxidation of Fe(II) in the presence of non-Fe metabolizing cells had no effect on the identity of the mineral but influenced the morphology and size of the particles, in which case small-sized lepidocrocite particles formed in the presence of cell surfaces (Châtellier et al., 2001;

Châtellier et al., 2004). Consistent with previous studies, the relatively broad XRD peaks corresponding to goethite within BIOS from site CA-03 suggest that this mineral exists as a nanoparticulate phase (Figure 1). Although it is possible that the cell derived organic matter within BIOS may have played a role in controlling the crystal size, the XRD pattern corresponding to goethite resembles that of synthetic high surface area goethite, which forms by the slow oxidation of a pH-neutral solution containing Fe(II) and bicarbonate (Schwertmann and Cornell, 2008). Bicarbonate promotes the formation of goethite over other iron oxides, in particular lepidocrocite, and given that the tailings at Calumet Mine contain carbonate-rich minerals they could potentially serve as a source of bicarbonate leading to the formation of conditions favorable for the precipitation of high surface area goethite at site CA-03 (Schwertmann and Cornell, 2008). Thus, nanoparticulate goethite may have simply formed in solution and later passively adsorbed to cell derived organic matter (Warren and Ferris, 1998; Rancourt et al., 2005). The apparent lack of goethite at site CA-04 could be attributed to the differences in Fe(II) oxidation rates between the two sites (Figure 1). However, it is possible that goethite may occur within BIOS from site CA-04 at levels below the detection limit of bulk XRD (~5% by weight), as chemical extractions revealed that BIOS from site CA-04 were comprised of ~12% of crystalline Fe-bearing minerals which could correspond to both magnetite and goethite (Table 2).

It is well known that 2-line ferrihydrite is thermodynamically unstable and eventually transforms into goethite and/or hematite which are the most stable end members in the environment, the kinetics of which are dependent on the prevailing geochemical conditions (e.g. pH and temperature) (Cornell and Schwertmann, 2003). For example, it took ~10 years for synthetic 2-line ferrihydrite to partially transform (~60%) into a mixture of goethite and hematite at 4°C and pH-neutral conditions (Schwertmann et al., 2004). In contrast, synthetic 2-line

ferrihydrite transformed into hematite after ageing for 2 days at 80°C and pH-neutral conditions (Kennedy et al., 2004). The incorporation/adsorption of foreign species (e.g. Al, Si, organic matter) by ferrihydrite also influence the rate of transformation and, depending on the concentration, may completely inhibit transformation (Cornell and Schwertmann, 2003). A number of studies showed that the intermixed organic component within BIOS inhibits the transformation of ferrihydrite into crystalline phases by binding ferrihydrite nanoparticles to functional groups thereby preventing particle rotation and aggregation (Banfield et al., 2000; Kennedy et al., 2004; Toner et al., 2009; Chan et al., 2011; Toner et al., 2012; Vollrath et al., 2013). In agreement with previous findings, a comparison between the XRD diffraction patterns obtained from fresh and aged BIOS from site CA-04 showed no differences (Figure 1). In contrast, the higher peak intensity corresponding to goethite for aged BIOS from site CA-03 when compared to that of fresh BIOS from the same site may suggest some changes in the mineralogical composition may have occurred as a consequence of ageing, in which case the goethite fraction may have increased at the expense of ferrihydrite (Figure 1). These apparent changes, however, cannot be quantified by bulk XRD. Fresh BIOS from sites CA-04 and CA-03 were previously analyzed by extended x-ray absorption fine structure (EXAFS) to determine the relative proportions of Fe-bearing minerals (Cotroneo and Fortin, 2013). Although we did not analyze the aged BIOS by EXAFS in this study, we previously found that proportions of Fe-bearing minerals determined by chemical extractions agreed well with those determined by EXAFS, thus chemical extraction provide a reliable alternative (Najem et al., 2016). Within error, the proportions of the poorly ordered and crystalline iron-bearing minerals determined by chemical extractions for aged BIOS in this study were in good agreement of those previously determined for fresh BIOS by EXAFS (Table 2 and S36, Cotroneo and Fortin, 2013). Therefore, XRD, chemical extractions, and EXAFS indicate that ageing did not significantly affect

the mineralogical composition of the samples and the apparent changes in peak intensities of goethite within aged BIOS from site CA-03 likely reflect the heterogeneity of the natural samples. Thus, the combined influence of the low temperature at which BIOS were stored in this study (-15°C) together with the presence of intermixed organic matter significantly hindered/inhibited transformation (Figure 1).

4.2. Anaerobic reduction of HFO and BIOS

4.2.1. Effects of phosphate

The initial lag period observed prior the onset of HFO reduction by *S. putrefaciens* CN32 in the presence of 3.9mM or lower concentrations of phosphate was previously observed by studies using similar experimental protocols followed in this study (Glasauer et al., 2003; Langley et al., 2009b; Langley et al., 2009c; Langley et al., 2009d; Revesz et al., 2015). During such period, the facultative DIRB acclimate to the nutrient concentrations and the anaerobic conditions imposed by the growth medium. The shorter lag period and faster establishment of reducing conditions within biotic microcosms containing 3.9mM relative to microcosms containing 10μM of phosphate suggests that 3.9mM of phosphate may have stimulated the activity/growth of DIRB (Figures S2 and S3). Despite such stimulation, however, the rates of HFO reduction were found to be similar between the two phosphate treatments (at corresponding molybdate:sulfate concentrations) (Table 4). Phosphate is a well-known growth-limiting nutrient for bacteria in the environment as it is an essential constituent of phospholipids, nucleotides, proteins, nucleic acids, and cell membranes (Fredrickson et al., 1998; Glasauer et al., 2003). Thus, the addition of phosphate could be expected to stimulate the growth of bacteria and in turn enhance the rate and extent of Fe(III) reduction. Plate counts, however, showed that the viable cell numbers were similar between the two phosphate treatments during the first 12 days of the experiment (Figure S4),

suggesting that cell number was not the primary factor determining the rates of reduction. The initial concentrations of phosphate measured in solution within biotic microcosms conducted with 3.9mM of phosphate indicated that ~20% of the added phosphate quickly adsorbed to the surface of HFO (Table S4). Continued adsorption of phosphate to the mineral surface could block reactive sites thereby preventing the direct contact between DIRB and the mineral surface which could have, potentially, counteracted the observed "stimulation" and lowered the rates of reduction (Figure 3, Table 4) (Borch et al., 2007; O'Loughlin et al., 2010; Amstaetter et al., 2012). On the other hand, given the large surface area of HFO (~700m^2/g) (Cornell and Schwertmann, 2003), the initial adsorption of phosphate may have not blocked a significant proportion of the reactive mineral surface, and the observed rates of reduction were simply limited by physicochemical properties of HFO, thus the concentration of phosphate may have simply played no role in determining the rates of reduction. The adsorption of 10μM of phosphate to the surface of HFO is not expected to block a significant proportion of mineral reactive sites from DIRB, but it is expected to limit the bioavailability of phosphate for DIRB. Despite such limitation, however, we found that cells remained viable throughout the duration experiment and the cell numbers were comparable to those determined in the presence of 3.9mM of phosphate (Figure S4). Even as HFO reduction reached a plateau at day 6 within microcosms containing 10μM of phosphate, cell numbers remained constant suggesting that cells were able to derive sufficient energy and yet no significant increase in Fe(II) occurred (Figure 3). The observed cessation of HFO reduction could be attributed to a number of factors.

As Fe(III) reduction proceeds in the presence of 10μM of phosphate, Fe(II) is released into solution which adsorbs to the mineral surface since Fe(II) has a strong affinity for iron oxides (Hansel et al., 2003a; Hansel et al., 2005; Langley et al., 2009b). Fe(II) also binds to the negatively

charged functional groups on the cell surface of DIRB (Urrutia et al., 1998; Glasauer et al., 2003). These reactions lead to the passivation of the mineral and cell surfaces by Fe(II) which blocks DIRB from accessing the remaining Fe(III) from enzymatic reduction (Urrutia et al., 1998; Fredrickson et al., 1998; Zachara et al., 2002; Roden and Urrutia, 2002). In addition, the interaction of Fe(II) with the meta-stable HFO catalytically transforms this mineral into crystalline iron oxides such as goethite or magnetite, as we observed in this study (Figure 7), which possess a lower surface area than HFO further limiting microbial reduction (Roden and Zachara, 1996; Cornell and Schwertmann, 2003; Hansel et al., 2003a; Hansel et al., 2005). Moreover, magnetite reduction by DIRB is thermodynamically favorable at pH<7 but not at pH>7 (Fredrickson et al., 1998; Dong et al., 2000; Hansel et al., 2003a). Finally, the released Fe(II) will likely react with the limited phosphate available in the media to form in-accessible vivianite ($Fe_3(PO_4)_2 \bullet 8H_2O$) which has a low solubility (log K_{sp} of -36), thus DIRB will also have to compete with Fe(II) for limited phosphate which will further impede microbial growth (Postma, 1981; Glasauer et al., 2003). During the plateau period where limited Fe(III) reduction could occur together with limited nutrient availability, DIRB may have existed as cell clusters to increase survival via cell-cell cooperation and they may have utilized organic by-products as alternative electron acceptors originating from lysed cells (Glasauer et al., 2003). As resources were depleted, cell viability eventually drops at the end of the experiment (Figure S4). In contrast to experiments conducted with 10μM of phosphate, as reduction of HFO proceeds in the presence of excess phosphate (3.9mM) the released Fe(II) reacts with phosphate to form strong aqueous complexes and precipitate as vivianite (Fredrickson et al., 1998; Kukkadapu et al., 2004). Such notion is supported by the low concentration of dissolved Fe(II) measured within biotic microcosms containing 3.9mM of phosphate and the decline of dissolved phosphate concentration at the end of the experiments

(Figure 3, Table S4). Through these reactions, phosphate counteracts the passivation of mineral and cell surfaces by Fe(II) thereby thermodynamically driving Fe(III) reduction forward, leading to a higher amount of Fe(III) reduced relative to experiments conducted with 10μM of phosphate (Figure 3, Table 4) (Fredrickson et al., 1998; Kukkadapu et al., 2004). Additionally, phosphate strongly binds to HFO preventing the interaction of Fe(II) with HFO and in turn inhibits the transformation of HFO into goethite or magnetite (Fredrickson et al., 1998; Galvez et al., 1999). Nonetheless, the extent of reduction of HFO in the presence of 3.9mM of phosphate only reached 75-90%, which is likely due to the decline of cell viability at the end of the experiments (Figure S4), and the passivation of mineral and cell surfaces with vivianite thereby blocking DIRB from accessing available Fe(III) (Roden and Urrutia, 2002).

In this study, the rate and extent of HFO reduction by *S. putrefaciens* CN32 determined in the presence of 3.9mM of phosphate and the absence of molybdate, did not agree well with previous studies using similar experimental procedures (Table 4). For example, Glasauer et al. (2003) reported rates of reduction of synthetic HFO of ~0.02 and 0.04 day^{-1}, and the maximum amount of Fe(III) reduced after 50-100 days reached 40 to 60%. In contrast, Langley et al. (2009b) found that synthetic HFO was reduced at a rate of ~0.162 day^{-1} and the maximum amount of Fe(III) reduced after 7 days of incubation reached ~78%. At present, we cannot explain the discrepancy between these studies, including this one, as all variables and culture conditions were replicated according to the methodology and protocols established by these studies. One possibility could be attributed to the health and viability of *S. putrefaciens* CN32, as noted by Glasauer et al. (2003), small variations in the pH, temperature, inoculum size, and the state of the cells could all affect the health and cell numbers of DIRB, which will in turn influence the rate and extent of Fe(III) reduction. Despite these possible variations, however, we found that the overall trends in the

growth of *S. putrefaciens* CN32 throughout the experimental duration in the presence of 3.9mM phosphate agreed well with previous studies, suggesting that cell growth and activity were proceeding normally. Another possibility, as noted by Langley et al. (2009b), could be attributed to the subtle differences in the mineralogy of HFO that are not readily detected by bulk XRD. Given the heterogeneous chemical composition and amorphous nature of HFO, such notion could offer an explanation (Cornell and Schwertmann, 2003).

Anaerobic incubations of non-sterilized BIOS amended with acetate and/or lactate as electron donor(s) by a number of studies revealed that BIOS serve as an excellent terminal electron acceptor for native iron-reducing bacteria (Emerson and Revsbech, 1994; Blöthe and Roden, 2009; Bruun et al., 2010). Such notion is supported by our results, which showed that significant Fe(III)-reduction occurred within control microcosms conducted with non-irradiated BIOS in the presence of 3.9mM or 10μM of phosphate (Figures 4 and 5, Table S5). Although the composition of the microbial community within the iron microbial mats at the Calumet New Mine was not determined in this study, studies that have probed the phylogeny of other iron microbial mats reported sequences related to fermenting bacteria, FeOB (*Gallionella* spp., *Leptothrix* spp., *Sideroxydans* spp.), DIRB (*Geobacter* spp., *Shewanella* spp., *Rhodoferax ferrireducens*, *Aeromonas*), SRB (*Desulfovibrio* spp., *Desulfosporosinus* spp.), and methanogens (Blöthe and Roden, 2009; Bruun et al., 2010; Gault et al., 2011; Gault et al., 2012; Roden et al., 2012; Fabisch et al., 2016). Thus, Fe(III) reduction within our samples may have been driven by native DIRB such as *Geobacter* spp. and *Shewanella* spp., however some fermenting bacteria (e.g. *Clostridium butyricum, Pelobacter propionicus*) and even SRB (e.g. *Desulfovibrio* spp.) are capable of enzymatically reducing Fe(III) (Coleman et al., 1993; Lovley et al., 1993; Dominik et al., 2002). Moreover, SRB such as *Desulfovibrio desulfuricans* or *Desulfovibrio vulgaris* could potentially derive energy from

the enzymatic reduction of Fe(III) to maintain cell growth and may have contributed to the observed production of Fe(II) within control microcosms (Figures 4 and 5, Table S5) (Coleman et al., 1993; Lovley et al., 1993). The lag period observed prior to the production of Fe(II) (8-12 days) within the control microcosms conducted with non-irradiated BIOS could be attributed to the acclimation of the native microbes to the medium, during that period the decline in Eh could be mediated by the outgassing of oxygen to reach equilibrium with the anaerobic atmosphere and heterotrophic bacteria that couple the oxidization of available organic matter to the reduction of dissolved O_2 thereby establishing conditions that favor fermentation, and Fe(III) and SO_4^{-2} reduction (Appelo and Postma, 2004). Although lactate may not be directly utilized by some Fe(III)-reducing bacteria and SRB as a carbon and electron source, fermentation of 3 moles of lactate by fermenting bacteria yields 1 mole of acetate and 2 moles of propionate according to the reaction (Bruun et al., 2010):

$$3C_3H_5O_3^- \rightarrow C_2H_3O_2^- + 2C_2H_5O_2^- + CO_2 + H_2O$$

The reaction by-products (acetate and propionate) could be utilized by native Fe(III)-reducing bacteria and SRB to further mediate Fe(III) and SO_4^{-2} reduction. The faster establishment of reducing conditions within control microcosms conducted with 3.9mM of phosphate and non-irradiated BIOS is likely due to the favorable nutrient conditions which stimulate the growth of native bacteria to mediate the aforementioned reactions (Figures 4 and 5). Under these conditions we found that Fe(III) and SO_4^{-2} reduction occurred simultaneously, more specifically it appears that after 8-10 days of incubation the concentration of sulfide and total Fe(II) increased together (Figures 4 and 5, S10 and S11). Lactate or acetate oxidation coupled to sulfate reduction by SRB leads to the production of reduced sulfide species that readily reduce iron oxides according to the reactions (Hansel et al., 2015):

$$2C_3H_5O_3^- + SO_4^{-2} \rightarrow 2C_2H_3O_2^- + 2HCO_3^- + HS^- + H^+ \quad (1)$$

$$C_2H_3O_2^- + SO_4^{-2} \rightarrow 2HCO_3^- + HS^- \quad (2)$$

$$HS^- + 2Fe(OH)_3(s) + 5H^+ \rightarrow 2Fe^{2+} + S^0 + 6H_2O \quad (3)$$

$$C_3H_5O_3^- + 2S^0 + 2H_2O \rightarrow C_2H_3O_2^- + HCO_3^- + 2HS^- + 3H^+ \quad (4)$$

$$Fe^{2+} + HS^- \rightarrow FeS_{(s)} + H^+ \quad (5)$$

Where $Fe(OH)_3$ corresponds to ferrihydrite (i.e. biogenic ferrihydrite), and $FeS_{(s)}$ corresponds to amorphous ferrous sulfide which gradually crystallizes to mackinwaite (FeS) (Stumm and Morgan, 2012). Assuming that a complete reduction of 0.14mM of sulfate from the media by SRB occurs, which yields 0.14mM HS^- (1:1 molar ratio (1) or (2)), and this amount reduces 0.28mM of Fe(III) (1:2 molar ratio (3)) which corresponds to 7% of total Fe(III) added to the media (4mM Fe(III)) and this amount is negligible. In fact, taking into account the speciation of reduced sulfur species and the volatility of H_2S leads to even lower concentration of HS^- available to reduce Fe(III). However, the abiotic reduction of Fe(III) by HS^- generates elemental sulfur (S^0 (5)), and probably other sulfur intermediates (e.g. sulfite) that could be reduced by SRB such as *Desulfovibrio* spp. or other bacteria that were found to occur within microbial iron mats, which leads to the perpetual recycling of sulfur species and the subsequent reduction of a significant amount of Fe(III) (3 and 4) (Gault et al., 2011; Lohmayer et al., 2014; Hansel et al., 2015). Therefore, the increase of Fe(II) within the control microcosms conducted with non-irradiated BIOS and 3.9mM of phosphate could be attributed to the indirect and/or direct reduction by SRB (reactions 1-5). However, the fact that Fe(II) also significantly increased within control microcosms conducted with non-irradiated BIOS and 10µM of phosphate and where no sulfate reduction occurred (Figures 4 and 5, S10 and S11), suggests that both native Fe(III)-reducing bacteria and SRB were likely operating simultaneously. The presence of excess phosphate (3.9mM) and lactate (20mM) likely supported both native Fe(III)-reducing bacteria and SRB without leading to the competitive exclusion of SRB by Fe(III)-

reducing bacteria under otherwise carbon substrate limited conditions as previously reported in sediments (Lovley and Phillips, 1987; Chapelle and Lovley, 1992; Appelo and Postma, 2004).

Similar trends in the changes of Eh were observed across all biotic microcosms conducted with non-irradiated BIOS indicating that, as opposed to HFO and regardless of the phosphate concentration, reducing conditions were established at an equal rate and extent (Figures S5-S8). We also found that reducing conditions were established much faster within microcosms conducted with non-irradiated BIOS relative to microcosms conducted with HFO (Figures S2 and S3, S5-S8). Consequently, the lag period before the onset of reduction of non-irradiated BIOS was either abbreviated or absent (Figures 4 and 5). These observations are in good agreement with previous studies that utilized BIOS as terminal electron acceptors (Langley et al., 2009b; Langley et al., 2009c). In contrast to HFO, the concentration of phosphate was found to have contrasting effects on the rates of reduction of non-irradiated BIOS, but overall, 3.9mM of phosphate significantly enhanced the extent of reduction (Figures 4 and 5, Table 4). The concentration of phosphate did not significantly influence the rates of reduction of non-irradiated from site CA-04 but it significantly influenced the rates of reduction of non-irradiated from site CA-03, in which case the rates of reduction of BIOS from site CA-03 in the presence of 10μM of phosphate were significantly slower than those determined in the presence of 3.9mM of phosphate (Table 4). The higher rate of reduction of non-irradiated BIOS from site CA-03 in the presence of 3.9mM of phosphate could be attributed to the increase of cell number of DIRB observed within 2 days of inoculation, whereas cell numbers of DIRB within biotic microcosms containing 10μM of phosphate slightly declined (Figure S9). These changes in cell numbers, however, were also observed within microcosms conducted with non-irradiated BIOS from site CA-04, and yet the rates of reduction did not vary between the phosphate treatments (Figure S9). It is possible that the

native Fe(III)-reducing bacteria may have contributed to the production of Fe(II), a higher cell density of native Fe(III)-reducing bacteria within non-irradiated BIOS from site CA-04 relative to non-irradiated BIOS from site CA-03 would lead to the production of a higher amount of Fe(II) thereby enhancing the rate of reduction in the presence of 10μM of phosphate (Table S5). If that was indeed the case, then the rate of reduction of non-irradiated BIOS would have also proceeded at a faster rate than the rate of reduction of non-irradiated BIOS from site CA-03 in the presence of 3.9mM of phosphate, which we did not observe (Table 4). At this time, we cannot explain the observed enhanced rate of reduction of non-irradiated BIOS from site CA-04 relative to the rates of reduction determined for non-irradiated BIOS from site CA-03 in the presence of 10μM of phosphate.

The effects of phosphate on the rate and extent of reduction BIOS were more apparent for experiments conducted with γ-irradiated BIOS, in which case the rates and extent of reduction of BIOS increased with increasing phosphate concentration (Figures 4 and 5, Table 4). Such difference could be attributed to the change in DIRB cell numbers between the two phosphate treatments, in which case cell numbers were found to increase for the first half of the experiment within biotic microcosms containing 3.9mM of phosphate, whereas the cell numbers within biotic experiments containing 10μM of phosphate exhibited an overall decline throughout the duration of the experiment (Figure S16). Thus, in addition to abiotic effects, 3.9mM of phosphate enhanced the bioreduction of BIOS via stimulation of cell biosynthesis. The fact that the rates of reduction of Fe(III) did not significantly vary between the two sites at corresponding phosphate concentrations, suggests that the BIOS samples did not exhibit different physicochemical properties (Table 4). We also found that the rates of reduction of HFO determined in the absence of molybdate were not significantly different than those determined for γ-irradiated BIOS in the

presence of 3.9mM of phosphate (Table 4). Under the same conditions, however, HFO was reduced to a significantly higher extent than γ-irradiated BIOS (Table 4). In contrast to our results, Langley et al. (2009a) and Langley et al. (2009b) investigated the reactivity of marine and freshwater γ-irradiated BIOS in the presence of 3.9mM of phosphate and found that BIOS were reduced at a much higher rate and to a higher extent than HFO. The enhanced reduction was attributed to the presence of cell derived organic matter which stimulated reduction by providing additional nutrient sources for DIRB, acting as electron shuttles, or complexing released Fe(II) thereby preventing it from blocking reactive sites on the oxide and DIRB surface (Langley et al., 2009b; Langley et al., 2009c). We also found that the rates and extents of reduction determined for γ-irradiated BIOS from sites CA-04 and CA-03 in the presence of 3.9mM of phosphate were significantly lower than those previously reported by Cotroneo and Fortin (2013) (Table 4). However, it should be noted that the measured changes in viable cell numbers along with Eh and pH during the reduction of γ-irradiated BIOS in the presence of 3.9mM of phosphate in this study were comparable to those previously reported by Langley et al. (2009b) and Cotroneo and Fortin (2013). This suggests that other factors related to the physicochemical properties of the BIOS samples used were responsible for the observed discrepancy between these studies and this one. We previously found that long-term ageing of BIOS (~5 years) at 4ºC promoted the aggregation of the iron oxide nanoparticles and in turn significantly lowered the reactivity of BIOS towards microbial reduction (Najem et al., 2016). In this study, our samples were stored at -15ºC for ~2 years, thus a similar operating mechanism maybe responsible for the apparent drop in reactivity of frozen BIOS. In agreement with such notion, recent work showed that freezing 6-line ferrihydrite at -15ºC significantly lowered its capacity to adsorb copper ions, and such decline was attributed to the aggregation of ferrihydrite nanoparticles (Gilbert et al., 2009). Apparently, freezing results

in the loss of interstitial water and pore spaces between nanoparticles thereby inducing compaction and aggregation which could in turn lead to the decline of surface area (Gilbert et al., 2009). Surface area is often used as a quantitative indicator of the reactive site density available for microbial iron reduction (Roden and Zachara, 1996; Roden, 2003). Accordingly, surface area could be used as a predictor of the potential iron reduction rate whereby an increase in mineral surface area tends to promote the microbial iron reduction and vice versa (Roden and Zachara, 1996; Roden, 2003). Although, the surface area of the BIOS samples in this study was not measured, previous work by our group showed that surface area measurements of BIOS by N_2 BET analysis were often highly variable, which was attributed to the presence of variable proportions of microbial cells and their exudates within the samples (Langley et al., 2009b; Langley et al., 2009c; Najem et al., 2016). Recent studies also found that surface area was generally a poor predictor of reactivity of BIOS and impure ferrihyrites (Cutting et al., 2009; Langley et al., 2009d; Ekstrom et al., 2010). Therefore, surface area measurements of BIOS used in the present study would have provided no usable information.

The rate of reduction of HFO determined in the absence of molybdate was significantly higher than those determined for γ-irradiated BIOS in the presence of 10μM of phosphate, whereas the amount of Fe(III) reduced for HFO was not significantly higher than the amount of Fe(III) reduced for γ-irradiated BIOS from site CA-04, but it was significantly higher than the amount of Fe(III) reduced for γ-irradiated BIOS from site CA-03 (Table 4). These results are rather unexpected as the presence of cell derived organic matter within BIOS was previously proposed to promote microbial reduction of Fe(III), presumably by binding Fe(II) away from DIRB and mineral surfaces thereby counteracting surface passivation by Fe(II) (Langley et al., 2009b). Thus, a higher rate and extent of reduction of Fe(III) would be expected for BIOS than HFO, particularly

at low phosphate concentrations. However, the concentrations of dissolved Fe(II) during the reduction of γ-irradiated BIOS reached ~60% of total Fe(II) similar to the amount determined during the reduction of HFO (Figures 3-5). This suggests that cell derived organic matter played no role in forming soluble Fe(II) complexes. Thus, it is possible that the aggregated mineral fraction may have protected the organic fraction from microbial degradation. The lower rates of reduction of γ-irradiated BIOS relative to the rate of reduction of HFO in the presence of 10μM of phosphate could be attributed to aggregation, Fe(II) passivation, and differences in DIRB growth dynamics. As previously mentioned within biotic microcosms conducted with HFO, cell counts remained relatively constant for ~12 days, whereas cell number of DIRB within microcosms conducted with γ-irradiated BIOS exhibited an overall decline throughout the duration of the experiment (Figure S16). Therefore, the decline in the viability of DIRB would likely explain the observed low rates of reduction and such decline could be attributed to the possible toxicity induced by Zn, Cu, and Pb previously adsorbed on the BIOS, which were likely released during the reductive dissolution of BIOS (Table 3) (Stone et al., 2006). DIRB may have overcome such toxicity under conditions favorable for growth (3.9mM phosphate) where we noted an increase in DIRB cell number (Figure S16), whereas under growth limiting conditions DIRB may have been more susceptible towards toxicity. Despite the possible toxic effects of Zn and Pb, the native bacteria were capable of reducing a significant amount of Fe(III) within control microcosms conducted with non-irradiated BIOS probably because the native bacteria were acclimated to the concentrations of Zn and Pb within the BIOS samples (Figures 4 and 5, Table S5).

In summary, we found that the concentration of phosphate had contrasting effects on the rates of Fe(III) reduction by *S. putrefaciens* CN32, but, overall, 3.9mM of phosphate significantly enhanced the extent of Fe(III) reduction (Figures 3-5, Table 4). Our results are in general

agreement with previous studies, albeit the reported effects of phosphate in the literature are somewhat contradictory. For example, phosphate at a concentration of 4.3mM was found to enhance the rate of reduction of Ni- or Co-substituted goethite, but did not affect the overall amount of Fe(III) reduced when compared to experiments conducted without phosphate (Zachara et al., 2001). At similar concentrations, phosphate had no effect on the extent of reduction of Ni-substituted ferrihydrite (Fredrickson et al., 2001), and it did not influence the rate or extent of reduction of naturally occurring iron oxides (Zachara et al., 1998). In contrast, phosphate (up to 20mM) was found to enhance the rate and extent of reduction of Si-substituted ferrihydrite in the presence of an electron shuttle (Kukkadapu et al., 2004). Similarly, phosphate at a concentration of 3.9mM enhanced the bioreduction of ferrihydrite relative to microcosms conducted with 0.4mM of phosphate, despite the apparent similarity of viable cell numbers between the two treatments (Glasauer et al., 2003). Others reported that the addition of 0.8mM of phosphate lowered the rate but did not affect the extent of reduction of ferrihydrite (Amstaetter et al., 2012), whereas the addition of 0.5mM of phosphate lowered the rate but significantly enhanced the extent of reduction of lepidocrocite when compared to experiments conducted without phosphate (O'Loughlin et al., 2010). In contrast to previous studies where phosphate was added to the media as an aqueous phase and where an excess amount of electron donor was added, increasing the concentration of phosphate pre-adsorbed to the surface of ferrihydrite-coated sand was found to limit the amount of Fe(III) reduced by *S. putrefaciens* CN32 in the presence of low amount of electron donor (Borch et al., 2007). On the other hand, increasing the amount of bound (occluded/incorporated) phosphate into lepidocrocite (P/Fe molar ratio of 0-0.1) lowered the rate of Fe(III) reduction, but at P/Fe>0, phosphate enhanced the extent of Fe(III) reduction by *S. putrefaciens* CN32 in the presence of excess electron donor (O'Loughlin et al., 2013). The discrepancy between these studies, including

this one, could be attributed to differences in experimental setup (Borch et al., 2007), including: cell preparation (Glasauer et al., 2003), buffer used in the media (HCO_3^- vs. PIPES) (Fredrickson et al., 1998; Zachara et al., 2002; Borch et al., 2007), mode of phosphate addition (pre-adsorbed / bound vs. aqueous addition) (Borch et al., 2007; O'Loughlin et al., 2013), and concentration of electron donor (Fredrickson et al., 2003; Borch et al., 2007).

4.2.2. Effects of molybdate

Oxyanions stereochemically similar to SO_4^{-2} including CrO_4^{-2}, MoO_4^{-2}, WO_4^{-2} and SeO_4^{-2} are known to inhibit sulfate reduction by SRB and the approximate order of effectiveness of inhibition was reported to be $CrO_4^{-2} > MoO_4^{-2} = WO_4^{-2} > SeO_4^{-2}$ (Taylor and Oremland, 1979; Oremland and Capone, 1988). Despite its effectiveness, CrO_4^{-2} is not considered a specific inhibitor for SRB as it is highly toxic to other bacteria (Oremland and Capone, 1988), thus it was not chosen as an inhibitor for this study. In contrast, depending on the concentration, MoO_4^{-2} was found to specifically inhibit SRB without affecting other bacteria, in particular DIRB (Oremland and Capone, 1988; Lovley et al., 1993). Sulfate reduction proceeds by first activating the sulfate anion, whereby adenosine 5'-triphosphate (ATP) and ATP sulfurylase catalyze the conversion of sulfate to adenosine 5'-phosphosulfate (APS) and pyrophosphate (PPi) (Taylor and Oremland, 1979; Oremland and Capone, 1988; Muyzer and Stams, 2008)

$$ATP + SO_4^{-2} \rightarrow APS + PPi \quad (6)$$

APS is stable and is required for subsequent steps to recover energy for the cell (Oremland and Capone, 1988). Reduction of APS proceeds by APS reductase to form sulfite and adenosine 5'-monophosphate (AMP)

$$APS + 2e^- \rightarrow AMP + SO_3^{-2} \quad (7)$$

AMP is subsequently converted into two molecules of adenosine diphosphate (ADP) by ATP-dependent enzyme adenylate kinase and sulfite is catalytically reduced by sulfite reductase into sulfide, consequently two ATP molecules are required for sulfate activation (Oremland and Capone, 1988; Muyzer and Stams, 2008). Molybdate inhibits ATP sulfurylase and leads to the production of APMo instead of APS in reaction (6) which is unstable and, presumably, breaks down into AMP + molybdate (Taylor and Oremland, 1979; Oremland and Capone, 1988). The result of using molybdate is that ATP (energy) is used for substrate activation but an appropriate electron acceptor was not generated, which eventually leads to cell death from energy exhaustion (Taylor and Oremland, 1979; Oremland and Capone, 1988; Biswas et al., 2009). In other words, SRB preferentially utilize molybdate as a terminal electron acceptor since the Mo(VI)-Mo(IV) couple (Eh^0=0.58V, see Appendix for calculations) is slightly above that of the SO_4^{-2}/HS^- couple (Eh^0=0.25V, see Appendix for calculations) but cannot maintain growth (Tucker et al., 1997). The efficiency of molybdate as an inhibitor was assessed by a number studies in pure culture, natural sediments, and wastewater (Taylor and Oremland, 1979; Oremland and Capone, 1988; Yadav and Archer, 1989; Tanaka and Lee, 1997; Chen et al., 1998; Ranade et al., 1999; Nemati et al., 2001; Isa and Anderson, 2005; Fleming et al., 2006; Biswas et al., 2009; Avramescu et al., 2011). Presumably, since molybdate competes with sulfate, previous studies suggested that molybdate should be added at concentration equimolar to ambient sulfate in order to inhibit sulfate reduction by SRB (Taylor and Oremland, 1979; Oremland and Capone, 1988). Others, however, observed complete inhibition of sulfate reduction at molybdate:sulfate concentration of 0.002-0.33 in pure culture (Chen et al., 1998; Nemati et al., 2001; Biswas et al., 2009), and complete or temporary inhibition at molybdate:sulfate concentration of 0.03-0.1 in wastewater (Tanaka and Lee, 1997; Ranade et al., 1999; Isa and Anderson, 2005). In contrast, simultaneous reduction of molybdate

and sulfate occurred at equimolar concentrations by a pure culture of the SRB *Desulfovibriode sulfuricans* or *Desulfovibrio vulgaris* (Tucker et al., 1997). The discrepancy between these studies suggests that the efficiency of molybdate to inhibit SRB depends on a number factors including: (1) the mode of addition, continuous vs. single addition which could lead to the adaptation of SRB (Yadav and Archer, 1989; Tanaka and Lee, 1997; Ranade et al., 1999; Isa and Anderson, 2005), (2) pure culture vs. natural sample, in which case a higher concentration of molybdate is required for inhibition for natural samples indicating that the composition of the microbial community plays an important role (Nemati et al., 2001), (3) the metabolic state and density of SRB (Tucker et al., 1997; Nemati et al., 2001), (4) strain and thus the sensitivity of the sulfate reducing bacterium (Biswas et al., 2009), (5) the hydrodynamic state of SRB (biofilm vs. freely suspended) (Nemati et al., 2001), and (6) the bioavailability of molybdate in solution which is controlled by sorption reactions in the presence of clays and iron oxides (Oremland and Capone, 1988). The fact that sulfate reduction occurred in our experiments despite the addition of molybdate at concentrations higher than the amount utilized by previous studies where complete inhibition of SRB was reported, suggests that a combination of the aforementioned factors may have played a role in determining the efficiency of molybdate inhibition in this study.

With respect to the sorption of molybdate to HFO and BIOS in our experiments, we found that molybdate was quickly adsorbed to HFO but not BIOS in the presence of 10μM of phosphate (Table S4). The initial slight increase in pH following the addition of molybdate to microcosms conducted with HFO and 10μM of phosphate is likely due to the displacement of OH^- groups on the oxide surface by molybdate anions which bind to HFO via an inner-sphere monodentate complex (Gustafsson, 2003; Xu et al., 2006). In contrast to the positively charged HFO, BIOS are often negatively charged at neutral-pH conditions which is due to the incorporation of cell derived

organic matter that modify the zero-point charge (zpc) of the mineral fraction, thus repulsion between the negative charges likely explains the lower amount of molybdate adsorbed to BIOS at the start of the experiment (Cornell and Schwertmann, 2003; Kleinert et al., 2011). As Fe(III) reduction proceeds, however, the concentration of dissolved molybdate eventually declines (Table S4), which is likely due to the incorporation of molybdate into secondary iron-bearing minerals (Section 4.2.4) or, potentially, the indirect reduction of molybdate (Mo(VI)) to reduced insoluble Mo-bearing species mediated by Fe(II) as previously observed with the reduction of chromate (Cr(VI)) to Cr(III)-bearing species (Wielinga et al., 2001; Hansel et al., 2003b). Thermodynamic calculations revealed that abiotic reduction of molybdate by $Fe(II)_{diss}$ was energetically favorable (ΔG= -70.3kJ/mole, see Appendix for calculations). However, if Mo(VI) reduction did occur, we would have observed a change in the concentration of Fe(II) in which case a delay or a stagnation period in the production of Fe(II) would be expected in the presence of molybdate since Fe(II) would be oxidized to Fe(III) (Figures 3-5). The fact that we observed no delays or stagnation periods in the production of dissolved Fe(II) during the reduction of either HFO or BIOS in the presence of 1:1 or 2:1 molybdate:sulfate concentration and 10µM of phosphate, suggests that molybdate reduction by Fe(II) was not significant, or kinetically unfavorable. Therefore, the decline in the concentration of dissolved molybdate in the presence of 10µM of phosphate is likely due to the adsorption and/or incorporation of molybdate into secondary iron-bearing minerals (Section 4.2.4, Table S4).

In contrast to experiments conducted with 10µM of phosphate, molybdate remained in solution within microcosms containing 3.9mM of phosphate throughout the duration of the experiment (Table S4). Like molybdate, phosphate tends to bind to iron oxides via an inner-sphere monodentate complex but also forms an inner-sphere bidentate complex, thus both anions compete

for the same sites (Xu et al., 2006; Stumm and Morgan, 2012). Previous studies have shown that phosphate but not sulfate outcompetes molybdate for sorption sites at pH-neutral conditions (Gustafsson, 2003; Xu et al., 2006), as observed in this study (Table S4). In addition, despite the large surface area of HFO (~700m^2/g), the excess concentration of phosphate (3.9mM) used in this study oversaturates the adsorption capacity of HFO (assuming adsorption capacity of 2.5µmol phosphate/m^2) (Torrent et al., 1990; Glasauer et al., 2003). In contrast, 10µM of phosphate is not expected to significantly impact the adsorption of molybdate to HFO. The fact that the majority of molybdate remained in solution at the end of experiments conducted with 3.9mM of phosphate suggests molybdate was not sequestered by vivianite via adsorption or incorporation. The zpc of vivianite in water was previously reported to be ~5.3 which is negatively charged under pH-neutral conditions (Thinnappan et al., 2008), thus vivianite is not expected to adsorb molybdate (Table S4). Such notion is further supported by EDS analysis of the vivianite precipitates formed from the bioreduction of HFO in the presence of molybdate, in which case no signals belonging to Mo were detected (Figure S22). Collectively, for experiments conducted with non-irradiated BIOS, our results suggest that molybdate remained bioavailable, and where adsorption did occur, the concentration of dissolved molybdate:sulfate concentration at the end of the experiment remained at 0.6-1.4, well above the amount utilized by previous studies where complete inhibition of SRB was reported (0.002-0.33) (Tanaka and Lee, 1997; Ranade et al., 1999; Nemati et al., 2001; Isa and Anderson, 2005; Biswas et al., 2009). Thus, sorption reactions did not limit the bioavailability of molybdate to inhibit SRB in the presence of BIOS, suggesting that other factors played a role in determining the efficiency of molybdate to inhibit SRB.

In this study, we found that molybdate at concentrations equimolar to or double the concentration of sulfate within microcosms conducted with non-irradiated BIOS completely

inhibited SRB in some experiments whereas in others it either delayed sulfide production or it had no effect. Most notably, molybdate may have inhibited SRB in control microcosms conducted with non-irradiated BIOS and 10μM of phosphate whereas in the presence of 3.9mM of phosphate, molybdate had no effect on SRB across all microcosms conducted with non-irradiated BIOS (Figures S10 and S11). This suggests that nutrient availability (i.e. concentration of phosphate) together with other factors may also play an important role in determining the efficiency of inhibition of molybdate. Adding to the complexity of these systems is the capability of some SRB to potentially derive energy from using Fe(III) as an alternative electron acceptor, but not from the reduction molybdate (Coleman et al., 1993; Lovley et al., 1993; Tucker et al., 1997). Fe(III) utilization by SRB could have supported the growth of SRB to overcome the effects of molybdate. However, the significance of these reactions in our experiments is unknown and discussion pertaining to these reactions is limited by available data. Interestingly, for experiments conducted with non-irradiated BIOS, sulfide production was found to commence much earlier and reached higher concentrations within biotic microcosms when compared to controls (Figures S10 and S11). Within biotic microcosms, the metabolic activity of *S. putrefaciens* CN32 would have initiated the establishment of reducing conditions much quicker relative to control microcosms (Figures S10 and S11), and these conditions would have supported the faster growth and establishment of native SRB, thereby leading to the earlier production of sulfide. Sulfide production, however, was found to commence much sooner within biotic microcosms containing 3.9mM of phosphate when compared to those containing 10μM of phosphate, and this is likely due to the high nutrient conditions which favored the growth and establishment of SRB at an earlier stage in the experiment. The high nutrient conditions combined with excess electron donor present in the media would have also precluded the competition between *S. putrefaciens* CN32 and the native

bacteria. In contrast, in the presence of limited nutrients (10μM of phosphate), *S. putrefaciens* CN32 would have outcompeted the native SRB for nutrients during the early stages of the experiment. As Fe(III) reduction proceeds, however, and the released Fe(II) restricts further reduction by DIRB or the bioavailable Fe(III) fraction is depleted, SRB would now be capable of competing with DIRB for nutrients. Such notion is supported by the fact that sulfide production within microcosms containing 10μM of phosphate occurs as Fe(II) production ceases (Figures 4-5, and S10-S11). Conversely, molybdate may have simply interfered with SRB thereby delaying sulfide production. Such notion is supported by experiments conducted with non-irradiated BIOS from site CA-04 and 10μM of phosphate, in which case increasing the concentration of molybdate was found to further delay the production of sulfide. For example, sulfide was detected at day 11 or day 13 within experiments conducted with non-irradiated BIOS from site CA-04 and 10μM of phosphate with molybdate:sulfate concentrations of 1:1 or 2:1, respectively (Figure S10). The delaying effects are further supported by biotic experiments conducted with non-irradiated BIOS from site CA-04 and 10μM of phosphate but without adding molybdate, which showed that sulfide production commenced at day 10 (Figure S23). These trends, however, were not observed for biotic microcosms conducted with non-irradiated BIOS from site CA-03 and 10μM, probably due to differences in the abundance of SRB and composition of the microbial community between the two sites (Figure S10). Collectively, these results suggest that the activity of SRB and efficiency of molybdate were dependent on nutrient conditions. It should also be noted that sulfate concentrations were measured within the control microcosms conducted with non-irradiated BIOS and 10μM of phosphate at the start and end of the experiment to determine the potential for the BIOS samples to contribute additional sulfate to the media. We found that sulfate concentrations slightly increased at the end of the experiment (from 0.14mM to 0.15mM), indicating that

molybdate:sulfate concentrations remained more-or-less constant within microcosms containing 3.9mM of phosphate throughout the duration of the experiment.

The addition of molybdate did not have any significant effects on the bioreduction of BIOS in the presence of either 3.9mM or 10μM of phosphate (Table 4). To further test the effects of molybdate on the rate and extent of BIOS reduction, we conducted reduction experiments with non-irradiated BIOS from site CA-04 and 10μM of phosphate but without the addition of molybdate (Figure S23). We found that the rate of reduction in the absence of molybdate did not significantly differ from those determined in the presence of molybdate (Figure S23, Table 4). In contrast to BIOS, however, molybdate significantly enhanced the rate and extent of reduction of HFO in the presence of 10μM but not 3.9mM of phosphate (Table 4). In contrast to our results, O'Loughlin et al. (2010) found that the addition of 0.5mM molybdate or phosphate enhanced the extent but lowered the rate of reduction of lepidocrocite by *S. putrefaciens* CN32. O'Loughlin et al. (2010) attributed the lower rates of reduction to molybdate blocking reactive Fe(III) sites from DIRB. It should be noted that the concentrations of molybdate and lepidocrocite used by O'Loughlin et al. (2010) leads to molybdate occupying ~37% of the maximum adsorption capacity of lepidocrocite (lepidocrocite surface area of 73.13m^2/g and assuming an adsorption capacity of 2.5μmol molybdate/m^2) (Torrent et al., 1990). Similarly, in this study the concentrations of molybdate occupy ~19 and ~37% of the maximum adsorption capacity for HFO at molybdate concentrations of 0.14 and 0.28mM, respectively (assuming HFO surface area of 700m^2/g and an adsorption capacity of 2.5μmol molybdate/m^2) (Torrent et al., 1990; Cornell and Schwertmann, 2003). Thus, our results differ from those reported by O'Loughlin et al. (2010) despite the equivalent surface area occupied by molybdate on HFO and lepidocrocite. The contrasting results between this study and those reported by O'Loughlin et al. (2010) could be attributed differences

in the experimental setup, including cell preparation and the iron oxide used as the terminal electron acceptor. In contrast to O'Loughlin et al. (2010), in this study DIRB were grown in the presence of molybdate (0.14 or 0.28mM) to acclimate the cells to the conditions of the media which may have influenced the physiology or metabolic state of DIRB in an unknown matter. As previously stated by Glasauer et al. (2003), small variations in the pH, temperature, inoculum size, and the state of the cells could all affect the fitness and the numbers of DIRB which will in turn dictate the rate and extent of Fe(III) reduction. Plate counts, however, revealed no significant variation in cell viability between the molybdate treatments (Figure S4). This suggests that the observed effects are likely related to the physicochemical properties of the iron oxide and the interaction of molybdate with the iron oxide rather than the fitness or number of DIRB. It should be noted that experiment replications indicated that the observed effects of molybdate on the bioreduction of HFO was not spurious (data not shown). It is possible that the addition and subsequent adsorption of molybdate to HFO suspension may have influenced the flocculation and aggregation state of the HFO nanoparticles thereby increasing their bioavailability to DIRB (Kukkadapu et al., 2004). Such notion could be supported by the fact that molybdate had no significant effect on the bioreduction of BIOS in the presence of 10μM, since molybdate did not adsorb to the surface of BIOS as readily as with HFO (Table S4). As observed by O'Loughlin et al. (2010), we also found that molybdate enhanced the extent of Fe(III) reduction, and such enhancement could be attributed to molybdate controlling the formation of secondary iron minerals, in which case molybdate was found to inhibit the formation of magnetite which otherwise sequesters Fe(III) from reduction by DIRB (Figure 7) (Fredrickson et al., 1998; Dong et al., 2000). Therefore, it appears that the adsorption of molybdate to the surface of the oxide is

necessary to promote the reduction of Fe(III), presumably through controlling the aggregation state of HFO nanoparticles and the formation of secondary iron minerals.

4.2.3. Effects of γ-irradiation

Tests performed to determine the efficiency of γ-irradiation in sterilizing BIOS revealed that a dose of 14kGy was sufficient to eliminate or render inactive all culturable microbes without significantly altering the bulk mineralogy of the samples (data not shown). In agreement with our results, a number of studies found that γ-irradiation at the recommended doses (10-25kGy) were effective in sterilizing natural samples without inducing changes in the mineralogy higher than the detection limit of XRD (Herbert et al., 2005; Langley et al., 2009b). For example, Langley et al. (2009b) showed that γ-irradiation at a dose of 14kGy did not alter the bulk mineralogy of synthetic 2-line ferrihydrite and BIOS. Nonetheless, some changes may still occur below the detection limit of XRD. For example, Bank et al. (2008) found that γ-irradiation of sediments to a final dose of 20kGy did not alter the bulk mineralogy, but reduced the goethite content by an average of 7% as determined by Mössbauer. Whether or not the proportion of the minerals within irradiated BIOS from sites CA-04 and CA-03 were altered as in the study of Bank et al. (2008) is unknown, but any changes that may have occurred appear to be, on a bulk scale, insignificant (e.g. reduction of goethite by 7%).

In agreement with XRD, the rates of reduction of γ- and non-irradiated BIOS in the presence of 3.9mM of phosphate did not significantly vary indicating that irradiation had no significant impact on the mineralogy of BIOS (Table 4). This is surprising, because it would be expected that in addition to *S. putrefaciens* CN32 the native bacteria would contribute to the production of Fe(II) thereby enhancing the rate of reduction of non-irradiated BIOS. Previous studies showed that the rate of Fe(III) reduction is directly proportional to the number of viable

cells of DIRB, in which case as the number of DIRB increases the rate of reduction increases. However, this relationship eventually reaches a saturation point, in which case the rates of reduction become limited by the physicochemical properties of the iron oxide including aggregation state and surface area (Roden and Zachara, 1996). This relationship could potentially explain why the rates of reduction between γ- and non-irradiated BIOS in the presence of 3.9mM did not significantly vary, in which case, for non-irradiated BIOS, it is possible that the cell number of the native Fe(III)-reducing bacteria together with *S. putrefaciens* CN32 oversaturated the accessible Fe(III) sites which were also limited as a consequence of aggregation. In contrast to experiments conducted with 3.9mM of phosphate, the rates of reduction of γ-irradiated BIOS were significantly lower than those determined for non-irradiated BIOS in the presence of 10μM of phosphate. Such difference could be attributed to the contribution of the native bacteria to the reduction of non-irradiated BIOS as the overall growth pattern of *S. putrefaciens* CN32 was similar across all biotic microcosms conducted with BIOS and 10μM of phosphate (Figures S9 and S16). The contribution of the native bacteria to the reduction of non-irradiated BIOS is not surprising given the significant production of Fe(II) observed within control microcosms conducted with non-irradiated BIOS (Table S5).

We found that, at corresponding phosphate concentrations, a significantly higher amount of Fe(III) was reduced within biotic microcosms conducted with non-irradiated BIOS when compared to the amount of Fe(III) reduced for γ-irradiated BIOS (Figures 4 and 5, Table 4). For biotic experiments conducted with non-irradiated BIOS and 3.9mM of phosphate, we found that Fe(III) reduction increased during the later stages of the experiment (>10 days of incubation) and such increase was accompanied by the increase of sulfide production and the decline of DIRB (Figures 4 and 5, S9-S11). As previously discussed, the high nutrient conditions would have

supported the growth of native iron-reducing bacteria and SRB which would have contributed to the reduction of Fe(III) either directly or indirectly (reactions 1-5), thus explaining the observed trends. We also found that some sulfide production occurred within biotic microcosms conducted with γ-irradiated BIOS and 3.9mM of phosphate, but the concentration of sulfide was very low when compared to the amount produced within biotic microcosms conducted with non-irradiated BIOS (Figure S17). Such low concentrations of sulfide, however, are not expected to reduce a significant amount of Fe(III). In contrast to biotic experiments conducted with non-irradiated BIOS and 3.9mM of phosphate, the production of sulfide within biotic microcosms conducted with non-irradiated BIOS and 10μM of phosphate did not appear to influence the total amount of Fe(III) reduced, probably because the production of sulfide occurred much later and the concentration of sulfide was much lower within biotic microcosms containing 10μM of phosphate relative to the amount produced within biotic microcosms containing 3.9mM of phosphate (Figures 4 and 5, S10 and S11). This suggests that other factors contributed to the observed enhanced reduction of non-irradiated BIOS when compared to γ-irradiated BIOS in the presence of 10μM. The native Fe(III)-reducing bacteria would have likely contributed to the production of Fe(II). We also found that the proportion of dissolved Fe(II) during the reduction of γ-irradiated BIOS reached ~60% of total Fe(II) as opposed to ~80% of total Fe(II) determined during the reduction of non-irradiated BIOS in the presence of 10μM of phosphate (Figures 4 and 5). As previously discussed, surface passivation of the mineral and cell surfaces with Fe(II) block DIRB from accessing available Fe(III). The fact that a higher amount of dissolved Fe(II) was measured within biotic microcosms conducted with non-irradiated BIOS and 10μM of phosphate suggests that less Fe(II) was associated with the surface of BIOS. This would have allowed DIRB to access more Fe(III) thereby leading to a higher production of Fe(II) observed within microcosms conducted with non-

irradiated BIOS and 10µM of phosphate (Figures 4 and 5). Within these microcosms, the lower amount of Fe(II) associated with the surface of BIOS relative to the amount associated with the surface of γ-irradiated BIOS, suggests that Fe(II) formed soluble complexes with unidentified compounds (Figures 4 and 5). It is possible that Fe(II) was complexed by organic by-products produced by the active native bacteria, such as biofilms and extracellular organic matter. Thus, it is possible that a synergistic effect between *S. putrefaciens* CN32 and the native bacteria occurred, thereby enhancing the overall reduction of Fe(III) within biotic microcosms conducted with non-irradiated BIOS and 10µM of phosphate (Table 4).

Recent studies assessing the impact of γ-irradiation on the reactivity of iron oxides or Fe(III)-bearing sediments found that γ-irradiation enhanced the reduction of Fe(III) by DIRB. For example, Brown et al. (2014) found that the exposure of synthetic 2-line ferrihydrite and hematite to a dose of 1 MGy, ~70x higher than the dose used in this study, altered their crystalline structure, in which case 2-line ferrihydrite partially transformed into 6-line ferrihydrite or akaganeite, whereas hematite partially transformed into a poorly crystalline iron oxide. Consequently, the irradiated iron oxides were more prone to reduction by *Shewanella oneidensis* MR-1 in the presence of an electron shuttle (Brown et al., 2014). In another study, Brown et al. (2015) reported that γ-irradiation of sediment samples at doses of 0.6 and 38.6 kGy, may have enhanced the bioavailability of Fe(III) to reduction by *Geobacter sulfurreducens*. The contrasting results between this study and those reported by Brown et al. (2015) could be attributed to the experimental setup and the sample used. In their study, Brown et al. (2015) incubated the γ-irradiated sediments with *Geobacter sulfurreducens* without the addition of an electron donor. However, the highly ionizing energy of γ-irradiation leads to the generation of reactive radical species that form from the radiolysis of H_2O (e.g. $^{\bullet}OH$, $^{\bullet}e_{aq}^{-}$, $^{\bullet}H$, H_2O_2, $^{\bullet}O_2^{-}$) which react with

complex organic matter (McNamara et al., 2003; Berns et al., 2008; Yakabuskie et al., 2011). Radiation induced depolymerization of organic matter leads to the release of significant quantities of dissolved organic matter (DOC), which could be used by *Geobacter sulfurreducens* to mediate the reduction of Fe(III) (McNamara et al., 2003; Berns et al., 2008; Brown et al., 2015). Another potential effect of γ-irradiation is the removal of nitrate by radiolysis, which is thermodynamically more favorable as an electron acceptor for *Geobacter sulfurreducens* than Fe(III) (Stumm and Morgan, 2012; Brown et al., 2015). Collectively, the enhanced reduction of Fe(III) reported by Brown et al. (2015) could be attributed to changes in the chemistry of the sediment rather than the physical state of Fe(III)-bearing oxides within the sediments. In our study, radiation induced chemical changes in γ-irradiated BIOS may have occurred. However, the significance of these changes and their effects on Fe(III) reduction by *S. putrefaciens* CN32 are unknown, but given the favorable growth conditions (excess electron donor and 3.9mM of phosphate) they are not expected to significantly influence the reduction of BIOS. On the other hand, depolymerization of complex organic matter could release nutrients, including phosphate, which could stimulate the growth of DIRB and influence the reduction of BIOS particularly within biotic microcosms conducted with 10μM of phosphate (McNamara et al., 2003). However, we observed no differences in cell counts between biotic microcosms conducted with non- and γ-irradiated BIOS and 10μM of phosphate, suggesting that released phosphate, if any, had no significant impact on the viability of DIRB (Figures S9 and S16). We recently carried out microbial reduction experiments using non- and γ-irradiated (final dose of 30kGy) pure synthetic iron oxides (2-line ferrihydrite, goethite, and lepidocrocite), and synthetic iron oxides coprecipitated with organic matter (alginate) as terminal electron acceptors (Khan et al., manuscript in preparation). In agreement with our results in this study, we found no significant difference in the rates of microbial

reduction of Fe(III) between non- and γ-irradiated synthetic iron oxides (Khan et al., manuscript in preparation). This suggests that γ-irradiation at doses within or close to the recommended dose of sterilization (10-25kGy) do not significantly alter the physical state of iron oxides.

Finally, despite the apparent effectiveness of γ-irradiation in sterilizing the BIOS samples, sulfide production was detected within microcosms containing 3.9mM of phosphate. Previous studies have also noted the recovery of some microbial activity after ~1 week post-irradiation, which has been attributed to bacteria that are capable of forming endospores to survive under various environmental stresses, including γ-irradiation (Lotrario et al., 1995; McNamara et al., 2003; Brown et al., 2015). Previous studies that have probed the phylogeny of the microbial community within iron microbial mats have also identified sequences related to *Desulfosporosinus* spp., and this genus contains some radioresistant spore forming SRB (Brown et al., 2015; Fabisch et al., 2016). Thus, within our samples, the sulfide production could be attributed to spore forming SRB that may have survived γ-irradiation. Sulfide generation, however, was not detected within biotic microcosms conducted with γ-irradiated BIOS and 10μM of phosphate, and this could be attributed to the unfavorable conditions for SRB establishment, including low nutrients and, possibly, the higher redox potential measured, in which case reducing conditions were not as strongly established when compared to biotic microcosms conducted with 3.9mM of phosphate (Figures S14 and S15).

4.2.4 Post-reduction secondary minerals

The formation of a specific secondary iron mineral phase during the microbial reduction of Fe(III) is principally dictated by the concentration and flux of Fe(II) which are in turn controlled by a number of factors, including: the surface area, solubility and crystallinity of the Fe(III)-phase (Roden and Zachara, 1996; Bonneville et al., 2004; Cutting et al., 2009; Bonneville et al., 2009),

concentration of DIRB (Roden and Zachara, 1996; Zegeye et al., 2007; O'Loughlin et al., 2010), geochemical conditions (e.g. pH, bicarbonate as buffer, etc.) (Fredrickson et al., 1998; Zachara et al., 2002), presence of oxyanions (e.g. PO_4^{-3}, MoO_4^{-2}, etc.) (Fredrickson et al., 1998; O'Loughlin et al., 2010), presence of electron shuttles (Fredrickson et al., 1998), impurities (e.g. Al, Ni, adsorbed/coprecipitated organic matter) (Fredrickson et al., 2001; Ekstrom et al., 2010; Shimizu et al., 2013; Eusterhues et al., 2014), presence and nature of dissolved organic carbon (O'Loughlin, 2008), and orientation of the incubation vessel (Dippon et al., 2015). Consequently, a wide variety of secondary iron minerals have been identified during the microbial reduction of different iron oxides. A necessary requirement for the catalytic conversion of ferrihydrite into lepidocrocite, goethite, or magnetite is the adsorption of Fe(II) to the mineral surface and subsequent electron transfer. The proportions of the mineral products that form following the adsorption of Fe(II) to the surface of ferrihydrite depend on the concentration of Fe(II). For example, Hansel et al. (2005) showed that 2-line ferrihydrite transforms into lepidocrocite and goethite at low Fe(II) loading (<1.0 mmol Fe(II)/g 2-line ferrihydrite) whereas magnetite, lepidocrocite, and goethite are the dominant products at high Fe(II) loadings (>1.0 mmol Fe(II)/g 2-line ferrihydrite), the proportions of which were also depended on anions present in solution including Cl^-, SO_4^{-2}, and HCO_3^-. Phosphate, however, inhibits the formation of goethite and magnetite by (1) binding to the surface of ferrihydrite thereby preventing either dissolution and subsequent reprecipitation or internal recrystallization of ferrihydrite, and (2) forming vivianite and aqueous complexes with Fe(II) thereby preventing Fe(II) from reaching the required surface loading threshold to form goethite or magnetite (Fredrickson et al., 1998; Hansel et al., 2003a; Cornell and Schwertmann, 2003; Borch et al., 2007). Accordingly, vivianite was the dominant mineral identified in our experiments conducted with 3.9mM of phosphate and where Fe(III) reduction occurred, in agreement with

previous studies where a high concentration of phosphate was used (Figures 6, S18 and S19) (Fredrickson et al., 1998; Glasauer et al., 2003; Langley et al., 2009b). Nonetheless, under these conditions, it was proposed that magnetite could form in the adjacent environment of the iron reducing cell, whereby the alkaline microenvironment imposed by the cell together with the uptake of phosphate would lead to favorable conditions for the precipitation of magnetite. XRD analysis, however, failed to identify peaks that correspond to magnetite, although it may have formed below the detection limit of the instrument (~5% by weight) (Figure 6) (Glasauer et al., 2003).

The concentration of molybdate did not appear to influence the biomineralization products of HFO in the presence of 3.9mM phosphate (Figures 6, S18 and S19). In some instances, we observed a colour change of the media from light-yellow/green to red within microcosms conducted with non-irradiated BIOS, 3.9mM of phosphate, and where sulfide production had occurred. A similar change in colour was previously reported by a number of studies, which was attributed to the formation of Mo(V)-S complexes (Tucker et al., 1997; Chen et al., 1998; Biswas et al., 2009). Continued sulfidization of the Mo(V)-S complex eventually leads to the precipitation of Mo as molybdenite (MoS_2, Ksp = 10^{-43}) (Tucker et al., 1997; Wang, 2012). The formation of molybdenite would likely explain the slight decline of molybdate observed within the biotic microcosms at the end of the experiment (Table S4). In agreement with such notion, EDS analyses of the precipitates generated peaks that correspond to Mo and S (Figure S22). Molybdenite, however, was not detected by XRD which is probably due to its low abundance and attenuation of the peaks by vivianite (Figures S18 and S19). Interestingly, the intensity of the red colour was found to increase when suspensions of the post-reduction samples were left for >1 month under anaerobic conditions, which eventually led to the formation of a red precipitate. EDS analyses of the red precipitate generated strong spectra corresponding to Mo and S (data not shown). However,

XRD analysis of the red precipitate was not possible due to low sample quantity. The formation of Mo(V)-S complexes and molybdenite were also likely forming within biotic microcosms conducted with non-irradiated BIOS and 10μM of phosphate, since some sulfide production occurred, but it was difficult to visually detect the red colour.

Magnetite and goethite were the dominant minerals formed from the bioreduction of HFO in the presence of 10μM of phosphate (Figure 7). In agreement with our results, previous studies have also identified magnetite and/or goethite as biomineralization products of HFO in the presence of low concentrations or absence of phosphate (Fredrickson et al., 1998; Glasauer et al., 2003; Hansel et al., 2003a). The relatively broad peaks of goethite suggest that this mineral exists as a nanoparticulate phase in accordance with SEM (Figures 7 and 10). Similarly, SEM failed to resolve individual crystals of magnetite indicating that the magnetite crystals were also nanometer in size, in agreement with previous studies (Figure 10) (Fredrickson et al., 1998; Hansel et al., 2003a). The described morphology of magnetite further indicates that magnetite formed from the solid-state transformation of ferrihydrite, as magnetite retained the morphology of precursor ferrihydrite (Fredrickson et al., 1998). The formation of magnetite depends on the concentration and speciation of Fe(II), and pH (Hansel et al., 2003a; Hansel et al., 2005). As previously noted, a threshold value of >1.0 mmol Fe(II)/g 2-line ferrihydrite (equivalent to Fe(II)/Fe(III) of 0.11 mol/mol) is required for magnetite formation (Hansel et al., 2003a; Hansel et al., 2005), and this value was reached or exceeded at day 3 and throughout the duration of the experiment across all biotic microcosms conducted with HFO and 10μM of phosphate in the presence or absence of molybdate, and yet magnetite formation was diminished with increasing molybdate concentration (Figures 3 and 7). Magnetite formation also varies with pH, in which case the extent of magnetite precipitation increases with increasing pH (Hansel et al., 2005). However, the fact that the

measured pH values did not significantly vary between the molybdate treatments across all biotic microcosms precludes pH as a controlling factor (Figure S3). This suggests that molybdate played an important role in controlling the extent of magnetite precipitation. Similar to phosphate, the adsorption of molybdate to the ferrihydrite surface may have stabilized the nanoparticles into an immobile network thereby preventing the solid-state transformation of ferrihydrite into magnetite. In addition, molybdate may suppress the adsorption of Fe(II) to the surface of ferrihydrite via competition for reactive sites thereby interfering with Fe(II)-ferrihydrite reactions (Catalano et al., 2011). In accordance with this study, molybdate was found to inhibit the formation of magnetite and promote the formation of carbonate green-rust during the biotic reduction of lepidocrocite (O'Loughlin et al., 2010). Green-rust is a mixed-valent Fe(II)/Fe(III) mineral phase which possesses a hexagonal morphology and a variable composition as shown by the formula $[Fe^{II}_{(1-x)}Fe^{III}_{x}(OH)_2]^{x+}[(\frac{x}{n})A^{n-}\bullet(\frac{m}{n})H_2O]^{x-}$ where A corresponds to interlayer anions (Fredrickson et al., 1998; Ona-Nguema et al., 2002; Glasauer et al., 2003; O'Loughlin et al., 2013). Typical interlayer anions include Cl^-, CO_3^{-2}, SO_4^{-2}, and, possibly, PO_4^{-3}, but it is unknown if MoO_4^{-2} could be accommodated as an interlayer anion (Fredrickson et al., 1998; Ona-Nguema et al., 2002; Glasauer et al., 2003). XRD analyses of the precipitates formed in the presence of 10μM of phosphate and molybdate failed to detect green-rust, similarly SEM failed to detect any crystallites with a hexagonal morphology. Nonetheless, green-rust may have formed throughout the reduction period as a precursor to magnetite or goethite and it could be present below the detection of the instruments (Glasauer et al., 2003). The concentrations of molybdate were found to significantly decline at the end of the reduction experiments (Table S4). This is likely due to the adsorption and/or incorporation of molybdate into goethite and/or magnetite, in accordance with previous

studies which reported the adsorption/incorporation of As(V) into goethite or magnetite (Kocar et al., 2006; Tufano et al., 2008).

In contrast to synthetic HFO, delineating the secondary iron products of non- and γ-irradiated BIOS that formed in the presence of 10μM of phosphate is complicated by the fact that magnetite and/or goethite were originally present within the samples (Figure 1). Nonetheless, we can infer possible minerlization pathways based on the previously described trends. For example, molybdate did not adsorb to BIOS as readily as it did to HFO, correspondingly molybdate concentrations in solution remained higher at the end of the experiment within microcosms conducted with BIOS relative to those conducted with HFO in the presence of 10μM of phosphate (Table S4). This would suggest that the conditions would now be more favorable for the formation of magnetite given that most of the molybdate was not associated with the surface of BIOS. However, magnetite did not form within biotic microcosms conducted with non- and γ-irradiated BIOS from site CA-03 and 10μM of phosphate (Figure 9), despite Fe(II)/Fe(III) reaching and surpassing the required threshold for magnetite formation (Fe(II)/Fe(III) 0.11) (Figure 5). This suggests that, for BIOS, other factors inhibited the formation of magnetite. Recent studies showed that organic matter adsorbed and/or coprecipitated with HFO either completely inhibits the formation of crystalline iron oxides or modify the proportions/identity of the crystalline phases (Piepenbrock et al., 2011; Amstaetter et al., 2012; Henneberry et al., 2012; Shimizu et al., 2013; Eusterhues et al., 2014; Chen et al., 2015). Organic matter inhibits the reductive transformation of HFO via Fe(II) by (1) inhibiting the direct the adsorption of Fe(II) onto the Fe(III) mineral via complexation of Fe(II), and (2) stabilizing HFO nanoparticles and/or preventing the nucleation of crystalline phases in solution (Jones et al., 2009; Henneberry et al., 2012). Thus, the intermixed cell derived organic matter within BIOS likely played a role in inhibiting magnetite formation

during the reduction of BIOS from site CA-03. Furthermore, the maximum amounts of Fe(III) reduced within biotic microcosms conducted with non-irradiated BIOS from site CA-03 and 10μM of phosphate reached 65-70% well within the range of the ascorbate iron extractable fraction (~75%) (Tables 2 and 4). Recent studies showed that the maximum amount of iron extracted by ascorbate correlates linearly with the maximum concentration of Fe(III) that could be reduced by DIRB (Hyacinthe et al., 2006). Thus, most of the ferrihydrite fraction was reduced while leaving the crystalline goethite intact, which is recalcitrant to microbial reduction (Roden and Zachara, 1996). Although it is possible that these observations could be coincidental, further support for our interpretation comes from the fact that the maximum amount of Fe(III) reduced for γ-irradiated BIOS from site CA-03 in the presence of 3.9mM phosphate reached ~65%, which is also in the range of the ascorbate iron extractable fraction. The similarity between the maximum Fe(III) reduced for γ-irradiated BIOS from site CA-03 and 3.9mM of phosphate and those determined for non-irradiated BIOS from site CA-03 and 10μM of phosphate suggests that most of the ferrihydrite, if not all, was reduced, while leaving goethite intact. The fact that most of the ferrihydrite was reduced within microcosms conducted with non-irradiated BIOS from site CA-03 and 10μM of phosphate suggests that minimal transformation of ferrihydrite to goethite or magnetite occurred, likely due to intermixed cell derived organic matter and, possibly, extracellular organic matter generated by the native bacteria, which complexed most of Fe(II) preventing a direct interaction between Fe(II) and Fe(III) (Section 4.2.3.). However, it is unknown if the proportion of goethite increased during the reduction of γ-irradiated BIOS from site CA-03 in the presence of 10μM of phosphate, as the maximum amount of Fe(III) reduced reached ~30% (Table 4). Nonetheless, it is clear that magnetite did not form during the reduction of γ-irradiated

BIOS from site CA-03 in the presence of 10μM of phosphate lending support to the inhibition of magnetite formation by intermixed cell derived organic matter within BIOS.

The secondary iron products that formed form the reduction BIOS from site CA-04 are more difficult to delineate than those for BIOS from site CA-03. The maximum amounts of Fe(III) reduced within biotic microcosms conducted with non-irradiated BIOS from site CA-04 and 10μM of phosphate reached 70-75% well below the ascorbate extraction Fe(III) fraction (~90%) (Tables 2 and 4). The similarity between the maximum Fe(III) reduced for γ-irradiated BIOS from site CA-04 and 3.9mM of phosphate and those determined for non-irradiated BIOS from site CA-04 and 10μM of phosphate suggests that most of the ferrihydrite was reduced. However, it appears that there is a discrepancy between the ascorbate extractable Fe(III) and the maximum Fe(III) reduced (i.e. ~20% of Fe(III) unaccounted for). As noted by Hyacinthe et al. (2006), some Fe(III) may reside within regions accessible to the ascorbate ions but inaccessible to the relatively large DIRB. Thus, ~20% of Fe(III) may reside within sites that are not easily accessed by DIRB within BIOS from site CA-04. Fe(III) may also reside within silicate minerals that are not directly accessible by DIRB, as XRD analysis of BIOS from site CA-04 revealed the presence of greater abundance of silicate minerals when compared to BIOS from site CA-03 (Figure 1). This further complicates data interpretation with regards to the secondary iron minerals that may have formed. XRD analysis of the residual products revealed new peaks which corresponded to goethite (Figures 8 and S20). Thus, goethite may have formed from the reductive transformation of ferrihydrite, or it may have been originally intermixed within the BIOS samples (Table 2). Based on our data interpretation from the reduction of BIOS from site CA-03 we could safely assume that magnetite formation is also likely to be inhibited by the intermixed cell derived organic matter and/or extracellular organic matter generated by the native microbes that complex Fe(II). Recent studies,

however, showed that the degree of transformation inhibition of HFO by organic matter is concentration dependent, in which case increasing the organic matter content was found to preserve ferrihydrite against reductive dissolution by Fe(II) and subsequent transformation (Shimizu et al., 2013; Eusterhues et al., 2014; Chen et al., 2015). The lower organic matter content of BIOS from site CA-04 relative to BIOS from site CA-03 could potentially allow the transformation of ferrihydrite into goethite and/or magnetite (Table 3). This could potentially explain why magnetite originally occurs within BIOS from site CA-04.

Most of the secondary iron products reported herein were also predicted from modeling of the present data using a geochemical computer software (PHREEQ-C). Where sulfide production had occurred, it was found that the solutions were supersaturated with respect to an amorphous FeS phase along with mackinawite, XRD, however, failed to detect these phases in the residual products probably due to their amorphous nature, low abundance, and attenuation of their peaks by other mineral phases including vivianite and silicates. Biotic experiments conducted with HFO or BIOS with 3.9mM of phosphate were supersaturated with respect to vivianite, whereas biotic experiments conducted with 10μM of phosphate were found to be supersaturated with respect to goethite and magnetite.

5. Conclusions

The concentration of phosphate was found to have contrasting effects on the reduction of HFO, non- and γ-irradiated BIOS by *S. putrefaciens* CN32, but in general 3.9mM of phosphate enhanced the extent of Fe(III) reduction. The concentration of phosphate was also found to influence the secondary iron mineral products that formed form the reduction of HFO and BIOS. With respect to BIOS, the intermixed cell derived organic matter together with extracellular organic matter generated by the native bacteria were also found to impact the formation of

secondary iron minerals. The possible inhibition of secondary iron mineral formation by the intermixed cell derived organic matter under environmentally relevant conditions suggests that the organic fraction may promote the reduction of BIOS which could in turn lead to the remobilization of associated contaminants rather than the sequestration of contaminants into secondary iron minerals. Incubations of non-irradiated BIOS with 10μM of phosphate further revealed a secondary mechanism which may inhibit the formation of magnetite and/or goethite, we found that the native microbes may excrete extracellular organic matter that complex Fe(II) which could thermodynamically favor the reductive dissolution of BIOS. In addition, within the environment these complexes may be re-oxidized by FeOB to form iron oxides and re-capture mobilized contaminants. Characterization of these complexes and whether or not they are accessible for FeOB represents a research opportunity.

The concentration of molybdate had contrasting effects on the reduction of HFO and BIOS which were also dependent on the concentration of phosphate and the physicochemical properties of the iron oxide. The concentration of molybdate influenced the reduction of HFO in the presence of 10μM of phosphate but not 3.9mM of phosphate, which in turn influenced the identity of the secondary iron minerals. Molybdate had no effect on the reduction of BIOS regardless of the concentration of phosphate. However, we found that the efficiency of molybdate to inhibit sulfate reducing bacteria depended on the phosphate concentration present in solution. The efficiency of molybdate may have also depended on the microbial community, this could also influence the efficiency of other chemical inhibitors often used in the literature. In order to inhibit the activity of the native microbes we found that γ-irradiation at 14kGy was effective and minimally invasive. We found that γ-irradiation did not alter the mineralogy of BIOS, and it did not alter the reactivity of BIOS towards reduction by *S. putrefaciens* CN32. Nonetheless, we observed some production

of sulfide, this suggests that for long-term experiments a higher dose of γ-irradiation may be required.

Finally, we found that freezing of BIOS at -4ºC for ~2 years had a profound impact on their reactivity with respect to microbial iron reduction. XRD and chemical extractions, however, revealed no significant changes in mineralogy of frozen BIOS when compared to their fresh counterparts. Despite the apparent similarity of mineralogy, the rates of reduction of frozen BIOS were significantly lower than their fresh counterparts. Freezing likely promoted dewatering and compaction of ferrihydrite nanoparticles leading to aggregation which in turn lowered the reactivity of BIOS towards reduction. Freezing is a natural phenomenon, we previously observed frozen BIOS during Winter season which could lead to aggregation. Aggregation of ferrihydrite particles could reduce the reactive surface area available to uptake metal contaminants (Gilbert et al., 2009). Aggregation on the other hand may lead to the binding of metal contaminants within aggregate pore spaces/interfaces, and hence a greater retention and sequestration of associated metals (Kim et al., 2007; Gilbert et al., 2009; Stegemeier et al., 2015; Dale et al., 2015). Remobilization of retained metal contaminants is likely to occur upon burial and the onset of anoxia in the presence of DRIB, as ferrihydrite remained bioavailable but at a lower rate. This also suggests that the reactivity of BIOS in natural environments may not be easy to predict, and therefore the effects of freezing on the reactivity of BIOS have to be considered within the framework of iron biogeochemistry.

References

Amstaetter, K., Borch, T., Kappler, A., 2012. Influence of humic acid imposed changes of ferrihydrite aggregation on microbial Fe(III) reduction. Geochim. Cosmochim. Acta, 85, 326-341.

Appelo, C.A.J., Postma, D., 2004. Geochemistry, groundwater and pollution. CRC press.

Avramescu, M.-L., Yumvihoze, E., Hintelmann, H., Ridal, J., Fortin, D., R.S. Lean, D., 2011. Biogeochemical factors influencing net mercury methylation in contaminated freshwater sediments from the st. Lawrence river in cornwall, ontario, canada. Sci. Total Environ., 409, 968-978.

Baken, S., Verbeeck, M., Verheyen, D., Diels, J., Smolders, E., 2015. Phosphorus losses from agricultural land to natural waters are reduced by immobilization in iron-rich sediments of drainage ditches. Water research, 71, 160-170.

Banfield, J.F., Welch, S.A., Zhang, H., Ebert, T.T., Penn, R.L., 2000. Aggregation-based crystal growth and microstructure development in natural iron oxyhydroxide biomineralization products. Science, 289, 751-754.

Bank, T.L., Kukkadapu, R.K., Madden, A.S., Ginder-Vogel, M., Baldwin, M., Jardine, P., 2008. Effects of gamma-sterilization on the physico-chemical properties of natural sediments. Chem. Geol., 251, 1-7.

Berns, A., Philipp, H., Narres, H.D., Burauel, P., Vereecken, H., Tappe, W., 2008. Effect of gamma-sterilization and autoclaving on soil organic matter structure as studied by solid state nmr, uv and fluorescence spectroscopy. European Journal of Soil Science, 59, 540-550.

Biswas, K.C., Woodards, N.A., Xu, H., Barton, L.L., 2009. Reduction of molybdate by sulfate-reducing bacteria. Biometals, 22, 131-139.

Blöthe, M., Roden, E.E., 2009. Microbial iron redox cycling in a circumneutral-ph groundwater seep. Appl. Environ. Microbiol., 75, 468-473.

Boland, D.D., Collins, R.N., Glover, C.J., Payne, T.E., Waite, T.D., 2014. Reduction of U(VI) by Fe(II) during the Fe(II)-accelerated transformation of ferrihydrite. Environ. Sci. Technol., 48, 9086-9093.

Bonneville, S., Van Cappellen, P., Behrends, T., 2004. Microbial reduction of iron(III) oxyhydroxides: Effects of mineral solubility and availability. Chem. Geol., 212, 255-268.

Bonneville, S., Behrends, T., Van Cappellen, P., 2009. Solubility and dissimilatory reduction kinetics of iron(III) oxyhydroxides: A linear free energy relationship. Geochim. Cosmochim. Acta, 73, 5273-5282.

Borch, T., Masue, Y., Kukkadapu, R.K., Fendorf, S., 2007. Phosphate imposed limitations on biological reduction and alteration of ferrihydrite. Environ. Sci. Technol., 41, 166-172.

Borch, T., Kretzschmar, R., Kappler, A., Cappellen, P.V., Ginder-Vogel, M., Voegelin, A., Campbell, K., 2009. Biogeochemical redox processes and their impact on contaminant dynamics. Environ. Sci. Technol., 44, 15-23.

Borisover, M., Keren, Y., Usyskin, A., Bukhanovsky, N., 2016. Effects of γ-irradiation of original and organic matter-amended soils on the sorption of triclosan and diuron from aqueous solutions. Chemosphere, 152, 62-70.

Brown, A.R., Wincott, P.L., LaVerne, J.A., Small, J.S., Vaughan, D.J., Pimblott, S.M., Lloyd, J.R., 2014. The impact of γ radiation on the bioavailability of Fe(III) minerals for microbial respiration. Environ. Sci. Technol., 48, 10672-10680.

Brown, A.R., Boothman, C., Pimblott, S.M., Lloyd, J.R., 2015. The impact of gamma radiation on sediment microbial processes. Appl. Environ. Microbiol., 81, 4014-4025.
Bruun, A.-M., Finster, K., Gunnlaugsson, H.P., Nørnberg, P., Friedrich, M.W., 2010. A comprehensive investigation on iron cycling in a freshwater seep including microscopy, cultivation and molecular community analysis. Geomicrobiology Journal, 27, 15-34.
Buerge, I.J., Hug, S.J., 1999. Influence of mineral surfaces on chromium (VI) reduction by iron(II). Environ. Sci. Technol., 33, 4285-4291.
Catalano, J.G., Luo, Y., Otemuyiwa, B., 2011. Effect of aqueous iron(II) on arsenate sorption on goethite and hematite. Environ. Sci. Technol., 45, 8826-8833.
Chan, C.S., De Stasio, G., Welch, S.A., Girasole, M., Frazer, B.H., Nesterova, M.V., Fakra, S., Banfield, J.F., 2004. Microbial polysaccharides template assembly of nanocrystal fibers. Science, 303, 1656-8.
Chan, C.S., Fakra, S.C., Edwards, D.C., Emerson, D., Banfield, J.F., 2009. Iron oxyhydroxide mineralization on microbial extracellular polysaccharides. Geochim. Cosmochim. Acta, 73, 3807-3818.
Chan, C.S., Fakra, S.C., Emerson, D., Fleming, E.J., Edwards, K.J., 2011. Lithotrophic iron-oxidizing bacteria produce organic stalks to control mineral growth: Implications for biosignature formation. ISME J, 5, 717-27.
Chapelle, F.H., Lovley, D.R., 1992. Competitive exclusion of sulfate reduction by Fe(III)-reducing bacteria: A mechanism for producing discrete zones of high-iron ground water. Ground water, 30, 29-36.
Châtellier, X., Fortin, D., West, M.M., Leppard, G.G., Ferris, F.G., 2001. Effect of the presence of microbial surfaces during the synthesis of fe oxides by oxidation of ferrous ions. European Journal of Mineralogy, 13, 705-714.
Châtellier, X., West, M.M., Rose, J., Fortin, D., Leppard, G.G., Ferris, F.G., 2004. Characterization of iron-oxides formed by oxidation of ferrous ions in the presence of various microbial species and inorganic ligands. Geomicrobiology Journal, 21, 99-112.
Chen, C., Kukkadapu, R., Sparks, D.L., 2015. Influence of coprecipitated organic matter on Fe2+(aq)-catalyzed transformation of ferrihydrite: Implications for carbon dynamics. Environ. Sci. Technol., 49, 10927-10936.
Chen, G., Ford, T., Clayton, C., 1998. Interaction of sulfate-reducing bacteria with molybdenum dissolved from sputter-deposited molybdenum thin films and pure molybdenum powder. J. Colloid Interface Sci., 204, 237-246.
Cline, J.D., 1969. Spectrophotometric determination of hydrogen sulfide in natural waters. Limnology and Oceanography, 14, 454-458.
Coleman, M.L., Hedrick, D.B., Lovley, D.R., White, D.C., Pye, K., 1993. Reduction of Fe(III) in sediments by sulphate-reducing bacteria.
Cooper, D.C., Picardal, F., Rivera, J., Talbot, C., 2000. Zinc immobilization and magnetite formation via ferric oxide reduction by shewanella putrefaciens 200. Environ. Sci. Technol., 34, 100-106.
Cooper, D.C., Neal, A.L., Kukkadapu, R.K., Brewe, D., Coby, A., Picardal, F.W., 2005. Effects of sediment iron mineral composition on microbially mediated changes in divalent metal speciation: Importance of ferrihydrite. Geochim. Cosmochim. Acta, 69, 1739-1754.
Cornell, R.M., Schwertmann, U., 2003. The iron oxides: Structure, properties, reactions, occurrences and uses. John Wiley & Sons.

Cotroneo, S.E., Fortin, D., 2013. Redox stability and microbial characterization of zinc-rich bacteriogenic iron oxides (BIOS). Undergraduate Thesis, University of Ottawa.

Cummings, D.E., Caccavo, F., Fendorf, S., Rosenzweig, R.F., 1999. Arsenic mobilization by the dissimilatory Fe(III)-reducing bacterium shewanella alga bry. Environ. Sci. Technol., 33, 723-729.

Cutting, R.S., Coker, V.S., Fellowes, J.W., Lloyd, J.R., Vaughan, D.J., 2009. Mineralogical and morphological constraints on the reduction of Fe(III) minerals by *Geobacter sulfurreducens*. Geochim. Cosmochim. Acta, 73, 4004-4022.

Dale, J., Stegemeier, J., Kim, C., 2015. Aggregation of nanoscale iron oxyhydroxides and corresponding effects on metal uptake, retention, and speciation: I. Ionic-strength and ph. Geochim. Cosmochim. Acta, 148, 100-112.

Dippon, U., Schmidt, C., Behrens, S., Kappler, A., 2015. Secondary mineral formation during ferrihydrite reduction by shewanella oneidensis mr-1 depends on incubation vessel orientation and resulting gradients of cells, Fe^{2+} and Fe minerals. Geomicrobiology Journal, 32, 878-889.

Dominik, P., Pohl, H.N., Bousserrhine, N., Berthelin, J., Kaupenjohann, M., 2002. Limitations to the reductive dissolution of al-substituted goethites by *Clostridium butyricum*. Soil Biology and Biochemistry, 34, 1147-1155.

Dong, H., Fredrickson, J.K., Kennedy, D.W., Zachara, J.M., Kukkadapu, R.K., Onstott, T.C., 2000. Mineral transformations associated with the microbial reduction of magnetite. Chem. Geol., 169, 299-318.

Ekstrom, E.B., Learman, D.R., Madden, A.S., Hansel, C.M., 2010. Contrasting effects of Al substitution on microbial reduction of Fe(III) (hydr)oxides. Geochim. Cosmochim. Acta, 74, 7086-7099.

Emerson, D., Revsbech, N.P., 1994. Investigation of an iron-oxidizing microbial mat community located near aarhus, denmark: Field studies. Appl. Environ. Microbiol., 60, 4022-4031.

Eusterhues, K., Hädrich, A., Neidhardt, J., Küsel, K., Keller, T., Jandt, K., Totsche, K., 2014. Reduction of ferrihydrite with adsorbed and coprecipitated organic matter: Microbial reduction by geobacter bremensis vs. Abiotic reduction by na-dithionite. Biogeosciences, 11, 4953-4966.

Fabisch, M., Freyer, G., Johnson, C., Büchel, G., Akob, D., Neu, T., Küsel, K., 2016. Dominance of 'G*allionella capsiferriformans*' and heavy metal association with Gallionella-like stalks in metal-rich pH 6 mine water discharge. Geobiology, 14, 68-90.

Ferris, F., Konhauser, K., Lyven, B., Pedersen, K., 1999. Accumulation of metals by bacteriogenic iron oxides in a subterranean environment. Geomicrobiology Journal, 16, 181-192.

Ferris, F.G., Hallberg, R., Lyven, B., Pedersen, K., 2000. Retention of strontium, cesium, lead and uranium by microbial iron oxides from a subterranean environment. Applied Geochemistry, 15, 1035-1042.

Ferris, F.G., 2005. Biogeochemical properties of bacteriogenic iron oxides. Geomicrobiology Journal, 22, 79-85.

Fleming, E.J., Mack, E.E., Green, P.G., Nelson, D.C., 2006. Mercury methylation from unexpected sources: Molybdate-inhibited freshwater sediments and an iron-reducing bacterium. Appl. Environ. Microbiol., 72, 457-464.

Fortin, D., Leppard, G.G., Tessier, A., 1993. Characteristics of lacustrine diagenetic iron oxyhydroxides. Geochim. Cosmochim. Acta, 57, 4391-4404.

Fortin, D., Langley, S., 2005. Formation and occurrence of biogenic iron-rich minerals. Earth-Science Reviews, 72, 1-19.
Fredrickson, J., Kota, S., Kukkadapu, R., Liu, C., Zachara, J., 2003. Influence of electron donor/acceptor concentrations on hydrous ferric oxide (HFO) bioreduction. Biodegradation, 14, 91-103.
Fredrickson, J.K., Zachara, J.M., Kennedy, D.W., Dong, H., Onstott, T.C., Hinman, N.W., Li, S.-m., 1998. Biogenic iron mineralization accompanying the dissimilatory reduction of hydrous ferric oxide by a groundwater bacterium. Geochim. Cosmochim. Acta, 62, 3239-3257.
Fredrickson, J.K., Zachara, J.M., Kukkadapu, R.K., Gorby, Y.A., Smith, S.C., Brown, C.F., 2001. Biotransformation of ni-substituted hydrous ferric oxide by an Fe(III)-reducing bacterium. Environ. Sci. Technol., 35, 703-712.
Frierdich, A.J., Catalano, J.G., 2012a. Controls on Fe(II)-activated trace element release from goethite and hematite. Environ. Sci. Technol., 46, 1519-1526.
Frierdich, A.J., Catalano, J.G., 2012b. Fe(II)-mediated reduction and repartitioning of structurally incorporated Cu, Co, and Mn in iron oxides. Environ. Sci. Technol., 46, 11070-11077.
Galvez, N., Barron, V., Torrent, J., 1999. Effect of phosphate on the crystallization of hematite, goethite, and lepidocrocite from ferrihydrite. Clays and Clay Minerals, 47, 304-311.
Gault, A.G., Ibrahim, A., Langley, S., Renaud, R., Takahashi, Y., Boothman, C., Lloyd, J.R., Clark, I.D., Ferris, F.G., Fortin, D., 2011. Microbial and geochemical features suggest iron redox cycling within bacteriogenic iron oxide-rich sediments. Chem. Geol., 281, 41-51.
Gault, A.G., Langley, S., Ibrahim, A., Renaud, R., Takahashi, Y., Boothman, C., Lloyd, J.R., Clark, I.D., Ferris, F.G., Fortin, D., 2012. Seasonal changes in mineralogy, geochemistry and microbial community of bacteriogenic iron oxides (BIOS) deposited in a circumneutral wetland. Geomicrobiology Journal, 29, 161-172.
Gilbert, B., Ono, R.K., Ching, K.A., Kim, C.S., 2009. The effects of nanoparticle aggregation processes on aggregate structure and metal uptake. J. Colloid Interface Sci., 339, 285-295.
Glasauer, S., Weidler, P.G., Langley, S., Beveridge, T.J., 2003. Controls on Fe reduction and mineral formation by a subsurface bacterium. Geochim. Cosmochim. Acta, 67, 1277-1288.
Gustafsson, J.P., 2003. Modelling molybdate and tungstate adsorption to ferrihydrite. Chem. Geol., 200, 105-115.
Hallberg, R., Ferris, F.G., 2004. Biomineralization by Gallionella. Geomicrobiology Journal, 21, 325-330.
Hansel, C.M., Benner, S.G., Neiss, J., Dohnalkova, A., Kukkadapu, R.K., Fendorf, S., 2003a. Secondary mineralization pathways induced by dissimilatory iron reduction of ferrihydrite under advective flow. Geochim. Cosmochim. Acta, 67, 2977-2992.
Hansel, C., Wielinga, B., Fendorf, S., 2003b. Structural and compositional evolution of Cr/Fe solids after indirect chromate reduction by dissimilatory iron-reducing bacteria. Geochim. Cosmochim. Acta, 67, 401-412.
Hansel, C.M., Benner, S.G., Nico, P., Fendorf, S., 2004. Structural constraints of ferric (hydr)oxides on dissimilatory iron reduction and the fate of Fe(II). Geochim. Cosmochim. Acta, 68, 3217-3229.
Hansel, C.M., Benner, S.G., Fendorf, S., 2005. Competing Fe(II)-induced mineralization pathways of ferrihydrite. Environ. Sci. Technol., 39, 7147-7153.

Hansel, C.M., Learman, D.R., Lentini, C.J., Ekstrom, E.B., 2011. Effect of adsorbed and substituted al on Fe(II)-induced mineralization pathways of ferrihydrite. Geochim. Cosmochim. Acta, 75, 4653-4666.

Hansel, C.M., Lentini, C.J., Tang, Y., Johnston, D.T., Wankel, S.D., Jardine, P.M., 2015. Dominance of sulfur-fueled iron oxide reduction in low-sulfate freshwater sediments. The ISME journal, 9, 2400-2412.

Hao, L., Guo, Y., Byrne, J.M., Zeitvogel, F., Schmid, G., Ingino, P., Li, J., Neu, T.R., Swanner, E.D., Kappler, A., 2016. Binding of heavy metal ions in aggregates of microbial cells, EPS and biogenic iron minerals measured in-situ using metal-and glycoconjugates-specific fluorophores. Geochim. Cosmochim. Acta, 180, 66-96.

Henneberry, Y.K., Kraus, T.E.C., Nico, P.S., Horwath, W.R., 2012. Structural stability of coprecipitated natural organic matter and ferric iron under reducing conditions. Organic Geochemistry, 48, 81-89.

Herbert, R.B., Malmström, M., Ebenå, G., Salmon, U., Ferrow, E., Fuchs, M., 2005. Quantification of abiotic reaction rates in mine tailings: Evaluation of treatment methods for eliminating iron-and sulfur-oxidizing bacteria. Environ. Sci. Technol., 39, 770-777.

Hyacinthe, C., Bonneville, S., Van Cappellen, P., 2006. Reactive iron(iii) in sediments: Chemical versus microbial extractions. Geochim. Cosmochim. Acta, 70, 4166-4180.

Isa, M.H., Anderson, G., 2005. Molybdate inhibition of sulphate reduction in two-phase anaerobic digestion. Process Biochemistry, 40, 2079-2089.

Islam, F.S., Gault, A.G., Boothman, C., Polya, D.A., Charnock, J.M., Chatterjee, D., Lloyd, J.R., 2004. Role of metal-reducing bacteria in arsenic release from bengal delta sediments. Nature, 430, 68-71.

James, R.E., Ferris, F.G., 2004. Evidence for microbial-mediated iron oxidation at a neutrophilic groundwater spring. Chem. Geol., 212, 301-311.

Jones, A.M., Collins, R.N., Rose, J., Waite, T.D., 2009. The effect of silica and natural organic matter on the Fe(II)-catalysed transformation and reactivity of Fe(III) minerals. Geochim. Cosmochim. Acta, 73, 4409-4422.

Kennedy, C.B., Scott, S.D., Ferris, F.G., 2004. Hydrothermal phase stabilization of 2-line ferrihydrite by bacteria. Chem. Geol., 212, 269-277.

Khan, B., Najem, T., & Fortin, D. The effects of gamma irradiation on the redox stability, mineralogy and physicochemical properties of the iron oxyhydroxides ferrihydrite, lepidocrocite, and goethite.

Kim, C.S., Lentini, C.J., Waychunas, G.A., 2007. Chapter 6 associations between iron oxyhydroxide nanoparticle growth and metal adsorption/structural incorporation. In: Mark, O.B., Douglas, B.K. (Eds.), Developments in earth and environmental sciences. Elsevier, pp. 153-185.

Kleinert, S., Muehe, E.M., Posth, N.R., Dippon, U., Daus, B., Kappler, A., 2011. Biogenic Fe(III) minerals lower the efficiency of iron-mineral-based commercial filter systems for arsenic removal. Environ. Sci. Technol., 45, 7533-7541.

Kocar, B.D., Herbel, M.J., Tufano, K.J., Fendorf, S., 2006. Contrasting effects of dissimilatory iron (III) and arsenic (V) reduction on arsenic retention and transport. Environ. Sci. Technol., 40, 6715-6721.

Kostka, J.E., Luther, G.W., 1994. Partitioning and speciation of solid phase iron in saltmarsh sediments. Geochim. Cosmochim. Acta, 58, 1701-1710.

Kukkadapu, R.K., Zachara, J.M., Fredrickson, J.K., Kennedy, D.W., 2004. Biotransformation of two-line silica-ferrihydrite by a dissimilatory Fe(III)-reducing bacterium: Formation of carbonate green rust in the presence of phosphate. Geochim. Cosmochim. Acta, 68, 2799-2814.

Langley, S., Gault, A.G., Ibrahim, A., Takahashi, Y., Renaud, R., Fortin, D., Clark, I.D., Ferris, F.G., 2009a. Sorption of strontium onto bacteriogenic iron oxides. Environ. Sci. Technol., 43, 1008-1014.

Langley, S., Gault, A., Ibrahim, A., Renaud, R., Fortin, D., Clark, I.D., Ferris, F.G., 2009b. A comparison of the rates of Fe(III) reduction in synthetic and bacteriogenic iron oxides by shewanella putrefaciens CN32. Geomicrobiology Journal, 26, 57-70.

Langley, S., Gault, A.G., Ibrahim, A., Takahashi, Y., Renaud, R., Fortin, D., Clark, I.D., Ferris, F.G., 2009c. Strontium desorption from bacteriogenic iron oxides (BIOS) subjected to microbial Fe(III) reduction. Chem. Geol., 262, 217-228.

Langley, S., Igric, P., Takahashi, Y., Sakai, Y., Fortin, D., Hannington, M.D., Schwarz-Schampera, U., 2009d. Preliminary characterization and biological reduction of putative biogenic iron oxides (BIOS) from the tonga-kermadec arc, southwest pacific ocean. Geobiology, 7, 35-49.

Lee, W., Batchelor, B., 2002. Abiotic reductive dechlorination of chlorinated ethylenes by iron-bearing soil minerals. 1. Pyrite and magnetite. Environ. Sci. Technol., 36, 5147-5154.

Lohmayer, R., Kappler, A., Lösekann-Behrens, T., Planer-Friedrich, B., 2014. Sulfur species as redox partners and electron shuttles for ferrihydrite reduction by *Sulfurospirillum deleyianum*. Appl. Environ. Microbiol., 80, 3141-3149.

Lotrario, J., Stuart, B., Lam, T., Arands, R., O'Connor, O., Kosson, D., 1995. Effects of sterilization methods on the physical characteristics of soil: Implications for sorption isotherm analyses. Bull. Environ. Contam. Toxicol., 54, 668-675.

Lovley, D.R., Phillips, E.J., 1987. Competitive mechanisms for inhibition of sulfate reduction and methane production in the zone of ferric iron reduction in sediments. Appl. Environ. Microbiol., 53, 2636-2641.

Lovley, D.R., Roden, E.E., Phillips, E., Woodward, J., 1993. Enzymatic iron and uranium reduction by sulfate-reducing bacteria. Mar. Geol., 113, 41-53.

Lovley, D.R., Holmes, D.E., Nevin, K.P., 2004. Dissimilatory Fe(III) and Mn(IV) reduction, Adv. Microb. Physiol. Academic Press, pp. 219-286.

MacLatchy, J., 2013. Onsite discussion on the history of the new calumet mine. Calumet mine, grand calumet island, quebec, canada. May, 2013.

Masue-Slowey, Y., Loeppert, R.H., Fendorf, S., 2011. Alteration of ferrihydrite reductive dissolution and transformation by adsorbed as and structural al: Implications for as retention. Geochim. Cosmochim. Acta, 75, 870-886.

McCormick, M.L., Bouwer, E.J., Adriaens, P., 2002. Carbon tetrachloride transformation in a model iron-reducing culture: Relative kinetics of biotic and abiotic reactions. Environ. Sci. Technol., 36, 403-410.

McNamara, N.P., Black, H.I.J., Beresford, N.A., Parekh, N.R., 2003. Effects of acute gamma irradiation on chemical, physical and biological properties of soils. Applied Soil Ecology, 24, 117-132.

Melton, E.D., Swanner, E.D., Behrens, S., Schmidt, C., Kappler, A., 2014. The interplay of microbially mediated and abiotic reactions in the biogeochemical fe cycle. Nat Rev Micro, 12, 797-808.

Moorhouse, W.W., 1941. Geology of the zinc-lead deposit on calumet island, quebec. GSA Bulletin, 52, 601-632.
Muehe, E.M., Scheer, L., Daus, B., Kappler, A., 2013a. Fate of arsenic during microbial reduction of biogenic versus abiogenic As–Fe(III)–mineral coprecipitates. Environ. Sci. Technol., 47, 8297-8307.
Muehe, E.M., Adaktylou, I.J., Obst, M., Zeitvogel, F., Behrens, S., Planer-Friedrich, B., Kraemer, U., Kappler, A., 2013b. Organic carbon and reducing conditions lead to cadmium immobilization by secondary fe mineral formation in a ph-neutral soil. Environ. Sci. Technol., 47, 13430-13439.
Muehe, E.M., Obst, M., Hitchcock, A., Tyliszczak, T., Behrens, S., Schröder, C., Byrne, J.M., Michel, F.M., Krämer, U., Kappler, A., 2013c. Fate of cd during microbial Fe(III) mineral reduction by a novel and cd-tolerant geobacter species. Environ. Sci. Technol., 47, 14099-14109.
Muyzer, G., Stams, A.J., 2008. The ecology and biotechnology of sulphate-reducing bacteria. Nature Reviews Microbiology, 6, 441-454.
Najem, T., Langley, S., Fortin, D., 2016. A comparison of Fe(III) reduction rates between fresh and aged biogenic iron oxides (BIOS) by shewanella putrefaciens CN32. Chem. Geol., 439, 1-12.
Nemati, M., Mazutinec, T., Jenneman, G., Voordouw, G., 2001. Control of biogenic H2S production with nitrite and molybdate. J. Ind. Microbiol. Biotechnol., 26, 350-355.
O'Loughlin, E.J., 2008. Effects of electron transfer mediators on the bioreduction of lepidocrocite (γ-feooh) by shewanella putrefaciens cn32. Environ. Sci. Technol., 42, 6876-6882.
O'Loughlin, E.J., Gorski, C.A., Scherer, M.M., Boyanov, M.I., Kemner, K.M., 2010. Effects of oxyanions, natural organic matter, and microbial cell numbers on the bioreduction of lepidocrocite (γ-FeOOH) and the formation of secondary mineralization products. Environ. Sci. Technol., 44, 4570-4576.
O'Loughlin, E.J., Boyanov, M.I., Flynn, T.M., Gorski, C.A., Hofmann, S.M., McCormick, M.L., Scherer, M.M., Kemner, K.M., 2013. Effects of bound phosphate on the bioreduction of lepidocrocite (γ-FeOOH) and maghemite (γ-Fe_2O_3) and formation of secondary minerals. Environ. Sci. Technol., 47, 9157-9166.
Ona-Nguema, G., Abdelmoula, M., Jorand, F., Benali, O., Gehin, A., Block, J.-C., Génin, J.-M.R., 2002. Iron (II, III) hydroxycarbonate green rust formation and stabilization from lepidocrocite bioreduction. Environ. Sci. Technol., 36, 16-20.
Oremland, R.S., Capone, D.G., 1988. Use of "specific" inhibitors in biogeochemistry and microbial ecology. In: Marshall, K.C. (Ed.), Adv. Microb. Ecol. Springer US, Boston, MA, pp. 285-383.
Parmar, N., Warren, L.A., Roden, E.E., Ferris, F.G., 2000. Solid phase capture of strontium by the iron reducing bacteria shewanella alga strain bry. Chem. Geol., 169, 281-288.
Parmar, Y.G., TJ Beveridge, FG Ferris, N, 2001. Formation of green rust and immobilization of nickel in response to microbial reduction of hydrous ferric oxide. Geomicrobiology Journal, 18, 375-385.
Piepenbrock, A., Dippon, U., Porsch, K., Appel, E., Kappler, A., 2011. Dependence of microbial magnetite formation on humic substance and ferrihydrite concentrations. Geochim. Cosmochim. Acta, 75, 6844-6858.
Plötze, M., Kahr, G., Stengele, R.H., 2003. Alteration of clay minerals—gamma-irradiation effects on physicochemical properties. Applied Clay Science, 23, 195-202.

Posth, N.R., Canfield, D.E., Kappler, A., 2014. Biogenic Fe(III) minerals: From formation to diagenesis and preservation in the rock record. Earth-Science Reviews, 135, 103-121.
Postma, D., 1981. Formation of siderite and vivianite and the pore-water composition of a recent bog sediment in denmark. Chem. Geol., 31, 225-244.
Praharaj, T., Fortin, D., 2008. Seasonal variations of microbial sulfate and iron reduction in alkaline pb–zn mine tailings (ontario, canada). Applied Geochemistry, 23, 3728-3740.
Raiswell, R., Vu, H.P., Brinza, L., Benning, L.G., 2010. The determination of labile fe in ferrihydrite by ascorbic acid extraction: Methodology, dissolution kinetics and loss of solubility with age and de-watering. Chem. Geol., 278, 70-79.
Ranade, D., Dighe, A., Bhirangi, S., Panhalkar, V., Yeole, T., 1999. Evaluation of the use of sodium molybdate to inhibit sulphate reduction during anaerobic digestion of distillery waste. Bioresource technology, 68, 287-291.
Rancourt, D.G., Thibault, P.-J., Mavrocordatos, D., Lamarche, G., 2005. Hydrous ferric oxide precipitation in the presence of nonmetabolizing bacteria: Constraints on the mechanism of a biotic effect. Geochim. Cosmochim. Acta, 69, 553-577.
Revesz, E., Fortin, D., Paktunc, D., 2015. Reductive dissolution of scorodite in the presence of *Shewanella* sp. CN32 and shewanella sp. Ana-3. Applied Geochemistry, 63, 347-356.
Roden, E.E., Zachara, J.M., 1996. Microbial reduction of crystalline iron(III) oxides: Influence of oxide surface area and potential for cell growth. Environ. Sci. Technol., 30, 1618-1628.
Roden, E.E., Urrutia, M.M., 2002. Influence of biogenic Fe(II) on microbial crystalline Fe(III) oxide reduction. Geomicrobiology journal, 19, 209-251.
Roden, E.E., Leonardo, M.R., Ferris, F.G., 2002. Immobilization of strontium during iron biomineralization coupled to dissimilatory hydrous ferric oxide reduction. Geochim. Cosmochim. Acta, 66, 2823-2839.
Roden, E.E., 2003. Fe(III) oxide reactivity toward biological versus chemical reduction. Environ. Sci. Technol., 37, 1319-1324.
Roden, E.E., McBeth, J.M., Blöthe, M., Percak-Dennett, E.M., Fleming, E.J., Holyoke, R.R., Luther III, G.W., Emerson, D., Schieber, J., 2012. The microbial ferrous wheel in a neutral ph groundwater seep. The microbial ferrous wheel: iron cycling in terrestrial, freshwater, and marine environments, 199.
Salonius, P.O., Robinson, J.B., Chase, F.E., 1967. A comparison of autoclaved and gamma-irradiated soils as media for microbial colonization experiments. Plant and Soil, 27, 239-248.
Schaller, J., Weiske, A., Dudel, E.G., 2011. Effects of gamma-sterilization on doc, uranium and arsenic remobilization from organic and microbial rich stream sediments. Sci. Total Environ., 409, 3211-3214.
Schwertmann, U., Stanjek, H., Becher, H.-H., 2004. Long-term in vitro transformation of 2-line ferrihydrite to goethite/hematite at 4, 10, 15 and 25 c. Clay Minerals, 39, 433-438.
Schwertmann, U., Cornell, R.M., 2008. Iron oxides in the laboratory: Preparation and characterization. John Wiley & Sons.
Shimizu, M., Zhou, J., Schröder, C., Obst, M., Kappler, A., Borch, T., 2013. Dissimilatory reduction and transformation of ferrihydrite-humic acid coprecipitates. Environ. Sci. Technol., 47, 13375-13384.
Stegemeier, J., Reinsch, B., Lentini, C., Dale, J., Kim, C., 2015. Aggregation of nanoscale iron oxyhydroxides and corresponding effects on metal uptake, retention, and speciation: II. Temperature and time. Geochim. Cosmochim. Acta, 148, 113-129.

Stone, J.J., Burgos, W.D., Royer, R.A., Dempsey, B.A., 2006. Impact of zinc on biological Fe(III) and nitrate reduction by *Shewanella putrefaciens* CN32. Environ. Eng. Sci., 23, 691-704.
Stookey, L.L., 1970. Ferrozine---a new spectrophotometric reagent for iron. Anal. Chem., 42, 779-781.
Stumm, W., Morgan, J.J., 2012. Aquatic chemistry: Chemical equilibria and rates in natural waters, 126. John Wiley & Sons.
Tanaka, S., Lee, Y.-H., 1997. Control of sulfate reduction by molybdate in anaerobic digestion. Water science and technology, 36, 143-150.
Tang, J., Zhuang, L., Ma, J., Tang, Z., Yu, Z., Zhou, S., 2016. Secondary mineralization of ferrihydrite affect microbial methanogenesis in geobacter/methanosarcina co-cultures. Appl. Environ. Microbiol.
Taylor, B.F., Oremland, R.S., 1979. Depletion of adenosine triphosphate indesulfovibrio by oxyanions of group vi elements. Curr. Microbiol., 3, 101-103.
Tessier, A., Fortin, D., Belzile, N., DeVitre, R.R., Leppard, G.G., 1996. Metal sorption to diagenetic iron and manganese oxyhydroxides and associated organic matter: Narrowing the gap between field and laboratory measurements. Geochim. Cosmochim. Acta, 60, 387-404.
Thinnappan, V., Merrifield, C., Islam, F., Polya, D., Wincott, P., Wogelius, R., 2008. A combined experimental study of vivianite and As(V) reactivity in the pH range 2–11. Applied Geochemistry, 23, 3187-3204.
Toner, B.M., Santelli, C.M., Marcus, M.A., Wirth, R., Chan, C.S., McCollom, T., Bach, W., Edwards, K.J., 2009. Biogenic iron oxyhydroxide formation at mid-ocean ridge hydrothermal vents: Juan de fuca ridge. Geochim. Cosmochim. Acta, 73, 388-403.
Toner, B.M., Berquó, T.S., Michel, F.M., Sorensen, J.V., Templeton, A.S., Edwards, K.J., 2012. Mineralogy of iron microbial mats from loihi seamount. Frontiers in Microbiology, 3.
Torrent, J., Barron, V., Schwertmann, U., 1990. Phosphate adsorption and desorption by goethites differing in crystal morphology. Soil Science Society of America Journal, 54, 1007-1012.
Tucker, M.D., Barton, L.L., Thomson, B.M., 1997. Reduction and immobilization of molybdenum by desulfovibrio desulfuricans. J. Environ. Qual., 26, 1146-1152.
Tufano, K.J., Reyes, C., Saltikov, C.W., Fendorf, S., 2008. Reductive processes controlling arsenic retention: Revealing the relative importance of iron and arsenic reduction. Environ. Sci. Technol., 42, 8283-8289.
Tuominen, L., Kairesalo, T., Hartikainen, H., 1994. Comparison of methods for inhibiting microbial activity in sediment. Appl. Environ. Microbiol., 60, 3454-3457.
Urrutia, M.M., Roden, E.E., Fredrickson, J.K., Zachara, J.M., 1998. Microbial and surface chemistry controls on reduction of synthetic Fe(III) oxide minerals by the dissimilatory iron-reducing bacterium shewanella alga. Geomicrobiology Journal, 15, 269-291.
Viollier, E., Inglett, P.W., Hunter, K., Roychoudhury, A.N., Van Cappellen, P., 2000. The ferrozine method revisited: Fe(II)/Fe(III) determination in natural waters. Applied Geochemistry, 15, 785-790.
Vollrath, S., Behrends, T., Koch, C.B., Cappellen, P.V., 2013. Effects of temperature on rates and mineral products of microbial Fe(II) oxidation by leptothrix cholodnii at microaerobic conditions. Geochim. Cosmochim. Acta, 108, 107-124.
Wang, D., 2012. Redox chemistry of molybdenum in natural waters and its involvement in biological evolution. Frontiers in microbiology, 3, 427.

Warren, L.A., Ferris, F.G., 1998. Continuum between sorption and precipitation of Fe(III) on microbial surfaces. Environ. Sci. Technol., 32, 2331-2337.
Wielinga, B., Mizuba, M.M., Hansel, C.M., Fendorf, S., 2001. Iron promoted reduction of chromate by dissimilatory iron-reducing bacteria. Environ. Sci. Technol., 35, 522-527.
Wolf, D., Dao, T., Scott, H., Lavy, T., 1989. Influence of sterilization methods on selected soil microbiological, physical, and chemical properties. J. Environ. Qual., 18, 39-44.
Xu, N., Christodoulatos, C., Braida, W., 2006. Adsorption of molybdate and tetrathiomolybdate onto pyrite and goethite: Effect of ph and competitive anions. Chemosphere, 62, 1726-1735.
Yadav, V.K., Archer, D.B., 1989. Sodium molybdate inhibits sulphate reduction in the anaerobic treatment of high-sulphate molasses wastewater. Appl. Microbiol. Biotechnol., 31, 103-106.
Yakabuskie, P., Joseph, J., Keech, P., Botton, G., Guzonas, D., Wren, J., 2011. Iron oxyhydroxide colloid formation by gamma-radiolysis. Phys. Chem. Chem. Phys., 13, 7198-7206.
Zachara, J.M., Fredrickson, J.K., Li, S.-M., Kennedy, D.W., Smith, S.C., Gassman, P.L., 1998. Microbial reduction of crystalline Fe^{3+} oxides in single phase suspensions and subsurface materials. American Mineralogist, 83, 1426-1443.
Zachara, J.M., Fredrickson, J.K., Smith, S.C., Gassman, P.L., 2001. Solubilization of Fe(III) oxide-bound trace metals by a dissimilatory Fe(III) reducing bacterium. Geochim. Cosmochim. Acta, 65, 75-93.
Zachara, J.M., Kukkadapu, R.K., Fredrickson, J.K., Gorby, Y.A., Smith, S.C., 2002. Biomineralization of poorly crystalline Fe(III) oxides by dissimilatory metal reducing bacteria (DMRB). Geomicrobiology Journal, 19, 179-207.
Zegeye, A., Ruby, C., Jorand, F., 2007. Kinetic and thermodynamic analysis during dissimilatory γ-FeOOH reduction: Formation of green rust 1 and magnetite. Geomicrobiology Journal, 24, 51-64.

Tables

Table 3-1: Microcosm and treatment set-up used in this study. 0:1, 1:1, 2:1 correspond to molybdate:sulfate concentrations.

Table 3-2: Non-sequential chemical extractions of the solid Fe phase of BIOS from sites CA-04 and CA-03. Also shown is the amorphous and crystalline iron fractions determined by the ascorbate extraction. Data represents mean and standard deviation of 3 replicates for each chemical treatment.

Table 3-3: Chemical composition of BIOS collected from sites CA-04 and CA-03, and HFO. Data represents mean and standard deviation of 4 replicates for elemental analyses and 2 replicates for loss on ignition.

Table 3-4: Maximum percentage of total Fe reduced, linear reduction rates and correlation coefficients for the linear reduction rates for HFO, non-irradiated BIOS, and γ-irradiated BIOS. H and L refer to the concentration of phosphate added to the media (H – 3.9mM, L – 10μM), whereas 0:1, 1:1, and 2:1 refer to the concentration of molybdate:sulfate added to the media. Data represents mean and standard deviation of 3 replicates for each experiment conducted with HFO and non-irradiated BIOS, whereas data corresponding to γ-irradiated BIOS represents mean and standard deviation of 2 replicates for each experiment.

Table 3-1: Microcosm and treatment set-up used in this study. 0:1, 1:1, 2:1 correspond to molybdate:sulfate concentrations.

Sample	Treatment					
	Molybdate:sulfate			Phosphate		γ-irradiated
	0:1	1:1	2:1	3.9mM	10μM	14kGy
HFO	Yes	Yes	Yes	Yes	Yes	No
N-CA-04	Yes	Yes	Yes	Yes	Yes	No
N-CA-03	No	Yes	Yes	Yes	Yes	No
γ-CA-04	Yes	No	No	Yes	Yes	Yes
γ-CA-03	Yes	No	No	Yes	Yes	Yes

Table 3-2: Non-sequential chemical extractions of the solid Fe phase of BIOS from sites CA-04 and CA-03. Also shown is the amorphous and crystalline iron fractions determined by the ascorbate extraction. Data represents mean and standard deviation of 3 replicates for each chemical treatment.

	Solid Phase Iron (mg/gdwt)				Fraction (%)	
Sample	HCl (H)	Ascorbate (A)	Oxalate (O)	Dithionite (D)	Amorphous[a]	Crystalline[b]
CA-04	205.5±5.8	207.1±6.7	263.6±5.1	234.8±5.1	88.2±3.4	11.8±3.6
CA-03	296.3±4.0	309.6±9.1	403.3±19	418.2±17	74.1±3.8	25.9±4.8

[a]Amorphous fraction calculated from: $\left(\frac{A}{D}\right)\times 100$

[b]Crystalline fraction calculated from: $\left(\frac{D-A}{D}\right)\times 100$

Table 3-3: Chemical composition of BIOS collected from sites CA-04 and CA-03, and HFO. Data represents mean and standard deviation of 4 replicates for elemental analyses and 2 replicates for loss on ignition.

Element (wt%)	CA-04	CA-03	HFO
Fe	22.7±0.79	39.3±0.27	46.70±1.14
Zn	0.19±0.04	0.19±0.003	0.004±0.001
Pb	0.08±0.01	0.01±0.05	bd[a]
P	bd	bd	bd
Mo	bd	bd	bd
Loss on ignition	10.3±0.001	15.1±0.006	nd[b]

[a] Below detection limit of the instrument

[b] Not determined

The limits of detection for the elements analyzed are (ppm): Fe 0.006, Zn 0.004, Pb 0.057, P 1.00, and Mo 0.015.

Table 3-4: Maximum percentage of total Fe reduced, linear reduction rates and correlation coefficients for the linear reduction rates for HFO, non-irradiated BIOS, and γ-irradiated BIOS. H and L refer to the concentration of phosphate added to the media (H – 3.9mM, L – 10μM), whereas 0:1, 1:1, and 2:1 refer to the concentration of molybdate:sulfate added to the media. Data represents mean and standard deviation of 3 replicates for each experiment conducted with HFO and non-irradiated BIOS, whereas data corresponding to γ-irradiated BIOS represents mean and standard deviation of 2 replicates for each experiment.

Sample	Maximum Fe Reduced (%)	Reduction Rate (day^{-1})	R^2
HFO H 0:1	90.5±0.8[a]	0.065±0.011	0.984
HFO H 1:1	75.5±1.8	0.080±0.011	0.989
HFO H 2:1	75.2±6.6	0.087±0.019	0.980
HFO L 0:1	39.6±1.4	0.054±0.004	0.997
HFO L 1:1	45.8±1.0	0.073±0.005	0.997
HFO L 2:1	48.9±2.5	0.086±0.005	0.997
N-CA-04 H 1:1[b]	89.3±5.0	0.066±0.004	0.997
N-CA-04 H 2:1	87.0±3.3	0.066±0.012	0.982
N-CA-04 L 1:1	77.5±2.2	0.066±0.006	0.995
N-CA-04 L 2:1	71.0±1.1	0.067±0.006	0.996
N-CA-03 H 1:1	86.6±5.5	0.070±0.005	0.997
N-CA-03 H 2:1	87.5±1.3	0.061±0.004	0.991
N-CA-03 L 1:1	64.5±3.9	0.047±0.005	0.994
N-CA-03 L 2:1	71.7±3.2	0.046±0.006	0.988
γ-CA-04 H	71.1±2.2	0.068±0.006	0.995
Fresh γ-CA-04 H[c]	100	0.214±0.013	0.998
γ-CA-04 L	41.1±0.1	0.035±0.005	0.987
γ-CA-03 H	65.1±0.4	0.061±0.015	0.981
Fresh γ-CA-03 H[c]	100	0.205±0.003	0.999
γ-CA-03 L	32.7±1.1	0.028±0.001	0.999

[a] – Maximum Fe reduced determined after 18 days of incubation, the amount of Fe reduced after 14 days was determined to be 77.9±4.8%

[b] – N refers to non-irradiated BIOS

[c] – Data correspond to fresh γ-irradiated BIOS collected in July 2013, data acquired from Cotroneo and Fortin (2013)

Figures

Figure 3-1: X-ray diffraction patterns of synthetic HFO, as well as fresh and frozen BIOS collected from sites CA-04 and CA-03. The main reflections of the reference data for 2-line ferrihydrite, goethite, and magnetite are presented at the bottom of the graph. The broad reflections centered at ~2.5 and 1.5 Å correspond to the poorly ordered iron oxide mineral 2-line ferrihydrite. The crystalline iron oxide minerals, magnetite, was also identified in BIOS samples collected from sites CA-04, whereas goethite was detected in BIOS samples collected from site CA-03. Other sharp peaks correspond to silicate weathering minerals and calcite. For clarity, all patterns have been vertically separated on an arbitrary y-axis. Data for fresh BIOS was obtained from Cotroneo and Fortin (2013).

Figure 3-2: SEM micrographs of BIOS collected from sites CA-04 (A) and CA-03 (B), showing the abundance of sheath-like and twisted structures reminiscent of the iron oxidizing bacteria *Leptothrix* spp. (L) and *Gallionella* spp. (G), respectively, scale bars = 3µm (A) and 1 µm (B).

Figure 3-3: Changes in total Fe(II) ($Fe(II)_{tot}$) and dissolved Fe(II) ($Fe(II)_{diss}$) relative to total Fe during the reduction of HFO by *S. putrefaciens* CN32 with 3.9mM or 10µM of phosphate with molybdate:sulfate concentrations of 0:1, 1:1, or 2:1. The concentrations of Fe(II) were determined with the ferrozine method. "Biotic" refers to microcosms to which bacteria were added, whereas "Control" refers to microcosms to which no bacteria were added. Data markers represent means and standard deviations of 3 replicates for each biotic experiment. Solid lines represent 3-parameter sigmoid lines of best fit to the data.

Figure 3-4: Changes in total Fe(II) ($Fe(II)_{tot}$) and dissolved Fe(II) ($Fe(II)_{diss}$) relative to total Fe during the reduction of non-irradiated and γ-irradiated BIOS collected from site CA-04 with 3.9mM or 10µM of phosphate. 1:1 or 2:1 refer to the molybdate:sulfate concentration. The concentrations of Fe(II) were determined with the ferrozine method. "Biotic" refers to microcosms to which bacteria were added, whereas "Control" refers to microcosms to which no bacteria were added. Data markers represent means and standard deviations of 3 replicates for biotic experiments conducted with non-irradiated BIOS and 2 replicates for those conducted with γ-irradiated BIOS. Solid lines represent 3-parameter sigmoid lines of best fit to the data.

Figure 3-5: Changes in total Fe(II) ($Fe(II)_{tot}$) and dissolved Fe(II) ($Fe(II)_{diss}$) relative to total Fe during the reduction of non-irradiated and γ-irradiated BIOS collected from site CA-03 with 3.9mM or 10µm of phosphate with molybdate:sulfate concentrations of 1:1 or 2:1. The concentrations of Fe(II) were determined with the ferrozine method. "Biotic" refers to microcosms to which bacteria were added, whereas "Control" refers to microcosms to which no bacteria were added. Data markers represent means and standard deviations of 3 replicates for biotic experiments conducted with non-irradiated BIOS and 2 replicates for those conducted with γ-irradiated BIOS. Solid lines represent 3-parameter sigmoid lines of best fit to the data.

Figure 3-6: X-ray diffraction patterns of post-reduction precipitates formed during the microbial reduction of HFO by *S. putrefaciens* CN32 in the presence of 3.9mM of phosphate and molybdate:sulfate concentrations of 0:1, 1:1, or 2:1. In all the treatments, vivianite was the dominant mineral. For clarity, all patterns have been vertically separated on an arbitrary y-axis.

Figure 3-7: X-ray diffraction patterns of post-reduction precipitates formed during the microbial reduction of HFO by *S. putrefaciens* CN32 in the presence of 10μM of phosphate and molybdate:sulfate concentrations of 0:1, 1:1, or 2:1. Data shows the progressive decrease in magnetite with increasing molybdate content, with goethite being the dominant mineral. Red arrows point to peaks that correspond to magnetite. Dashed lines highlight the peaks from the sample holder. For clarity, all patterns have been vertically separated on an arbitrary y-axis.

Figure 3-8: X-ray diffraction patterns of post-reduction precipitates formed during the microbial reduction of non- and γ-irradiated BIOS from site CA-04 conducted with 10μM of phosphate. 0:1, 1:1, 2:1 refer to the molybdate:sulfate concentrations. Dashed lines highlight the peaks from the sample holder. For clarity, all patterns have been vertically separated on an arbitrary y-axis.

Figure 3-9: X-ray diffraction patterns of post-reduction precipitates formed during the microbial reduction of non- and γ-irradiated BIOS from site CA-03 conducted with 10μM of phosphate. 1:1 and 2:1 correspond to the molybdate:sulfate concentrations. Dashed lines highlight the peaks from the sample holder. For clarity, all patterns have been vertically separated on an arbitrary y-axis.

Figure 3-10: SEM micrographs of post-reduction precipitates formed during the microbial reduction of BIOS from sites CA-04 (A and D) and CA-03 (B and E), and HFO (C and F) with 3.9mM (A-C) or 10μM (D-F) of phosphate by *S. putrefaciens* CN32.

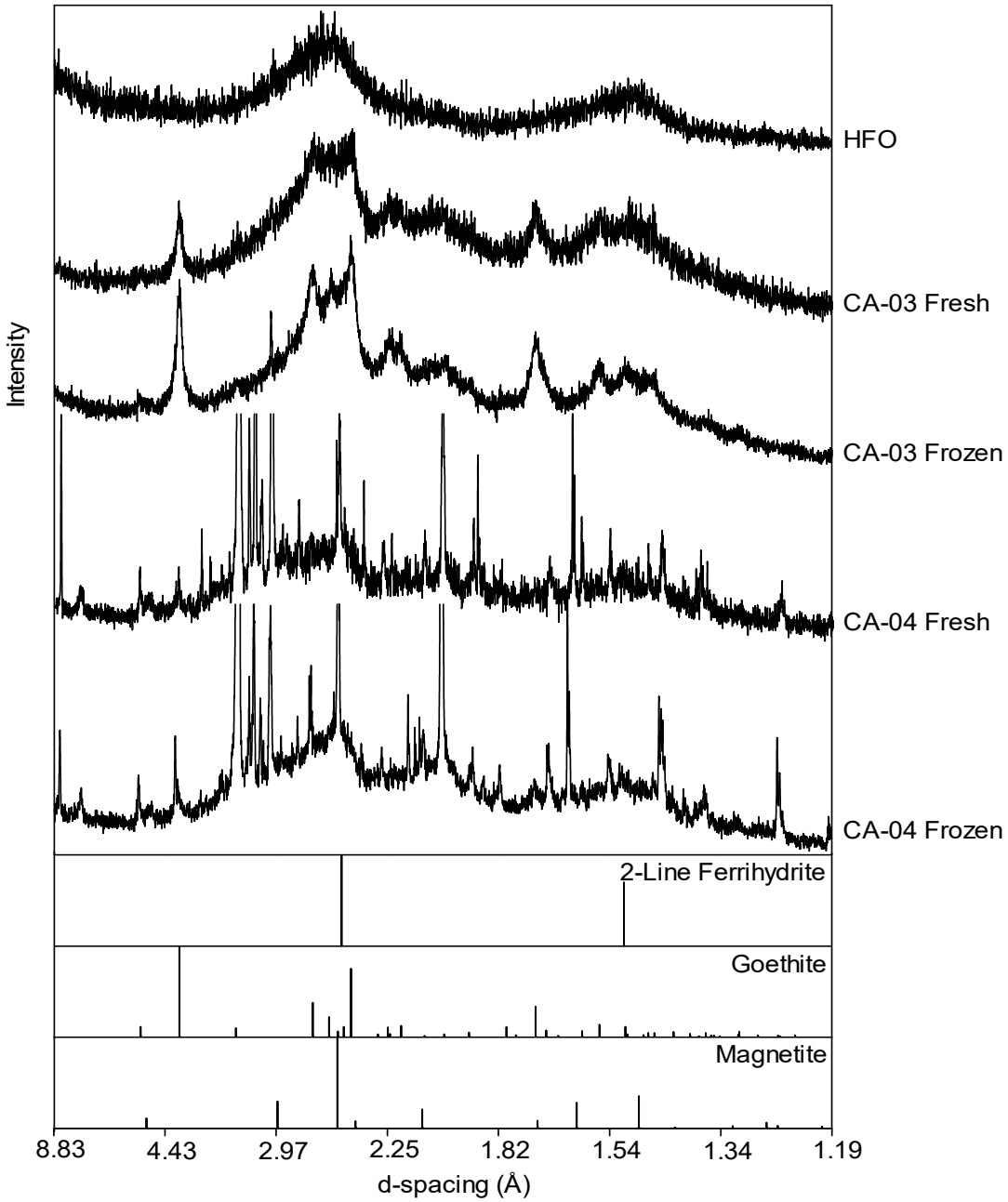

Figure 3-1: X-ray diffraction patterns of synthetic HFO, as well as fresh and frozen BIOS collected from sites CA-04 and CA-03. The main reflections of the reference data for 2-line ferrihydrite, goethite, and magnetite are presented at the bottom of the graph. The broad reflections centered at ~2.5 and 1.5 Å correspond to the poorly ordered iron oxide mineral 2-line ferrihydrite. The crystalline iron oxide minerals, magnetite, was also identified in BIOS samples collected from sites CA-04, whereas goethite was detected in BIOS samples collected from site CA-03. Other sharp peaks correspond to silicate weathering minerals and calcite. For clarity, all patterns have been vertically separated on an arbitrary y-axis. Data for fresh BIOS was obtained from Cotroneo and Fortin (2013).

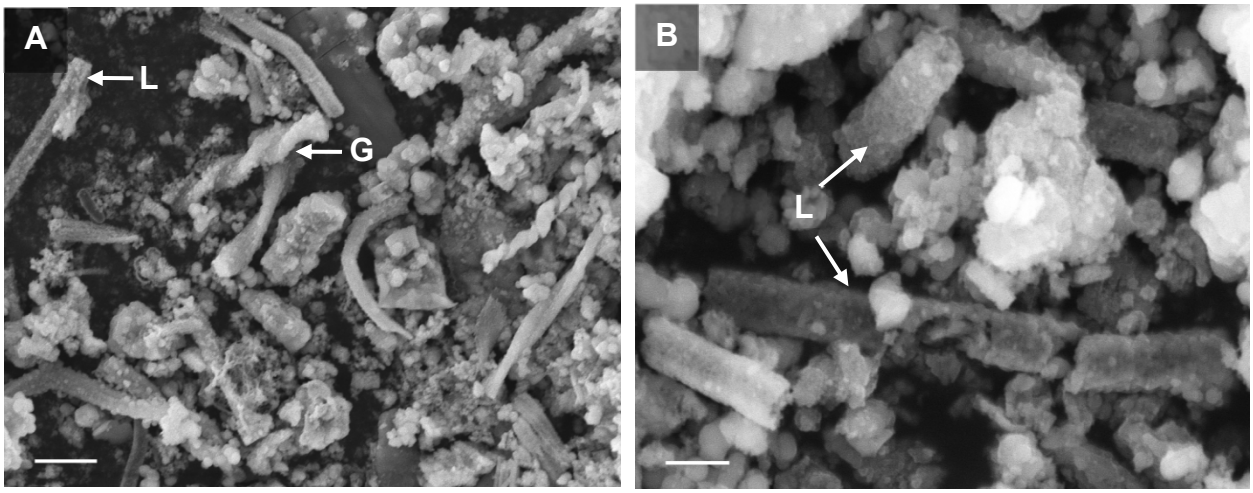

Figure 3-2: SEM micrographs of BIOS collected from sites CA-04 (A) and CA-03 (B), showing the abundance of sheath-like and twisted structures reminiscent of the iron oxidizing bacteria *Leptothrix* spp. (L) and *Gallionella* spp. (G), respectively, scale bars = 3µm (A) and 1 µm (B).

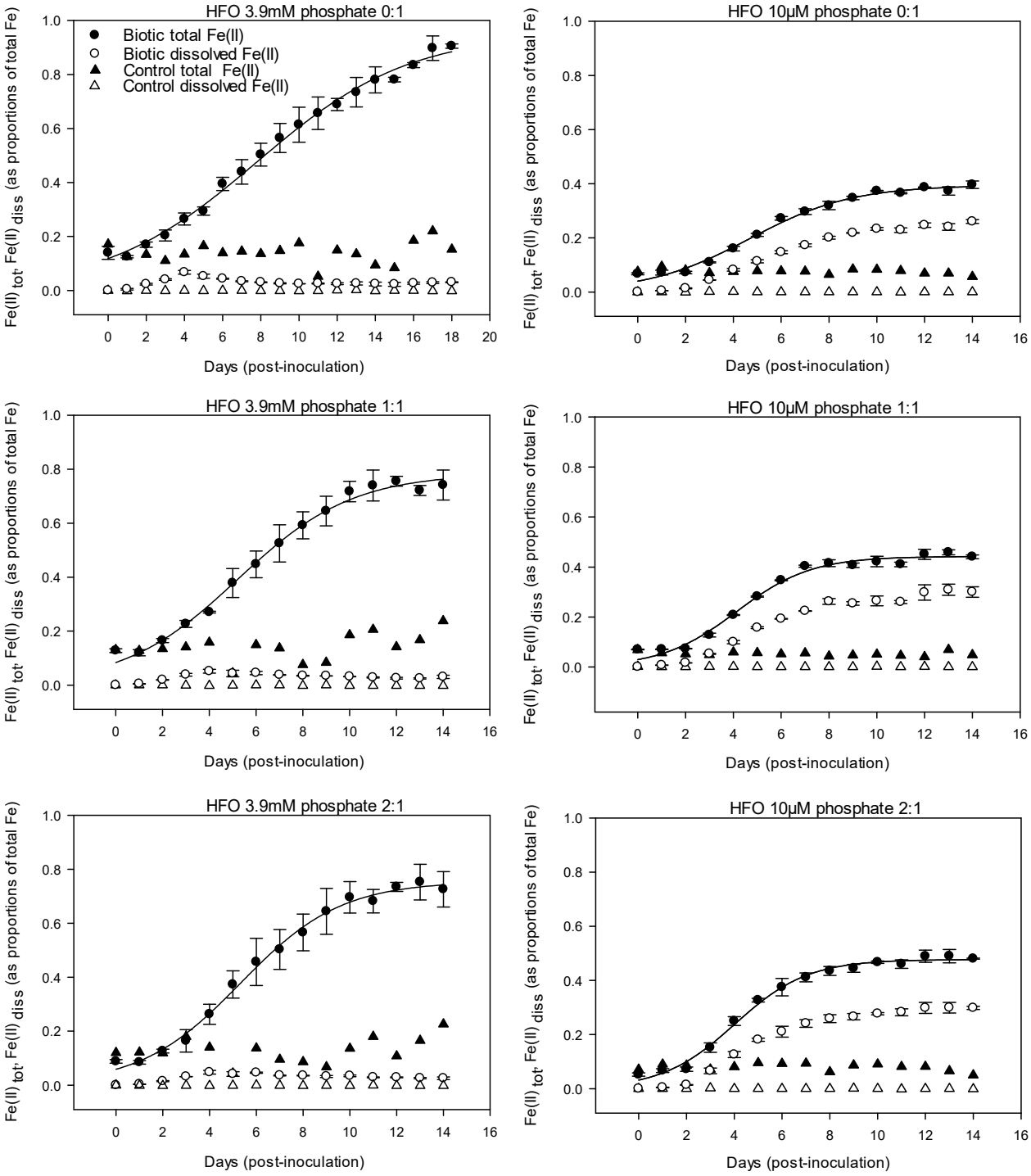

Figure 3-3: Changes in total Fe(II) ($Fe(II)_{tot}$) and dissolved Fe(II) ($Fe(II)_{diss}$) relative to total Fe during the reduction of HFO by *S. putrefaciens* CN32 with 3.9mM or 10µM of phosphate with molybdate:sulfate concentrations of 0:1, 1:1, or 2:1. The concentrations of Fe(II) were determined with the ferrozine method. "Biotic" refers to microcosms to which bacteria were added, whereas "Control" refers to microcosms to which no bacteria were added. Data markers represent means and standard deviations of 3 replicates for each biotic experiment. Solid lines represent 3-parameter sigmoid lines of best fit to the data.

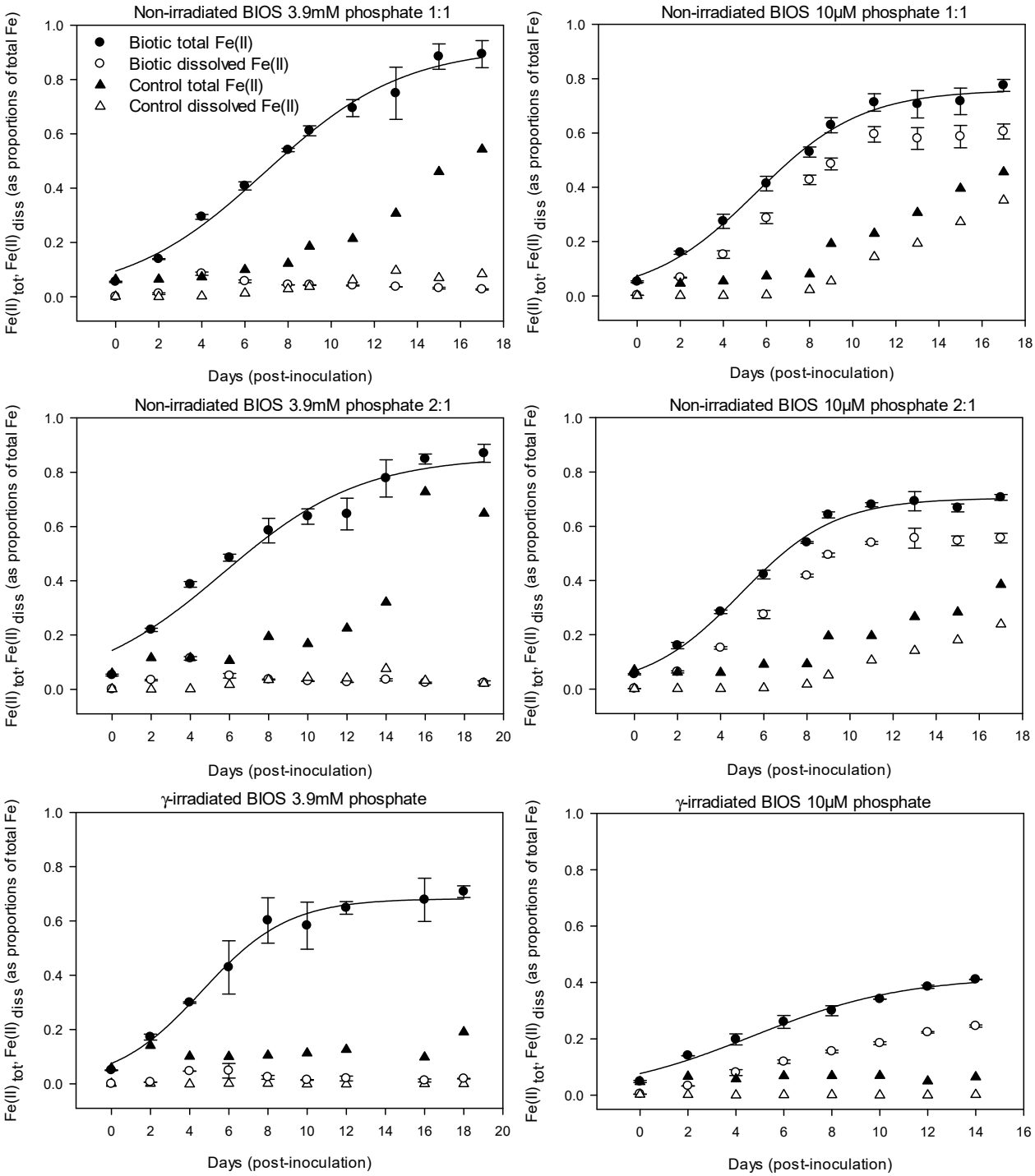

Figure 3-4: Changes in total Fe(II) ($Fe(II)_{tot}$) and dissolved Fe(II) ($Fe(II)_{diss}$) relative to total Fe during the reduction of non-irradiated and γ-irradiated BIOS collected from site CA-04 with 3.9mM or 10µM of phosphate. 1:1 or 2:1 refer to the molybdate:sulfate concentration. The concentrations of Fe(II) were determined with the ferrozine method. "Biotic" refers to microcosms to which bacteria were added, whereas "Control" refers to microcosms to which no bacteria were added. Data markers represent means and standard deviations of 3 replicates for biotic experiments conducted with non-irradiated BIOS and 2 replicates for those conducted with γ-irradiated BIOS. Solid lines represent 3-parameter sigmoid lines of best fit to the data.

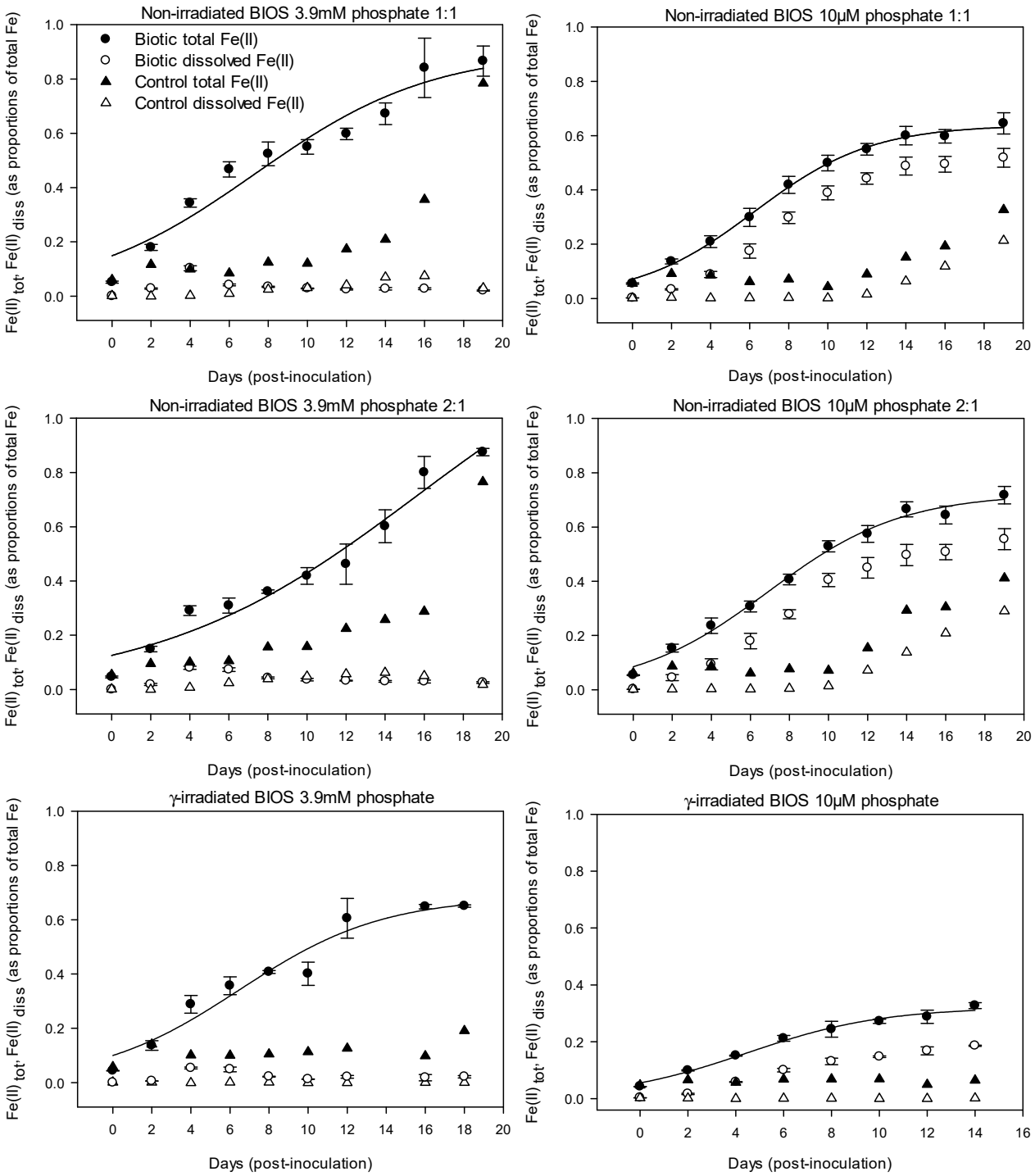

Figure 3-5: Changes in total Fe(II) ($Fe(II)_{tot}$) and dissolved Fe(II) ($Fe(II)_{diss}$) relative to total Fe during the reduction of non-irradiated and γ-irradiated BIOS collected from site CA-03 with 3.9mM or 10µm of phosphate with molybdate:sulfate concentrations of 1:1 or 2:1. The concentrations of Fe(II) were determined with the ferrozine method. "Biotic" refers to microcosms to which bacteria were added, whereas "Control" refers to microcosms to which no bacteria were added. Data markers represent means and standard deviations of 3 replicates for biotic experiments conducted with non-irradiated BIOS and 2 replicates for those conducted with γ-irradiated BIOS. Solid lines represent 3-parameter sigmoid lines of best fit to the data.

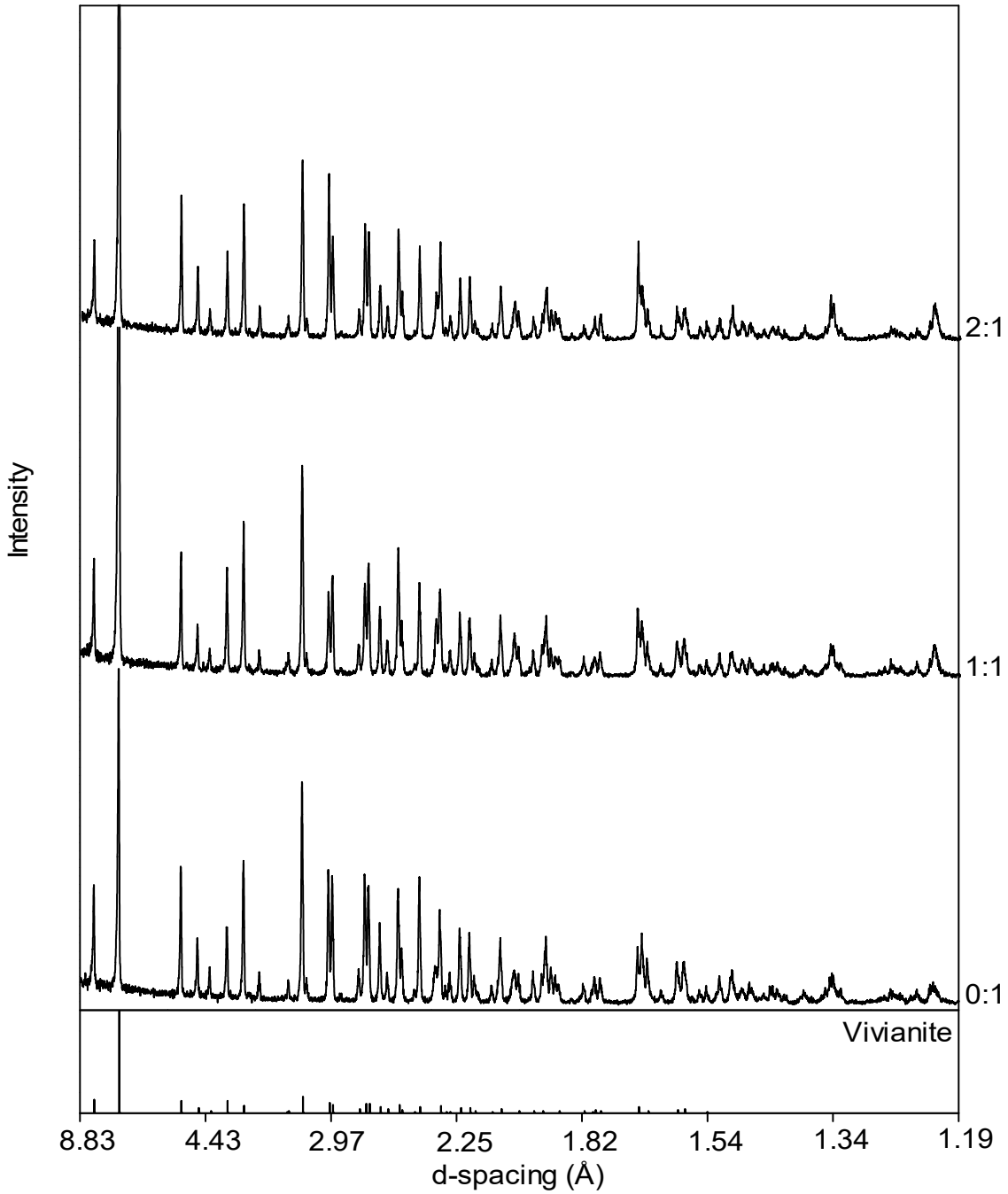

Figure 3-6: X-ray diffraction patterns of post-reduction precipitates formed during the microbial reduction of HFO by *S. putrefaciens* CN32 in the presence of 3.9mM of phosphate and molybdate:sulfate concentrations of 0:1, 1:1, or 2:1. In all the treatments, vivianite was the dominant mineral. For clarity, all patterns have been vertically separated on an arbitrary y-axis.

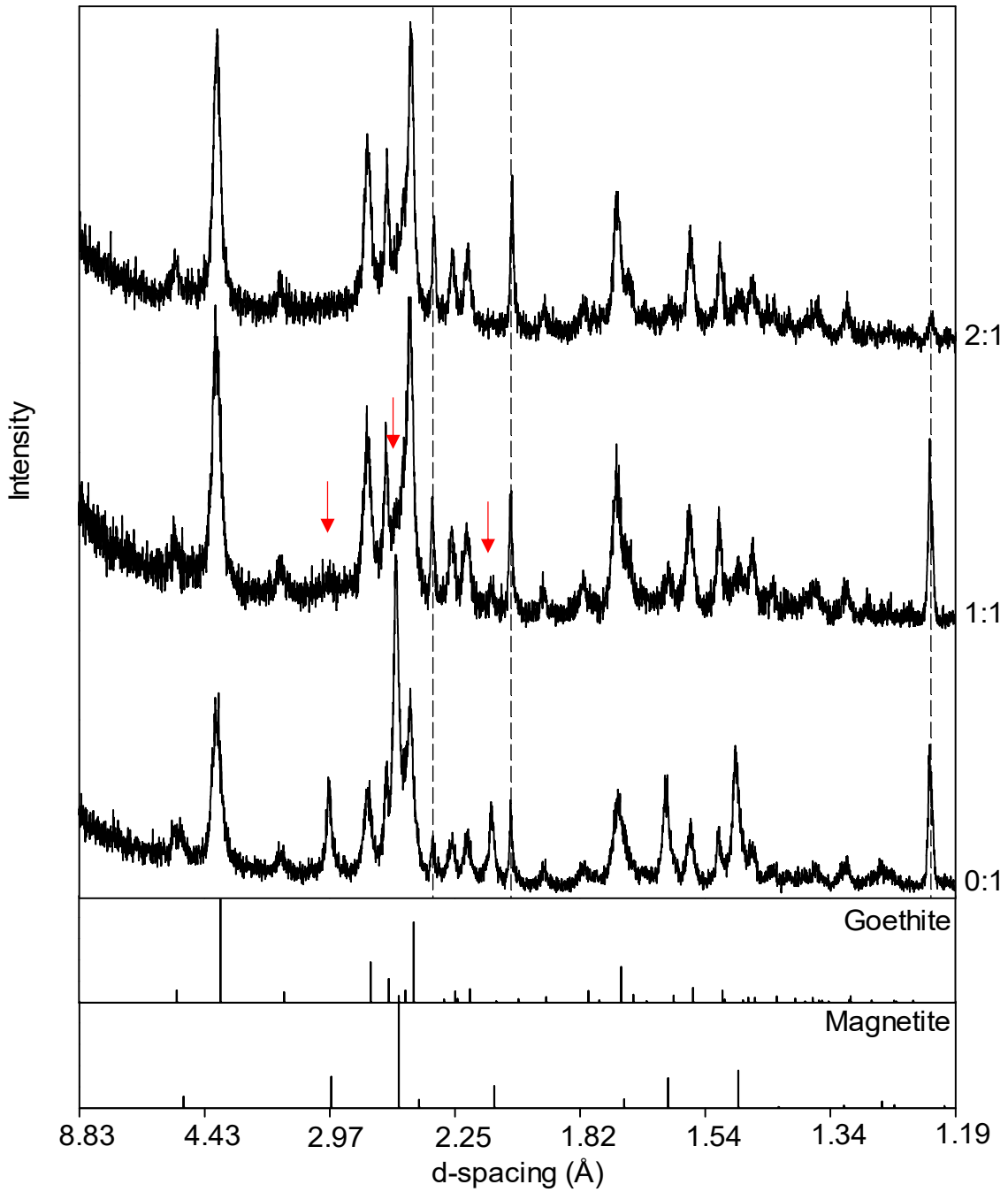

Figure 3-7: X-ray diffraction patterns of post-reduction precipitates formed during the microbial reduction of HFO by *S. putrefaciens* CN32 in the presence of 10μM of phosphate and molybdate:sulfate concentrations of 0:1, 1:1, or 2:1. Data shows the progressive decrease in magnetite with increasing molybdate content, with goethite being the dominant mineral. Red arrows point to peaks that correspond to magnetite. Dashed lines highlight the peaks from the sample holder. For clarity, all patterns have been vertically separated on an arbitrary y-axis.

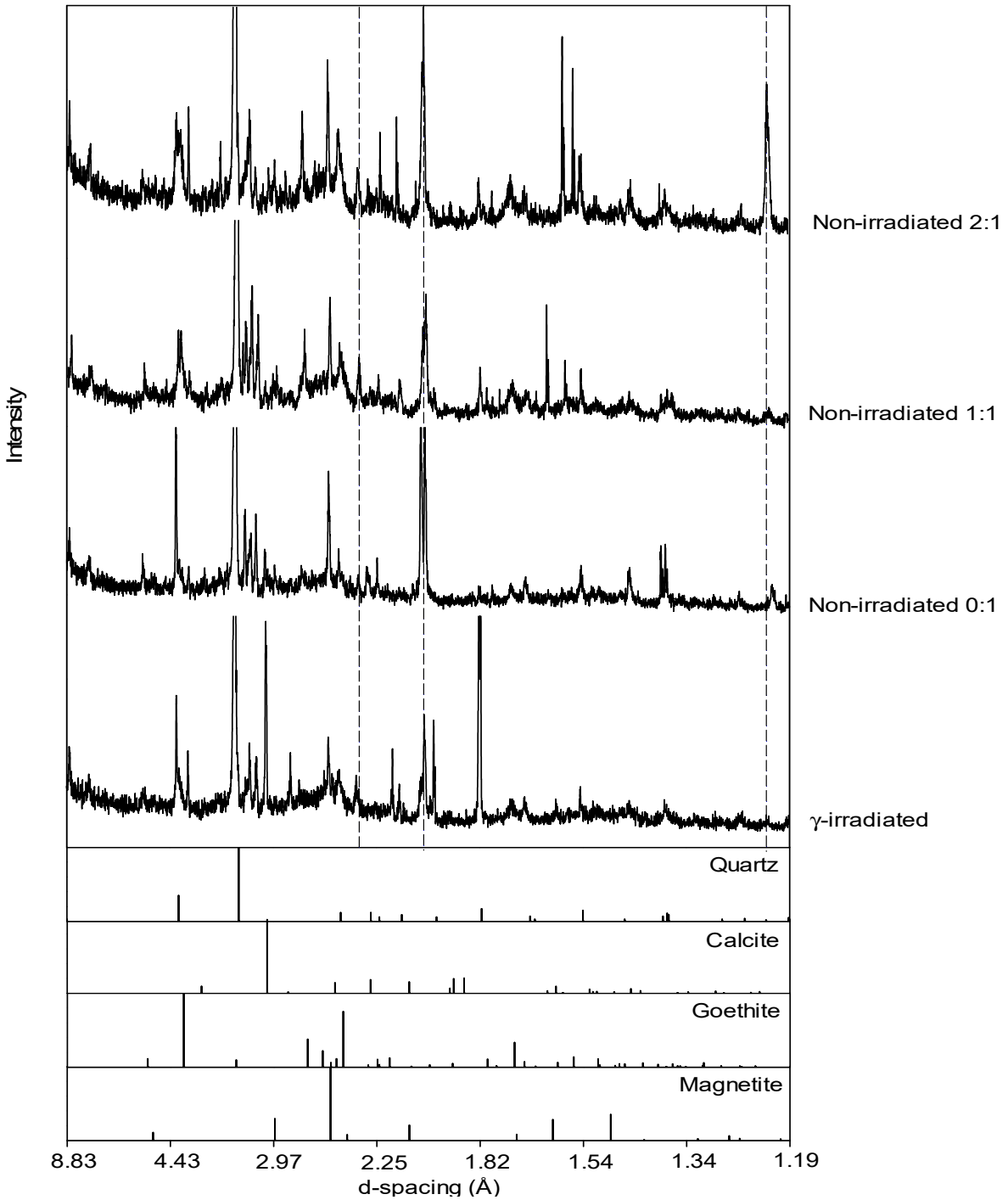

Figure 3-8: X-ray diffraction patterns of post-reduction precipitates formed during the microbial reduction of non- and γ-irradiated BIOS from site CA-04 conducted with 10μM of phosphate. 0:1, 1:1, 2:1 refer to the molybdate:sulfate concentrations. Dashed lines highlight the peaks from the sample holder. For clarity, all patterns have been vertically separated on an arbitrary y-axis.

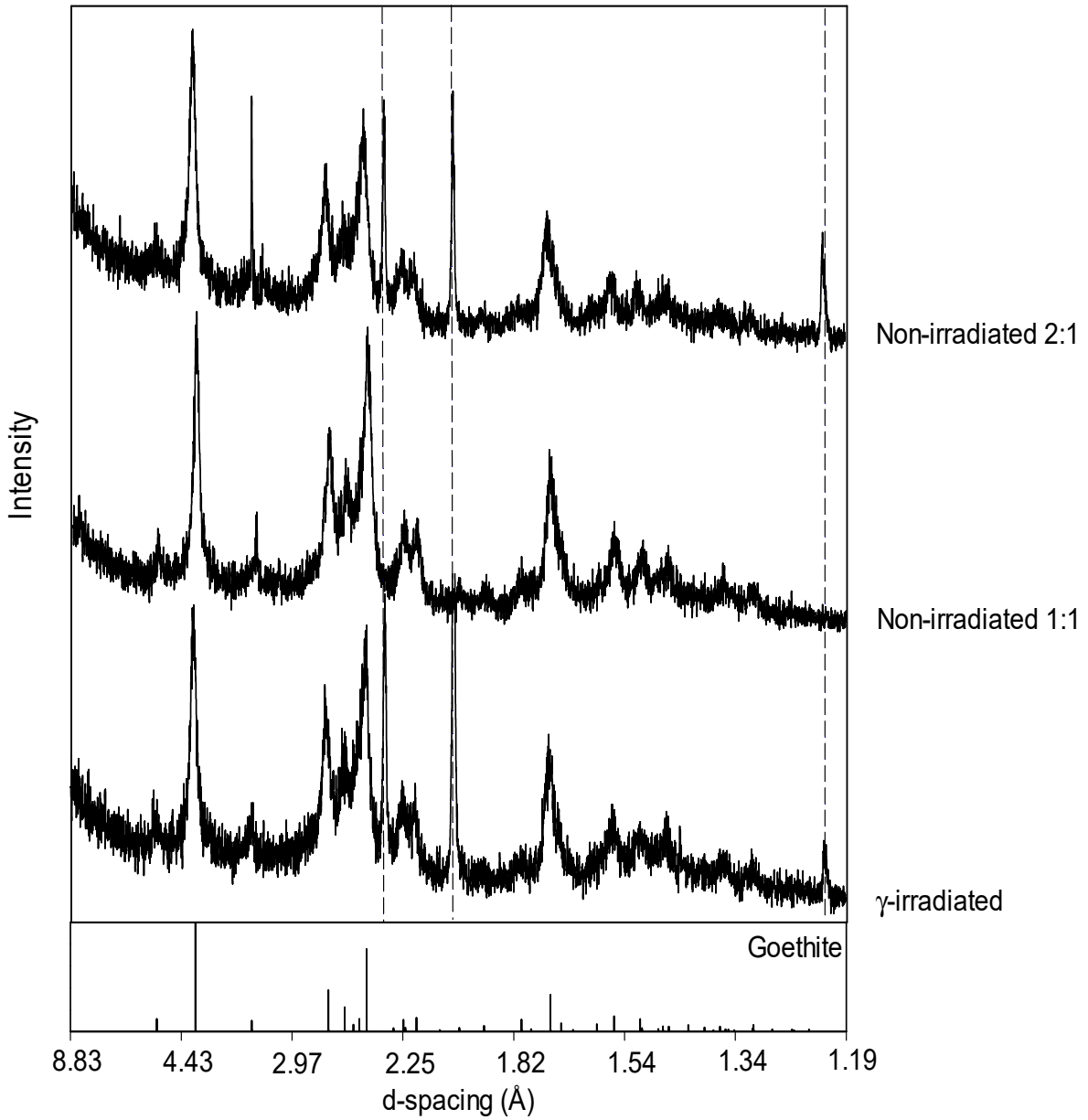

Figure 3-9: X-ray diffraction patterns of post-reduction precipitates formed during the microbial reduction of non- and γ-irradiated BIOS from site CA-03 conducted with 10μM of phosphate. 1:1 and 2:1 correspond to the molybdate:sulfate concentrations. Dashed lines highlight the peaks from the sample holder. For clarity, all patterns have been vertically separated on an arbitrary y-axis.

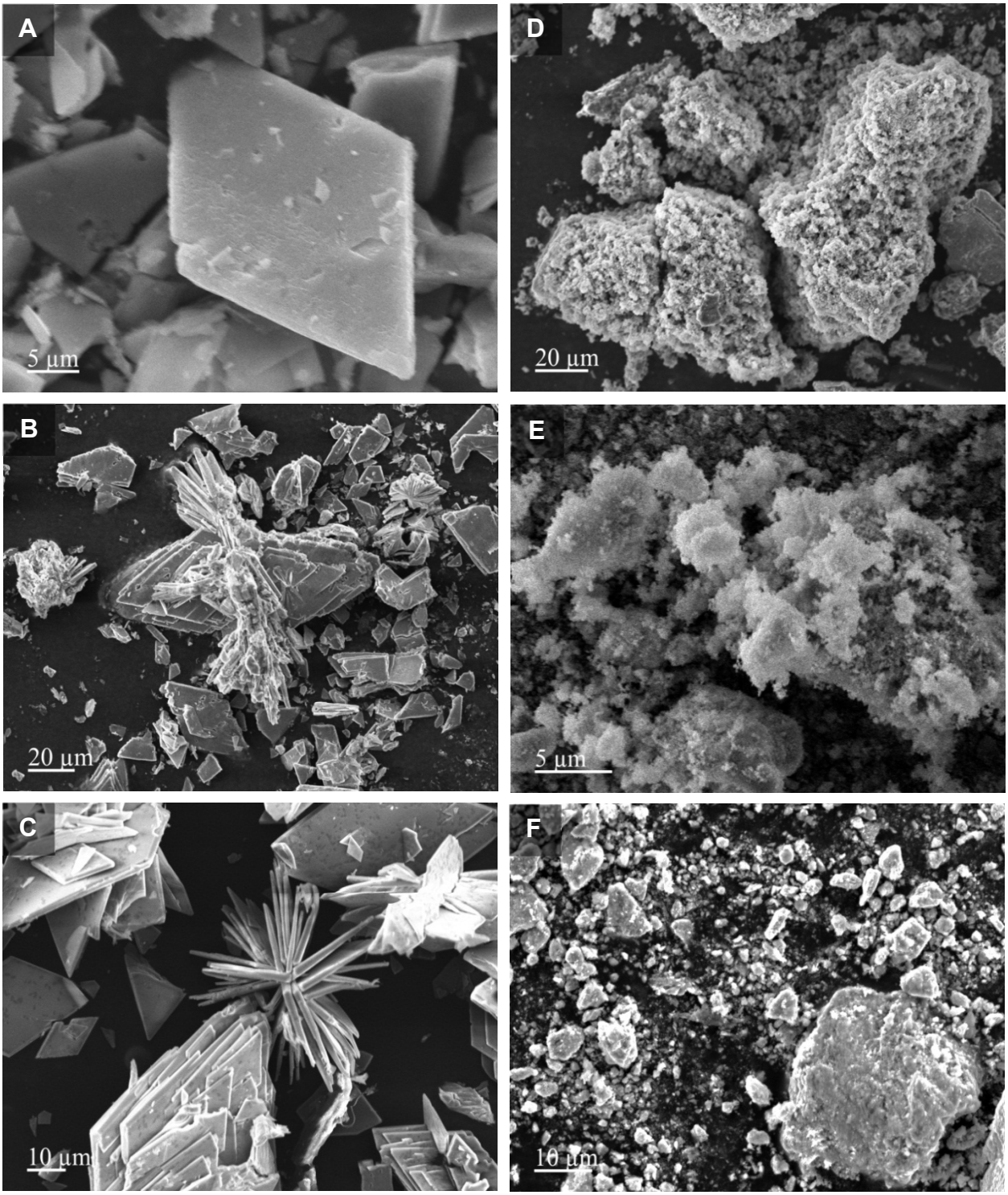

Figure 3-10: SEM micrographs of post-reduction precipitates formed during the microbial reduction of BIOS from sites CA-04 (A and D) and CA-03 (B and E), and HFO (C and F) with 3.9mM (A-C) or 10µM (D-F) of phosphate by *S. putrefaciens* CN32.

Chapter 4: Summary and Future Research

The following general conclusions can be made from the research conducted:

1. Simulated diagenesis (ageing) of BIOS under environmentally conditions did not influence their mineralogical composition. Despite the similarity of mineralogy between aged and fresh BIOS, aged BIOS were found to be significantly less reactive than their fresh counterparts. Ageing likely promoted the aggregation of ferrihydrite nanoparticles thereby diminishing the reactive site density available for access by DIRB.
2. The concentration of phosphate had varying effects on the rates of reduction of ferrihydrite, non- and γ-irradiated BIOS. Excess concentration of phosphate enhanced the extent but not the rate of Fe(III) reduction. Phosphate had a significant impact on the identity of the secondary iron minerals that formed. In the presence of environmentally relevant concentration of phosphate, goethite and magnetite were the primary mineral products. However, the intermixed organic component within BIOS likely inhibited the formation of magnetite, and, possibly, goethite.
3. The effects of molybdate on the rate and extent of reduction of ferrihydrite, non- and γ-irradiated BIOS were found to be dependent on the terminal acceptor type, and the concentration of phosphate. Molybdate was also found to influence the formation of magnetite in some experiments. Finally, the efficiency of molybdate to inhibit sulfate reducing bacteria strongly depended on the concentration of phosphate.
4. γ-irradiation at a dose of 14kGy did not alter the bulk mineralogy nor the reactivity of BIOS, and it was concluded to be a suitable and minimally invasive sterilization technique for BIOS.

5. As previously found with simulated diagenesis, freezing of BIOS at -15ºC likely promoted the aggregation of ferrihydrite nanoparticles which diminished the reactivity of BIOS towards microbial reduction.

Future Research:

The research conducted was based on the principles discussed in the papers and future work will look to expand on those elements including additional future work. Thus, I propose:

1. Given the inherent complexity of naturally occurring BIOS, and to circumvent the use of molybdate or γ-irradiation, the use of pure-strains of microaerophilic iron-oxidizing bacteria/laboratory grown BIOS is now an attractive and a plausible option. Recent advancement made it possible to grow an appreciable amount of BIOS via a diffusion-chamber (Kikuchi et al., 2014). The diffusion-chamber offers a controlled environment which makes it possible to test numerous factors and a combination of factors on the mineralogy and, possibly, population distribution of the microbial community. Thus, I propose the following:

- Determine the impact of temperature, [O_2], dissolved inorganic carbon, aluminum, ionic strength, pH, etc… on the rate of Fe(II) oxidation and in turn the mineralogy of BIOS.
- Determine the impact of oxyanions PO_4, SiO_4, As(V), As(III) on the mineralogy of BIOS. The addition of oxyanions can be added to simulate adsorption (addition after formation of BIOS) or to simulate co-precipitation (addition during the formation of BIOS). The timing of addition of oxyanions will likely influence the crystallinity of the BIOS differently.

- Given the recent interest in the interaction of rare earth metals (REEs) and biofilms within natural environments and given the inherent complexity of the naturally occurring biofilms. Studying the interactions of various REEs with pure phases of BIOS will prove to be useful to determine the partitioning of REEs between the mineral and organic fraction under controlled settings. It is possible to add complexity to these systems by adding different impurities/compounds to slowly mimic the environment, and to determine their influence on REEs uptake and partitioning.
- The generated BIOS from previous proposed experiments could be exposed to anaerobic conditions to determine if geochemical changes/impurities influence the reactivity of BIOS in the presence of an iron reducing bacteria. These changes may not be easily detected by bulk XRD or EXAFS, thus iron reducing bacteria may prove to be useful to delineate changes.
- Recent work showed that stalks were reduced at a lower rate than sheaths (Langley et al., 2009). This suggests that sheaths and stalks possess different reactivity, this could also suggest that contaminants may be distributed differently within stalks when compared to sheaths. Determine the binding capacity of sheaths vs. stalks for various oxyanions and metal contaminants, investigate the distribution of the different metals/oxyanions between sheaths vs. stalks using confocal laser scanning microscopy combined with metal- and polysaccharide-specific fluorophores (Hao et al., 2016; Fabisch et al., 2016).
- Inoculating the diffusion chamber with a "dirty" sample (i.e. BIOS collected from field) together with changing various geochemical parameters of the media within the diffusion chamber (SO_4^{-2}, S^0, NO_3^-, Mn, etc…) may lead to conditions that favor the

growth of previously undefined iron-oxidizing bacteria. Probing the phylogeny of the microbial community could provide clues of the changing community dynamics. In combination, a micro-probe could be easily installed to determine geochemical changes at the micron scale and relate how the changing parameters influence the composition of the microbial community.

- A number of combinations and a vast number of experiments can be made to add to our understanding of the behavior and reactivity of BIOS generated from microaerophilic iron oxidizing bacteria.

2. BIOS form in a broad range of environments suggesting that they are exposed to varying temperature and pressure. Conduct a controlled experiment to determine the impact of simulated diagenesis at varying temperature and/or pressure on the stability and reactivity of synthetic ferrihydrite, lepidocrocite, goethite, or akageneite co-precipitated with a polysaccharide (alginate) that compositionally resembles the extracellular polymeric substances produced by iron oxidizing bacteria (sheaths and stalks). Synthesize co-precipitates of the aforementioned iron oxides with varying concentrations of alginate (C/Fe) and expose them to simulated diagenesis to reflect carbon rich or carbon poor environments. Alginate can be replaced by or combined with other impurities that are often associated with iron oxides in the environment, including Al, Si, P, etc...

3. Recent work suggested that the distribution of sheaths forming- and stalk forming-iron oxidizing bacteria within the natural environment is dictated by the concentration of the dissolved organic carbon (DOC), perhaps the type, structural complexity, and composition of the DOC also play an important role (Fleming et al., 2014). Conduct field experiments to characterize DOC within waters of the BIOS mats using NRM, HPLC, etc. Once

characterized, conduct controlled experiments (i.e. pure strains) to determine the effect of DOC on the health of the iron oxidizing bacteria (i.e. mixotrophic growth).

4. Previous research showed that iron oxidizing bacteria are capable of accessing Fe(II) within a limited number of minerals (e.g. siderite, magnetite, FeS, etc.). Unknown is whether or not iron oxidizing bacteria are capable of accessing Fe(II) that is complexed with organic matter. These complexes are generally stable even under oxic conditions, and if they are accessible this would likely expand the niche for microaerophilic iron oxidizing bacteria. Design a controlled experiment with pure strains of bacteria along with various Fe(II)-organic complexes. Relate the findings of the experiments conducted in Point 3 to those in Point 4.
5. Explore the effects of γ-irradiation on mixed valent Fe(II)/Fe(III) iron oxides including magnetite and green-rust.
6. Determine if the effects of γ-irradiation on different iron oxide minerals is related to the crystal size of the mineral.

References

Fabisch, M., Freyer, G., Johnson, C., Büchel, G., Akob, D., Neu, T., Küsel, K., 2016. Dominance of '*Gallionella capsiferriformans*' and heavy metal association with gallionella-like stalks in metal-rich ph 6 mine water discharge. Geobiology, 14, 68-90.

Fleming, E.J., Cetinic, I., Chan, C.S., King, D.W., Emerson, D., 2014. Ecological succession among iron-oxidizing bacteria. The ISME Journal, 8, 804-815.

Hao, L., Guo, Y., Byrne, J.M., Zeitvogel, F., Schmid, G., Ingino, P., Li, J., Neu, T.R., Swanner, E.D., Kappler, A., 2016. Binding of heavy metal ions in aggregates of microbial cells, eps and biogenic iron minerals measured in-situ using metal-and glycoconjugates-specific fluorophores. Geochim. Cosmochim. Acta, 180, 66-96.

Kikuchi, S., Makita, H., Takai, K., Yamaguchi, N., Takahashi, Y., 2014. Characterization of biogenic iron oxides collected by the newly designed liquid culture method using diffusion chambers. Geobiology, 12, 133-145.

Langley, S., Gault, A., Ibrahim, A., Renaud, R., Fortin, D., Clark, I.D., Ferris, F.G., 2009. A comparison of the rates of Fe(III) reduction in synthetic and bacteriogenic iron oxides by Shewanella putrefaciens CN32. Geomicrobiology Journal, 26, 57-70.

Appendix

Table S1: Selected phyiscochemical parameters of groundwater-derived surface waters measured at the New Calumet Mine sites CA-04 and CA-03 during the spring of 2013. Data obtained from Cotroneo and Fortin (2013).

Site	pH	Eh (mV)	Temp (ºC)	Dissolved O_2 (mg/L)	Fe(II) (ppm)[a]	Fe(II) (ppm)[b]	SO_4 (ppm)[b]	Mo (ppm)[b]	DIC (ppm)	DOC (ppm)
CA-04	7.22	+42	13.5	0.8	12.91	9.89	714.74	bd[c]	80.28	5.26
CA-03	7.29	+152	12.18	4.23	37.15	35.31	743.01	bd	77.16	4.46

[a] Concentration of Fe(II) in the unfiltered water

[b] Concentrations determined in the filtered water (0.22µm)

[c] Below detection limit of the instrument (0.0041 ppm)

Table S2: Extraction efficiency of 0.5M and 6M HCl of microbially reduced solids collected from experiments conducted with 10µM of phosphate after incubation for 10 days. 0:1, 1:1, and 2:1 correspond to concentration of molybdate:sulfate. The concentration of Fe(II) was determined using the ferrozine method. Data represents mean and standard deviation of 3 replicates for each extraction.

Treatment	0:1 Fe(II) (mM)	1:1 Fe(II) (mM)	2:1 Fe(II) (mM)
0.5M HCl	1.39±0.022	1.69±0.013	1.77±0.023
6M HCl*	1.39±0.056	1.76±0.001	1.83±0.028

* 6M is the final concentration

For further confirmation of the extraction efficiency of 0.5M HCl, a concentrated suspension of post-secondary iron minerals originating from biotic microcosms conducted with HFO and 10µM of phosphate was extracted in 0.5M HCl and 3M HCl (final concentration) for 24 hours in the anaerobic chamber. Suspensions from biotic microcosms with HFO and low phosphate were chosen because the presence of magnetite was confirmed by XRD. Given that coarse magnetite is recalcitrant to dissolution in 0.5M HCl, such suspension would serve as an excellent representative to compare the extraction efficiency between weak and strong acid. After 24 hours of extraction, in contrast to the suspension extracted with 0.5M HCl, no solids remained in the tube where the suspension was extracted with 3M HCl. However, the concentrations of Fe(II) were comparable (data represents mean and standard deviation of 2 for each sample):

Treatment	Sample 1 (mM)	Sample 2 (mM)
0.5M HCl	1.66±0.01	1.61±0.01
3M HCl[a]	1.70±0.02	1.62±0.02

[a] 3M is the final concentration

Table S3: Iron extraction efficiency by dithionite compared to strong nitric acid and peroxide (HNO_3/H_2O_2) digestions. The HNO_3/H_2O_2 digests were analyzed with ICP-OES. Data expressed as mg per gram of dry sample. Data represents mean and standard deviation of 3 replicates for dithionite extractions and 4 replicates for HNO_3/H_2O_2 digestions.

Sample	Dithionite	HNO_3/H_2O_2
CA-04	234.8±5.1	227.1±7.9
CA-03	418.2±17.4	392.7±2.7

Table S4: Initial and final concentrations of phosphate and molybdate (mM) in biotic and control batch experiments conducted with HFO, and BIOS from sites CA-04 and CA-03. "Biotic" refers to microcosms to which *S. putrefaciens* CN32 were added, whereas "Control" refers to control microcosms to which no bacteria were added. 1 replicate, either Control or biotic, was analyzed for each treatment. H and L refer to the concentration of phosphate (H – 3.9mM, L – 10μM), whereas 0:1, 1:1, and 2:1 refer to the concentration of molybdate:sulfate added to the media.

Sample	Initial Phosphate		Final Phosphate		Initial Molybdate		Final Molybdate	
	Control	Biotic	Control	Biotic	Control	Biotic	Control	Biotic
HFO H 0:1	3.16	3.18	2.53	1.47	bd[a]	bd	bd	bd
HFO H 1:1	3.02	3.05	2.68	1.57	0.14	0.14	0.14	0.13
HFO H 2:1	3.25	3.31	2.78	1.61	0.30	0.30	0.28	0.26
HFO L 0:1	bd	bd	bd	bd	bd	bd	bd	bd
HFO L 1:1	bd	bd	bd	bd	0.07	0.07	0.05	0.02
HFO L 2:1	bd	bd	bd	bd	0.17	0.17	0.14	0.06
N-CA-04 H 1:1[b]	3.07	3.08	2.1	1.38	0.14	0.13	0.13	0.14
N-CA-04 H 2:1	3.80	3.30	1.36	1.47	0.29	0.26	0.25	0.25
N-CA-04 L 1:1	bd	bd	bd	bd	0.13	0.13	0.10	0.09
N-CA-04 L 2:1	bd	bd	bd	bd	0.27	0.27	0.20	0.20
N-CA-03 H 1:1	3.56	3.03	1.19	1.23	0.15	0.12	0.13	0.12
N-CA-03 H 2:1	3.49	3.18	1.26	1.14	0.28	0.25	0.24	0.24
N-CA-03 L 1:1	bd	bd	bd	bd	0.13	0.12	0.09	0.08
N-CA-03 L 2:1	bd	bd	bd	bd	0.29	0.24	0.18	0.14
γ-CA-04 H	3.81	3.86	3.22	1.88	bd	bd	bd	bd
γ-CA-04 L	nd[c]	nd	nd	nd	nd	nd	nd	nd
γ-CA-03 H	3.81	3.81	3.22	1.64	bd	bd	bd	bd
γ-CA-03 L	nd	nd	nd	nd	nd	nd	nd	nd

[a] – Below the detection limit of the instrument
[b] – N refers to non-irradiated BIOS
[c] – nd refers to not determined

Table S5: Maximum percentage of total Fe reduced, linear reduction rates and correlation coefficients for the linear reduction rates for control microcosms with non-irradiated BIOS. H and L refer to the concentration of phosphate added to the media (H – 3.9mM, L – 10μM), whereas 1:1, and 2:1 refer to the concentration of molybdate:sulfate added to the media. 1 replicate was employed for each treatment.

Sample	Maximum Fe Reduced (%)	Reduction Rate (day^{-1})	R^2
CA-04 H 1:1	54.3	0.057±0.010	0.986
CA-04 H 2:1	72.8	0.126±0.078	0.887
CA-04 L 1:1	45.6	0.039±0.010	0.970
CA-04 L 2:1	38.5	0.029±0.011	0.934
CA-03 H 1:1	78.4	0.120±0.032	0.974
CA-03 H 2:1	76.6	0.106±0.068	0.887
CA-03 L 1:1	32.7	0.033±0.007	0.976
CA-03 L 2:1	41.1	0.037±0.011	0.951

Statistical analyses: rate and extent of reduction

1. **Group 1: HFO**

The rates of HFO reduction by *S. putrefaciens* CN32 within experiments conducted with 3.9mM of phosphate and molybdate:sulfate concentrations of 0:1, 1:1, or 2:1 were determined to be, respectively, 0.065±0.011, 0.080±0.010, or 0.087±0.016 day^{-1} (Table 4). Interestingly, the rates of reduction of HFO by *S. putrefaciens* CN32 in the presence of 10μM of phosphate and molybdate:sulfate concentrations of 0:1, 1:1, or 2:1 approached those determined in the presence of 3.9mM of phosphate, in which case the rates were determined to be 0.054±0.004, 0.073±0.005, or 0.086±0.005 day^{-1}, respectively (Table 4). Two factor ANOVA revealed that the concentration of phosphate had no significant effect on the rate of reduction of HFO ($p>0.05$, Table S6), whereas molybdate had a significant effect ($p<0.05$, Table S6), and the effects of molybdate did not depend on the concentration of phosphate given that there was no significant interaction between phosphate and molybdate ($p>0.05$, Table S6). In contrast to the rates of reduction of HFO, two factor ANOVA revealed that the concentration of phosphate significantly affected the extent of HFO reduction (within 14 days of reduction) ($p<0.05$, Tables 4 and S7), whereas the concentration of molybdate had no significant effect ($p>0.05$, Table S7), and, interestingly, the effects of phosphate seem to be significantly influenced by the concentration of molybdate but may be fortuitous because of the strong effects of phosphate ($p<0.05$, Table S7). A comparison between the rates of reduction determined in the presence of 3.9mM of phosphate and those determined in the presence of 10uM phosphate at corresponding molybdate:sulfate concentrations revealed no significant difference (Tukey's Test $p>0.05$). In contrast, the extent of reduction of HFO determined in the presence of 3.9mM of phosphate were significantly higher than those determined in the presence of 10uM phosphate at corresponding molybdate:sulfate concentrations (Tukey's Test $p<0.05$, Table S8). Post-hoc analyses revealed that the rate and extent of reduction of HFO in the presence of 3.9mM of phosphate did not significantly vary as a function of molybdate concentration ($p>0.05$). In contrast, in the presence of 10μM of phosphate, paired comparisons revealed a significant difference in the rate and extent of reduction between those determined in the presence of 2:1 molybdate:sulfate and those determined in the absence of molybdate (0:1 molybdate:sulfate) ($p<0.05$, Tables S9 and S10), whereas no significant difference was found between other paired combinations ($p>0.05$, Tables S9 and S10). Given the larger variability around the rates of reduction determined in the presence of 3.9mM of phosphate and the smaller variability around the rates of reduction determined in the presence of 10μM of phosphate (Table 4), single factor ANOVA analyses were conducted on data grouped according to the phosphate concentration to determine the effects of the concentration of molybdate. Single factor ANOVA analyses revealed no significant effect of the concentration of molybdate on the rate of reduction of HFO in the presence of 3.9mM phosphate ($p>0.05$). In contrast, the concentration of molybdate was found to have a significant effect on the rate of reduction of HFO within experiments conducted with 10μM of phosphate ($p<0.05$, Table S11). Post-hoc analysis revealed that the rates of reduction were significantly different from each other, indicating that the rate of reduction increased as the concentration of molybdate increased ($p<0.05$, Tables 4 and S12). Single factor ANOVA revealed that the concentration of molybdate had no significant effect on the extent of reduction of HFO in the presence of 3.9mM phosphate ($p>0.05$). In contrast, the concentration of molybdate had a significant effect on the extent of reduction of HFO in the presence of 10μM of phosphate ($p<0.05$, Table S13). In contrast to the rates of reduction, the influence of molybdate on the extent of HFO reduction in the presence of 10μM phosphate had a saturating effect, in which case post-hoc analysis revealed no significant difference in the maximum amount of HFO reduced

between experiments conducted with molybdate:sulfate concentration of 1:1 or 2:1 ($p>0.05$, Table S14). However, a significant difference was observed in the maximum amount of HFO reduced between experiments conducted with molybdate:sulfate concentration of 1:1 or 2:1, and those to which no molybdate was added ($p<0.05$, Table S14).

Table S6: Summary of two factor ANOVA determining the effects of the concentration of phosphate and molybdate on the rate of HFO reduction by *S. putrefaciens* CN32.

Source of Variation	*SS*	*df*	*MS*	*F*	*P-value*	*F crit*
Phosphate	0.000166	1	0.000166	1.649308	0.223294	4.747225
Molybdate	0.00225	2	0.001125	11.1944	0.001805	3.885294
Interaction	8.23E-05	2	4.12E-05	0.40964	0.672831	3.885294
Within	0.001206	12	0.0001			
Total	0.003703	17				

Table S7: Summary of two factor ANOVA determining the effects of the concentration of phosphate and molybdate on the extent of HFO reduction.

Source of Variation	*SS*	*df*	*MS*	*F*	*P-value*	*F crit*
Phosphate	0.442677	1	0.442677	337.7472	3.74E-10	4.747225
Molybdate	0.003331	2	0.001666	1.270845	0.31579	3.885294
Interaction	0.011825	2	0.005913	4.511205	0.034593	3.885294
Within	0.015728	12	0.001311			
Total	0.473562	17				

Table S8: Pairwise comparisons between the extents of HFO reduction conducted in the presence of 3.9mM or 10µM of phosphate at corresponding molybdate:sulfate concentrations (0:1, 1:1, and 2:1). Comparisons were conducted by Tukey's post-hoc test after carrying out two factor ANOVA (Table S7).

Comparison	*Diff of Means*	*p*	*q*	*P*	*P<0.05*
3.9mM vs. 10µM at 0:1	0.384	2	18.359	<0.001	Yes
3.9mM vs. 10µM at 1:1	0.295	2	14.096	<0.001	Yes
3.9mM vs. 10µM at 2:1	0.263	2	12.561	<0.001	Yes

Table S9: Paired comparisons of the rates of reduction of HFO determined in the presence of 10µM of phosphate and 0:1, 1:1, or 2:1 molybdate:sulfate concentrations. Comparisons were conducted by Tukey's post-hoc test after carrying out two factor ANOVA (Table S6).

Comparison	*Diff of Means*	*p*	*q*	*P*	*P<0.05*
2:1 vs. 0:1	0.0324	3	5.603	0.005	Yes
2:1 vs. 1:1	0.0138	3	2.382	0.251	No
1:1 vs. 0:1	0.0186	3	3.221	0.098	No

Table S10: Paired comparisons of the extents of reduction of HFO determined in the presence of 10μM of phosphate and 0:1, 1:1, or 2:1 molybdate:sulfate concentrations. Comparisons were conducted by Tukey's post-hoc test after carrying out two factor ANOVA (Table S7).

Comparison	*Diff of Means*	*p*	*q*	*P*	*P<0.05*
2:1 vs. 0:1	0.0937	3	4.481	0.021	Yes
2:1 vs. 1:1	0.029	3	1.387	0.602	No
1:1 vs. 0:1	0.0647	3	3.094	0.114	No

Table S11: Summary of single factor ANOVA determining the effects of increasing concentration of molybdate on the rate of HFO reduction in the presence of 10μM of phosphate.

Source of Variation	*SS*	*df*	*MS*	*F*	*P-value*	*F crit*
Between Groups	0.001589	2	0.000794	169.5182	5.26E-06	5.143253
Within Groups	2.81E-05	6	4.69E-06			
Total	0.001617	8				

Table S12: Pairwise multiple comparison for the rates of HFO reduction conducted with 10μM of phosphate and various molybdate:sulfate concentrations (0:1, 1:1, and 2:1). Comparisons were conducted by Tukey's post-hoc test after carrying out single factor ANOVA (Table S11).

Comparison	*Diff of Means*	*P*	*q*	*p*	*p<0.05*
2:1 vs. 0:1	0.0324	3	25.943	<0.001	Yes
2:1 vs. 1:1	0.0138	3	11.028	<0.001	Yes
1:1 vs. 0:1	0.0186	3	14.915	<0.001	Yes

Table S13: Summary of single factor ANOVA determining the effects of increasing concentration of molybdate on the extent of HFO reduction in the presence of 10μM of phosphate.

Source of Variation	*SS*	*df*	*MS*	*F*	*P-value*	*F crit*
Between Groups	0.013793	2	0.006896	23.94183	0.001381	5.143253
Within Groups	0.001728	6	0.000288			
Total	0.015521	8				

Table S14: Pairwise multiple comparison for the extents of HFO reduction conducted with 10μM of phosphate and various molybdate:sulfate concentrations (0:1, 1:1, and 2:1). Comparisons were conducted by Tukey's post-hoc test after carrying out single factor ANOVA (Table S13).

Comparison	*Diff of Means*	*P*	*q*	*p*	*p<0.05*
2:1 vs. 0:1	0.0937	3	9.558	0.001	Yes
2:1 vs. 1:1	0.0290	3	2.959	0.172	No
1:1 vs. 0:1	0.0647	3	6.599	0.008	Yes

2. Group 2: Non-irradiated BIOS

The rates of reduction of non-irradiated BIOS from site CA-04 by *S. putrefaciens* CN32 within batch experiments conducted with molybdate:sulfate concentrations of 1:1 or 2:1 were determined to be, in the presence of 3.9mM of phosphate, 0.066±0.004 or 0.066±0.012 day^{-1}, respectively, whereas in the presence of 10μM of phosphate, the rates were determined to be 0.066±0.006 or 0.067±0.006 day^{-1}, respectively (Table 4). The rates of reduction of non-irradiated BIOS from site CA-03 by *S. putrefaciens* CN32 within batch experiments conducted with

molybdate:sulfate concentrations of 1:1 or 2:1 approached those determined for non-irradiated BIOS from site CA-04 in the presence of 3.9mM of phosphate, which were determined to be 0.070±0.005 or 0.061±0.010 day^{-1}, respectively (Table 4). In contrast, the rates of reduction of non-irradiated BIOS from site CA-03 by *S. putrefaciens* CN32 within batch experiments conducted with 10μM of phosphate and molybdate:sulfate concentrations of 1:1 or 2:1 were much lower, in which case the rates were determined to be 0.047±0.005 or 0.046±0.006 day^{-1}, respectively (Table 4). Two factor ANOVA revealed that the concentration of either phosphate or molybdate had no significant effect on the rate of reduction of non-irradiated BIOS from site CA-04 ($p>0.05$), and no significant interaction was found between phosphate and molybdate ($p>0.05$). In contrast, two factor ANOVA revealed that the concentration of phosphate had a significant effect on the extent of reduction of non-irradiated BIOS from site CA-04 ($p<0.05$, Table S15), and the concentration of molybdate had a significant effect on the extent of reduction but the data does not show a notable trend suggesting that the observed significance may be fortuitous because of the strong effects of phosphate ($p<0.05$, Tables 4 and S15), finally, the effects of phosphate were not significantly influenced by the concentration of molybdate given that no significant interaction was observed ($p>0.05$, Table S15). A comparison between the extent of reduction of non-irradiated BIOS from site CA-04 determined in the presence of 3.9mM of phosphate and those determined in the presence of 10uM phosphate at corresponding molybdate:sulfate concentrations revealed a significant difference (Tukey's Test $p<0.05$, Table S16). No significant difference was observed between the extent of reduction of non-irradiated BIOS from site CA-04 determined in the presence of 3.9mM of phosphate and the different molybdate treatments (Tukey's Test $p>0.05$). In contrast, a significant difference was observed between the extent of reduction of non-irradiated BIOS from site CA-04 in the presence of 10μM of phosphate and the different molybdate treatments, however in contrast to HFO, the extent of reduction did not increase with increasing molybdate concentration, rather an opposite trend was observed (Table 4). In contrast to non-irradiated BIOS from site CA-04, the concentration of phosphate was found to have a significant effect on the rate and extent of reduction of non-irradiated BIOS from site CA-03 (two factor ANOVA $p<0.05$, Tables S17 and S18), whereas the concentration of molybdate had a significant effect on the rate (two factor ANOVA $p<0.05$, Table S17) but not the extent (two factor ANOVA $p>0.05$, Table S18), and the effects of phosphate did not depend on the concentration of molybdate given that no significant interaction was observed (two factor ANOVA $p>0.05$, Tables S17 and S18). Although the concentration of molybdate appeared to significantly affect the rate of reduction, this could be attributed to chance given the strong effect of phosphate (Tables 4, S17 and S18). Post-hoc analyses revealed a significant difference in the extent and rate of reduction of non-irradiated BIOS from site CA-03 between those determined in the presence of 3.9mM phosphate and those determined in the presence of 10μM phosphate at corresponding molybdate:sulfate concentrations ($p<0.05$, Tables S19 and S20). For experiments conducted with 3.9mM of phosphate and non-irradiated BIOS from site CA-03, post-hoc analyses also revealed a significant difference in the rates but not extent of reduction between the different molybdate treatments (Tables S21 and S22). In contrast, a significant difference was observed in the extent but not rate of reduction between the different molybdate treatments in the presence of 10μM of phosphate (Table S21 and S22). However, no specific trend was observed as a function of molybdate concentration (Table 4).

Table S15: Summary of two factor ANOVA determining the effects of the concentration of phosphate and molybdate on the extent of reduction of non-irradiated BIOS from site CA-04.

Source of Variation	*SS*	*df*	*MS*	*F*	*P-value*	*F crit*
Phosphate	0.059241	1	0.059241	56.33663	6.89E-05	5.317655
Molybdate	0.006482	1	0.006482	6.164383	0.037945	5.317655
Interaction	0.001535	1	0.001535	1.459857	0.261453	5.317655
Within	0.008412	8	0.001052			
Total	0.07567	11				

Table S16: Pairwise comparisons between the extents of reduction of non-irradiated BIOS from site CA-04 conducted in the presence of 3.9mM or 10μM of phosphate at corresponding molybdate:sulfate concentrations (1:1 and 2:1). Comparisons were conducted by Tukey's post-hoc test after carrying out two factor ANOVA (Table S15).

Comparison	*Diff of Means*	*p*	*q*	*P*	*P<0.05*
3.9mM vs. 10μM at 1:1	0.118	2	6.298	0.002	Yes
3.9mM vs. 10μM at 2:1	0.163	2	8.714	<0.001	Yes

Table S17: Summary of two factor ANOVA determining the effects of the concentration of phosphate and molybdate on the rate of reduction of non-irradiated BIOS collected from site CA-03.

Source of Variation	*SS*	*df*	*MS*	*F*	*P-value*	*F crit*
Phosphate	0.001124	1	0.001124	98.54184	8.97E-06	5.317655
Molybdate	7.36E-05	1	7.36E-05	6.453183	0.034694	5.317655
Interaction	5.92E-05	1	5.92E-05	5.192354	0.052179	5.317655
Within	9.12E-05	8	1.14E-05			
Total	0.001348	11				

Table S18: Summary of two factor ANOVA determining the effects of the concentration of phosphate and molybdate on the extent of reduction of non-irradiated BIOS collected from site CA-03.

Source of Variation	*SS*	*df*	*MS*	*F*	*P-value*	*F crit*
Phosphate	0.109122	1	0.109122	81.85091	1.78E-05	5.317655
Molybdate	0.0047	1	0.0047	3.52547	0.09726	5.317655
Interaction	0.002776	1	0.002776	2.082305	0.187002	5.317655
Within	0.010665	8	0.001333			
Total	0.127263	11				

Table S19: Pairwise comparisons between the rates of reduction of non-irradiated BIOS from site CA-03 conducted in the presence of 3.9mM or 10μM of phosphate at corresponding molybdate:sulfate concentrations (1:1 and 2:1). Comparisons were conducted by Tukey's post-hoc test after carrying out two factor ANOVA (Table S17).

Comparison	*Diff of Means*	*p*	*q*	*P*	*P<0.05*
3.9mM vs. 10μM at 1:1	0.0238	2	12.205	<0.001	Yes
3.9mM vs. 10μM at 2:1	0.0149	2	7.648	<0.001	Yes

Table S20: Pairwise comparisons between the extents of reduction of non-irradiated BIOS from site CA-03 conducted in the presence of 3.9mM or 10μM of phosphate at corresponding molybdate:sulfate concentrations (1:1 and 2:1). Comparisons were conducted by Tukey's post-hoc test after carrying out two factor ANOVA (Table S18).

Comparison	*Diff of Means*	*p*	*q*	*P*	*P<0.05*
3.9mM vs. 10μM at 1:1	0.221	2	10.490	<0.001	Yes
3.9mM vs. 10μM at 2:1	0.160	2	7.604	<0.001	Yes

Table S21: Pairwise comparisons between the rates of reduction of non-irradiated BIOS from site CA-03 conducted in the presence of 3.9mM or 10μM of phosphate at corresponding molybdate:sulfate concentrations (1:1 and 2:1). Comparisons were conducted by Tukey's post-hoc test after carrying out two factor ANOVA (Table S17).

Comparison	*Diff of Means*	*p*	*q*	*P*	*P<0.05*
1:1 vs. 2:1 at 3.9mM	0.00940	2	4.819	0.009	Yes
1:1 vs. 2:1 at 10μM	0.000510	2	0.262	0.858	No

Table S22: Pairwise comparisons between the extents of reduction of non-irradiated BIOS from site CA-03 conducted in the presence of 3.9mM or 10μM of phosphate at corresponding molybdate:sulfate concentrations (1:1 and 2:1). Comparisons were conducted by Tukey's post-hoc test after carrying out two factor ANOVA (Table S18).

Comparison	*Diff of Means*	*p*	*q*	*P*	*P<0.05*
1:1 vs. 2:1 at 3.9mM	0.00916	2	0.435	0.767	No
1:1 vs. 2:1 at 10μM	0.0700	2	3.321	0.047	Yes

3. Group 3: γ-irradiated BIOS

The rates of reduction of γ-irradiated BIOS from sites CA-04 or CA-03 by *S. putrefaciens* CN32 in the presence of 3.9mM of phosphate approached those determined for non-irradiated BIOS, in which case the rates were determined to be 0.068±0.006 or 0.061±0.015 day^{-1}, respectively (Table 4). In contrast, in the presence of 10μM of phosphate, the rates of reduction of γ-irradiated BIOS from sites CA-04 or CA-03 by *S. putrefaciens* CN32 were slow, in which the case the rates were determined to be 0.035±0.005 or 0.028±0.001 day^{-1}, respectively (Table 4). Two factor ANOVA revealed that the site to which BIOS originated from did not significantly influence the rates of reduction ($p>0.05$, Table S23), but the concentration of phosphate had a significant effect on the rates of reduction ($p<0.05$, Table S23), and the effects of phosphate did not depend on the site ($p>0.05$, Table S23). Post-hoc analyses showed that the rates of reduction of γ-irradiated BIOS did not significantly differ between CA-04 and CA-03 BIOS at corresponding phosphate concentrations (Tukey's Test $p>0.05$). In contrast, for γ-irradiated BIOS collected from a specific site, post-hoc analyses revealed a significant difference in the rates of reduction between the different phosphate treatments (Tukey's Test $p<0.05$, Table S24). In contrast to the rates of reduction, two factor ANOVA revealed that the extent of reduction significantly depended on the site to which γ-irradiated BIOS originated from ($p<0.05$, Table S25), and the concentration had a significant effect on the extent of reduction ($p<0.05$, Table S25), but no significant interaction was observed between the site and concentration of phosphate ($p>0.05$, Table S25). Therefore, for γ-irradiated BIOS from sites CA-04 and CA-03, the amount of Fe(III) reduced was significantly higher in the presence of 3.9mM phosphate when compared to the amount of Fe(III) reduced in

the presence of 10μM of phosphate (Tukey's Test $p<0.05$, Table S26). Post-hoc analyses also revealed that regardless of the phosphate concentration, the amount of Fe(III) reduced was significantly higher for γ-irradiated BIOS from site CA-04 than the amount reduced for γ-irradiated BIOS from site CA-03 (Tukey's Test $p<0.05$, Table 27).

Table S23: Summary of two factor ANOVA determining the effects of the site to which BIOS originated from and the concentration of phosphate on the rate of reduction of γ-irradiated BIOS from sites CA-04 and CA-03.

Source of Variation	*SS*	*df*	*MS*	*F*	*P-value*	*F crit*
Site	9.11E-05	1	9.11E-05	1.392603	0.303352	7.708647
Phosphate	0.002211	1	0.002211	33.79117	0.004359	7.708647
Interaction	4.5E-08	1	4.5E-08	0.000688	0.980335	7.708647
Within	0.000262	4	6.54E-05			
Total	0.002564	7				

Table S24: Pairwise comparisons of the rates of reduction of γ-irradiated BIOS from sites CA-04 or CA-03 between the different phosphate treatments (3.9mM or 10μM). Comparisons were conducted by Tukey's post-hoc test after carrying out two factor ANOVA (Table S23).

Comparison	*Diff of Means*	*p*	*q*	*P*	*P<0.05*
3.9mM vs. 10μM for CA-04	0.0334	2	5.844	0.015	Yes
3.9mM vs. 10μM for CA-03	0.0331	2	5.791	0.015	Yes

Table S25: Summary of two factor ANOVA determining the effects of the site to which BIOS originated from and the concentration of phosphate on the extent of reduction of γ-irradiated BIOS from sites CA-04 and CA-03.

Source of Variation	*SS*	*df*	*MS*	*F*	*P-value*	*F crit*
Site	0.009863	1	0.009863	66.04516	0.001247	7.708647
Phosphate	0.192479	1	0.192479	1288.876	3.59E-06	7.708647
Interaction	0.000339	1	0.000339	2.272024	0.206208	7.708647
Within	0.000597	4	0.000149			
Total	0.203270	7				

Table S26: Pairwise comparisons of the extent of reduction of γ-irradiated BIOS from sites CA-04 or CA-03 between the different phosphate treatments (3.9mM or 10μM). Comparisons were conducted by Tukey's post-hoc test after carrying out two factor ANOVA (Table S25).

Comparison	*Diff of Means*	*p*	*q*	*P*	*P<0.05*
3.9mM vs. 10μM for CA-04	0.297	2	34.486	<0.001	Yes
3.9mM vs. 10μM for CA-03	0.323	2	37.512	<0.001	Yes

Table S27: Pairwise comparisons in the extent of reduction of γ-irradiated BIOS from sites CA-04 and CA-03 at different phosphate treatments (3.9mM or 10μM). Comparisons were conducted by Tukey's post-hoc test after carrying out two factor ANOVA (Table S25).

Comparison	*Diff of Means*	*p*	*q*	*P*	*P<0.05*
CA-04 vs. CA-03 at 3.9mM	0.0572	2	6.635	0.010	Yes
CA-04 vs. CA-03 at 10μM	0.0833	2	9.662	0.003	Yes

4. All groups

In order to determine whether or not the type of the iron oxide had a significant effect on the rate and extent of reduction, two factor ANOVA was conducted on data grouped according to the iron oxide type and site (HFO vs. CA-04 vs. CA-04) which were also grouped according to the concentration of phosphate and molybdate, the rates and extents of reduction for γ-irradiated BIOS were included in the analyses as experiments conducted with non-irradiated BIOS but without the addition of molybdate (i.e. 0:1 molybdate:sulfate concentration). For experiments conducted with 3.9mM of phosphate, two factor ANOVA revealed that the type of the iron oxide had a significant effect on the rate of reduction ($p<0.05$, Table S28), but molybdate had no significant effect ($p>0.05$, Table S28), and there was no significant interaction between the type of the iron oxide and the concentration of molybdate ($p>0.05$, Table S28). Post-hoc analyses revealed a significant difference in the rates of reduction only between HFO and non-irradiated BIOS from site CA-03 at corresponding molybdate:sulfate concentrations (Tukey's Test $p<0.05$, Table S29).

Across the entire data, the rates of reduction did not significantly vary suggesting that the rates of reduction for γ-irradiated BIOS were not significantly different than those determined for non-irradiated BIOS and in turn, the rates of reduction of non- and γ-irradiated BIOS did not significantly differ from the rates of reduction for HFO at corresponding molybdate:sulfate concentrations (Tukey's Test $p>0.05$, Table S29). For experiments conducted with 10μM of phosphate, two factor ANOVA revealed that the type of the iron oxide had a significant effect on the rate of reduction ($p<0.05$, Table S30), and the concentration of molybdate had a significant effect ($p<0.05$, Table S30), and there was a significant interaction between the type of the iron oxide and the concentration of molybdate ($p<0.05$, Table S30). Post-hoc analyses revealed that regardless of the molybdate concentration and in the presence of 10μM of phosphate, the rates of reduction of non-irradiated BIOS were significantly higher than those determined for γ-irradiated BIOS (Tukey's Test $p<0.05$, Table S31). Under the same conditions, no significant difference was found between the rates of reduction of γ-irradiated BIOS from sites CA-04 and CA-03 (Tukey's Test $p>0.05$, Table S31), whereas a significant difference was found between the rates of reduction of non-irradiated BIOS from sites CA-04 and CA-03 at corresponding molybdate:sulfate concentrations (Tukey's Test $p<0.05$, Table S31). A comparison of rates of reduction between HFO (at 0:1 molybdate:sulfate) and γ-irradiated BIOS determined in the presence of 10μM of phosphate revealed a significant difference, indicating that HFO was reduced at a faster rate (Tukey's Test $p<0.05$, Table S31). Also, the rates of reduction of HFO were significantly higher than those determined for non-irradiated BIOS from site CA-03 in the presence of 10μM of phosphate and at corresponding molybdate concentrations (Tukey's Test $p<0.05$, Table S31). In contrast, under the same conditions, no significant difference was observed between the rates of reduction of HFO and non-irradiated BIOS from site CA-04 in the presence of molybdate:sulfate concentration of 1:1 (Tukey's Test $p>0.05$, Table S31). However, the rate of reduction of HFO was significantly higher than that of non-irradiated BIOS from site CA-04 determined in the

presence of molybdate:sulfate concentration of 2:1 and 10μM of phosphate (Tukey's Test $p<0.05$, Table S31).

For experiments conducted with 3.9mM or 10μM of phosphate, two factor ANOVA revealed that the type of the iron oxide had a significant effect on the extent of reduction ($p<0.05$, Tables S32 and S33), and the concentration of molybdate had a significant effect ($p<0.05$, Tables S32 and S33), and there was a significant interaction between the type of the iron oxide and the concentration of molybdate ($p<0.05$, Tables S32 and S33). Post-hoc analyses revealed a significant difference between the maximum amount of Fe(III) reduced between non- and γ-irradiated BIOS, in which case a significantly higher amount of Fe(III) was reduced for non-irradiated BIOS when compared to γ-irradiated BIOS at corresponding phosphate concentrations (Tukey's Test $p<0.05$, Tables S34 and S35). A comparison of the maximum amount of Fe(III) reduced between non-irradiated BIOS from sites CA-04 and CA-03 at corresponding molybdate concentrations and in the presence of 3.9mM of phosphate revealed no significant difference (Tukey's Test $p>0.05$, Table S34). Under the same conditions, however, a significant difference was found when comparing the maximum amount of Fe(III) reduced between HFO and non-irradiated BIOS from site CA-04 or CA-03 at their corresponding molybdate concentrations suggesting that BIOS were reduced to a higher extent than HFO (Tukey's Test $p<0.05$, Table S34). It is important to note that HFO reduction conducted with molybdate was terminated after 14 days in comparison to non-irradiated BIOS where the experiments were terminated after 17-19 days, thus reduction of HFO could have potentially continued as observed for HFO conducted in the absence of molybdate but for 18 days (Table 4 and Figures 3-5). Therefore, the statistical analyses which determined that non-irradiated BIOS were reduced to a higher extent than HFO at corresponding molybdate:sulfate concentrations and 3.9mM of phosphate could be ignored. For experiments conducted with 3.9mM of phosphate, post-hoc analyses also showed a significant difference in the amount of Fe(III) reduced between HFO (in the absence of molybdate and after 14 days) and γ-irradiated BIOS from site CA-03 (Tukey's Test $p<0.05$, Table S34) but not from site CA-04 (Tukey's Test $p>0.05$, Table S34). Post-hoc analyses showed that a significantly higher amount of Fe(III) was reduced for non-irradiated BIOS from site CA-04 when compared to that of non-irradiated BIOS from site CA-03 in the presence of molybdate:sulfate concentration of 1:1 and 10μM of phosphate (Tukey's Test $p<0.05$, Table S35). Under similar conditions, however, no significant difference was found between the maximum amount of Fe(III) reduced for non-irradiated BIOS from sites CA-04 and CA-03 in the presence of molybdate:sulfate concentration of 2:1 (Tukey's Test $p>0.05$, Table S35). At corresponding molybdate:sulfate concentrations, a significantly higher amount of Fe(III) was reduced for non-irradiated BIOS when compared to HFO in the presence of 10μM of phosphate (Tukey's Test $p<0.05$, Table S35). Under similar conditions, however, no significant difference was found between the maximum amount of Fe(III) reduced for HFO (in the absence of molybdate) and γ-irradiated BIOS from site CA-04 (Tukey's Test $p>0.05$, Table S35), but a significantly higher amount of HFO was reduced when compared to that of γ-irradiated BIOS from site CA-03 (Tukey's Test $p<0.05$, Table S35).

Table S28: Summary of two factor ANOVA determining the effects of the iron oxide type and the concentration of molybdate on the rate of reduction of the different iron oxides in the presence of 3.9mM of phosphate.

Source of Variation	*SS*	*df*	*MS*	*F*	*P-value*	*F crit*
Oxide type	0.000763	2	0.000382	3.949	0.04	3.633723
Molybdate	0.000242	2	0.000121	1.253	0.312	3.633723
Interaction	0.000583	4	0.000146	1.508	0.247	3.006917
Within	0.00155	16	9.67E-05			
Total	0.00321	24				

Table S29: Pairwise comparisons between the rates of reduction of all the iron oxides utilized in this study in the presence of 3.9mM of phosphate and molybdate:sulfate concentrations of 0:1, 1:1, or 2:1. Comparisons were conducted by Tukey's post-hoc test after carrying out two factor ANOVA (Table S28).

Comparison	*Diff of Means*	*p*	*q*	*P*	*P<0.05*
0:1 vs. 1:1 within CA-04[a]	0.00186	3	0.294	0.977	No
0:1 vs. 2:1 within CA-04	0.00144	3	0.227	0.986	No
2:1 vs. 1:1 within CA-04	0.00042	3	0.0743	0.999	No
1:1 vs. 2:1 within CA-03	0.0094	3	1.655	0.487	No
1:1 vs. 0:1 within CA-03[a]	0.00939	3	1.479	0.56	No
0:1 vs. 2:1 within CA-03	7.43E-06	3	0.00117	1	No
CA-04 vs. CA-03 at 0:1	0.00688	3	0.989	0.767	No
CA-04 vs. HFO at 0:1	0.00305	3	0.481	0.939	No
HFO vs. CA-03 at 0:1	0.00383	3	0.603	0.905	No
HFO vs. CA-04 at 1:1	0.0129	3	2.265	0.274	No
HFO vs. CA-03 at 1:1	0.00848	3	1.494	0.554	No
CA-03 vs. CA-04 at 1:1	0.00437	3	0.771	0.851	No
HFO vs. CA-03 at 2:1	0.0258	3	4.547	0.014	Yes
HFO vs. CA-04 at 2:1	0.0204	3	3.588	0.054	No
CA-04 vs. CA-03 at 2:1	0.00544	3	0.959	0.779	No

[a]- data for 0:1 molybdate:sulfate corresponds to the rates of reduction of γ-irradiated BIOS from sites CA-04 and CA-03

Table S30: Summary of two factor ANOVA determining the effects of the iron oxide type and the concentration of molybdate on the rate of reduction of the different iron oxides in the presence of 10μM of phosphate.

Source of Variation	*SS*	*df*	*MS*	*F*	*P-value*	*F crit*
Oxide type	0.00389	2	0.00195	214.337	<0.001	3.633723
Molybdate	0.00326	2	0.00163	179.569	<0.001	3.633723
Interaction	0.000318	4	7.96E-05	8.766	<0.001	3.006917
Within	0.000145	16	9.08E-06			
Total	0.00737	24				

Table S31: Pairwise comparisons between the rates of reduction of all the iron oxides utilized in this study in the presence of 10μM of phosphate and molybdate:sulfate concentrations of 0:1, 1:1, or 2:1. Comparisons were conducted by Tukey's post-hoc test after carrying out two factor ANOVA (Table S30).

Comparison	*Diff of Means*	*p*	*q*	*P*	*P<0.05*
2:1 vs. 0:1 within CA-04[a]	0.0327	3	16.814	<0.001	Yes
2:1 vs. 1:1 within CA-04	0.00138	3	0.793	0.842	No
1:1 vs. 0:1 within CA-04	0.0313	3	16.105	<0.001	Yes
1:1 vs. 0:1 within CA-03[a]	0.0187	3	9.633	<0.001	Yes
1:1 vs. 2:1 within CA-03	0.00051	3	0.293	0.977	No
2:1 vs. 0:1 within CA-03	0.0182	3	9.371	<0.001	Yes
HFO vs. CA-03 at 0:1	0.0259	3	13.311	<0.001	Yes
HFO vs. CA-04 at 0:1	0.0193	3	9.929	<0.001	Yes
CA-04 vs. CA-03 at 0:1	0.00658	3	3.087	0.105	No
HFO vs. CA-03 at 1:1	0.0258	3	14.83	<0.001	Yes
HFO vs. CA-04 at 1:1	0.00663	3	3.814	0.05	No
CA-04 vs. CA-03 at 1:1	0.0192	3	11.016	<0.001	Yes
HFO vs. CA-03 at 2:1	0.0401	3	23.047	<0.001	Yes
HFO vs. CA-04 at 2:1	0.019	3	10.944	<0.001	Yes
CA-04 vs. CA-03 at 2:1	0.0211	3	12.103	<0.001	Yes

[a]- data for 0:1 molybdate:sulfate corresponds to the rates of reduction of γ-irradiated BIOS from sites CA-04 and CA-03

Table S32: Summary of two factor ANOVA determining the effects of the iron oxide type and the concentration of molybdate on the extent of reduction of the different iron oxides in the presence of 3.9mM of phosphate.

Source of Variation	*SS*	*df*	*MS*	*F*	*P-value*	*F crit*
Oxide type	0.0156	2	0.00782	4.445	0.029	3.633723
Molybdate	0.0741	2	0.0371	21.062	<0.001	3.633723
Interaction	0.0622	4	0.0155	8.833	<0.001	3.006917
Within	0.0282	16	0.00176			
Total	0.174	24				

Table S33: Summary of two factor ANOVA determining the effects of the iron oxide type and the concentration of molybdate on the extent of reduction of the different iron oxides in the presence of 10μM of phosphate.

Source of Variation	*SS*	*df*	*MS*	*F*	*P-value*	*F crit*
Oxide type	0.142	2	0.071	156.723	<0.001	3.633723
Molybdate	0.318	2	0.159	350.803	<0.001	3.633723
Interaction	0.0984	4	0.0246	54.348	<0.001	3.006917
Within	0.00724	16	0.000453			
Total	0.583	24				

Table S34: Pairwise comparisons between the extents of reduction of all the iron oxides utilized in this study in the presence of 3.9mM of phosphate and molybdate:sulfate concentrations of 0:1, 1:1, or 2:1. Comparisons were conducted by Tukey's post-hoc test after carrying out two factor ANOVA (Table S32).

Comparison	*Diff of Means*	*p*	*q*	*P*	*P<0.05*
1:1 vs. 0:1 within CA-04[a]	0.186	3	6.863	<0.001	Yes
1:1 vs. 2:1 within CA-04	0.0239	3	0.985	0.769	No
2:1 vs. 0:1 within CA-04	0.162	3	5.981	0.002	Yes
2:1 vs. 0:1 within CA-03[a]	0.225	3	8.306	<0.001	Yes
2:1 vs. 1:1 within CA-03	0.00916	3	0.378	0.962	No
1:1 vs. 0:1 within CA-03	0.216	3	7.968	<0.001	Yes
HFO vs. CA-03 at 0:1	0.13	3	4.783	0.01	Yes
HFO vs. CA-04 at 0:1	0.0723	3	2.671	0.174	No
CA-04 vs. CA-03 at 0:1	0.0572	3	1.928	0.383	No
CA-04 vs. HFO at 1:1	0.138	3	5.695	0.003	Yes
CA-04 vs. CA-03 at 1:1	0.0273	3	1.125	0.711	No
CA-03 vs. HFO at 1:1	0.111	3	4.569	0.014	Yes
CA-03 vs. HFO at 2:1	0.123	3	5.076	0.007	Yes
CA-03 vs. CA-04 at 2:1	0.00577	3	0.238	0.985	No
CA-04 vs. HFO at 2:1	0.117	3	4.837	0.009	Yes

[a]- data for 0:1 molybdate:sulfate corresponds to the rates of reduction of γ-irradiated BIOS from sites CA-04 and CA-03

Table S35: Pairwise comparisons between the extents of reduction of all the iron oxides utilized in this study in the presence of 10μM of phosphate and molybdate:sulfate concentrations of 0:1, 1:1, or 2:1. Comparisons were conducted by Tukey's post-hoc test after carrying out two factor ANOVA (Table S33).

Comparison	*Diff of Means*	*p*	*q*	*P*	*P<0.05*
1:1 vs. 0:1 within CA-04[a]	0.365	3	26.583	<0.001	Yes
1:1 vs. 2:1 within CA-04	0.0691	3	5.625	0.003	Yes
2:1 vs. 0:1 within CA-04	0.296	3	21.551	<0.001	Yes
2:1 vs. 0:1 within CA-03[a]	0.388	3	28.24	<0.001	Yes
2:1 vs. 1:1 within CA-03	0.07	3	5.698	0.003	Yes
1:1 vs. 0:1 within CA-03	0.318	3	23.144	<0.001	Yes
CA-04 vs. CA-03 at 0:1	0.0833	3	5.534	0.003	Yes
CA-04 vs. HFO at 0:1	0.0142	3	1.035	0.749	No
HFO vs. CA-03 at 0:1	0.069	3	5.027	0.007	Yes
CA-04 vs. HFO at 1:1	0.315	3	25.614	<0.001	Yes
CA-04 vs. CA-03 at 1:1	0.13	3	10.622	<0.001	Yes
CA-03 vs. HFO at 1:1	0.184	3	14.992	<0.001	Yes
CA-03 vs. HFO at 2:1	0.225	3	18.33	<0.001	Yes
CA-03 vs. CA-04 at 2:1	0.00861	3	0.701	0.874	No
CA-04 vs. HFO at 2:1	0.217	3	17.629	<0.001	Yes

[a]- data for 0:1 molybdate:sulfate corresponds to the rates of reduction of γ-irradiated BIOS from sites CA-04 and CA-03

Table S36: Proportions of iron-bearing phases in fresh BIOS collected from sites CA-04 and CA-03 determined by best fits of iron K-edge EXAFS spectra.

	Proportion of Iron-bearing Mineral (%)		
Sample	2-Line ferrihydrite	Lepidocrocite	Goethite
CA-04	100	-	-
CA-03	78	4	18

Source: Cotroneo and Fortin (2013)
Fitting error ±5% (Gault et al., 2011)

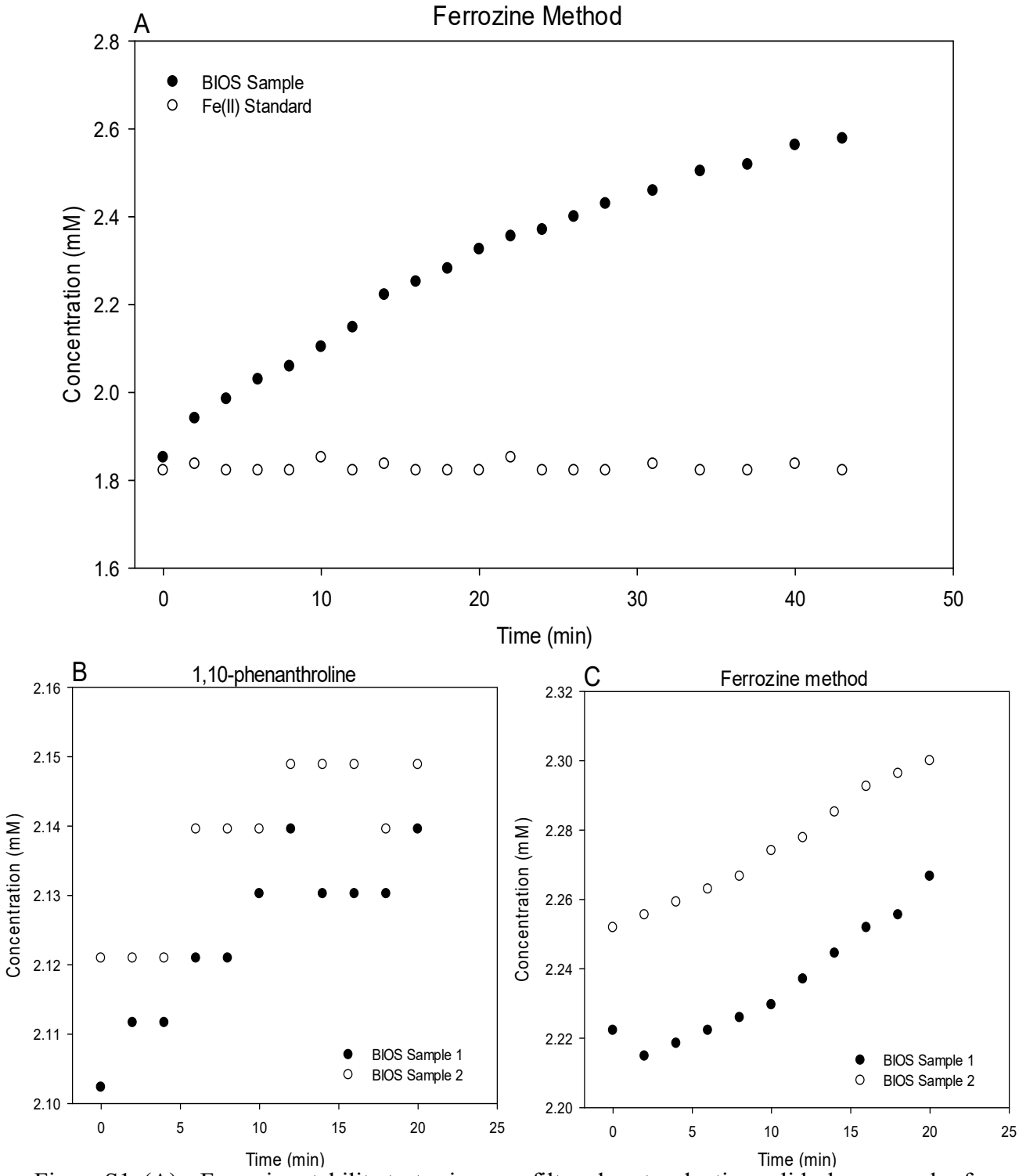

Figure S1: (A) – Ferrozine stability test using non-filtered post-reduction solid-phase samples from batch microcosms conducted with BIOS which were digested in 0.5M HCl for 24 hours compared to a Fe(II) standard (Iron(II) ethylenediammonium sulfate tetrahydrate). B and C – A comparison between 1,10-phenanthroline and ferrozine methods using non-filtered post-reduction solid-phase samples from batch experiments conducted with BIOS.

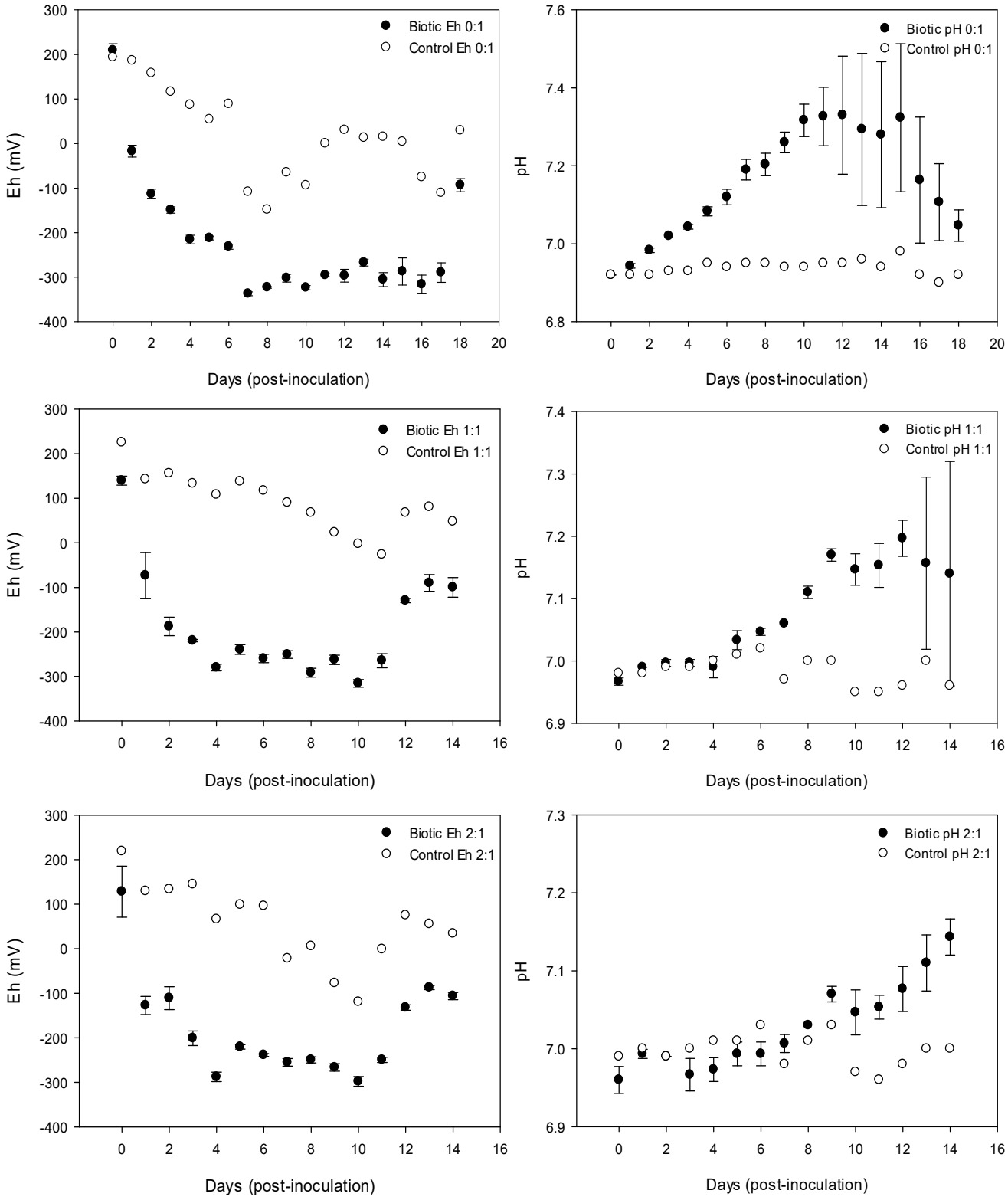

Figure S2: Changes in redox potential (Eh) (corrected to the standard hydrogen electrode; SHE) and pH during the reduction of HFO with molybdate:sulfate concentrations of 0:1, 1:1, and 2:1 and with 3.9mM of phosphate. "Biotic" refers to microcosms to which *S. putrefaciens* CN32 were added, whereas "Control" refers to control microcosms without bacteria. Data represents mean and standard deviation of 3 replicates for biotic experiments.

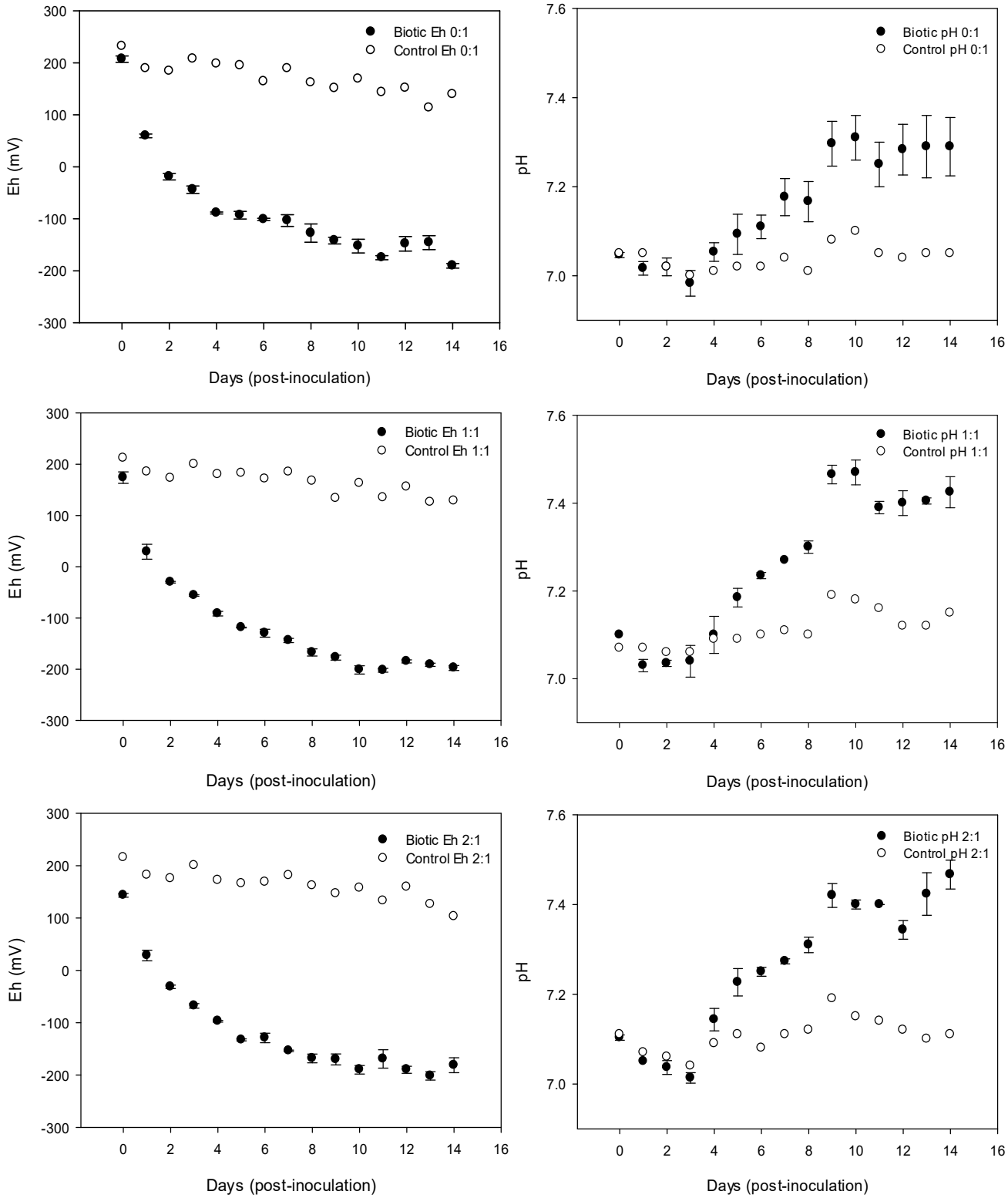

Figure S3: Changes in redox potential (Eh) (corrected to the standard hydrogen electrode; SHE) and pH during the reduction of HFO with molybdate:sulfate concentrations of 0:1, 1:1, and 2:1 and with 10µM of phosphate. "Biotic" refers to microcosms to which *S. putrefaciens* CN32 were added, whereas "Control" refers to control microcosms without bacteria. Data represents mean and standard deviation of 3 replicates for biotic experiments.

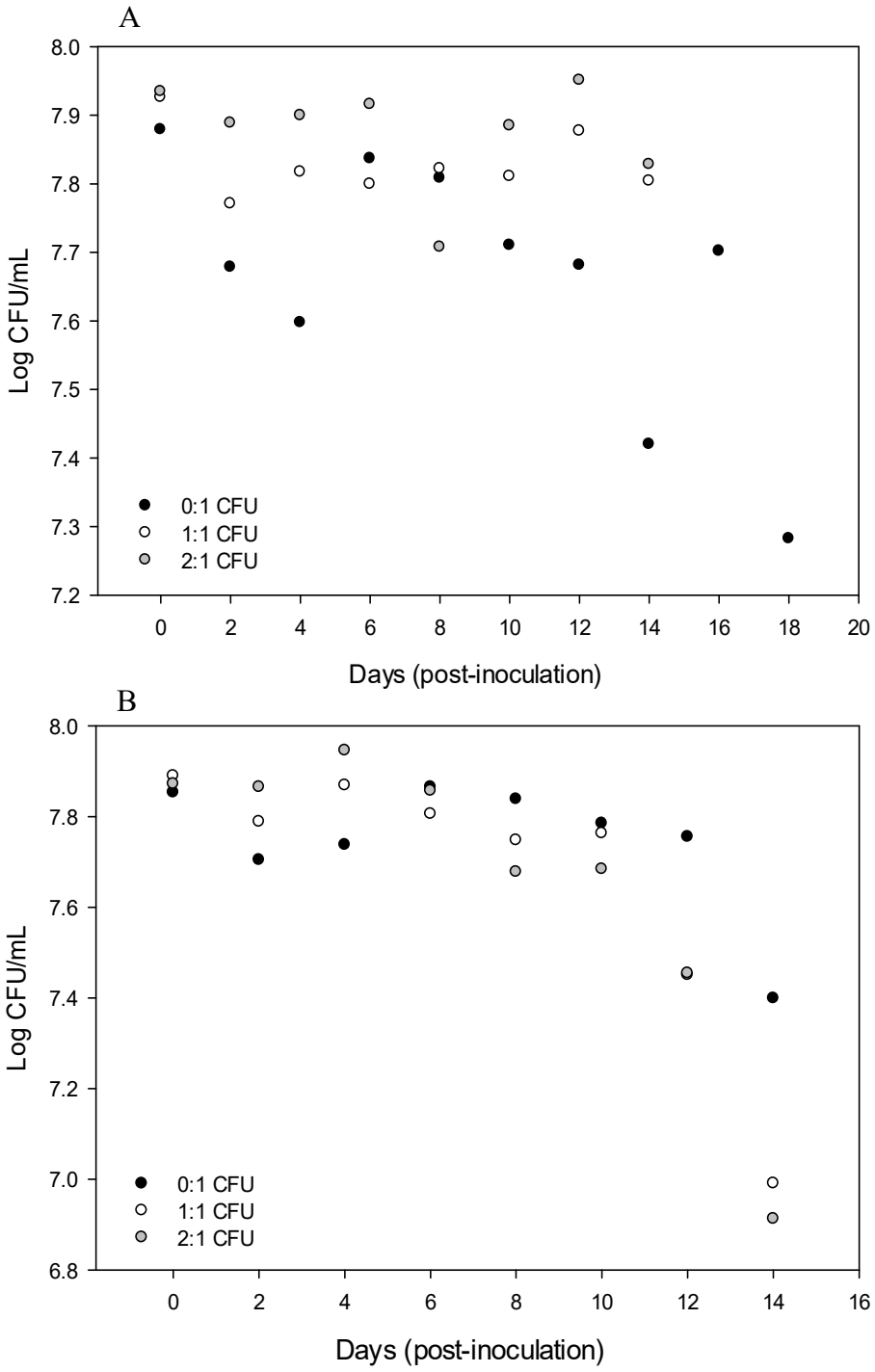

Figure S4: Changes in cell concentration of *S. putrefaciens* CN32 during the reduction of HFO with molybdate:sulfate concentrations of 0:1, 1:1, and 2:1 and with (A) 3.9mM and (B) 10µM of phosphate. No growth was observed in the control microcosms. Data represents mean of 3 replicates for each experiment.

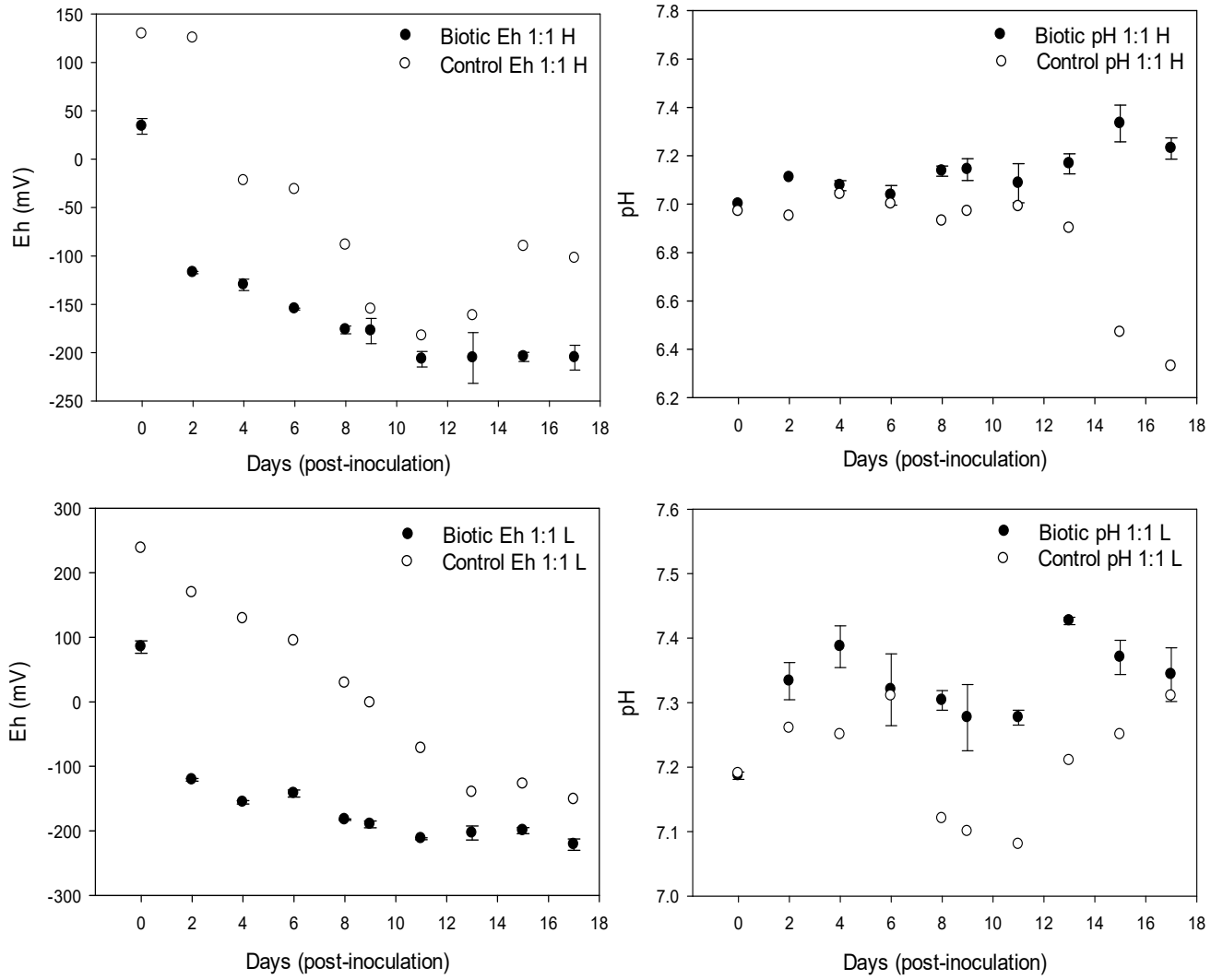

Figure S5: Changes in redox potential (Eh) (corrected to the standard hydrogen electrode; SHE) and pH during the reduction of non-irradiated BIOS collected from site CA-04 with molybdate:sulfate concentrations of 1:1, and 3.9mM (H) or 10µM (L) of phosphate. "Biotic" refers to microcosms to which *S. putrefaciens* CN32 were added, whereas "Control" refers to control microcosms to which no bacteria were added. Data represents mean and standard deviation of 3 replicates for biotic experiments.

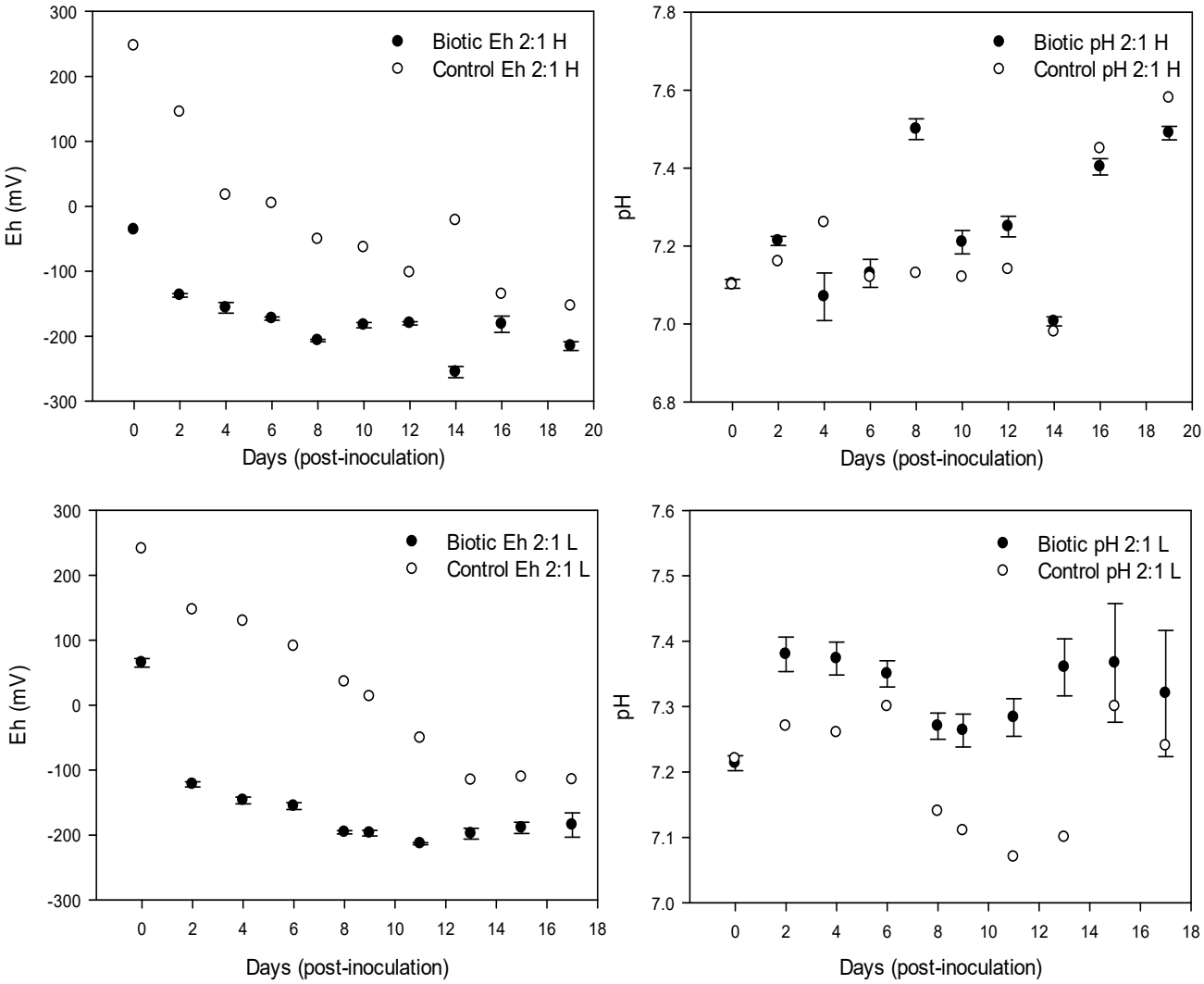

Figure S6: Changes in redox potential (Eh) (corrected to the standard hydrogen electrode; SHE) and pH during the reduction of non-irradiated BIOS collected from site CA-04 with molybdate:sulfate concentrations of 2:1, and 3.9mM (H) or 10µM (L) of phosphate. "Biotic" refers to microcosms to which *S. putrefaciens* CN32 were added, whereas "Control" refers to control microcosms to which no bacteria were added. Data represents mean and standard deviation of 3 replicates for biotic experiments.

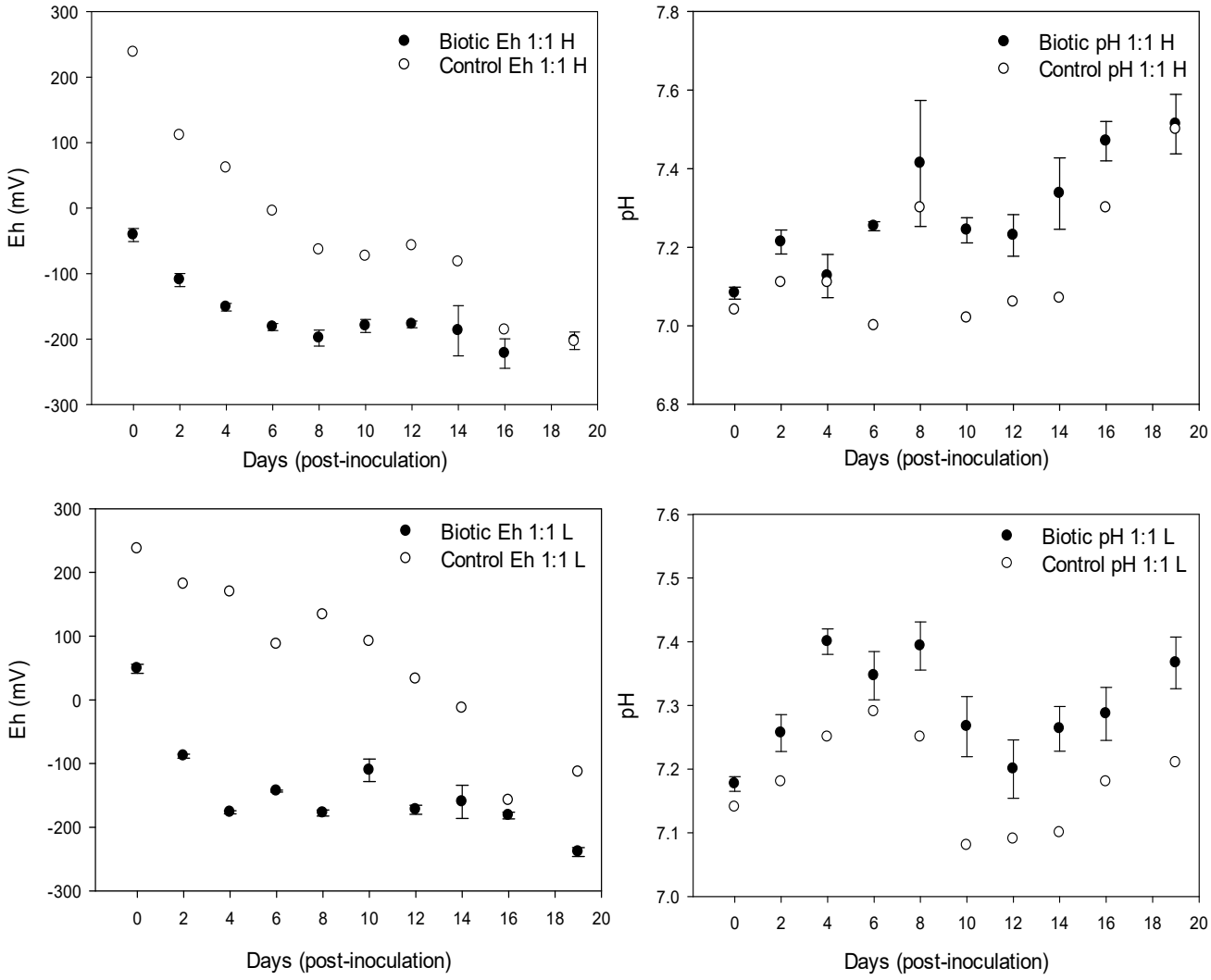

Figure S7: Changes in redox potential (Eh) (corrected to the standard hydrogen electrode; SHE) and pH during the reduction of non-irradiated BIOS collected from site CA-03 with molybdate:sulfate concentrations of 1:1, and 3.9mM (H) or 10µM (L) of phosphate. "Biotic" refers to microcosms to which *S. putrefaciens* CN32 were added, whereas "Control" refers to control microcosms to which no bacteria were added. Data represents mean and standard deviation of 3 replicates for biotic experiments.

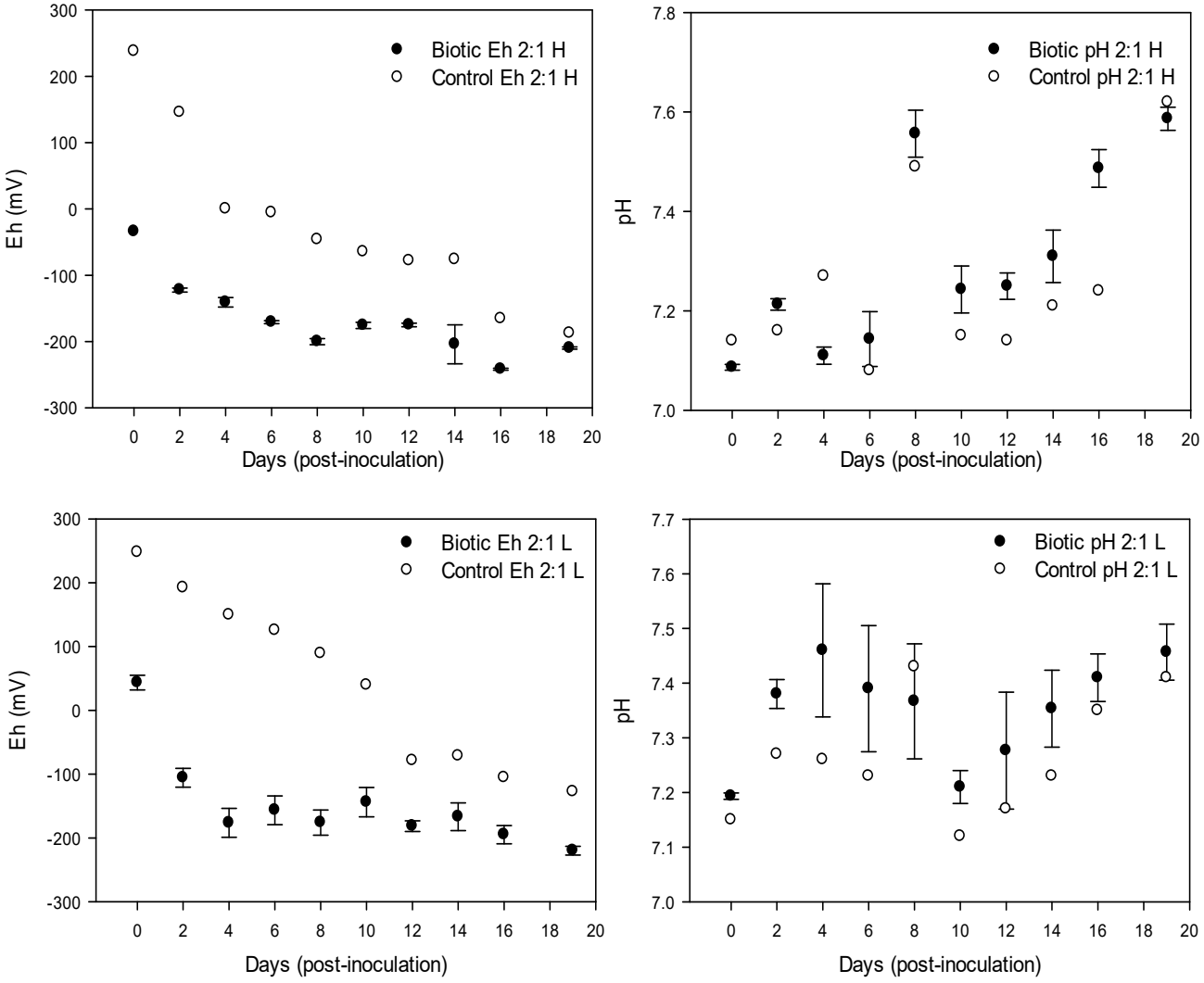

Figure S8: Changes in redox potential (Eh) (corrected to the standard hydrogen electrode; SHE) and pH during the reduction of non-irradiated BIOS collected from site CA-03 with molybdate:sulfate concentrations of 2:1, and 3.9mM (H) or 10µM (L) of phosphate. "Biotic" refers to microcosms to which *S. putrefaciens* CN32 were added, whereas "Control" refers to control microcosms to which no bacteria were added. Data represents mean and standard deviation of 3 replicates for biotic experiments.

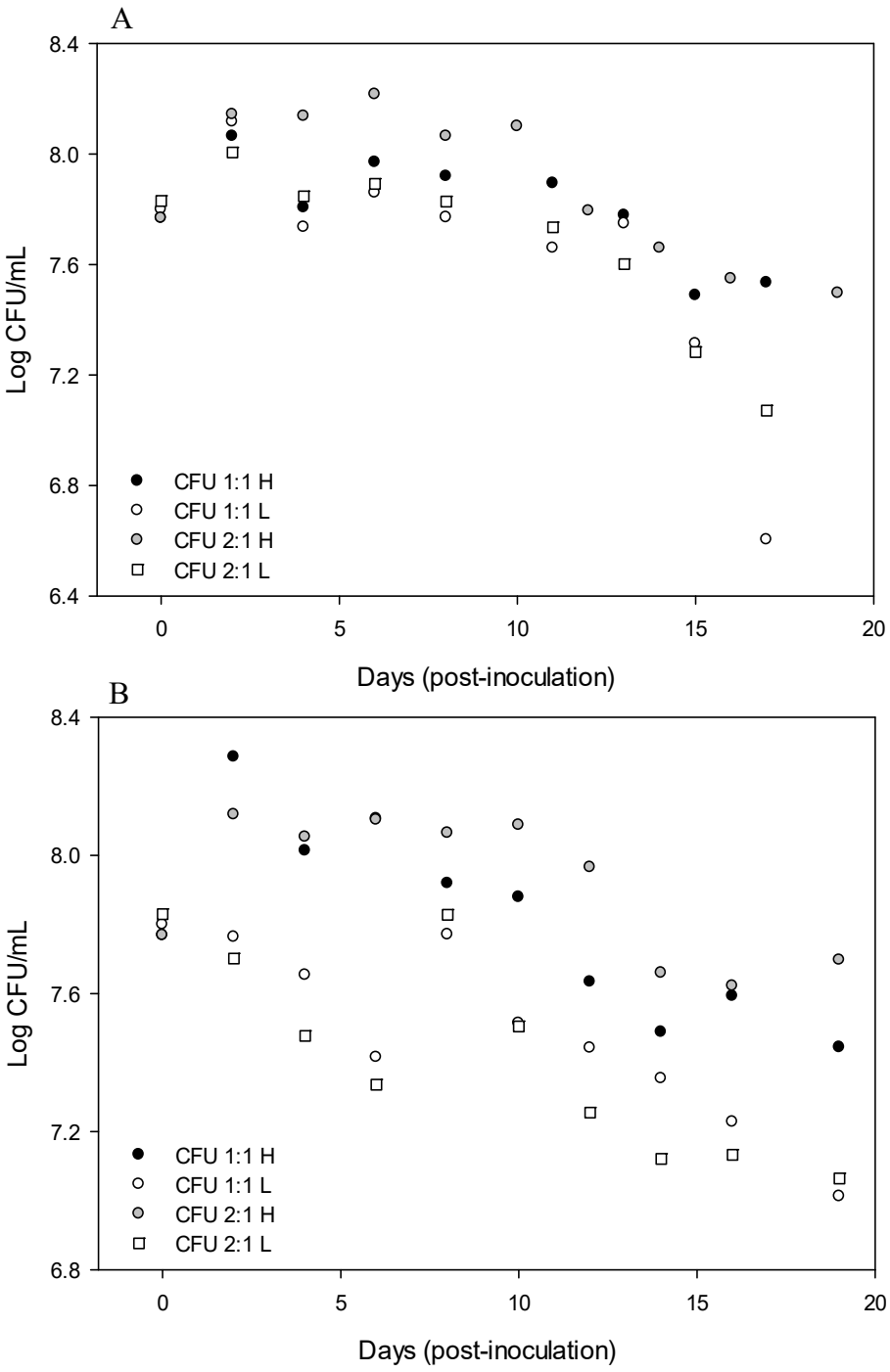

Figure S9: Changes in cell concentration of *S. putrefaciens* CN32 during the reduction of non-irradiated BIOS collected from sites (A) CA-04 and (B) CA-03 conducted with molybdate:sulfate concentrations of 1:1 or 2:1, and 3.9mM (H) or 10µM (L) of phosphate. No growth of *S. putrefaciens* CN32 was observed in the Control microcosms. Data represents mean of 3 replicates for each treatment.

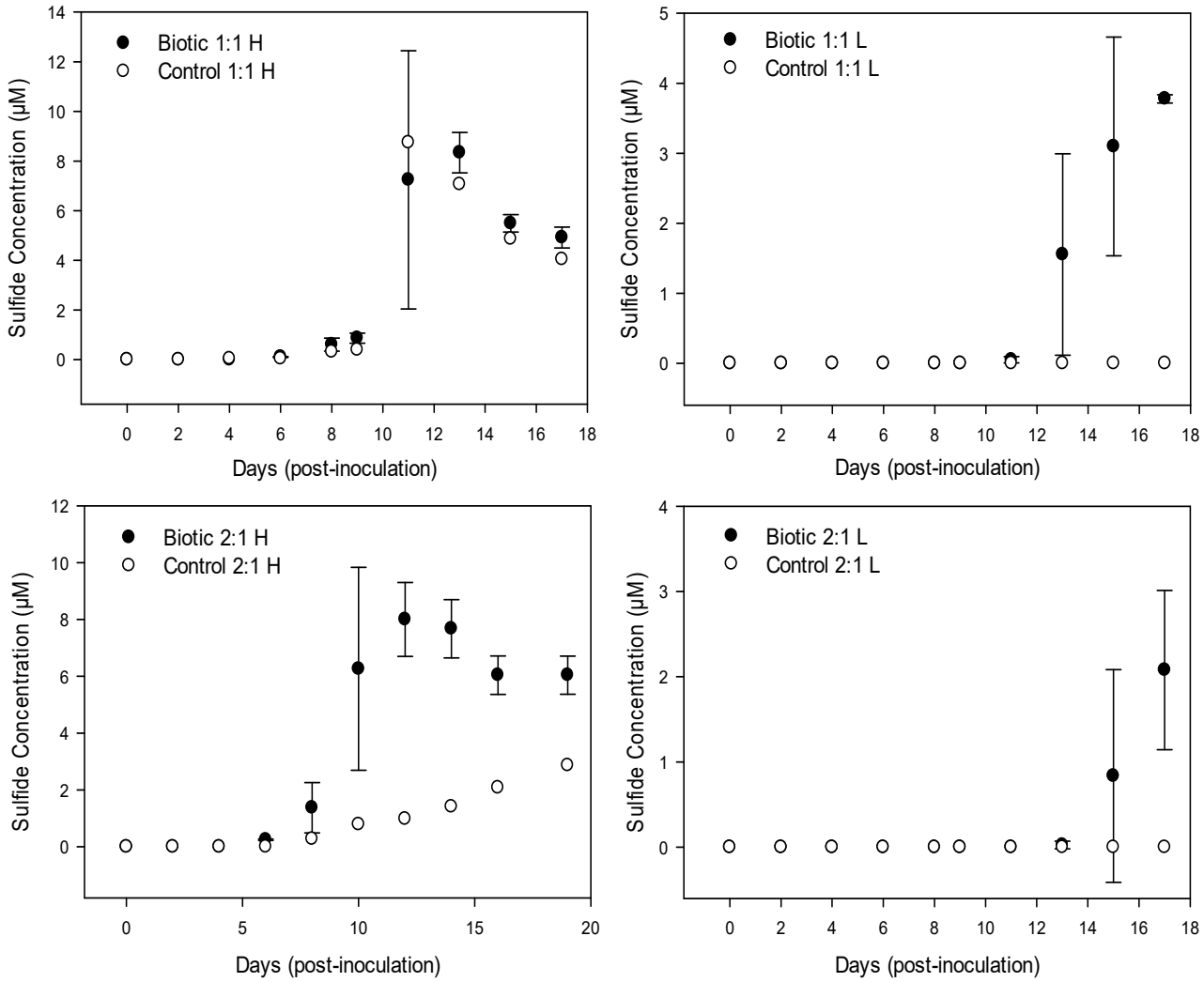

Figure S10: Changes in dissolved sulfide concentration (µM) during the reduction of non-irradiated BIOS collected from site CA-04 conducted with molybdate:sulfate concentrations of 1:1 or 2:1, and 3.9mM (H) or 10µM (L) of phosphate. "Biotic" refers to microcosms to which *S. putrefaciens* CN32 were added, whereas "Control" refers to control microcosms to which no bacteria were added. Data represents mean of 3 replicates for biotic experiments.

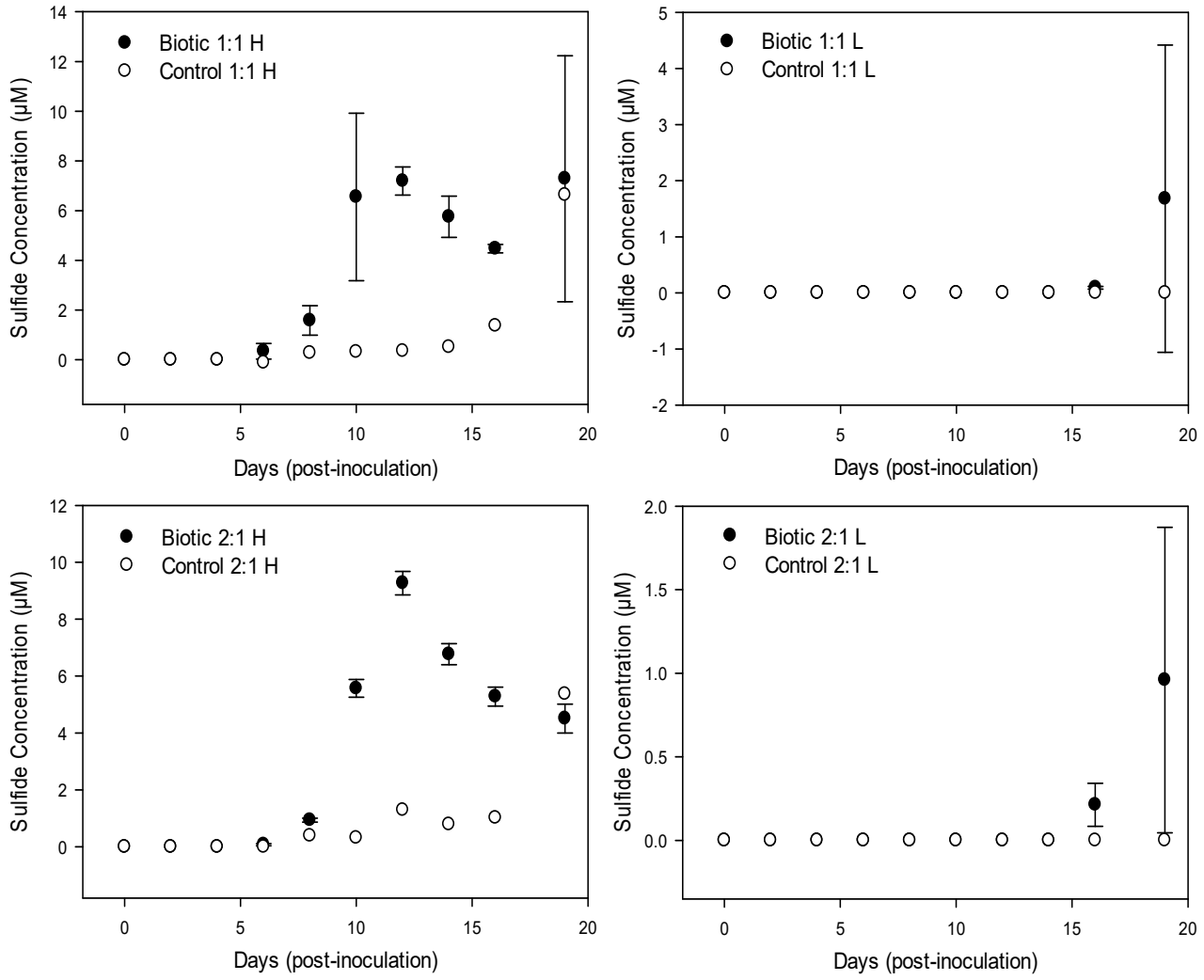

Figure S11: Changes in dissolved sulfide concentration (µM) during the reduction of non-irradiated BIOS collected from site CA-03 conducted with molybdate:sulfate concentrations of 1:1 or 2:1, and 3.9mM (H) or 10µM (L) of phosphate. "Biotic" refers to microcosms to which *S. putrefaciens* CN32 were added, whereas "Control" refers to control microcosms to which no bacteria were added. Data represents mean of 3 replicates for biotic experiments.

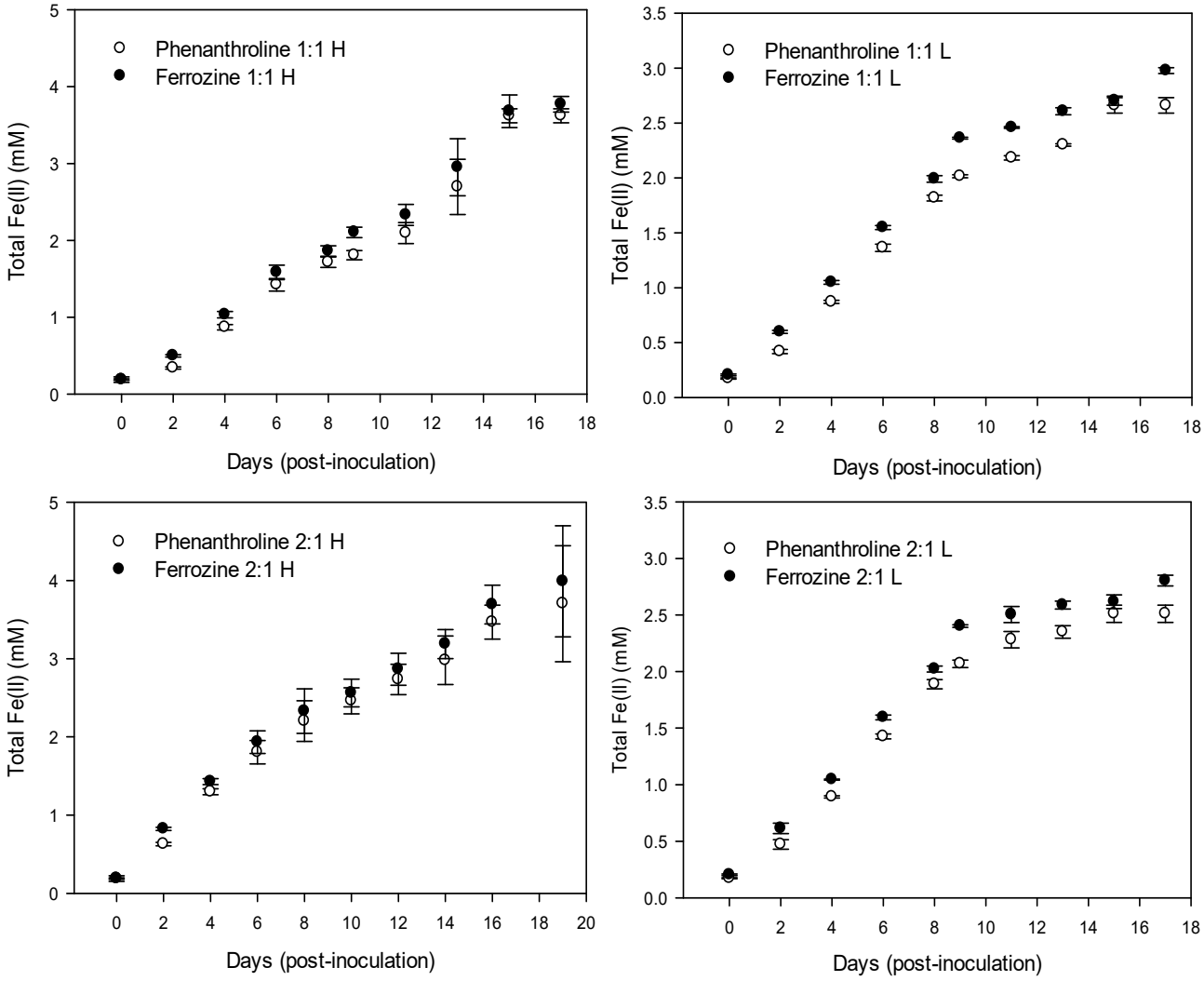

Figure S12: Changes in total Fe(II) (mM) during the reduction of non-irradiated BIOS collected from site CA-04 with molybdate:sulfate concentrations of 1:1 or 2:1, and 3.9mM (H) or 10µM (L) of phosphate. The concentration of total Fe(II) was determined using 2 spectrophotometric methods, the ferrozine method and 1,10-phenanthroline. As the graphs show, no major differences were found between the two methods. Data represents mean and standard deviation of 3 replicates.

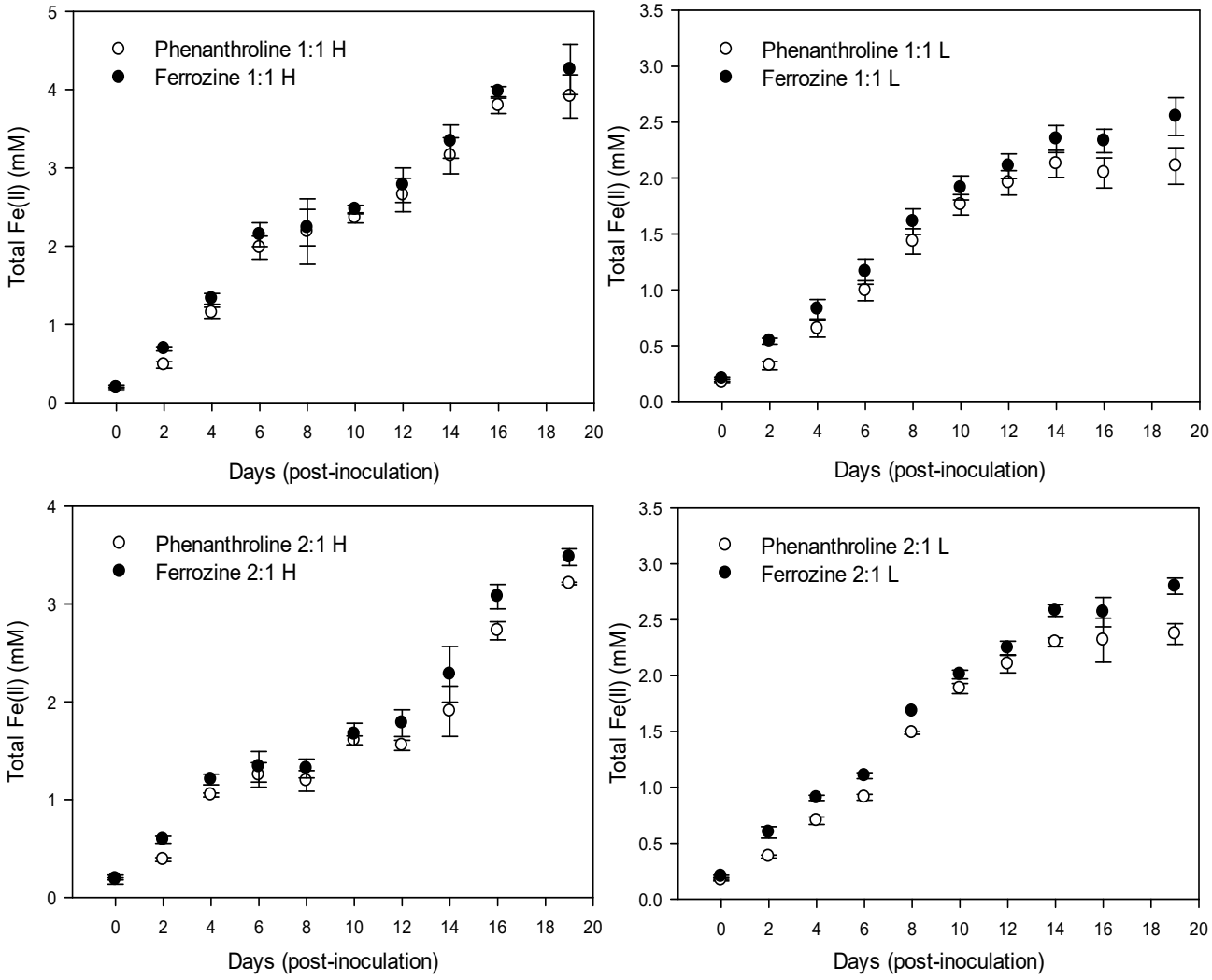

Figure S13: Changes in total Fe(II) (mM) during the reduction of non-irradiated BIOS collected from site CA-03 with molybdate:sulfate concentrations of 1:1 or 2:1, and 3.9mM (H) or 10µM (L) of phosphate. The concentration of total Fe(II) was determined using 2 spectrophotometric methods, the ferrozine method and 1,10-phenanthroline. As the graphs show, no major differences were found between the two methods. Data represents mean and standard deviation of 3 replicates.

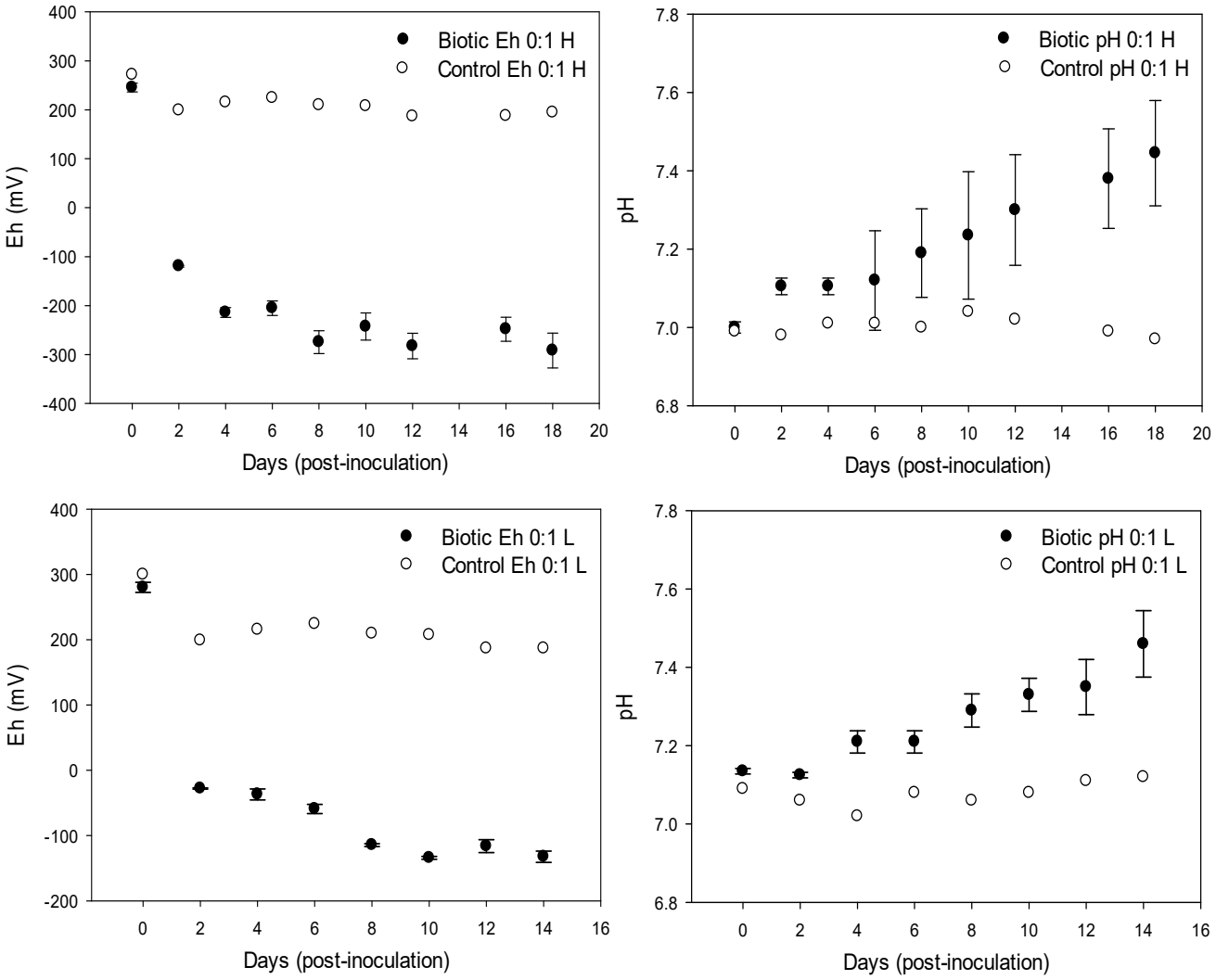

Figure S14: Changes in redox potential (Eh) (corrected to the standard hydrogen electrode; SHE) and pH during the reduction of γ-irradiated BIOS collected from site CA-04 with 3.9mM (H) or 10μM (L) of phosphate. "Biotic" refers to microcosms to which *S. putrefaciens* CN32 were added, whereas "Control" refers to control microcosms to which no bacteria were added. Data represents mean and standard deviation of 2 replicates for biotic experiments.

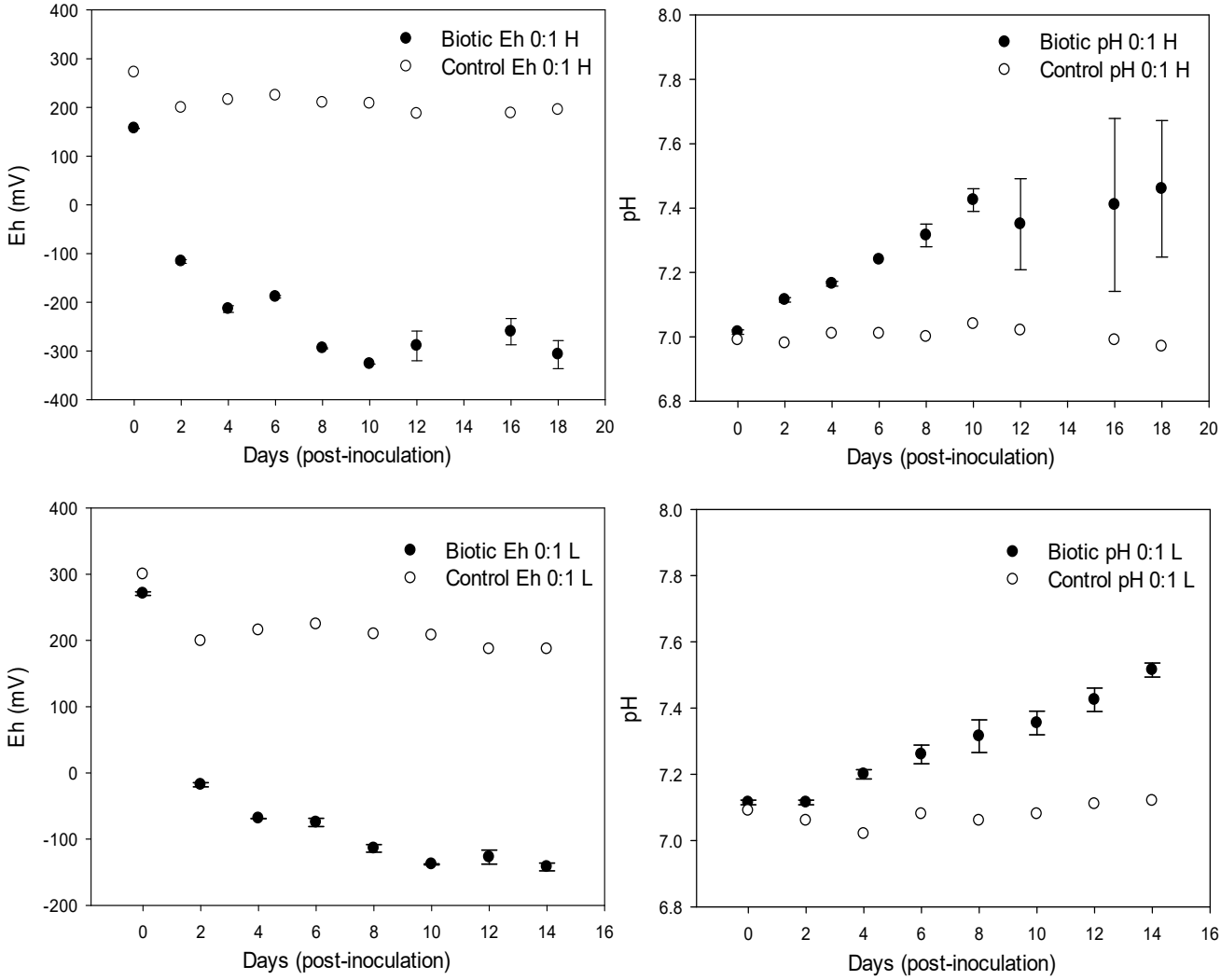

Figure S15: Changes in redox potential (Eh) (corrected to the standard hydrogen electrode; SHE) and pH during the reduction of γ-irradiated BIOS collected from site CA-03 with 3.9mM (H) or 10μM (L) of phosphate. "Biotic" refers to microcosms to which *S. putrefaciens* CN32 were added, whereas "Control" refers to control microcosms to which no bacteria were added. Data represents mean and standard deviation of 2 replicates for biotic experiments.

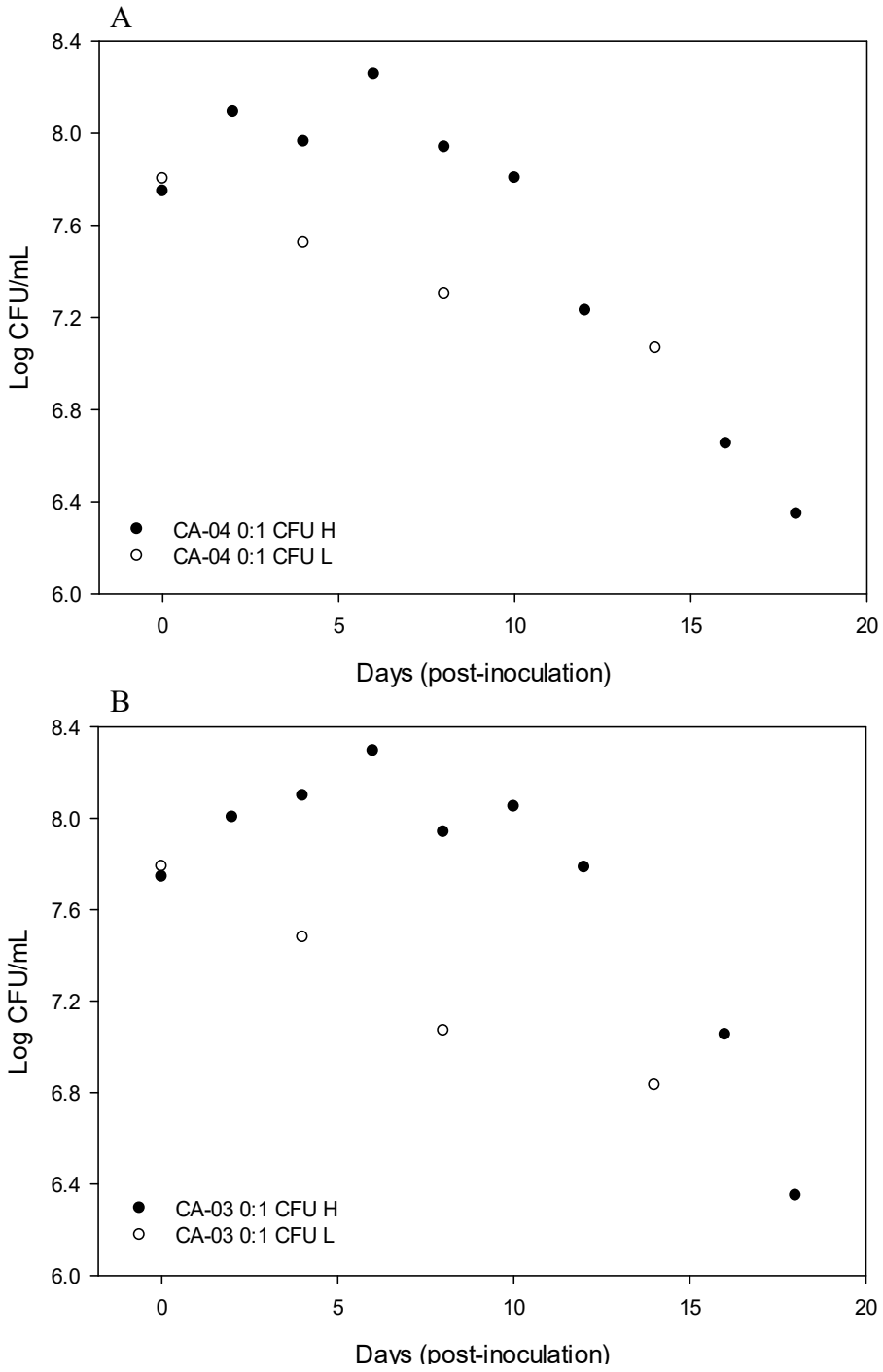

Figure S16: Changes in cell concentration of *S. putrefaciens* CN32 during the reduction of γ-irradiated BIOS collected from sites (A) CA-04 and (B) CA-03 with 3.9mM (H) or 10μM (L) of phosphate. No growth was observed in the control microcosms. Data represents mean of 2 replicates for each experiment.

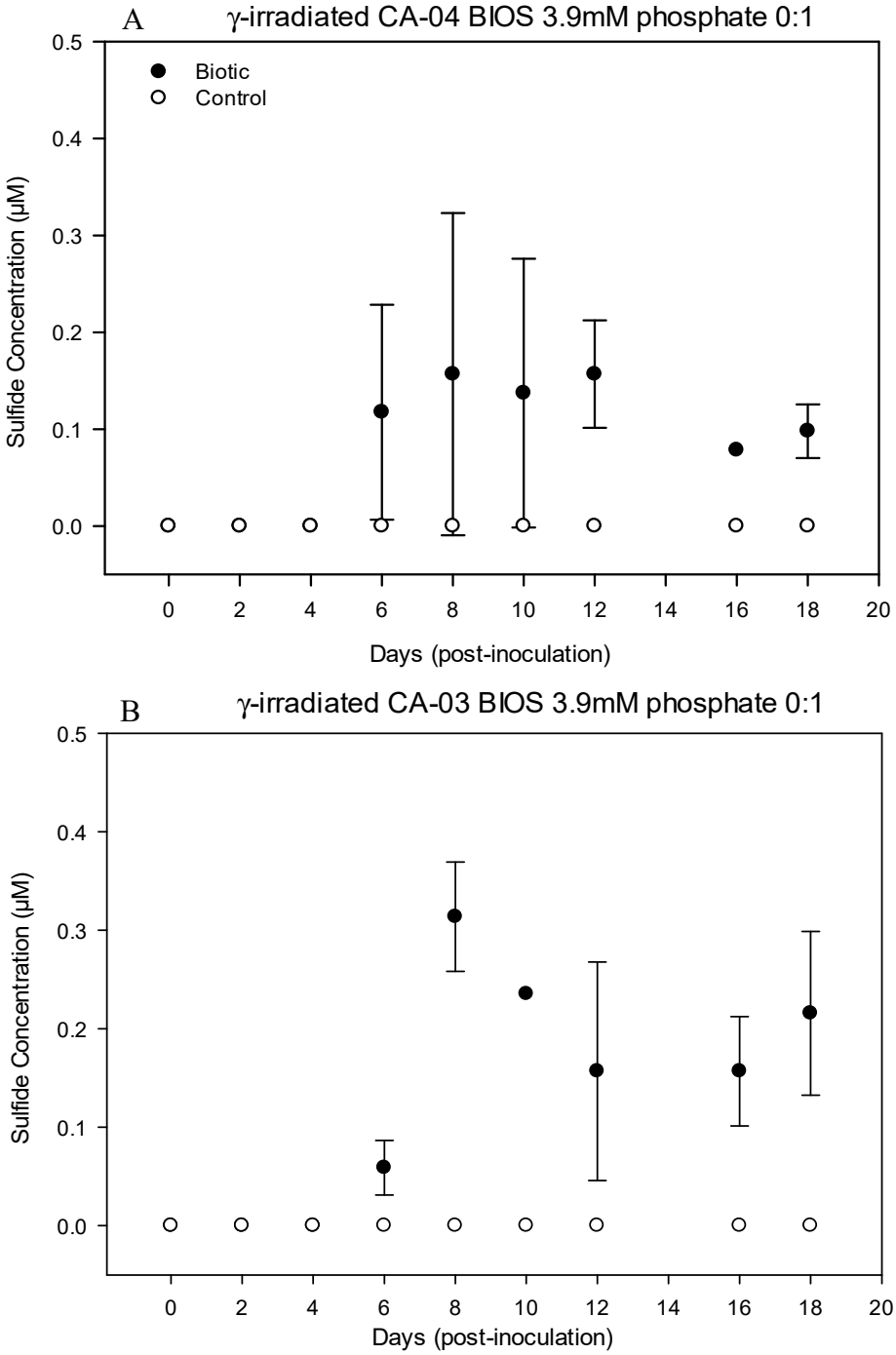

Figure S17: Changes in dissolved sulfide concentration (µM) during the reduction of γ-irradiated BIOS collected from sites CA-04 and CA-03 conducted with 3.9mM concentration of phosphate without the addition of molybdate (0:1). "Biotic" refers to microcosms to which *S. putrefaciens* CN32 were added, whereas "Control" refers to control microcosms to which no bacteria were added. Data represents mean of 2 replicates for biotic experiments.

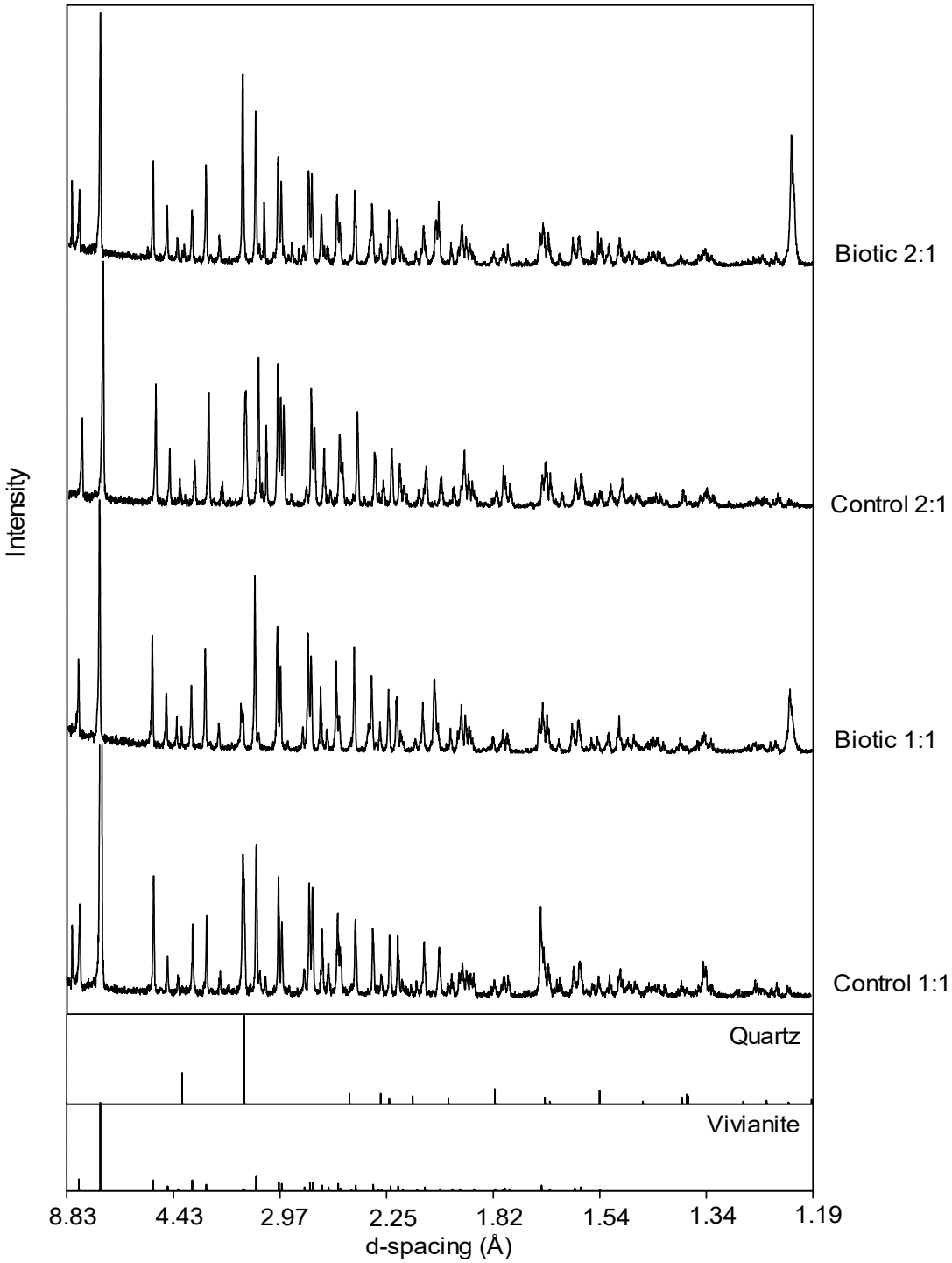

Figure S18: X-ray diffraction patterns of post-reduction precipitates formed during the microbial reduction of non-irradiated BIOS from site CA-04 by *S. putrefaciens* CN32 in the presence of 3.9mM of phosphate and molybdate:sulfate concentrations of 1:1 or 2:1. In all the treatments, vivianite was the dominant mineral. For clarity, all patterns have been vertically separated on an arbitrary y-axis.

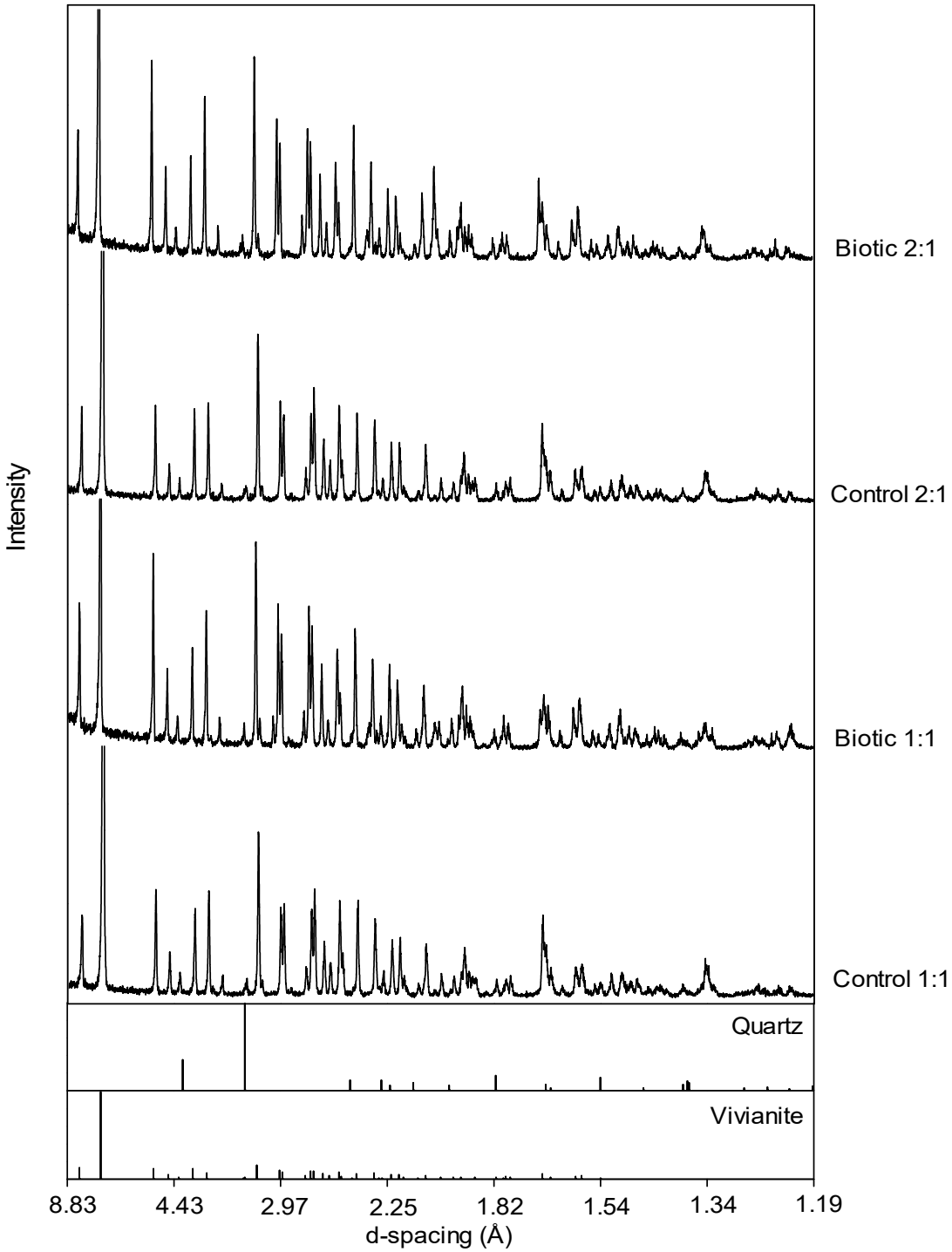

Figure S19: X-ray diffraction patterns of post-reduction precipitates formed during the microbial reduction of non-irradiated BIOS from site CA-03 by *S. putrefaciens* CN32 in the presence of 3.9mM of phosphate and molybdate:sulfate concentrations of 1:1 or 2:1. In all the treatments, vivianite was the dominant mineral. For clarity, all patterns have been vertically separated on an arbitrary y-axis.

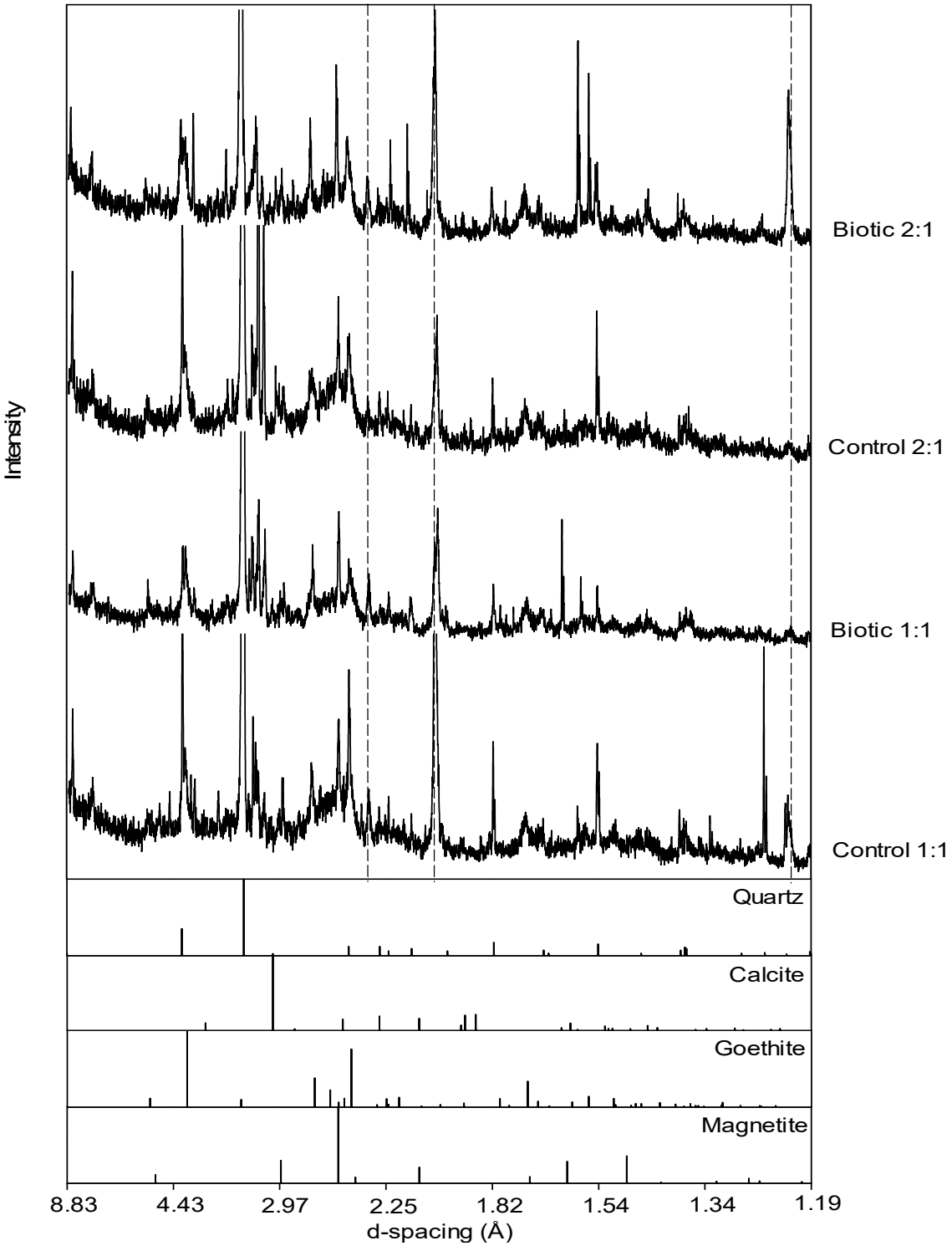

Figure S20: X-ray diffraction patterns of post-reduction precipitates formed during the microbial reduction of non-irradiated BIOS from site CA-04 conducted with 10μM of phosphate and molybdate:sulfate concentrations of 1:1 or 2:1. Dashed lines highlight the peaks from the sample holder. For clarity, all patterns have been vertically separated on an arbitrary y-axis.

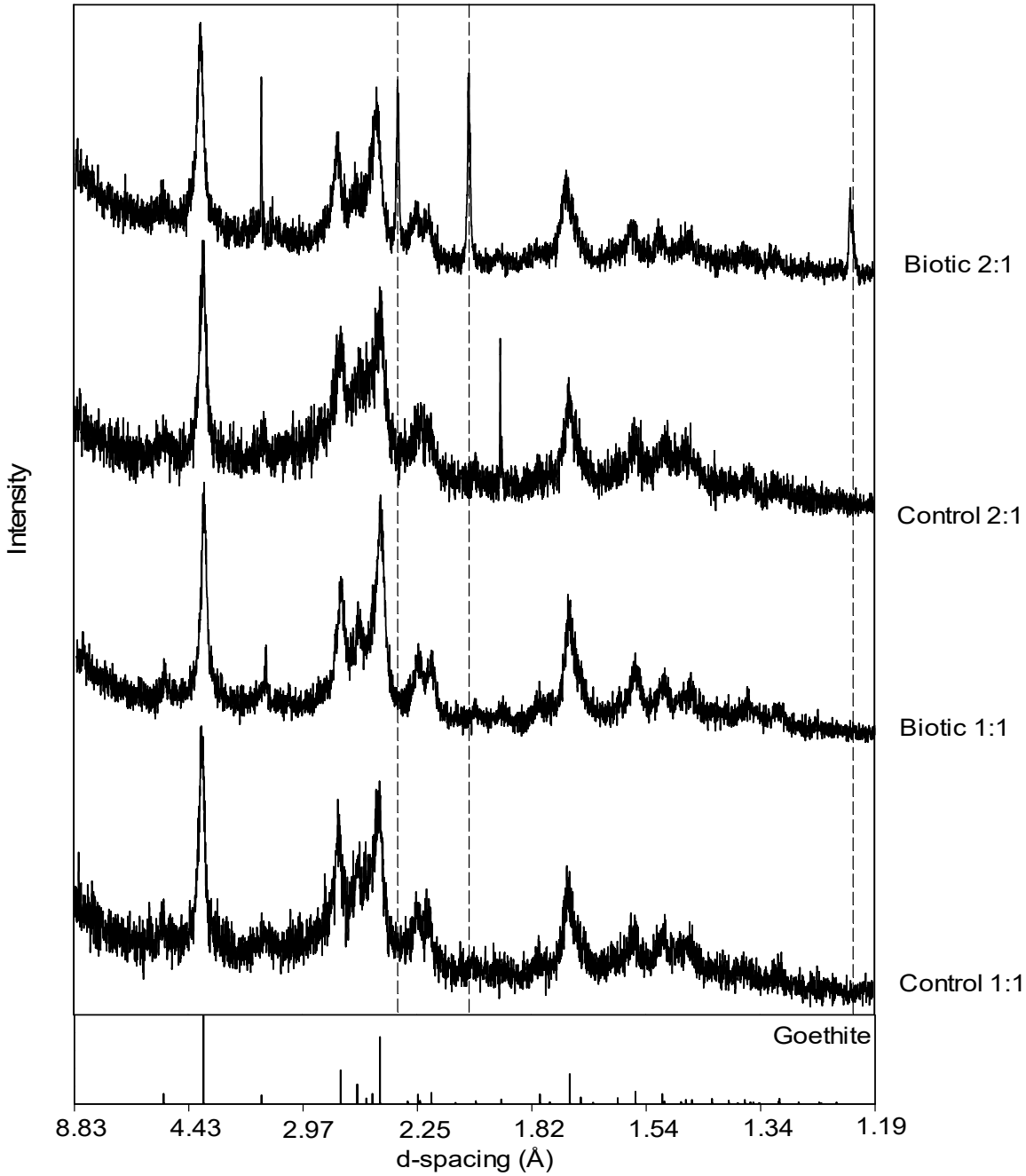

Figure S21: X-ray diffraction patterns of post-reduction precipitates formed during the microbial reduction of non-irradiated BIOS from site CA-03 conducted with 10μM of phosphate and molybdate:sulfate concentrations of 1:1 or 2:1. Dashed lines highlight the peaks from the sample holder. For clarity, all patterns have been vertically separated on an arbitrary y-axis.

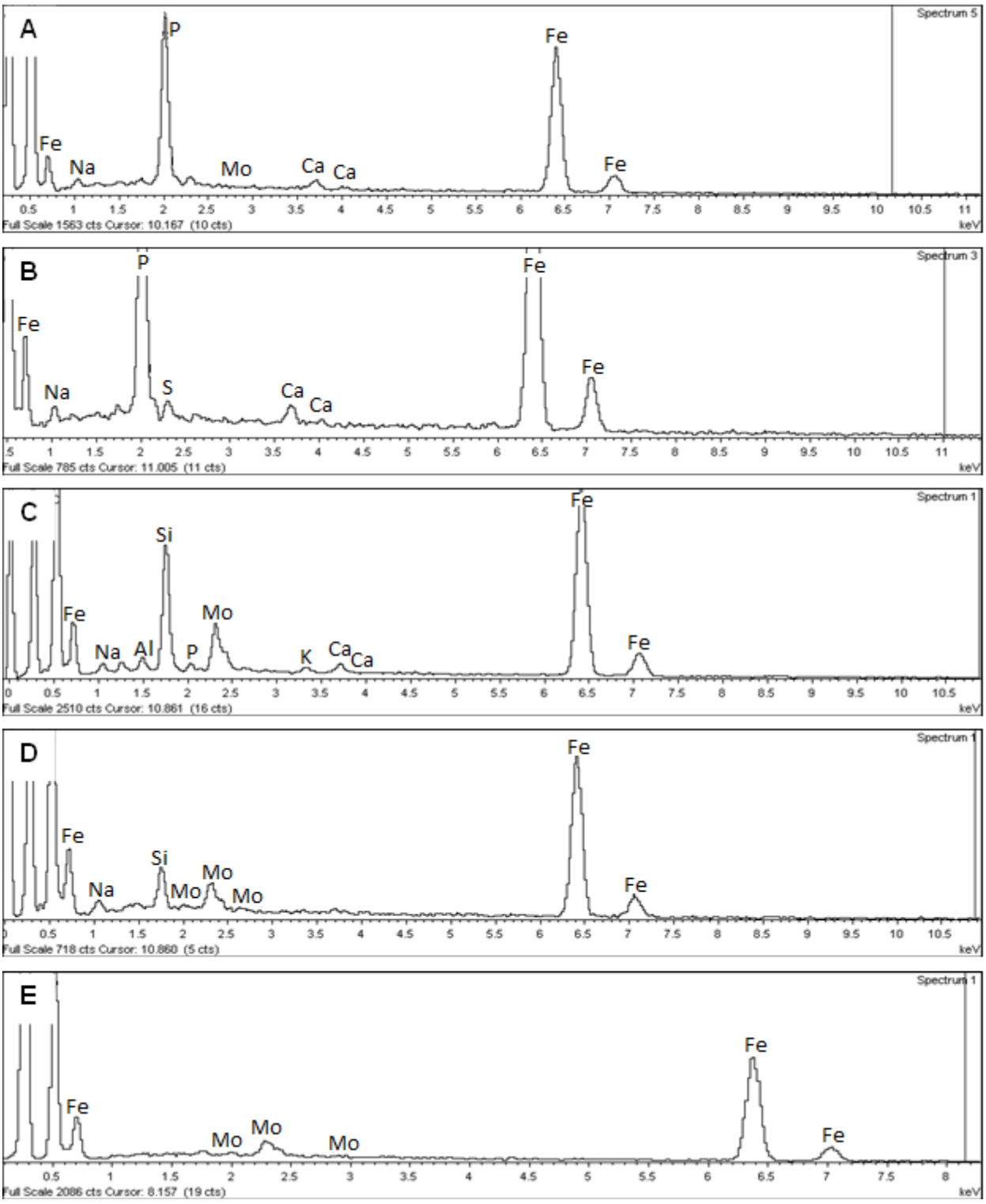

Figure S22: EDS analyses of post-reduction precipitates formed during the microbial reduction of BIOS from sites CA-04 and CA-03 conducted with 3.9mM (A and B) or 10µM (C and D) of phosphate with molybdate:sulfate concentration of 2:1 in the presence of *S. putrefaciens* CN32. Also shown is the EDS analysis of the post-reduction precipitate from biotic batch experiments conducted with HFO, 10 µM of phosphate, and molybdate:sulfate concentration of 2:1 (E).

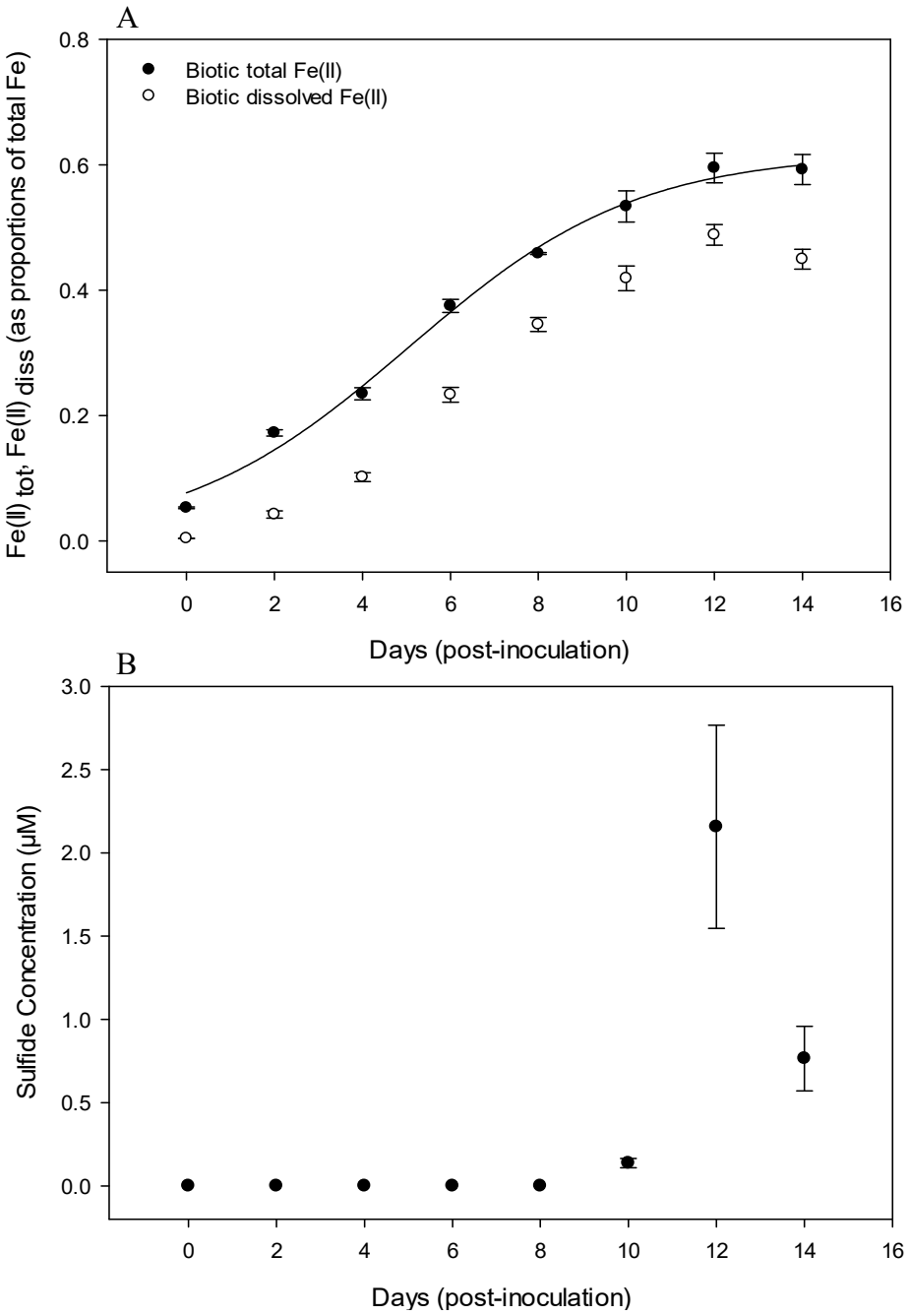

Figure S23: (A) Changes in total Fe(II) ($Fe(II)_{tot}$) and dissolved Fe(II) ($Fe(II)_{diss}$) relative to total Fe, and (B) dissolved sulfide concentration during the reduction of non-irradiated BIOS from site CA-04 by *S. putrefaciens* CN32 conducted with 10µM of phosphate but without the addition of molybdate. The rate of Fe(III) reduction was determined to be 0.056±0.014 day^{-1} (R^2 0.982) and the maximum amount of Fe(III) reduced was determined to be 59.5±2.3%. Data represents mean and standard deviation of 2 replicates.

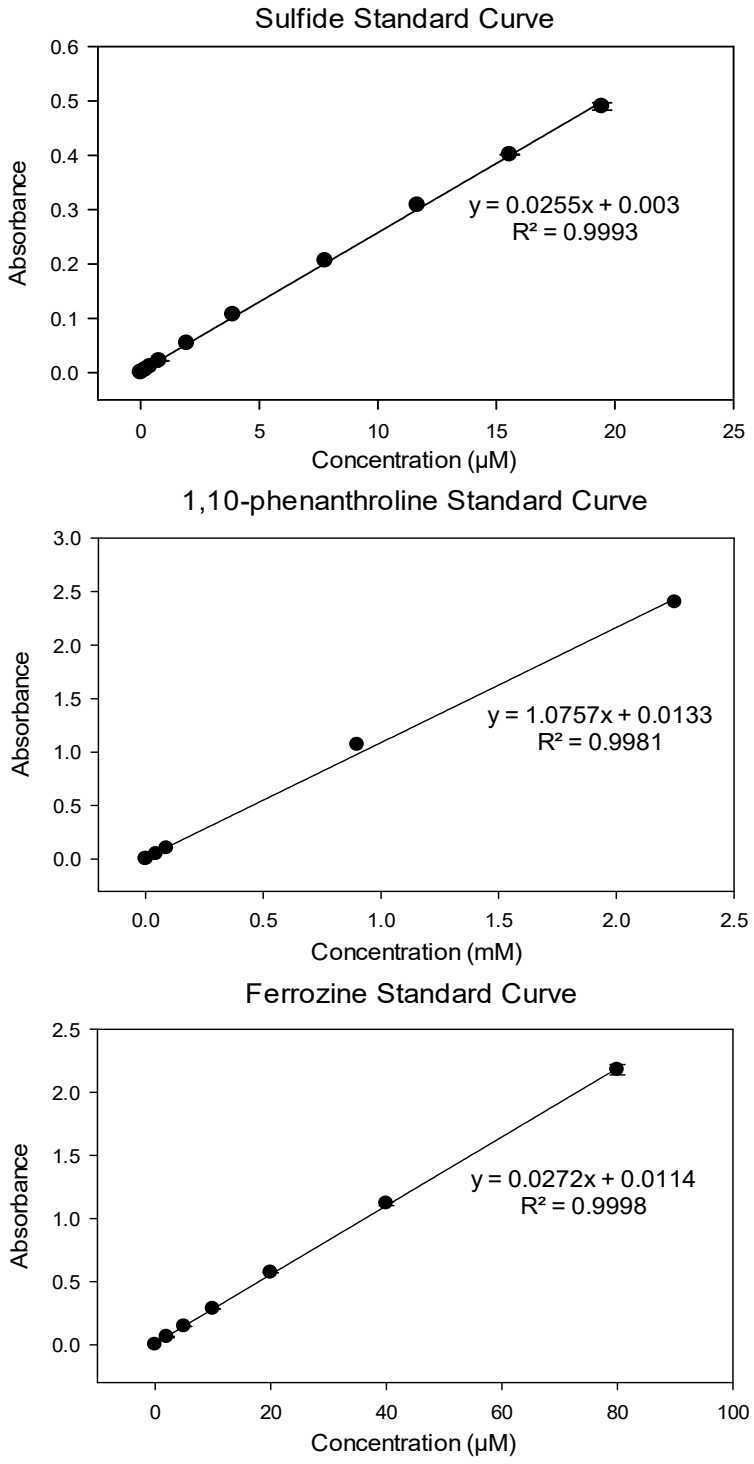

Figure S24: Standard curves for the determination of dissolved sulfide, and ferrous iron.

Calculations

Table S37: Thermodynamic data

Species	ΔG_f° kJ/mol	Reference
Fe^{3+}	-8.56	Clark (2015)
Fe^{2+}	-82.88	Clark (2015)
HS^-	12.08	Clark (2015)
SO_4^{2-}	-744.0	Clark (2015)
H_2O	-237.14	Clark (2015)
$HMoO_4^-$	-893.70	Brookins (2012)
$MoO_2(s)$	-532.99	Brookins (2012)
MoO_2^+	-513.79	Brookins (2012)

Standard redox couple:

Sulfate reduction proceeds as:

$$8e^- + 9H^+ + SO_4^{-2} \rightarrow HS^- + 4H_2O$$

$\Delta G^{\circ} = \sum products - \sum reactants$
ΔG° = (12.08 + 4(-237.14)) – (-744)
ΔG° = -192.48 kJ/mol

Since: ΔG° = - nFE°_{cell}
$E^{\circ}_{cell} = -\frac{\Delta G^{\circ}}{nF}$
n = moles of electron
F = Farady's constant 96.5 kJ/mol

$$E^{\circ}_{cell}\, SO_4^{-2}/HS^- = -\frac{-192.48}{8\times 96.5} = 0.25\text{V}$$

Molybdate reduction proceeds as:

$$2e^- + 3H^+ + HMoO_4^- \rightarrow MoO_{2(s)} + 2H_2O$$

ΔG° = (2(-237.14) + -532.99) – (-893.7)
ΔG° = -113.58 kJ/mol

$$E^{\circ}_{cell}\, HMoO_4^-/MoO_2 = -\frac{-113.58}{2\times 96.5} = 0.58\text{V}$$

Is Fe^{2+} oxidation energetically favorable by $HMoO_4^-$?

$$2e^- + 3H^+ + HMoO_4^- \rightarrow MoO_{2(s)} + 2H_2O$$
$$(Fe^{2+} \rightarrow Fe^{3+} + e^-)\times 2$$
$$3H^+ + HMoO_4^- + 2Fe^{2+} \rightarrow MoO_2(s) + 2Fe^{3+} + 2H_2O$$

$\Delta G^\circ = \sum products - \sum reactants$
ΔG° = (2(-8.56) + 2(-237.14) + (-532.99)) – ((-893.7) + 2(-82.88))
ΔG° = 35.1 kJ/mol

Since $\Delta G^\circ = -RTlnK$ *or* Log K= $-\frac{\Delta G^\circ}{5.708}$
Thus, for the reaction:
Log K= $-\frac{35.1}{5.708}$
Log K = -6.15
K = $7.08\text{x}10^{-7}$

Therefore, for the reaction: $3H^+ + HMoO_4^- + 2Fe^{2+} \rightarrow MoO_2(s) + 2Fe^{3+} + 2H_2O$
K = $7.08\text{x}10^{-7}$

$\Delta G = RT \ln \frac{Q}{K}$
Where:
Q = reaction quotient
K = equilibrium constant
R = gas constant 0.0083143 kJ/molK
T = temperature in kelvins 298.16

$$3H^+ + HMoO_4^- + 2Fe^{2+} \rightarrow MoO_2(s) + 2Fe^{3+} + 2H_2O$$
$$Q = \frac{[Fe^{3+}]^2}{[HMoO_4^-][Fe^{2+}]^2[H^+]^3}$$

From measured data collected from microcosms conducted with HFO, 10μM of phosphate, and 2:1 molybdate:sulfate concentration:
$[Fe^{2+}]_{diss}$ = 1.14mM
$[HMoO_4^-]_{diss}$ = 0.06mM
$[Fe^{3+}]_{diss}$ = $4.13\text{x}10^{-17}$mM
pH = 7.4

Concentration of $[Fe^{3+}]$ can be calculated from the Nernst equation:
Eh = -200mV → -0.2V

$$Eh = E^\circ + \frac{RT}{nF} \ln \frac{[Fe^{3+}]}{[Fe^{2+}]}$$

$$\text{Eh} = 0.77 + 0.059 \log \frac{[\text{Fe}^{3+}]}{[\text{Fe}^{2+}]}$$

$$-0.2 = 0.77 + 0.059 \log \frac{[\text{Fe}^{3+}]}{[1.14]}$$

$$[\text{Fe}^{3+}] = 4.13 \times 10^{-17} \text{mM}$$

Therefore:

$$Q = \frac{[4.13 \times 10^{-17}]^2}{[0.06][1.14]^2[4 \times 10^{-5}]^3}$$

Q = 3.43×10^{-19}

Remember that $\Delta G = RT \ln \frac{Q}{K}$

$$\Delta G = 0.0083143 \times 298.16 \ln \left(\frac{3.43 \times 10^{-19}}{7.08 \times 10^{-7}} \right)$$

$$\boldsymbol{\Delta G = -70.3\ kJ/mole}$$

Therefore, the reaction is thermodynamically favorable

Surface site occupancy calculations:
A range of values for the phosphate adsorption capacity of ferrihydrite have been published in the literature: 2.4 – 3.9µmol phosphate/m^2 (Torrent et al., 1990; Glasauer et al., 2003; Mengistu et al., 2015).

For calculations: a value of 2.5µmol phosphate/m^2 was arbitrarily chosen. Given the similarity of structures between PO_4^{-3} and MoO_4^{-2}, and the fact that compete for the same sites we assumed that molybdate occupies the same surface area as phosphate, i.e. 2.5µmol molybdate/m^2 (Gustafsson, 2003; Xu et al., 2006). The surface area of ferrihydrite (HFO) is also variable, we chose a value of 700m^2/g, which corresponds to the surface area of HFO that is in suspension (not dry) (Cornell and Schwertmann, 2003).

The maximum adsorption capacity of ferrihydrite (HFO):
Assuming the general formula for HFO: $Fe(OH)_3$ = 106.867 $\frac{g}{mole}$

$$2.5\frac{\mu mol}{m^2}\times 700\frac{m^2}{g}=1750\ \frac{\mu mole}{g}\rightarrow 1.75\times 10^{-3}\frac{mole}{g}$$

$$1.75\times 10^{-3}\frac{mole}{g}\times 106.867\frac{g}{mole}=0.187\ \frac{mole}{mole}$$

For our experiments, we used 4mM of Fe as HFO, thus:

$$0.187\ \frac{mole}{mole}\times\left(4mM\times\frac{1mole}{1000mmole}\right)=7.48\times 10^{-4}mole/L\ \rightarrow 0.748\ mM \text{ of phosphate}$$

Therefore, the maximum amount of phosphate that ferrihydrite can uptake at 4mM HFO is 0.75mM.

Phosphate concentration in our experiment was 3.9mM, therefore the amount of phosphate that is left in solution after 1 hour of equilibration should be:

3.9mM – 0.75mM = 3.15mM of phosphate or ~80% of phosphate left in solution
It is clear that phosphate oversaturates the adsorption capacity of HFO in our experiments.

Molybdate concentrations used in our experiments were 0.14mM and 0.28mM (molybdate:sulfate concentrations of 1:1 and 2:1, respectively):

At 0.14mM molybdate occupies:
$\frac{0.14}{0.75}=\sim 19\%$ of the available sites

At 0.28mM molybdate occupies:
$\frac{0.28}{0.75}=\sim 37\%$ of the available sites

The maximum adsorption capacity of lepidocrocite (O'Loughlin et al., 2010):
General formula for lepidocrocite: FeOOH = 88.85 $\frac{g}{mole}$
The surface area of lepidocrocite used by O'Loughlin et al. (2010) was reported to be 73.13 m^2/g
Assuming that the value of 2.5µmole phosphate or molybdate/m^2 also applies to lepidocrocite:

$$2.5\frac{\mu mol}{m^2}\times 73.13\frac{m^2}{g}=182.8\ \frac{\mu mole}{g}\rightarrow 1.83\times 10^{-3}\frac{mole}{g}$$

$1.83\times10^{-3}\,\frac{\text{mole}}{\text{g}}\times88.85\,\frac{\text{g}}{\text{mole}}=0.016\,\frac{\text{mole}}{\text{mole}}$

For their experiments, O'Loughlin et al. (2010) used 80mM of Fe as lepidocrocite, thus:
$0.016\,\frac{\text{mole}}{\text{mole}}\times\left(80mM\times\frac{1mole}{1000mmole}\right)=1.29\times10^{-3}mole/L\;\rightarrow 1.29\,mM$
Therefore, the maximum amount of phosphate that lepidocrocite can uptake at a concentration of 80mM is 1.29mM

Molybdate concentration used by O'Loughlin et al. (2010) experiments was 0.5mM, thus:
$\frac{0.5}{1.29}=\sim38\%$

Therefore, molybdate occupies ~38% of the available sites.

References:

Brookins, D.G., 2012. Eh-ph diagrams for geochemistry. Springer Science & Business Media.

Cotroneo, S.E., Fortin, D., 2013. Redox stability and microbial characterization of zinc-rich bacteriogenic iron oxides (BIOS). Undergraduate Thesis, University of Ottawa.

Clark, I., 2015. Groundwater geochemistry and isotopes. CRC Press.

Cornell, R.M., Schwertmann, U., 2003. The iron oxides: Structure, properties, reactions, occurrences and uses. John Wiley & Sons.

Gault, A.G., Ibrahim, A., Langley, S., Renaud, R., Takahashi, Y., Boothman, C., Lloyd, J.R., Clark, I.D., Ferris, F.G., Fortin, D., 2011. Microbial and geochemical features suggest iron redox cycling within bacteriogenic iron oxide-rich sediments. Chem. Geol., 281, 41-51.

Glasauer, S., Weidler, P.G., Langley, S., Beveridge, T.J., 2003. Controls on fe reduction and mineral formation by a subsurface bacterium. Geochim. Cosmochim. Acta, 67, 1277-1288.

Gustafsson, J.P., 2003. Modelling molybdate and tungstate adsorption to ferrihydrite. Chem. Geol., 200, 105-115.

Mengistu, H.A., Tessema, A., Demlie, M.B., Abiye, T.A., Roeyset, O., 2015. Surface-complexation modelling for describing adsorption of phosphate on hydrous ferric oxide surface. Water SA, 41, 157-168.

O'Loughlin, E.J., Gorski, C.A., Scherer, M.M., Boyanov, M.I., Kemner, K.M., 2010. Effects of oxyanions, natural organic matter, and microbial cell numbers on the bioreduction of lepidocrocite (γ-FeOOH) and the formation of secondary mineralization products. Environ. Sci. Technol., 44, 4570-4576.

Torrent, J., Barron, V., Schwertmann, U., 1990. Phosphate adsorption and desorption by goethites differing in crystal morphology. Soil Science Society of America Journal, 54, 1007-1012.

Xu, N., Christodoulatos, C., Braida, W., 2006. Adsorption of molybdate and tetrathiomolybdate onto pyrite and goethite: Effect of ph and competitive anions. Chemosphere, 62, 1726-1735.